

# GUIDE TO THIN SECTION MICROSCOPY

Second Edition

MICHAEL M. RAITH, PETER RAASE  
& JÜRGEN REINHARDT



---

ISBN 978-3-00-037671-9 (PDF)

© 2012 by M.M. Raith (University of Bonn) , P. Raase (University of Kiel), J. Reinhardt (University of KwaZulu-Natal)

All rights reserved. No part of this e-book may be reproduced, in any form or by any means, without the prior written permission of the authors.

Mailing and E-Mail addresses:

Prof. Dr. Michael M. Raith, Roidestraße 19, 53359 Rheinbach, Germany. E-Mail: m.raith@uni-bonn.de

Dr. Peter Raase, Steendiek 1, 24220 Schönhorst, Germany. E-Mail: pr@min.uni-kiel.de

Dr. Jürgen Reinhardt, School of Agricultural, Earth & Environmental Sciences, Department of Geology, University of KwaZulu-Natal, Durban 4000, South Africa. E-Mail: reinhardtj@ukzn.ac.za



## Contents

<b>Prefaces .....</b>	I-II
<b>Literature.....</b>	III
<b>Note on nomenclature and abbreviations.....</b>	IV
<b>1. 1 The petrographic microscope:</b>	
1.1 Magnifying glass (loupe) and microscope	
1.1.1 Imaging by a converging lens (objective).....	1-2
1.1.2 Magnification with the loupe (ocular, eyepiece).....	3
1.1.3 The compound microscope.....	3-6
1.2 Objectives and oculars	
1.2.1 Objective.....	6-8
1.2.2 Ocular.....	8-9
1.2.3 Tube, objective and ocular.....	10
1.3 Illumination	
1.3.1 Aperture of illumination.....	10-11
1.3.2 Light field.....	11
1.3.3 Glass diffusers and filters.....	11-13
1.4 Light paths in the microscope	
1.4.1 Köhler illumination.....	14
1.4.2 Orthoscopic mode.....	14
1.4.3 Conoscopic mode.....	15
1.5 Centring the microscope.....	15-18
1.6 Polarizer und Analyzer.....	18-21
1.7 Trouble-shooting	
1.7.1 Optimising the image of the specimen.....	22
1.7.2 Eliminating poor illumination.....	22-23
1.7.3 Sources of errors in the crossed-polarizers mode.....	23
1.7.4 Microscope care and maintenance.....	23
<b>2. Measuring angles, lengths and thickness:</b>	
2.1 Measurement of angles.....	24-25
2.2 Measurement of lengths.....	26-27
2.3 Determination of thin section thickness.....	28-30

**3. Morphological properties:**

3.1 Grain shape and symmetry.....	31-39
3.2 Cleavage, fracture, deformation-recrystallization phenomena.....	40-46
3.3 Twinning.....	47-50
3.4 Inclusions, intergrowths, alteration products .....	51-59

**4. Optical properties:**

## 4.1 Some basic principles

4.1.1 Nature of light, refraction .....	60-62
4.1.2 Isotropy and anisotropy.....	63-67

## 4.2 Optical characteristics used for mineral determination

4.2.1 Colour and pleochroism.....	68-76
4.2.2 Light refraction (relief, chagrin, Becke line).....	77-79
4.2.3 Double refraction (extinction behaviour, interference colour).....	80-99
4.2.4 Extinction positions in birefringent crystal sections.....	100-111
4.2.5 Conoscopic methods (optical character).....	112-126

**5. Routine mineral determination.....** 127



## Preface to the Second Edition

The main changes for the second edition concern chapters 1.6 (Polarizer and analyzer), 3.2 (Cleavage, fracture, deformation and recrystallization phenomena), 3.4 (Inclusions, intergrowths, alteration products) and 4.2.3 (Double refraction). Otherwise, only minor editorial modifications have been made, including the replacement of some photomicrographs.

Chapter 1.6 has been reorganized to describe the necessary checks and adjustment procedures for the two polarizers step-by-step. Chapter 3.2 has been extended to include deformation-related features at the grain or thin section scale, as far as such features can be observed in the transmitted-light microscope. The text and figures of chapter 3.4 have been revised and extended. Chapter 4.2.3, which includes aspects of optical mineralogy that are notoriously difficult to grasp for novices, has undergone a major revision. We added more figures and text that should help to understand the physical background to some basic optical phenomena such as retardation and interference colours. Furthermore, the upgrade involves new calculated interference colour charts, including a previously unpublished  $\Delta n - d$  chart.

Users of this guidebook will notice that the photomicrographs do not include a scale. Scales were left out here for two simple reasons: firstly, because the size of the thin section details shown to demonstrate optical or morphological properties is commonly not critical, and secondly, because we felt that the insertion of scales would clutter up the plates without serving much of a purpose. It needs to be stressed that scales on photomicrographs attached to any particular mineralogical or petrological study are essential information that must be generally included.

As explained on page IV, we decided to discontinue the use of the symbols  $\delta$  and  $\Delta$  for birefringence and retardation, respectively. We hope those professionals who have been brought up with the “deltas” will forgive us for breaking with this tradition.

M.M.R  
P.R.  
J.R.

February 2012

## Preface to the First Edition

The microscopic investigation of materials such as minerals, rocks, ores, technical and other synthetic products in transmitted and reflected light remains one of the classic, and to this day indispensable, mineralogical methods of analysis. Polarized-light microscopy provides a non-destructive way to identify solid substances (whether crystalline or amorphous) with relatively high spatial resolution, while the phases can be studied within their textural framework. It allows an estimate of chemical compositions and provides clues to the history of formation of the material, using specific textural characteristics (structure, fabric, phase assemblage, phase relationships, reaction textures). Thus, in many respects polarized-light microscopy has distinct advantages over bulk-analytical methods that use sample powders for phase identification (XRD) or for the analysis of chemical composition (XRF, AAS). The limitations of polarized-light microscopy are obvious where the chemical composition of complex solid solutions has to be determined, or where the material is too fine-grained to allow the identification of single phases. Depending on the specific objectives and the nature of the material to be investigated, a modern study in material science will therefore aim to combine polarized-light microscopy with complementary non-destructive methods of high spatial resolution (EMPA, SEM-EDX, TEM).

There are numerous textbooks that provide detailed accounts of the determinative techniques of polarized-light microscopy as well as the crystal-optical background for examining transparent amorphous and crystalline phases (glasses, minerals, synthetic substances). Hence, there is no need for a comprehensive presentation of that material in the following introduction to mineral determination in thin section. For practical work at the polarized-light microscope it is sufficient to summarise the necessary facts such that even users without an in-depth knowledge of mineralogy can follow the instructions. Fundamentals of crystal optics and crystallography are included only where they are crucial for explaining the observed optical phenomena and the morphological properties of crystals.

The identification of minerals under the polarized-light microscope is based on optical and morphological properties. Books that contain extensive listings of such properties provide the data basis for the vast number of natural minerals and synthetic phases (see reference list).

This guide is based on a previously published text that has been widely used in the German-speaking world, but is now out of print: "Methoden der Dünnschliffmikroskopie" by G. Müller and M. Raith (Clausthaler Tektonische Hefte, vol.14). We adopted this text to a large degree, revising the figures using modern graphics software, and adding many more figures and photomicrographs to illustrate the various phenomena described in the text.

We hope that this guide will provide students with the necessary basics to master and successfully apply polarized-light microscopy.

Suggestions are always welcome!

## Bibliography

### Optical crystallography and techniques in mineralogical and petrographic microscopy

- Bloss, F.D. (1999): Optical Crystallography. Mineralogical Society of America, Washington, D.C. 239 p.
- Dyar M.D., Gunter, M.E. & Tasa, D. (2008): Mineralogy and Optical Mineralogy. Mineralogical Society of America, Chantilly, Va. 708 p.
- Ehlers, E.G. (1987): Optical Mineralogy, Vol. 1. Theory and Technique. Blackwell Scientific Publ., Palo Alto. 158 p.
- Nesse, W.D. (2003): Introduction to Optical Mineralogy (3rd ed.). Oxford University Press, New York. 348 p.
- Phillips, W.R. (1971): Mineral Optics – Principles and Techniques. Freeman and Company, San Francisco. 249 p.
- Stoiber, R.E. & Morse, S.A. (1994): Crystal identification with the Polarizing Microscope. Chapman & Hall. 358 p.
- Wahlstrom, E.E. (1979): Optical Crystallography (5th ed.). John Wiley & Sons, New York. 488 p.

### Mineral determination

- Deer, W.A., Howie, R.A. & Zussman, J. (1992): An Introduction to the Rock-Forming Minerals (2nd edition). Longman, London. 696 p. \*
- Ehlers, E.G. (1987): Optical Mineralogy, Vol. 2. Mineral Descriptions. Blackwell Scientific Publ., Palo Alto. 286 p. \*
- Heinrich, E.W. (1965): Microscopic Identification of Minerals. McGraw-Hill, New York. 414 p. \*
- Kerr, P.F. (1977): Optical Mineralogy (4th ed.). McGraw-Hill, New York. 492 p. \*
- MacKenzie, W.S. & Adams, A.E. (1994): A Colour Atlas of Rocks and Minerals in Thin Section. Manson Publ. 192 p.
- MacKenzie, W.S. & Guilford, C. (1980): Atlas of Rock-Forming Minerals in Thin Section. Longman, London. 98 p.
- Nesse, W.D. (2003): Introduction to Optical Mineralogy (3rd ed.). Oxford University Press, New York. 348 p. \*
- Perkins, D. & Henke, K.R. (2003): Minerals in Thin Section (2nd ed.). Prentice Hall, Upper Saddle River. 176 p. \*
- Phillips, W.R. & Griffen, D.T. (1981): Optical Mineralogy. The Nonopaque Minerals. W.H. Freeman, San Francisco. 677 p. \*
- Tröger, W.E., Bambauer, H.U., Taborszky, F. & Trochim, H.D. (1979): Optical Determination of Rock-Forming Minerals. Part 1: Determinative Tables. Schweizerbart, Stuttgart. 188 p. \*

\* books with more or less extensive mineral data compilations



## A note on terminology and some abbreviations used in this book

When using a polarized-light microscope, communicating directions in an unequivocal way is important. The cross-hairs in the ocular, the directions of light polarization and the microscope axis are the main reference directions. The four cardinal points (and intermediate directions derived from those) are commonly used to express and distinguish directions, with no geographical meaning, obviously. For a standard microscope set-up, "N-S" means parallel to the "vertical" cross-hair or parallel to a line running from brow to chin between the two eyes of the observer; "E-W" means parallel to the "horizontal" cross-hair or parallel to a line across the centre of both eyes. Diagonal directions are thus referred to as NW-SE and NE-SW.

The Greek letters  $\alpha$ ,  $\beta$ ,  $\gamma$ ,  $\varepsilon$ ,  $\omega$  are used by some authors as subscripts to refractive indices ( $n$ ). In this text, we follow the terminology of Tröger et al. (1979) and others which is logical and intuitive in the sense that the refractive indices  $n_x$ ,  $n_y$  and  $n_z$  correlate with the axes X, Y and Z of the coordinate system in which the shape of the indicatrix of biaxial crystals is defined. Furthermore,  $\alpha$ ,  $\beta$ ,  $\gamma$  are crystallographic cell parameters, and hence any potential confusion with optical parameters should be avoided. In the same way as in  $n_x$ ,  $n_y$  and  $n_z$ , the subscripts o and e relate to refractive indices of O- and E-rays or O- and E-waves in uniaxial crystals.

As pointed out in the previous edition of the guidebook, many (though not all) authors of optical mineralogy textbooks use the Greek letter *delta* for two different parameters that are related to each other:  $\delta$  stands for birefringence and  $\Delta$  for retardation ( $\Delta = \delta * d$ ;  $d$  = thickness of crystal plate). To add to the potential confusion,  $\Delta$  is the symbol for birefringence in the widely used Tröger tables (Tröger et al., 1979). Although the use of  $\delta$  and  $\Delta$  may be standard symbols in the teaching of crystal optics in some institutions, we decided to abandon these for the 2012 edition in order to make the shorthand terminology less confusing for those being introduced to optical mineralogy. We will use the symbol  $\Delta$  strictly in its standard mathematical sense (i.e., "difference"). Hence, birefringence can simply be expressed as  $\Delta n$  ( $= n_z - n_x$ , for example). The symbol for retardation is the Greek letter  $\Gamma$  (hence,  $\Gamma = \Delta n * d$ ).

In science the common symbol for wavelength is  $\lambda$ , but in optical mineralogy  $\lambda$  is also used for indicating the interference colour order ( $1\lambda$  = first order red,  $2\lambda$  = second order red, etc.). We have tried to circumvent reference to the latter, but the use of terms such as " $\lambda$ -plate" (meaning  $1\lambda$  or 551 nm retardation corresponding to 1st order red) and " $\lambda/4$ -plate" are somewhat entrenched and thus hard to avoid.

## 1. The petrographic microscope

### 1.1 Magnifying glass (loupe) and microscope

In order to examine the microtextural and mineralogical features in the thin section of a rock with higher resolution than that of the naked eye, a microscope is used. A microscope has two systems of lenses. The first lens system (objective) produces a magnified image of the object. This real image is viewed by the second lens system (ocular or eyepiece) that also provides further magnification.

#### 1.1.1 Imaging by a converging lens (objective)

Optical images of an object are formed by converging lenses, i.e. spherical lenses with outward bulging surfaces (biconvex lenses). An inverted real image is formed if the object is placed beyond the focal length ( $f$ ) of the lens. This image can be projected on a screen (which is the principle behind the camera and the human eye; Fig. 1-1, upper part).

The distances from the object to the lens ( $a$ ) and from the lens to the image ( $b$ ) are related to the focal lengths ( $f$ ) of the biconvex lens by the following equation (lens formula, Fig. 1-1, lower part):

$$\frac{1}{a} + \frac{1}{b} = \frac{1}{f}$$

The magnification of the lens is given by:

$$M = \frac{B}{A} = \frac{b}{a} = \frac{b-f}{f} = \frac{f}{a-f}$$

The size of the real image ( $B$ ) is larger than that of the object ( $A$ ), if

$$\frac{b-f}{f} > 1 \text{ i.e. } 2f < b \text{ resp. } \frac{f}{a-f} > 1 \text{ i.e. } a < 2f.$$

Example: If an object is placed at a distance of 33 mm in front of a biconvex lens with a focal length of 30 mm, the lens will produce a 10-times magnified image ( $M = 10:1$ ) at a distance of 330 mm behind the lens.

The human eye can modify the focal length by changing the curvature of its lens such that it can project sharp images on the retina of objects ranging in distance from about 250 mm to infinity.

As an object approaches the human eye from a greater distance it is seen at increasing visual angles ( $\alpha$ ) and, with the concomitant increasing magnification, the image on the retina becomes progressively larger (Fig. 1-2, upper part).

The shortest possible distance of focused vision varies individually. It has been set at 250 mm by the optical industry in order to standardize the calculation of magnification values.

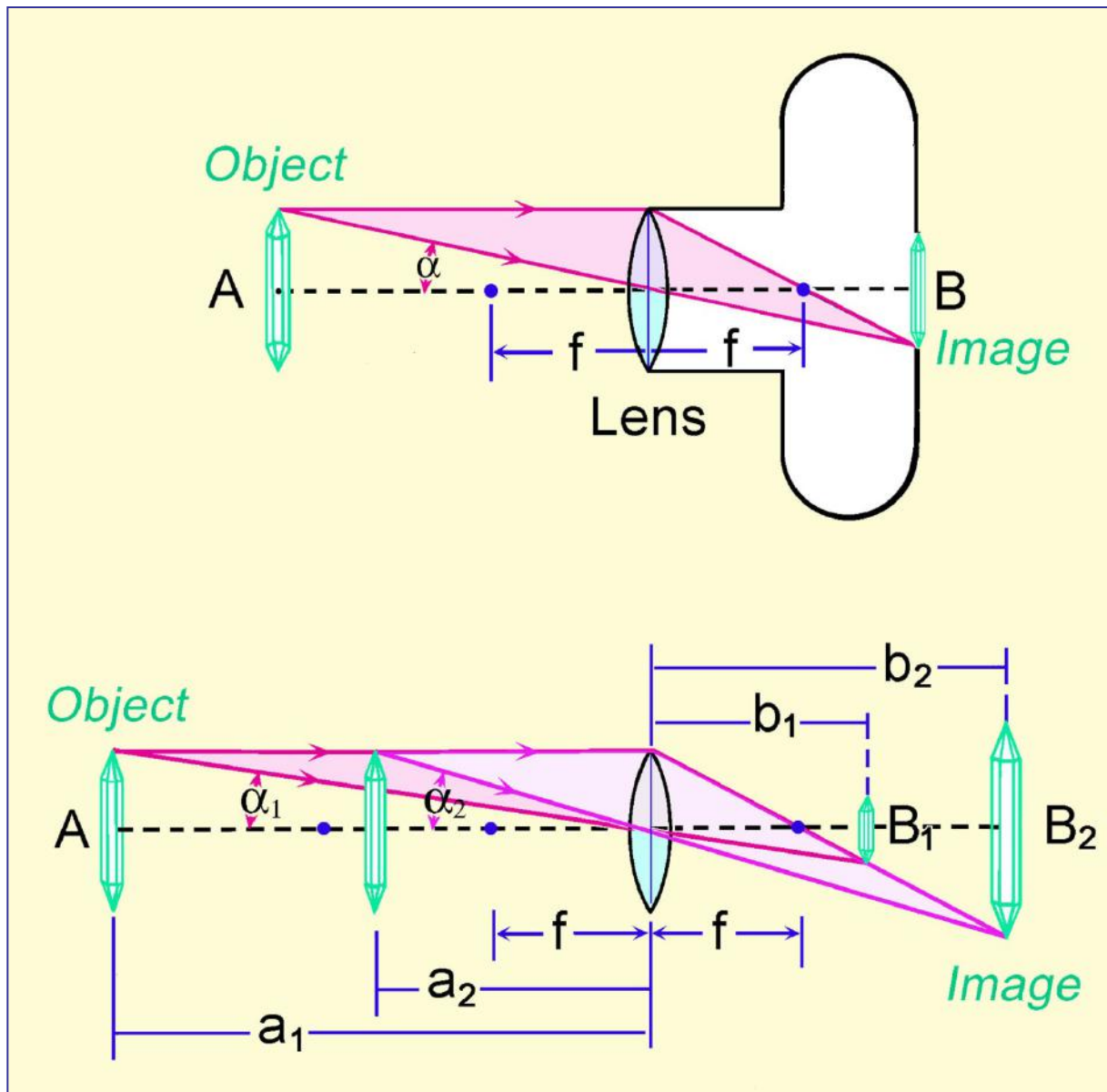


Figure 1-1. Optical imaging of a crystal by a biconvex lens

Placed at the shortest distance of focused vision, the object is seen at the largest possible visual angle and thus with the highest possible magnification. Fine structures of an object, when observed at the shortest distance of vision, can only be resolved, however, if they appear at visual angles larger than  $1'$  (about  $0.02^\circ$ ).

Structural details that remain below this limit of vision can still be resolved through further magnification with a magnifying glass (loupe) or microscope.

### 1.1.2 Magnification with the loupe (ocular, eyepiece)

The most simple device to increase the visual angle is a magnifying glass (loupe). It consists of a biconvex lens with a focal length that is smaller than the minimum distance of vision (<250 mm). If an object (A) is placed in the focal point F of the lens, the user sees an enlarged upright image (B) which appears to be located behind the loupe (i.e., on the object side) and appears to come from infinite distance (virtual image; Fig. 1-2, lower part).

The human eye now views the object at an increased visual angle  $\alpha'$ . As a consequence, the image B projected on the retina is significantly enlarged.

The magnifying power of a loupe is defined as the ratio of the tangent values of the visual angles (or the sizes of the images) at which the object is seen with and without the lens at the minimum distance of vision of 250 mm (Fig. 1-2, upper und lower parts):

$$M_L = \frac{\tan\alpha'}{\tan\alpha} = \frac{B'/250}{A/250} = \frac{A/f}{A/250} = \frac{250}{f} \quad (\text{loupe equation})$$

The magnification of a loupe  $M_L$  is thus defined as the ratio of the minimum distance of vision (250 mm) and the focal length ( $f$ ) of the lens.

Example: A loupe with a focal length of 31.25 mm produces eightfold magnified images:  $250/31.25 = 8 \times$ .

If the object is not placed in the focal point of the loupe but within the focal length, (Fig. 1-2, middle part), the magnification can vary up to a value of

$$M_L = \frac{250}{f} + 1$$

$M_L$  values engraved on the casing of the loupe refer specifically to the magnification that applies if the object is placed in the focal point of the lens.

### 1.1.3 The compound microscope

In the most simple case, the magnification of an object in the *microscope* is achieved in two steps through a combination of two biconvex lenses (compound microscope; Fig. 1-3).

In a first imaging step (Fig. 1-3, upper part), a convex lens (*objective*) produces a real, enlarged and inverted image of the object at a magnification scale M.

In a second imaging step (Fig. 1-3, middle part), the real image is viewed by a magnifying glass (*ocular, eyepiece*), providing further magnification. To ensure that this virtual image can be viewed with a relaxed eye focused on infinity, the real image is placed in the focal plane of the ocular (Fig. 1-3, lower part).

The final image is created on the retina of the human eye.

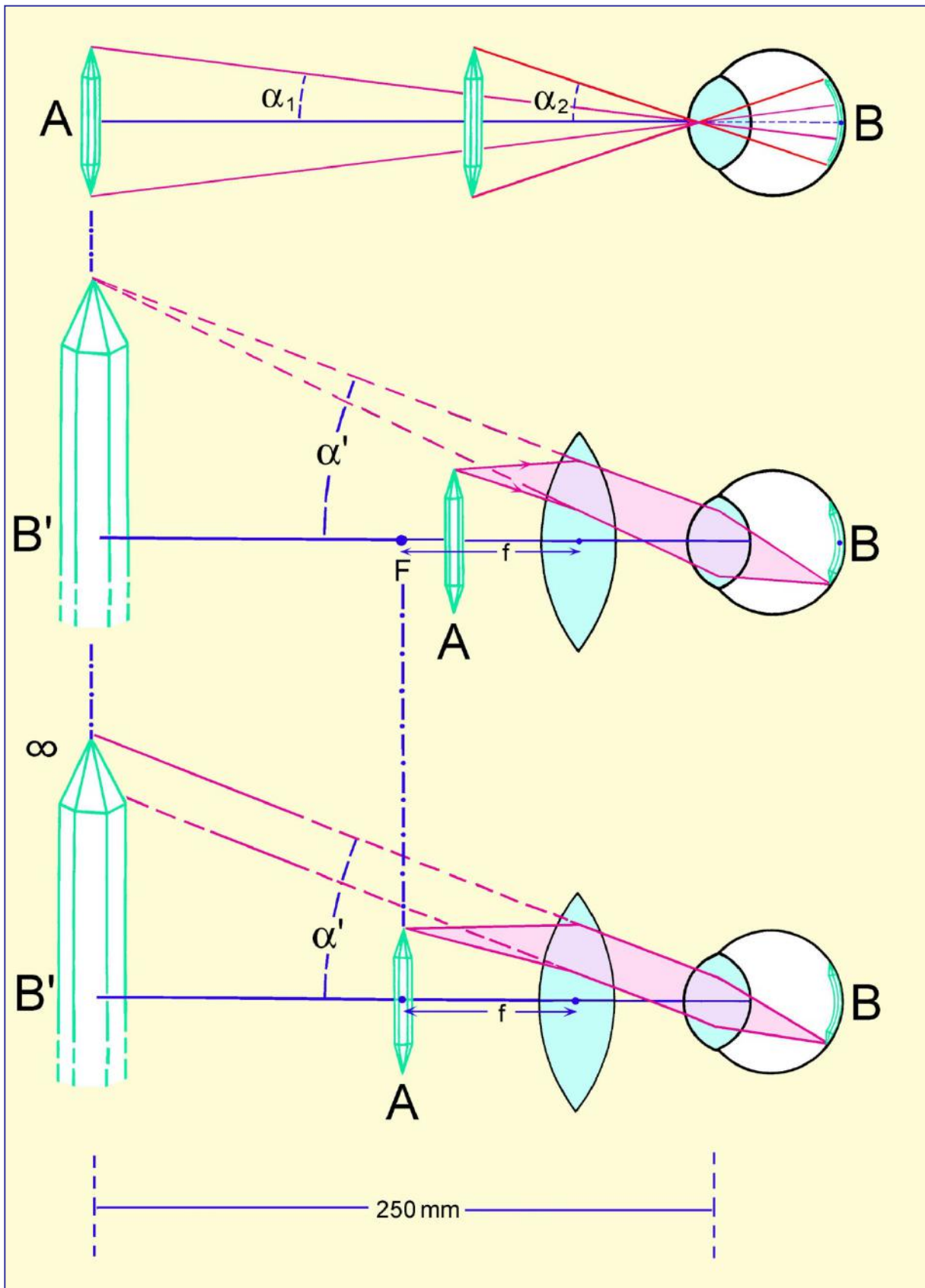
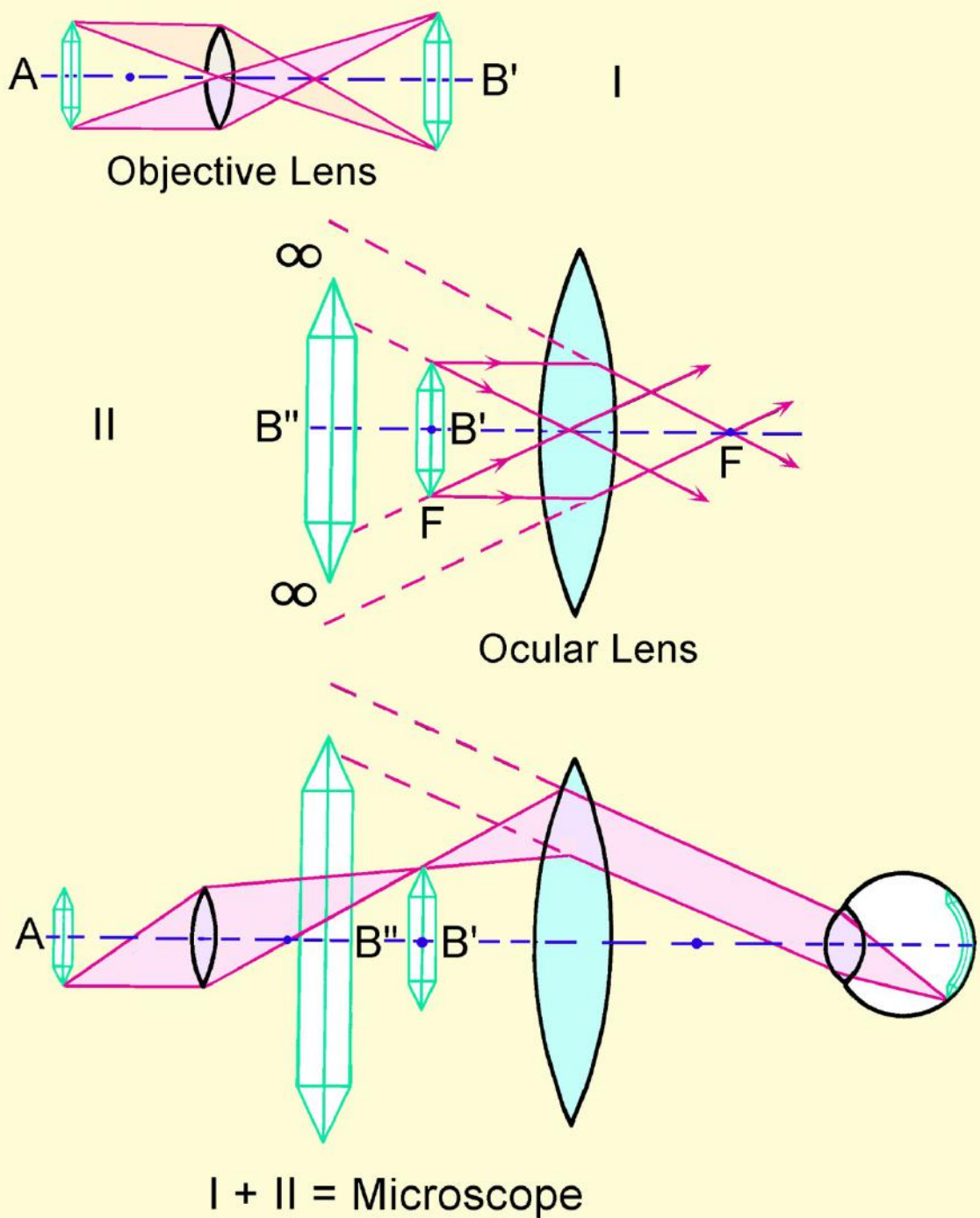


Figure 1- 2. Magnification of a crystal by a biconvex lens (magnifying glass, loupe, ocular)



**Figure 1-3.** Two-step magnification of a crystal by the compound microscope



The total magnification  $M$  of a compound microscope is the product of objective magnification ( $M_O$ ) and ocular magnification ( $M_L$ ):

$$M = M_O * M_L$$

**Example:** A microscope equipped with an objective  $M_O = 50$  and an ocular  $M_L = 10$  has a final magnification of  $50 \times 10 = 500$ .

In modern compound microscopes (with infinity-corrected optical systems) the magnification of the object is performed in a somewhat different way. The specimen is placed in the lower focal plane of the objective, so that its image is projected at infinity. An auxiliary lens (tube lens or telan) placed within the tube between the objective and the eyepiece brings the parallel light rays into focus and produces the real image which then is viewed with the ocular. The infinity-corrected imaging technique allows to insert accessory components such as analyzer, compensators or beam splitters into the light path of parallel rays between the objective and the tube lens with only minimal effects on the quality of the image. It further provides a better correction of spherical and chromatic aberration.

## 1.2 Objective and ocular (eyepiece)

### 1.2.1 Objective

The quality of the observed image is largely determined by the objective. The objective is thus a key component in the microscope, being responsible for the primary image, its magnification and the resolution under which fine details of an object can be observed. The ocular merely serves to further magnify the fine details that are resolved in the intermediate image, so that they exceed the angular resolution limits of the human eye and can be viewed at visual angles larger than  $1'$  (Ch. 1.1.1, loupe).

The important properties of an objective are its magnification, its numerical aperture and the degree of aberration correction, whereby the latter two determine the quality of the intermediate image.

### Aberration

Simple biconvex lenses produce imperfect, distorted images that show spherical and chromatic aberrations. In modern objectives, such optical aberrations are compensated to a large extent by a combination of converging and diverging lenses that are made of materials with different refractive indices and dispersion. Remaining aberrations are compensated by oculars with complementary corrections.

At high magnification and large aperture, the cover glass of thin sections introduces chromatic and spherical aberrations which have an adverse effect on image quality. This is because light rays emerging from an object point P are refracted at the boundary cover glass/air. As a consequence, the backward extensions of the light rays do not focus in a spot, but form a blurry, defocused area (Fig. 1-4A, grey areas). With increasing thickness of the cover glass the blurring effect becomes more pronounced. High-power objectives are therefore corrected for this type of cover glass aberration, commonly for a standard glass thickness of 0.17 mm. Hence, the cover glass forms part of the objective system! Any thickness deviating from 0.17 mm affects the intermediate image. Furthermore, if the cover glass is too thick, it may not be possible to focus the specimen using high-power objectives, due to the short free working distances of such objectives (see Table 1).

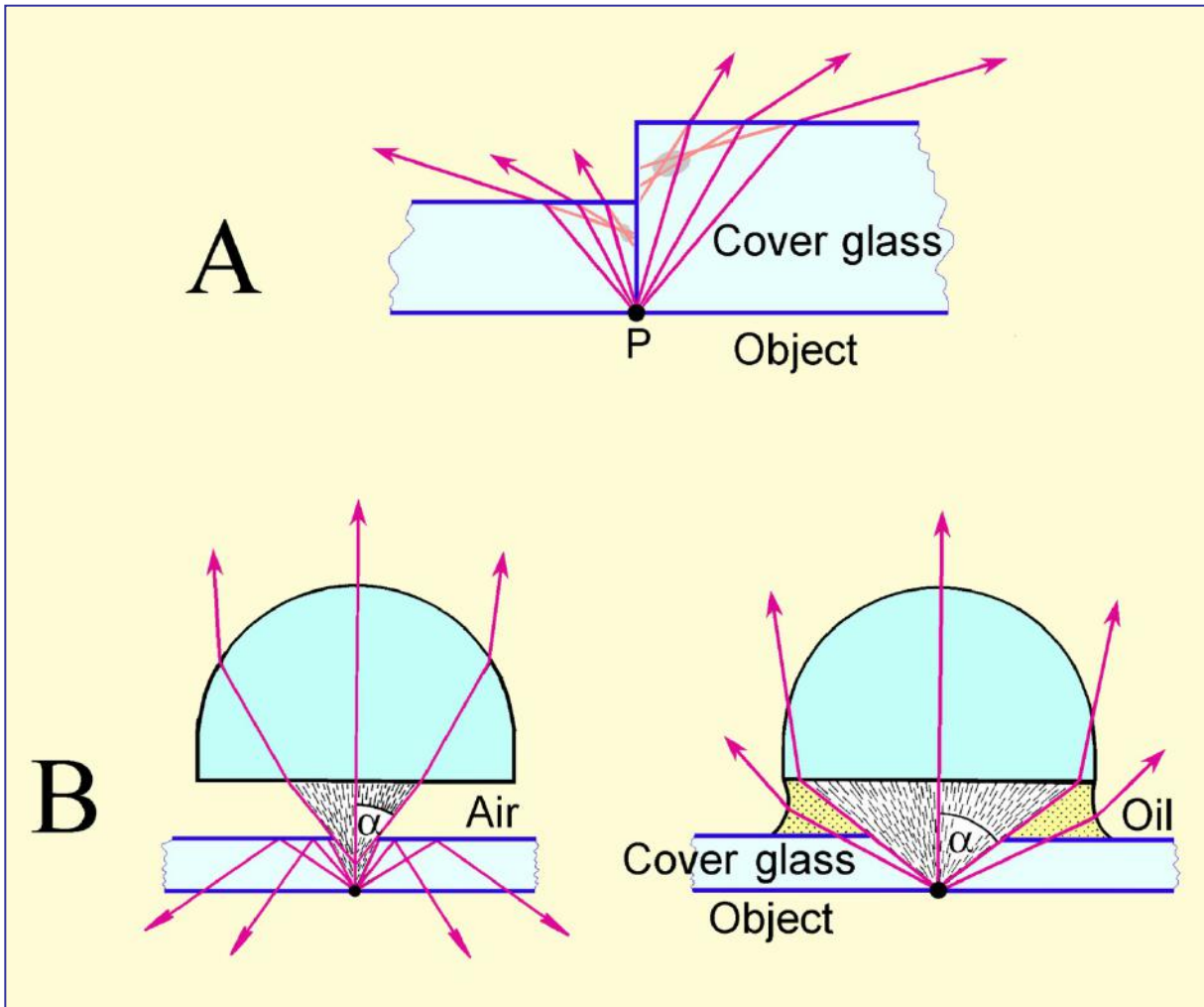


**Figure 1-4.** A. Aberration of light rays in the cover glass; B. Aperture of the objective

### Aperture and resolution

The numerical aperture (N.A.) of the objective is a measure of the quantity of light taken up by the objective lens. The N.A. is proportional to the angular aperture  $\alpha$  of the cone of light rays emitted from a point on the specimen that enters the objective, and to the refractive index  $n$  of the medium which separates the specimen from the front lens of the objective (e.g. 1.0 for air, 1.33 for water, and  $\sim 1.56$  for oil):  $N.A. = n * \sin\alpha$  (Fig. 1-4B).

When viewing the specimen with objectives of increasing numerical aperture, the cone of light rays entering the front lens of the objective increases in width. This is of great importance in microscopy, because the resolving power of the objective, i.e. the ability of the objective to visualize fine details of the specimen in the intermediate image, increases with its numerical aperture. Resolution is defined as the shortest distance  $d$  at which two narrowly spaced points on the specimen are still visualized as separate entities in the intermediate image. The resolution limit  $d$  depends only on the numerical aperture and the wavelength  $\lambda$  of the light used:  $d = 0.5 \lambda / N.A.$ .

It follows that, in order to resolve finest details, the specimen should be viewed with a high-power objective with large numerical aperture and under short-wavelength monochromatic light.

The numerical aperture of the objective, and hence its resolution, can be increased by filling the space between the front lens of the objective and the specimen with an immersion liquid of suitably high refractive index (oil;  $n \sim 1.56$ ). Thereby the refraction of light rays at the interface between the cover glass and oil is minimised, and a wider cone of light rays enters the objective (Fig. 1-4B).

For this purpose special objective systems with small focal length and short free working distance have been designed: oil-immersion objectives. While “dry” objectives operating in air do not have numerical apertures beyond 0.95 (the theoretical limit being N.A. = 1), aperture values up to 1.40 can be achieved with oil-immersion objectives, depending on the refractive index of the appropriate immersion liquid (water = 1.333; glycerine = 1.455; immersion oil = 1.515; methylene iodide = 1.744).

Specific properties of the objective such as magnification, numerical aperture, optical tube length, degree of aberration correction, and cover glass thickness are engraved on the outer objective barrel (Fig. 1-5, Table 1). Objectives designed for polarized-light microscopy consist of strain-free lens systems and are marked with the inscription P, PO, or Pol. Table 1 also gives the free working distance (FWD) between the specimen and the front lens of the objective for selected objectives of some major manufacturers.

### 1.2.2 Ocular (Eyepiece)

Fine structures in the intermediate image are only resolved by the human eye if they are viewed at visual angles  $>1'$ . Commonly, this requires a further magnification of the intermediate image by the ocular. The optimal resolution is achieved if the total magnification of the microscope is the numerical aperture of the objective multiplied by 500 to 1000:

$$M = M_O * M_L = 500 * \text{N.A.} \leftrightarrow 1000 * \text{N.A.}$$

If the total magnification lies below this range, finest structures in the intermediate image remain invisible. If it is higher, the intermediate image is magnified without any further gain in resolution (= empty magnification).

Modern oculars consist of two multi-lens components, the “eye lens” and the “field lens”, that correct optical aberrations of the ocular itself and eliminate residual aberrations of the intermediate image. A Periplan ocular, for example, contains seven lenses that are cemented into a single doublet, a single triplet, and two individual lenses. A fixed internal diaphragm is positioned in the focal plane of the ocular, between the “eye lens” and “field lens” components, in focus with the intermediate image, and defines the circular field of view.

For polarized-light microscopy, an ocular with exactly adjusted crosshairs (or a crossed micrometer disc) mounted on the fixed diaphragm not only provides the ‘N-S’ and ‘E-W’ reference directions for the vibration directions of the polarizer and analyzer, but also serves to measure angles (Ch. 2.1, 4.2.1). For measuring and counting objects in a thin section, glass discs with engraved linear and crossed micrometers or grids can be placed in the diaphragm plane. By adjusting the height of the eye lens, diaphragm and reticule are brought into focus with the intermediate image.

The specific properties of oculars are inscribed on their casing (Fig. 1-5, Table 1).

**Table 1.** Objectives and oculars of some renowned manufacturers

**I. Strain-free objectives for polarizing microscopy**

<b>Company</b>	<b>Designation</b>	<b>M</b>	<b>NA</b>	<b>FWD (mm)</b>	<b>Cover glass thickness</b>
<b>Leica</b>	Hi Plan Pol	4	0.10	26.2	-
	Hi Plan Pol	10	0.22	7.8	-
	Hi Plan Pol	20	0.40	0.9	0.17
	Hi Plan Pol	40	0.65	0.31	0.17
	Hi Plan Pol	63	0.75	0.31	0.17
<b>Nikon</b>	CFI Achromat P	4	0.10	30	-
	CFI Achromat P	10	0.25	6.1	-
	CFI Achromat P	20	0.40	3	0.17
	CFI Achromat P	40	0.65	0.65	0.17
<b>Zeiss</b>	A-Plan	2.5	0.06	9.4	-
	A-Plan	5	0.12	9.9	-
	A-Plan	10	0.25	4.4	-
	A-Plan	20	0.45	0.51	0.17
	A-Plan	40	0.65	0.43	0.17
<b>Olympus</b>	PLN4xP	4	0.10	18.5	-
	ACHN10xP	10	0.25	6	-
	ACHN20xP	20	0.40	3	0.17
	ACHN40xP	40	0.65	0.45	0.17

**II. Oculars**

<b>Company</b>	<b>Designation</b>	<b>Magnification</b>	<b>Field number (mm)</b>
<b>Leica</b>	Periplan	10	20
	Periplan crossed micrometer	10	20
<b>Nikon</b>	CFI	10	22
	CFI CM crossed micrometer	10	22
<b>Zeiss</b>	W-PL, focusable	10	23
<b>Olympus</b>	WHN10x	10	22
	WHN10x-H, focusable	10	22

Objective

Magnification 20x

Numerical aperture 0.40

Tube length  $\infty$

Cover glass 0.17mm thickness

Free working WD 3.9mm distance



Periplan-Ocular

Magnification 10x

Field number 20

Ocular for spectacle wearer

Reticule plate

**Figure 1-5.** Objective (Example: Nikon CFI Achromat 20x P) and ocular (Example: Leica Periplan with reticule plate)

### 1.2.3 Tube, objective and ocular

Objective and ocular are connected by a microscope tube. In older microscopes the tube has a specified length (Nikon, Olympus, Zeiss: 160 mm; Leitz: 170 mm) because the objectives project the real images onto a fixed plane. In modern microscopes the tube length can vary as infinity-corrected objectives are used. In such systems, the tube length is referred to as the reference focal length and ranges between 165 mm (Zeiss) and 200 mm (Leica, Nikon).

The ocular is inserted into the upper end of the tube. Two small slots at the tube edge ensure that the ocular position is fixed, with the crosshairs oriented either N-S and E-W or diagonally at 45° to these directions. To account for variable eyesight, the crosshairs can be focused by adjusting the height of the eye lens.

The objective is mounted at the lower end of the tube. The single-objective holders common in former petrographic microscopes are nowadays only used in reflected-light, interference and universal-stage microscopy. In modern microscopes, the objectives are mounted on a quadruple or quintuple revolving nosepiece (turret) accommodating 4 to 5 objectives of different magnification which can thus be quickly selected for observation (Fig. 1-6). A click-stop mechanism ensures an accurate position when changing objectives. When objectives of different magnification are used on the same object, it is desirable that the images remain focused. Thus, modern objectives have a fixed distance from the nosepiece objective mounting hole to the point of focus on the specimen (= parfocal distance; Leica, Zeiss: 45mm; Nikon: 60 mm).

## 1.3 Illumination

To be viewed with the microscope, the specimens, unless they fluoresce, must be illuminated. Opaque specimens (e.g. ore minerals, metals) are imaged with the proportion of light that is reflected from the specimen (reflected-light microscopy). Transparent or weakly absorbent specimens are observed using the light that passes through them (transmitted-light microscopy). The images reveal only those structures of the specimen where the colour and intensity of the transmitted light is modified through absorption, diffraction and reflection.

In older microscopes the illumination of a translucent specimen is achieved by directing the light from the sun or from a matted bulb via a planar or concave mirror and a subsequent focusing lens system (condenser) through the specimen.

In modern microscopes a built-in light source in the base of the microscope provides the specimen illumination. Commonly a 6V 20W halogen bulb is used with variable brightness control. The light emitted from the bulb is focused by a simple lens system (collector) and then directed via the condenser through the specimen (Fig. 1-7).

### 1.3.1 Aperture of illumination

A homogeneous illumination of the observed specimen area is essential for the quality of the microscopic image. Furthermore, in order to achieve optimal resolution, the cone of light rays passing through the specimen should have the largest possible opening angle (cf. Ch. 1.2.1, Aperture).

As a rule, the aperture of illumination should equate or be slightly less than the aperture of the objective. Larger apertures would cause a loss of contrast, smaller apertures a reduction of resolution. The aperture of illumination is adjusted with a diaphragm which is located below the condenser lenses (*iris diaphragm or aperture diaphragm*) (Fig. 1-7; Ch. 1.4.1). By closing the diaphragm, the illumination aperture is reduced, resulting in increased image contrast and depth of field. Opening the diaphragm increases the aperture of illumination and leads to a loss of image contrast.

### 1.3.2 Light field

Depending on their magnification, objectives cover specimen areas of different size (object field). To avoid blooming of the fine image details by lateral stray light, the diameter of the illuminating light bundle (light field) should not exceed the size of the viewed object field. The light field can be adjusted to the required size by a diaphragm which is located above the collector lens of the illuminator (*field diaphragm*) (Fig. 1-7; Ch. 1.4.1).

Illumination aperture and light field can also be modified by changing the focal length of the condenser. For this purpose, modern condensers are equipped with a swing-in auxiliary condensing lens which, when inserted, changes the system from long focal length (low aperture, large light field) to short focal length (high aperture, small light field size).

To achieve complete illumination of specimens when using objectives of low magnification (e.g.  $M = 1.25$ ), the front lens, and in some cases the entire condenser, must be removed from the substage assembly.

A number of particular condensers has been designed for application in special imaging techniques (phase contrast, interference, fluorescence and dark field microscopy).

To ensure optimum illumination and resolution of fine specimen structures, a special illumination method was introduced by A. Köhler in 1893, which is still the most widely used method of specimen illumination in transmitted-light microscopy (see Ch. 1.4).

### 1.3.3 Glass diffuser and filters

Built into the lamphouse of modern microscopes, a thermal filter absorbs the heat produced by the halogen lamp, and an opal glass then diffuses the emitted light, thereby improving the homogeneous illumination of the specimen.

Various filters are either housed in the base of the microscope or can be placed in a port above the field diaphragm. Commonly, a blue daylight filter serves to condition the light emitted from the artificial light source to the quality of sunlight. Neutral density filters are used to attenuate the intensity of light without changing its spectral composition. Monochromatic light which is needed for special measurements, such as the determination of refractive indexes with the immersion method, is usually generated by interference filters (dichroic filters).

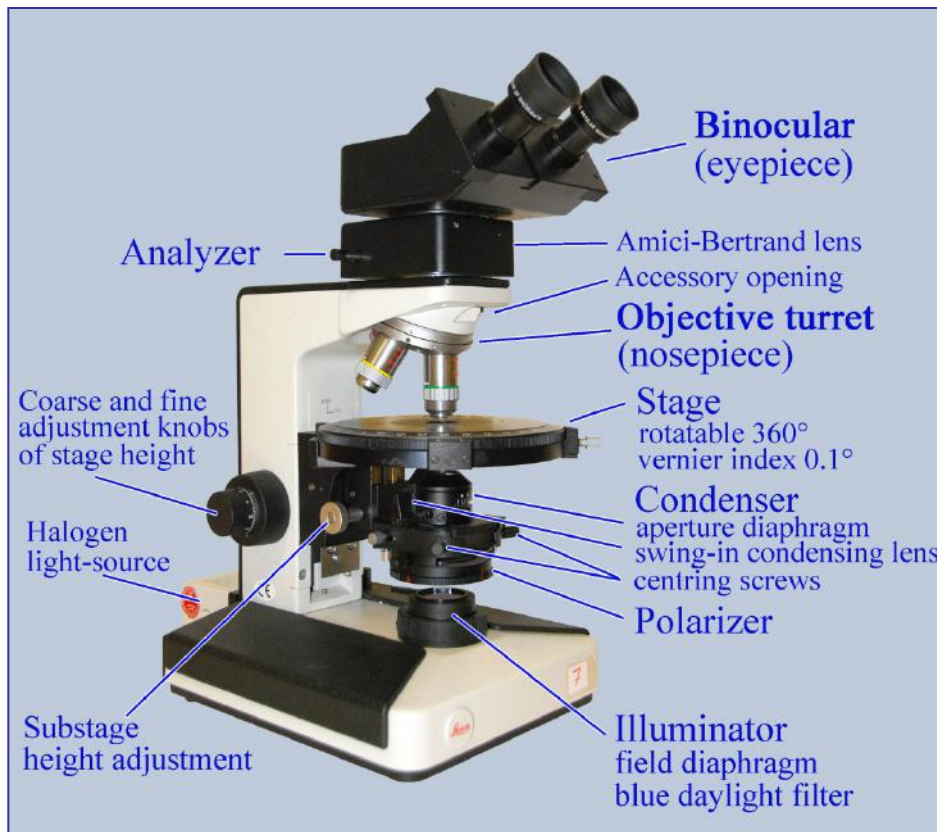


**Figure 1-6.** Design of polarized-light microscopes (Nikon Eclipse 50/Pol; Leica Laborlux 12 Pol)

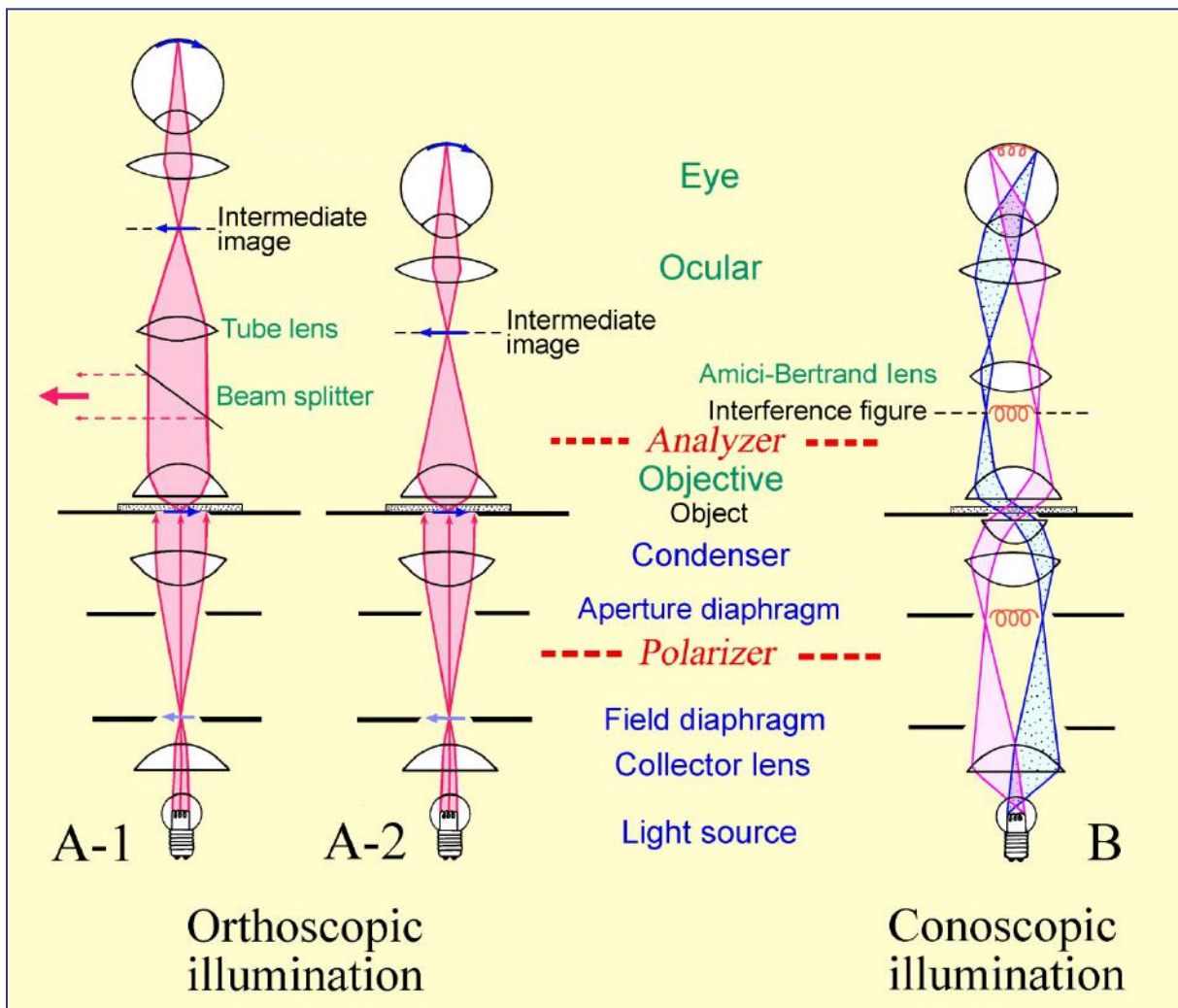


Figure 1-7. Orthoscopic and conoscopic ray paths in the microscope

**A: Orthoscopic illumination mode.** In finite tube-length microscopes, the objective produces a real inverted image (intermediate image) of the specimen which then is viewed with further enlargement through the ocular (A-2). In infinity-corrected microscopes, the objective projects the image of the specimen to infinity, and a second lens placed in the tube (tube lens) forms the intermediate image which then is viewed through the ocular (A-1). This imaging design allows to insert accessory components such as analyzer, compensators or beam splitters into the light path of parallel rays between the objective and the tube lens with only minor effects on the image quality.

**B: Conoscopic illumination mode.** Parallel rays of the light cone which illuminates the specimen create an image in the upper focal plane of the objective (B). In the case of anisotropic crystals, an interference image is generated which can be viewed as an enlargement by inserting an auxiliary lens (Amici-Bertrand lens). The interference image can also be directly observed in the tube through a pinhole which replaces the ocular.

## 1.4 Light paths in the microscope

### 1.4.1 Köhler illumination

The Köhler illumination is based on a specific geometry of light paths in the illuminating substage part of the microscope, and is achieved through a special arrangement of the light source, collector lens, field diaphragm, aperture diaphragm and condenser lens (Fig. 1-7). This special illumination mode ensures an even illumination of the viewed object field (light field) and further allows to independently adjust the illumination aperture and the size of the light field.

1. The collector lens projects an enlarged image of the light source (filament of the halogen lamp) onto the front focal plane of the condenser where the aperture diaphragm resides. As a result, the illuminating light beam is leaving the condenser as a light cone consisting of bundles of parallel rays (Fig. 1-7). The aperture of the illuminating cone can be modified by varying the aperture of the iris diaphragm. As each point in the object field receives light rays from each point of the filament of the halogen lamp, an even illumination of the entire object field is achieved. Further images of the light source (filament) are generated in the upper focal plane of the objective (resp. the tube lens) and the upper focal plane of the ocular.
2. The condenser lens projects an image of the field diaphragm onto the specimen plane, and hence, superposed images of both object and field diaphragm are generated by the objective in the intermediate image plane where they are jointly observed through the ocular. The size of the illuminated field of the specimen (light field) can be adjusted by varying the aperture of the field diaphragm without affecting the illumination aperture (Fig. 1-7).

The microscope alignment for Köhler illumination is described in Chapter 1.5.

The Köhler illumination allows to examine optically anisotropic minerals in two different modes:

### 1.4.2 Orthoscopic mode

The divergent light rays emanating from each point of a specimen are focused in the intermediate image plane, thereby creating the real image of the specimen (Fig. 1-7A).

In an optically anisotropic mineral, along each direction of the illuminating cone (Ch. 4.1) light waves with different velocity (birefringence; Ch. 4.2.3) and in part also different amplitude (absorption) pass through the grain. The light waves are superposed at each point of the object image. Therefore, the image of an individual mineral grain, when viewed under strongly convergent illumination, does not provide information on the optical behaviour in different directions of the mineral.

However, when the aperture of the illumination cone is reduced by closing down the aperture diaphragm, the optical phenomena observed in the intermediate image are dominated by the properties of light waves that pass through the mineral grain at right angle to the viewing plane: orthoscopic mode (Ch. 4). It follows that direction-dependent optical properties of an anisotropic mineral in thin section must be deduced from examining several grains cut in different crystallographic orientations.

### 1.4.3 Conoscopic mode

When a highly convergent light cone is generated (e.g. by inserting the condenser front lens into the light path), bundles of parallel light rays in a wide range of directions pass through the mineral grain. The parallel light rays are then focused in the rear focal plane of the objective, whereby rays with different tilt angles towards the microscope axis produce image points in different positions (Fig. 1-7B, Fig. 4-48).

This image therefore allows to examine the behaviour of light propagating along distinct crystallographic directions in a single grain: conoscopic mode. When viewed with crossed polarizers, characteristic interference figures are observed that reflect the symmetry and optical properties of the anisotropic mineral (Ch. 5).

The conoscopic interference figure only records those optical directions that are represented in the aperture cone (Ch. 1.2). In order to maximise the range of directions in a cone as wide as possible, the aperture of both objective and condenser must be large.

An enlarged interference image can be observed by inserting an auxiliary lens, the Amici-Bertrand lens, into the tube between analyzer and ocular (Fig. 1-7B). The interference image can be focused by adjusting the distance of the ocular to the Amici-Bertrand lens, provided the microscope allows such an adjustment. Some microscopes offer special devices for centring and focusing the Amici-Bertrand lens.

Alternatively, the interference figure can be directly viewed within the microscope tube after removing the ocular, or by looking through a pinhole which replaces the ocular. The image appears smaller and has better contrast compared to an interference figure observed through the Amici-Bertrand lens.

Practical guidance to the conoscopic imaging mode is given in Chapter 5, which also discusses the application of conoscopy to the identification of anisotropic minerals.

## 1.5 Centring the microscope

Apart from adjusting the substage illumination alignment according to Köhler, an optimal microscope performance requires that all optical components (light source, collector, condenser, objective, ocular) and the rotatable stage are aligned on a common central axis which coincides with the direction of the vertical light rays in the microscope. All components are centred to the axis of the rotating stage. The centring is done in three steps:

### A. Centring the objectives

The centre of the field of view, which corresponds to the lens axis of the objective, must be in alignment with the axis of the rotating stage. To check this, the thin section has to be put into focus, a minute grain or object in the sample is selected and shifted to the centre (Fig. 1-8, I). When rotating the microscope stage the following situations may occur:

- a) The particle remains stationary in its central position, indicating that the objective is precisely centred.

b) The particle is moving along a circular off-centre path (Fig. 1-8,II), indicating that the objective is not centred. The rotation axis of the image has to be shifted into the centre of the reticule. This is achieved by turning the two centering screws located in the objective casing or the nosepiece using the centring tools commonly provided with the microscope. Older microscopes may have centring rings on the objectives (and hence no special centring tools are required). The objectives are centred if the rotation centre of any circular particle path coincides with the crosshairs intersection. An alternative way of achieving this is to rotate the stage such that an observed particle is in the most distant off-centre position, 180° from its position at the crosshairs intersection. By turning the centring screws, the particle is then shifted half the distance towards the crosshairs intersection (Fig. 1-8,III).

To verify that the objective is precisely centred now, the particle is shifted into the crosshairs intersection by carefully moving the thin section. If the particle remains in its position when rotating the stage, the objective is centred (Fig. 1-8,IV). Otherwise, the centring procedure has to be repeated.

All the objectives on the nosepiece have to be centred this way. Should an objective of high magnification be already centred precisely, it is even easier to centre the lower-magnification objectives. A small grain or object is positioned in the crosshairs intersection using the high-magnification objective. Then the poorly centred objective is rotated into the optical path and the particle is moved to the crosshairs intersection using the centering devices.

Caution! It is important to ensure that the nosepiece is positioned correctly on the tube and the objective in use has clicked into place. Otherwise, centring can never be achieved (Ch. 1.7). Some microscopes (e.g., Olympus) have a stage that can be centred. The stage is then centred on a single fixed objective and has to be aligned first, with that particular objective in place, before the other objectives can be centred. Any attempt to centre the objectives with the stage being off-centre will result in a serious misalignment of the light path.

What applies to all microscopes: To avoid de-centring of the objectives, they must never be touched when changing magnification! Always grab the grooved rim of the nosepiece to change between objectives.

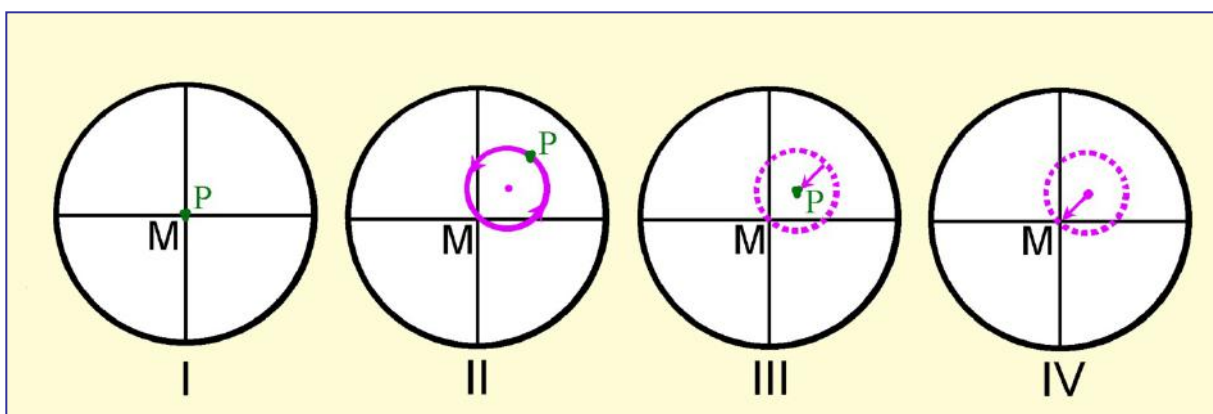


Figure 1-8. Centring the objective

## B. Centring the condenser for Köhler illumination

After focusing the thin section, the field diaphragm is closed, the front lens of the condenser inserted into the optical path, and the field diaphragm focused in the image plane by adjusting the substage height (Fig. 1-9 I→II). The following situations may be encountered:

- (a) The centre of the field diaphragm image coincides with the crosshairs intersection, i.e. the centre of the field of view, indicating that the condenser is perfectly centred (Fig. 1-9 III).
- (b) The field diaphragm image is offset with respect to the crosshairs. In this case, the field diaphragm image must be centred by turning the condenser-centring screws (Fig. 1-9 II→III).

Finally, in order to avoid glare by lateral stray light, the field diaphragm should be opened only slightly beyond the margin of the field of view (Fig. 1-9 IV).

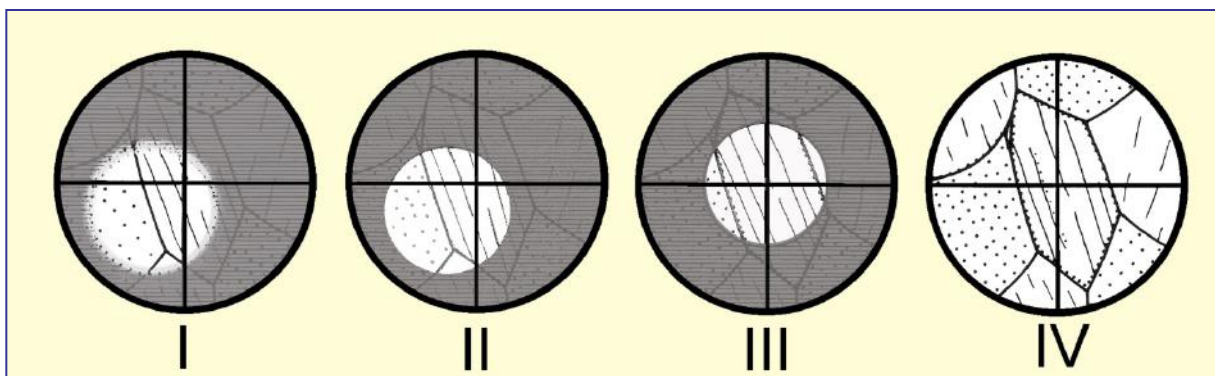


Figure 1-9. Centring the condenser

## C. Centring the light source

In modern microscopes, light source and collector are commonly integrated into the base of the microscope and thus need not be centred. In certain microscopes, centring bolts in the lamp case allow to centre the lamp socket. After the condenser has been centred, the lamp position is adjusted until the object field is evenly and brightly illuminated.

For precise Köhler illumination, the collector must be adjusted so that an image of the lamp filament is created in the plane of the aperture diaphragm of the condenser. This filament image can be made visible by putting tracing paper onto the aperture diaphragm. A further image of the filament is created in the upper focal plane of the objective which can be observed more conveniently in conoscopic mode.

Filament images can only be observed if frosted glass inserts are removed from the illumination path!

## D. Adjustment of the oculars

If a microscope is fitted with a binocular head, the eyepieces must be adjusted individually in order to obtain a focused image for both eyes, also after changing between different objectives. Furthermore, the oculars must be adjusted for the correct interpupillary distance, i.e. the distance between the eyes.

The oculars of infinity-corrected microscopes are adjusted as follows (whereby the ocular with the crosshairs should be placed in the right tube of the binocular):

- (1) Look through the oculars and close the left eye. The crosshairs in the right ocular is observed with the right eye and focused with the diopter adjustment ring on this ocular. Then the object image is focused by carefully adjusting the stage height with the fine adjustment knob.
- (2) Now close the right eye and observe the object image with the left eye through the left ocular, without adjusting the stage vertically. If the image is not properly focused, the adjustment must be made using the diopter adjustment ring on the left ocular.

When focusing the object image, it is important that both eyes are relaxed and focused to infinity.

## 1.6 Polarizer and analyzer

The **polarizer** (polarizing filter or nicol prism) resides below the condenser. It can be swung in and out of the light path, and in many microscopes it is possible to rotate the polarizer about a vertical axis. The light source emits waves that vibrate randomly in all possible planes. The polarizing filter used in modern microscopes consists of a stretched polyvinyl film which reduces the randomly vibrating light waves to waves of a single vibration direction (polarization plane). For simplicity, the term “pol-waves” is introduced here for the plane-polarized waves leaving the polarizer.

When passing through the thin section, the pol-waves may undergo diverse modifications (refraction, absorption, birefringence etc., Ch. 4.2). In order to detect and quantify such modifications, the polarization plane should correspond to an easily identifiable reference direction in the field of view. In modern microscopes, the reference direction for the lower polarizer is E-W, parallel to the “horizontal” crosshair. There are microscopes, however, where the orientation of the polarizers is different (lower polarizer N-S, analyzer E-W). Specific optical-microscopic phenomena relate directly to the polarizer orientation (such as pleochroism and relief change, where the vibration direction of the lower polarizer provides the reference direction in the field of view).

Therefore, apart from ensuring that the polarizers are aligned, the general orientation of the polarizers must be known to the operator before starting to work on thin sections. This routine check may be performed with a colored tourmaline crystal, whether as a loose grain or as a prismatic section in thin section. The maximum absorption will be observed if the c-axis is oriented perpendicular to the polarizer direction (Fig. 1-10). The same check can be done with biotite in sections roughly orthogonal to (001). Biotite is a common mineral in many rocks, and thus thin sections containing biotite should be easily available. Biotite in sections roughly orthogonal to (001) displays its prominent cleavage and shows its maximum absorption (i.e. deepest color) if its basal plane (001) or cleavage is sub-parallel to the lower polarizer direction (Fig. 1-10). Biotite should not be used for alignment, though, as it is monoclinic. The angles between its (001) plane and any of the crosshairs may be close to zero, but it can also deviate by as much as 10°, depending on composition.

In this guidebook, we generally assume that the lower polarizer is oriented E-W. In microscopes where it is N-S, a rotation of directions by 90° would apply to certain descriptions, sketches and photographs in chapters 4.2.1 and 4.2.3 (e.g., photomicrographs of Figs. 4-11 to 4-17, Figs. 4-22 to 4-26).

The **analyzer** (polarizing filter or nicol prism) is used to analyse the modifications the pol-waves have experienced in the thin section (Ch. 4.2). It is positioned between the objective and the ocular, and is either pushed or swung into the tube below the Amici-Bertrand lens. The polarization plane of the analyzer must be perpendicular to that of the lower polarizer (i.e., N-S if the lower polarizer direction is E-W).

Although microscopes should always be in proper working order, a routine check for alignment of polarizers and crosshairs should be performed if extinction positions are critical (e.g., when measuring extinction angles). This can be done by putting a strongly elongate mineral with well-developed, straight prism faces under crossed polarizers. Suitable are all minerals of orthorhombic or higher symmetry with interference colors of at least higher first order (e.g., sillimanite, orthoamphibole, tourmaline). If both polarizers and the ocular crosshairs are properly aligned, such crystals will be completely black when positioned exactly parallel to one of the crosshairs (Fig. 1-11). If polarizers are out of alignment, the procedures below can be followed to rectify the problem. The crosshairs in modern microscopes are mechanically fixed. Potential misalignment of the polarizers can occur either due to both polarizers being rotated with respect to the crosshairs (i.e., crystals as in Fig. 1-11 turn black under crossed polarizers, but there is an angle between the prism faces and the crosshairs), or the polarizers are not at precisely 90° to each other (i.e., the crystals will not turn completely black when rotated). The latter is more common as either of the two polarizers is in a fixed position in most standard-fitted microscopes. Hence, only one of the two can be easily adjusted. Nevertheless, the possibility remains that a fixed polarizing filter is misaligned in its casing.

**To align the polarization plane of the polarizer** (= vibration direction of the pol-wave) with the E-W thread of the crosshairs, a grain mount of fine, deeply coloured tourmaline needles can be used. These needles must lie exactly in the thin section plane, which is easier to achieve using loose grains than trying to find that orientation in a rock thin section. First, a tourmaline needle is aligned with its c-axis parallel to the N-S direction of the crosshairs and then the polarizer rotated until the needle shows maximum absorption (in the same way as shown in the thin section photograph of Fig. 1-10, left side). For this procedure, the analyzer is kept out of the light path.

**Explanation:** Tourmaline is a strongly dichroic mineral (dichroism, Ch. 4). Maximum absorption occurs perpendicular to the c-axis, i.e. in the vibration direction of the O-wave. **Caution!** Ensure that the adjusted position of the polarizer is not changed afterwards. If the microscope has a rotatable polarizer, the correct position can be marked on the holder or, if necessary, be fixed with adhesive tape.

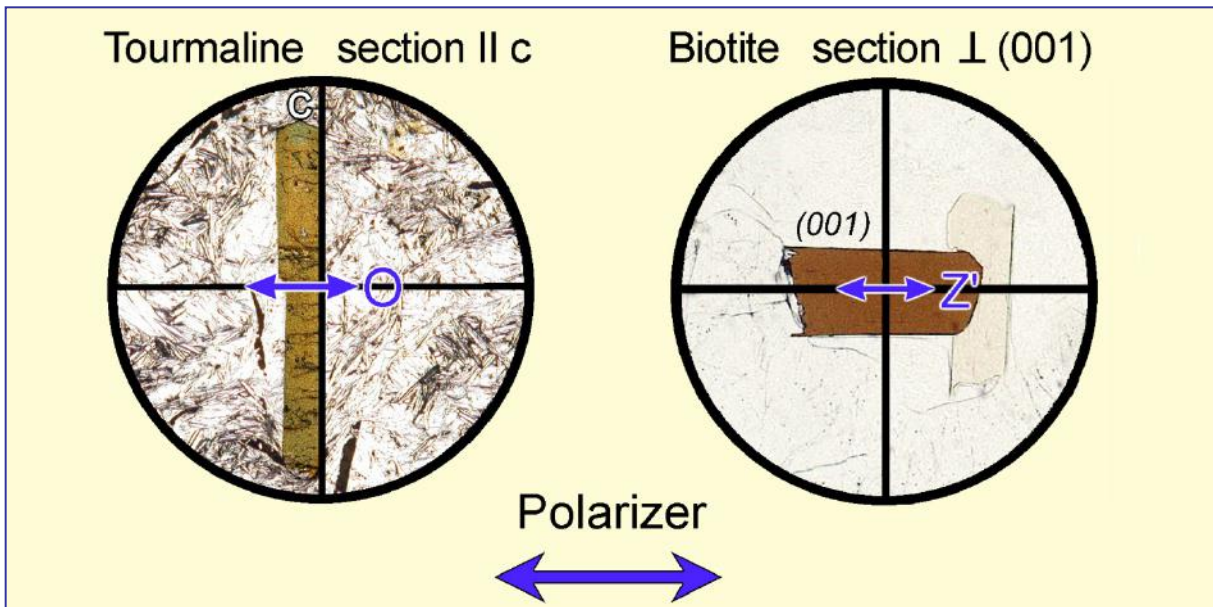


**Figure 1-10.** Routine check of lower polarizer orientation using tourmaline or biotite. In microscopes where the polarizer is oriented N-S, the directions of maximum absorption of the two minerals are rotated 90° with respect to the positions shown here.

Once the polarizer is properly oriented, ***the polarization plane of the analyzer is aligned*** with the N-S direction of the crosshairs. When inserting the analyzer into the light path (no specimen on the stage), the field of view should appear black if the polarization direction of the analyzer is oriented parallel N-S. If the field of view is not black, the analyzer must be adjusted. This adjustment can also be made using long-prismatic sections of minerals with orthorhombic or higher symmetry, as shown in Fig. 1-11. This set-up has the advantage that the precise alignment of the two polarizers and the crosshairs can be examined at the same time.

Rotatable analyzers allow to adjust the orientation of the polarization filter with a graduated spindle that can be locked after adjustment. In the more common swing-in or push-in analyzers, the correct position of the polarizing filter in the casing would have to be adjusted manually. As pointed out before, in many modern microscopes only one of the two polarizers can be adjusted while the orientation of either lower polarizer or analyzer is fixed.

If high-magnification objectives are used for observation (without any object in the light path!) and the aperture diaphragm is open, the field of view does not appear completely black under crossed polarizers. This is caused by a rotation of the E-W vibrating pol-waves at the strongly curved surfaces of the objective lenses. Under conoscopic illumination an interference image is observed which resembles the centred optic-axis interference figure of a weakly birefringent positive uniaxial crystal (Ch. 5).

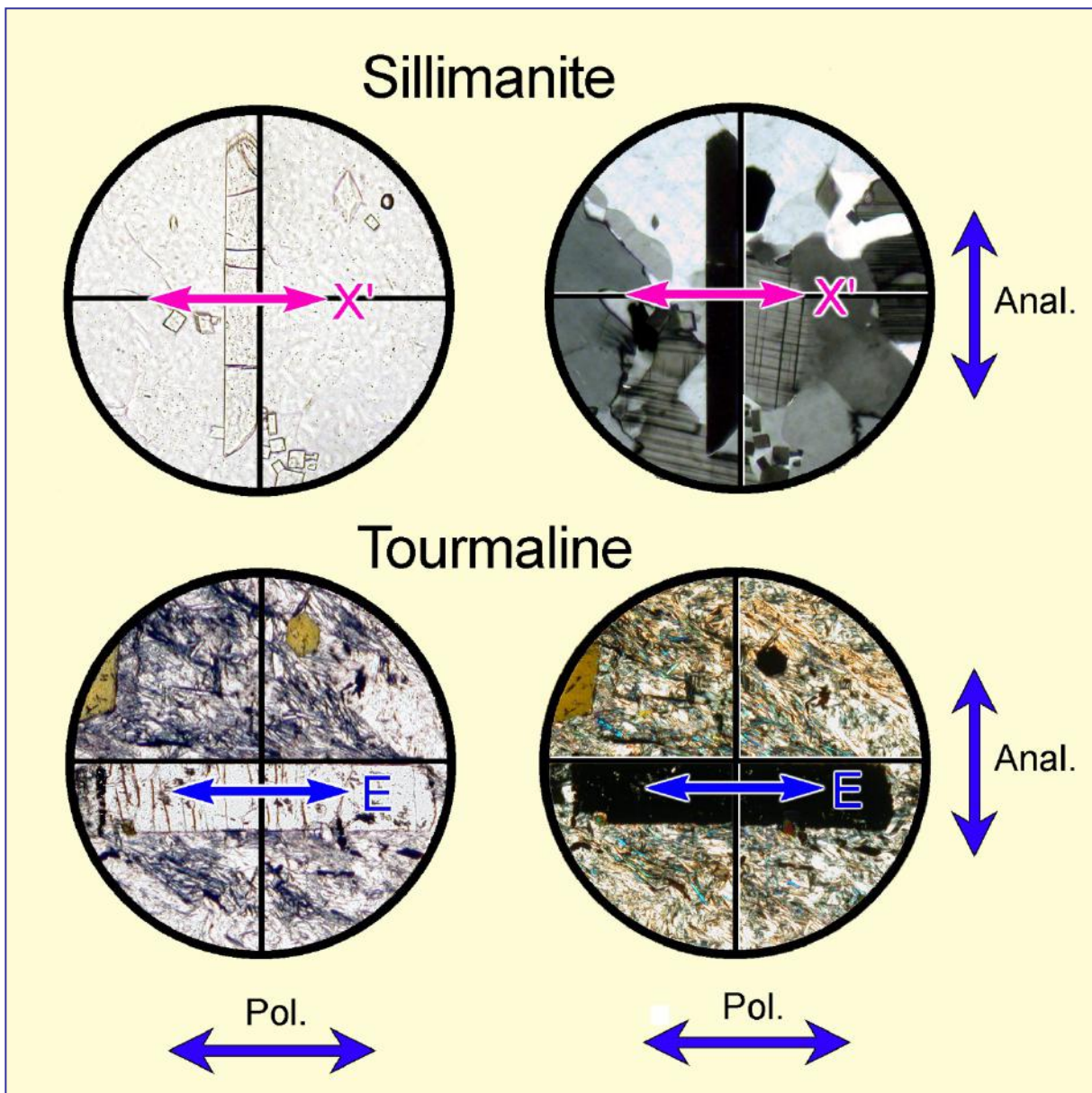


**Figure 1-11.** Testing the precise alignment of polarizer, analyzer and crosshairs with the help of prismatic sections of high-symmetry minerals.

If the angle between the extinction position and either of the crosshairs is exactly  $0^\circ$  (as seen here), all three elements are perfectly aligned. If the lower polarizer is correctly adjusted against the crosshairs, the analyzer can be adjusted such that the extinction position of the prismatic minerals corresponds with a parallel alignment of prism faces and crosshairs. Note that the orientation of the lower polarizer (E-W vs. N-S) cannot be checked under crossed polarizers.

## 1.7 Trouble-shooting

### 1.7.1 Optimising the image of the specimen

It is assumed that the microscope has been aligned for Köhler illumination (Ch. 1.5).

(1) If the thin section can be perfectly focused with low magnification objectives ( $M_O = 2.5$  to 10), but remains out of focus when objectives of higher magnification ( $M_O = 20, 40, 63$  etc.) are used, it should be checked whether the thin section is lying on its wrong side, i.e. with the cover glass down (see free working distance of objectives, Table 1).

(2) If the correctly placed thin section cannot be focused with high-magnification objectives, the cover glass is too thick and must be replaced by a cover glass of the standard thickness of 0.17 mm.

(3) Proper focusing may also be hampered by dusty surfaces of the optical components. The dust is best removed with a soft and completely grease-free brush.

(4) Indistinct and blurred images result when the front lenses of objectives and oculars are smudged with fingerprints resp. the grease of the eyelashes. In such cases it is advised to breathe on the lenses and then carefully clean them with a lens tissue or a lint-free paper tissue. Oily stains (e.g. by immersion liquids) are best removed with a cotton bud dipped in ether or ethyl alcohol. Solvents, however, should be applied with caution as the lenses are mounted in synthetic resins. To avoid fingerprints on the front lenses, objectives should always be changed with the fingers on the revolving turret, not on the objectives.

### 1.7.2 Eliminating poor illumination

The microscope alignment for Köhler illumination ensures a perfect, evenly illuminated field of view (Ch. 1.5). However, problems may still be encountered with the quality of illumination.

If the field of view is unevenly or not at all illuminated, although the light source is working and the field diaphragm illuminated, potential causes of such problems in the substage assembly are:

(a) The front lens of the condenser or an extra lens below the condenser have not been properly put into or out of the optical pathway. As a result, the lens mounts may partially or completely block the light beam.

(b) Filters are not correctly positioned.

(c) When using low-magnification objectives for observation, the field of view will be poorly illuminated if either the field diaphragm is closed down, the condenser is in a high position, or the front lens of the condenser is in the light path.

The sub-stage illumination is perfectly adjusted if the thin section, when viewed sideways from the top, shows an evenly and brightly illuminated round field which can be enlarged or reduced in size by opening or closing the field diaphragm.

If the image of the thin section remains imperfect when viewed through the oculars, the causes for poor illumination must be sought in the tube part of the microscope. The light path may be partially or completely blocked if:

(a) The revolving nosepiece was not properly mounted on the microscope stand or an objective has not clicked into place after a change of magnification.

- (b) An accessory plate has not been fully inserted into the tube.
- (c) The analyzer has not been fully inserted (swung-in) or removed (swung-out).
- (d) The Amici-Bertrand lens has been partially swung-in (out).
- (e) An accessory magnification lens (e.g. Optovar of the Zeiss Photomicroscope) has not properly clicked into position.

### 1.7.3 Sources of error in the crossed-polarizers mode

- (a) In a thin section of standard thickness ( $25\mu\text{m}$ ) quartz and feldspar grains show first-order grey-white interference colours. If instead brownish-white shades are observed, the polarizers are not precisely adjusted, i.e. their polarizing planes are not oriented perpendicular to one another. Hence, polarizer and analyzer must be adjusted following the instructions given in Ch. 1.6.
- (b) If the quartz and feldspars grains show blue-green and orange-red interference colours instead of the first-order grey-white colours, the first-order red plate ( $\lambda$ -plate) resides in the light path (cf. accessory plates, Ch. 4.2.4).
- (c) The crosshairs (or crossed micrometer) must be precisely oriented N-S and E-W. For this purpose the tube has two slots into which the notch on the ocular casing fits. These allow to fix the ocular with its crosshairs in the standard N-S–E-W orientation or, if needed, in a  $45^\circ$  diagonal orientation.

### 1.7.4 Microscope care and maintenance

The microscope should be kept in a dry laboratory and should not be exposed to direct sunlight. In humid climates, the laboratory should be air-conditioned.

To prevent the microscope from collecting dust, it must be under a suitable protective cover if not in use. Even if properly protected, dust will accumulate on the equipment eventually. Hence, the surfaces of the optically effective systems such as illumination set-up, filters, polarizer, condenser lenses and ocular need to be cleaned every few days with a soft brush. For longer periods of non-use, it is advisable to store microscopes in a cupboard.

When transporting microscopes they should be kept upright, such that filters or accessory plates that are not firmly attached cannot fall off and get potentially damaged. For longer transport, all these parts need to be removed. Furthermore, microscope manufacturers advise that the objectives should be taken off and stored separately, preferably in their original containers. It should be kept in mind that polarized-light microscopes are high-precision instruments, and any mishap during transport can seriously compromise the alignment of the optical systems. Thus, care must be taken that the microscope is safely secured. The storage cabinets previously supplied with each microscope have unfortunately become a thing of the past.

The bearings of the movable parts in the microscope are lubricated. The grease tends to become more viscous over time. Thus, the movable parts must be attended to by a trained precision mechanic in regular intervals. Although the lenses of modern microscopes are protected with anti-fungal coatings, the lens systems have to be cleaned regularly by a service person. Fungus growth can be a serious problem, particularly in tropical climates.

## 2. Measuring angles, lengths and thicknesses

### 2.1 Measurement of angles

The determination of an unknown mineral or the determination of the composition of a solid solution may require measuring an angle between two specific linear or planar features. Such features include crystal faces, cleavage planes, twin planes and vibration directions.

With the help of angles between cleavage sets, pyroxenes can be distinguished from amphiboles, for example. Of even greater importance is the determination of angles between mineral planes and optical vibration directions (Ch. 4.2.4).

Angles are determined using a polarized-light microscope with a  $360^\circ$  scale on the rotating stage. Furthermore, a reference direction is required which is provided by the crosshairs in the ocular. A prerequisite for a precise measurement is exact centring of the microscope and the use of a higher-magnification objective with a small depth of field. For the determination of angles between cleavage sets, the analyzer should be out of the light path.

Ideally the angle between cleavage planes, crystal faces etc. is measured on a grain or a grain domain where both planes are parallel to the viewing direction. If the thin section is defocused, whereby the aperture diaphragm is partially closed to obtain a sufficiently high contrast, fringes of equal brightness appear on both sides of the traces of such planes and migrate outwards in a symmetric fashion. Such an ideal grain orientation is rarely realised in thin section, though, and it is sufficient to find grains in which the traces of the cleavage planes appear as thin dark lines.

For measurement, the thin section is oriented, either by hand or using a mechanical stage, such that the intersection of the traces of the planes is in the centre of the crosshairs. By rotating the stage it can be tested whether the intersection remains centred. If it moves off-centre the objective will need to be centred. While rotating the stage avoid pressing against it unnecessarily.

Next, cleavage set 1 is rotated such that it lies parallel to the N-S thread of the crosshairs. Then, the angle I is read from the vernier at the stage edge (Fig. 2-1, left). Now the microscope stage is rotated until the cleavage set 2 is parallel to the N-S thread of the crosshairs, and angle II is read from the vernier (Fig. 2-1, right). The difference between I and II is the angle in question.

Note: If the  $360^\circ$  mark is crossed during the procedure, the two partial angles have to be added up.

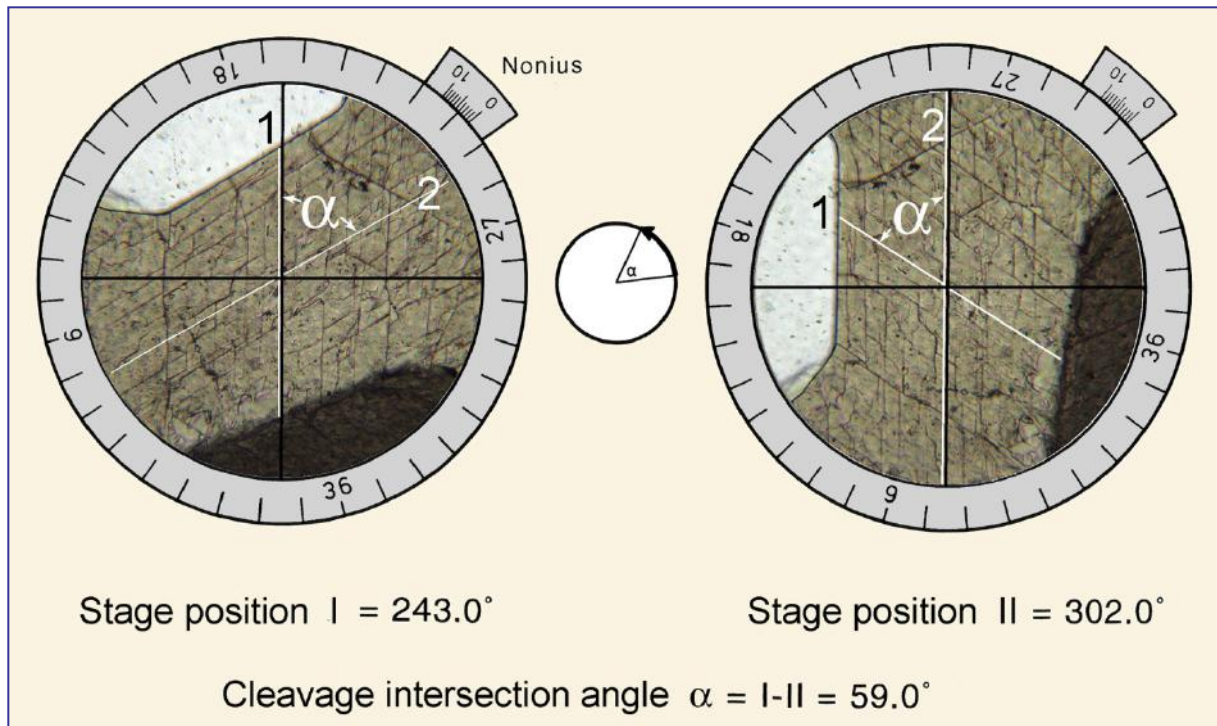


**Figure 2-1.** Measurement of the angle  $\alpha$  between two cleavage sets

The following may contribute to measuring errors:

1. Mechanical tolerance of the stage
2. Precision in reading the scale on the stage
3. Precision in placing the traces of planes parallel to one of the crosshairs
4. Precision in finding the exact extinction position, if angles are measured towards vibration directions
5. Quality of the planar elements used and their traces in the mineral grain

Assuming careful positioning of the traces of the planes and care in reading the scale, the cause of the largest error commonly relates to a badly defined cleavage. Particularly minerals with cleavage classified as poor or merely distinct may show cleavage traces that are either not exactly planar, or stepped, or too short. Furthermore, the cleavage may be bent due to deformation or it may host secondary minerals. During preparation, holes may form as mineral fragments break out along cleavages, or careful grinding may lead to very few cleavage planes opening up and becoming visible. Twin planes may also not follow the ideal crystallographic directions exactly.

A common problem is to find a grain of ideal crystallographic orientation in a thin section (the intersection line between two sets of planes being exactly vertical), and this may indeed prove to be impossible in certain cases. When using a grain with a slightly inclined orientation an error of a few degrees must be taken into consideration.

## 2.2 Measurement of lengths

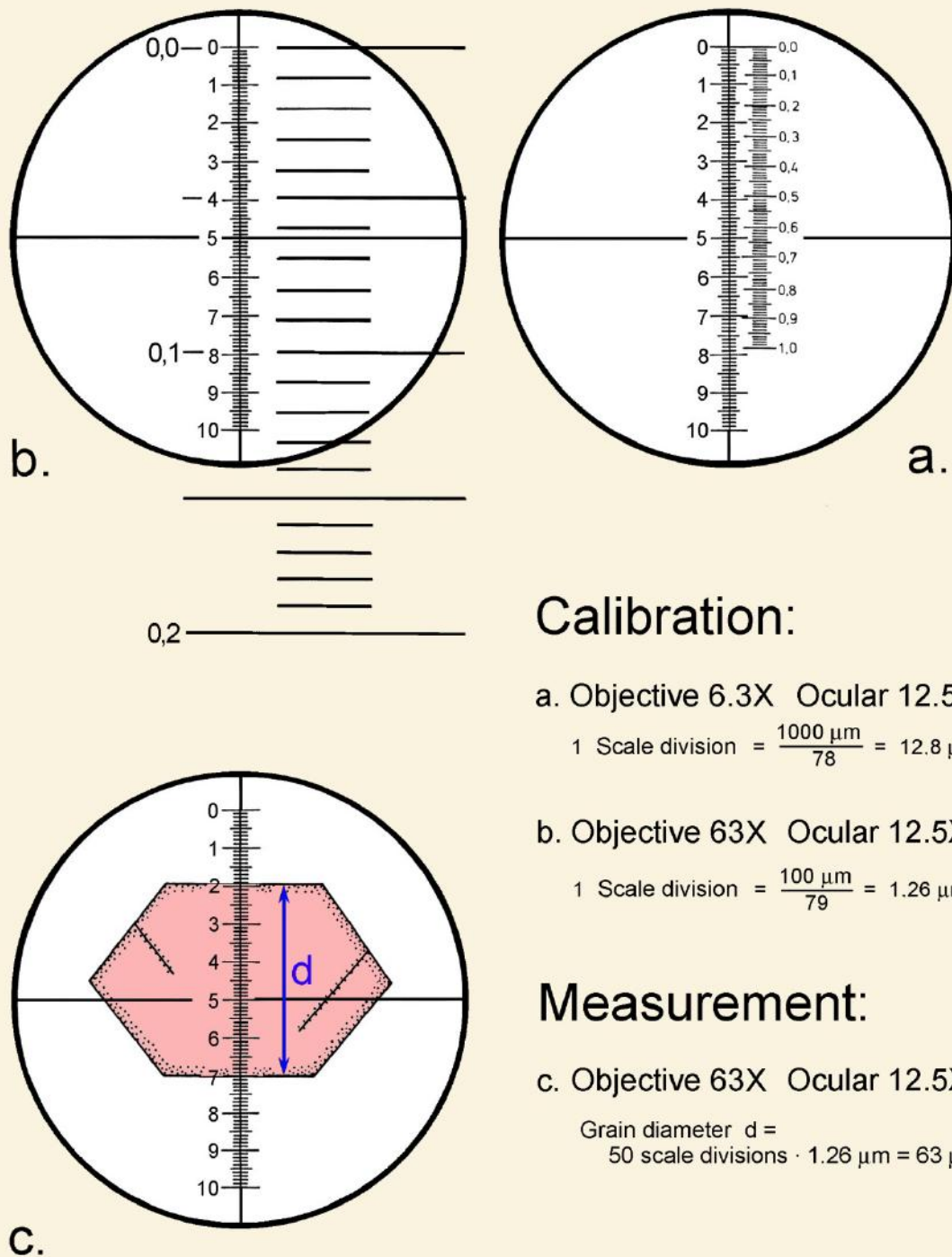
The measuring of distances is necessary for the determination of grain size, length-width ratios etc. For such measurements oculars are used that have a graticule (ocular micrometer) which must be calibrated. The graticule is commonly combined with the ocular crosshairs as a horizontally or vertically oriented scale attached to the E-W or N-S threads of the crosshairs, respectively (Fig. 2-2).

If objectives with increasing magnification are used, the image increases in size correspondingly. Therefore, the calibration of the graduations on the ocular scale must be carried out for each ocular-objective combination separately. The engraved magnification numbers on the objectives are only approximate values which would make a calibration based purely on calculations too imprecise.

For calibration, a specific scale is used, called an object micrometer, with a graduation of 10  $\mu\text{m}$  per mark; 100 graduation marks add up to 1 mm. The object micrometer is put in a central stage position and, after focusing, is placed parallel and adjacent to the ocular scale (Fig. 2-2). In example (a) 100 graduation marks of the object micrometer, adding up to 1000  $\mu\text{m}$ , correspond to 78 graduation marks on the ocular micrometer. At this magnification (objective 6.3x; ocular 12.5x) the distance between two graduation marks in the ocular is 1000  $\mu\text{m}$  divided by 78. The interval is therefore 12.8  $\mu\text{m}$ . Example (b) is valid for another combination (objective 63x; ocular 12.5x).

If, for example, a grain diameter needs to be determined, the number of graduation marks representing the grain diameter are counted and then multiplied by the calibration value for the particular objective-ocular combination (Fig. 2-2c).

The *total error* of the described procedure is a complex accumulated value. Both the object micrometer used for calibration and the ocular micrometer have a certain tolerance range. Errors occur with strongly magnifying lens systems because the image is not entirely planar, but has distortions in the peripheral domains. The largest error is commonly made by the human eye when comparing object and graduation. For increased accuracy it is important to use an objective with the highest possible magnification, such that the mineral grain covers a large part of the ocular scale.



## Calibration:

a. Objective 6.3X Ocular 12.5X

$$1 \text{ Scale division} = \frac{1000 \mu\text{m}}{78} = 12.8 \mu\text{m}$$

b. Objective 63X Ocular 12.5X

$$1 \text{ Scale division} = \frac{100 \mu\text{m}}{79} = 1.26 \mu\text{m}$$

## Measurement:

c. Objective 63X Ocular 12.5X

$$\begin{aligned} \text{Grain diameter } d &= \\ 50 \text{ scale divisions} \cdot 1.26 \mu\text{m} &= 63 \mu\text{m} \end{aligned}$$

**Figure 2-2.** Calibration of the ocular micrometer and measurement of distances

## 2.3 Determination of thin section thickness

The birefringence of anisotropic minerals can be determined in approximation by comparing the interference colours to those of the Michel-Lévy or Raith-Sørensen interference colour charts (Ch. 4.2.3), or it can be done precisely using the compensation method. For both methods the thickness of the mineral in thin section must be known. Commonly, the thin section thickness is standardised to 25 resp. 30 µm. Abundant minerals such as quartz and feldspar would then show an interference colour of first-order grey to white. If these minerals are not present in the thin section, thickness is difficult to estimate for the inexperienced. In such a case, the thickness can be determined via the vertical travel of the microscope stage.

For focusing the image, microscopes are equipped with focusing knobs for coarse and fine adjustment. The instruction manuals supplied by the manufacturers contain information on the vertical travel per graduation mark. This value is 2 µm for many microscopes.

For measuring the thickness, an objective with high magnification and small depth of field (40x or 63x) is chosen and the surface of the cover slip is put into focus. This surface can be recognised by the presence of dust particles. The inexperienced user may put a fingerprint onto the surface! Now the fine adjustment is turned in the appropriate direction to decrease the distance between sample and objective. Eventually, the focus plane has passed the cover slip, and the interface between the embedding medium and the minerals appears. This is recognised by the surface roughness and the grinding marks on the thin section. Reducing the distance between sample and microscope stage further, the lower surface of the thin section with all its uneven features comes into focus. The path through the thin section can also be followed along cleavage planes and inclusions. Inexperienced users should repeat this procedure a couple of times and maybe make notes about, and cross-check, the positions of the various boundary surfaces using the scale at the focusing knobs.

For a precise determination of thickness using the upper and lower boundary surfaces of the thin section, it is necessary to turn the focal adjustment in one direction only, eliminating the mechanical backlash. If the thickness from the lower to the upper surface is measured, the starting position of the focal plane must be in the 1 mm thick glass slide. If moving in the reverse sense, the starting position must be in the 0.17 mm thick cover glass above the mineral surface.

The number of graduation marks by which the fine adjustment is turned in order to shift the focus from the lower to the upper boundary surface (or in the reverse direction) multiplied by the value given per graduation mark (e.g., 2 µm) results in a vertical travel distance  $h$  in µm. However, this distance is commonly not the true thickness of the section.



Due to light refraction against air, both boundary surfaces of the mineral in the thin section are not observed in their true position. The apparent position of the lower surface is influenced further by the refractive index of the mineral (Fig. 2-3, top).

The thickness is thus:  $d = n_{\text{crystal}} / n_{\text{air}} * \Delta h$

whereby  $\Delta h$ , the vertical distance, is measured in number of graduation marks. The refraction index of the mineral should be known at least to the first decimal, which can be easily estimated.

For quartz, an example could be:  $d = 1.55/1.00 * 8.5$

If one graduation mark corresponds to  $2 \mu\text{m}$ , the result for the thin section thickness is:

$$d = 1.55/1.00 * 8.5 * 2 \mu\text{m} = 26.35 \mu\text{m}.$$

### Calibration of travel

If the vertical travel is not known or maybe modified from extensive use of the microscope, it has to be calibrated. To this end, a cover glass is broken in two, and the thickness of the glass is determined near the broken edge with a micrometer tool. Such devices are available in every mechanical workshop. The cover glass fragment is then put onto a glass slide, with the fracture in the centre of view. Depending on the orientation of the fracture surface, there are two ways of calibration which should lead to the same result (Fig. 2-3a,b):

a)  $d = \Delta h$

b)  $n = n_{\text{glass}} \sim 1.5;$   $d = \Delta h * 1.5$  (see above)

If the thickness of the cover glass measured with the micrometer tool was  $168.4 \mu\text{m}$ , and the travel was 67.3, respectively 44.9, graduation marks, the calibration value per graduation mark would be

in case a)  $168.4 \mu\text{m} / 67.3 = 2.5 \mu\text{m};$

in case b)  $168.4 \mu\text{m} / 44.9 / 1.5 (n_{\text{glass}}) = 2.5 \mu\text{m}.$

The *calibration error* can have a number of sources. Mechanical tolerances of the micrometer and the microscope are normally small in comparison to observational errors in determining the different positions of the boundary surfaces. This error may be established from a series of measurements.

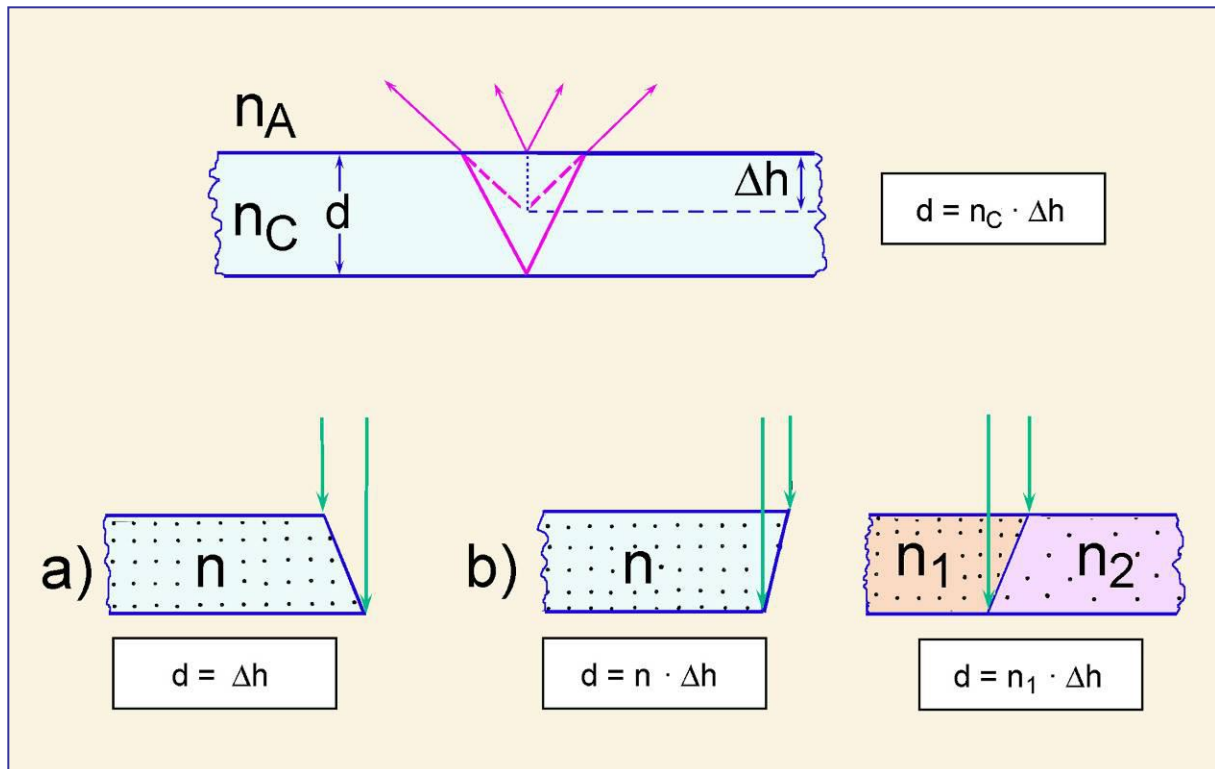


Figure 2-3. Calibration of vertical travel and measurement of thickness

### 3. Morphological properties

#### 3.1 Grain shape and symmetry

Natural minerals as well as synthetic crystalline phases show a considerable variety of crystal forms. The symmetry of the "outer" crystal form of a specific mineral species is an expression of the symmetry of the "inner" atomic structure. According to their symmetry characteristics all known crystalline phases can be assigned to one of the seven groups of symmetry (= crystal systems) (Fig. 3-1).

**Combination of crystal faces:** Depending on growth conditions, a mineral species can occur in different crystal forms through combinations of different crystal faces. Fig. 3-2 shows examples of the variety of crystal forms of natural occurring olivine and augite.

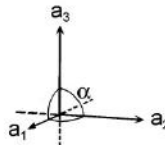
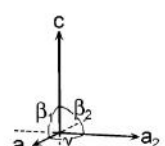
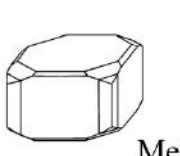
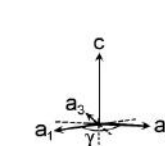
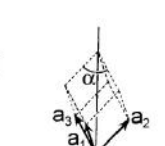
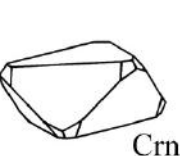
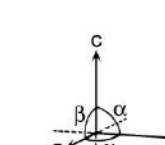
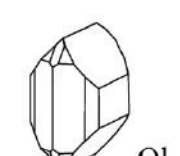
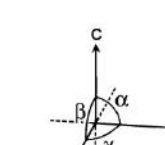
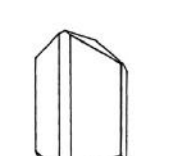
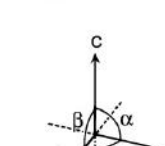
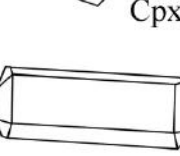
**Habit:** Crystals may also have different proportions, even if they have the same crystal faces developed. That means they differ in the relative size of crystal faces to each other. Figure 3-3 shows crystals of different habit using the examples spinel, garnet, sodalite and leucite (all equant), melilite, mica (flaky, platy to short-columnar) and clinopyroxene and amphibole (acicular, prismatic).

**Crystal form:** Euhedral crystals, which are crystals completely bound by rational crystal faces reflect unobstructed growth (such as crystallisation in a melt, Fig. 3-4, or in amygdales, caverns, pores etc.), or they form if a particular mineral has the tendency to impose its crystal shape and faces onto the adjacent, "weaker" ones (crystalloblastic series; Fig. 3-4).

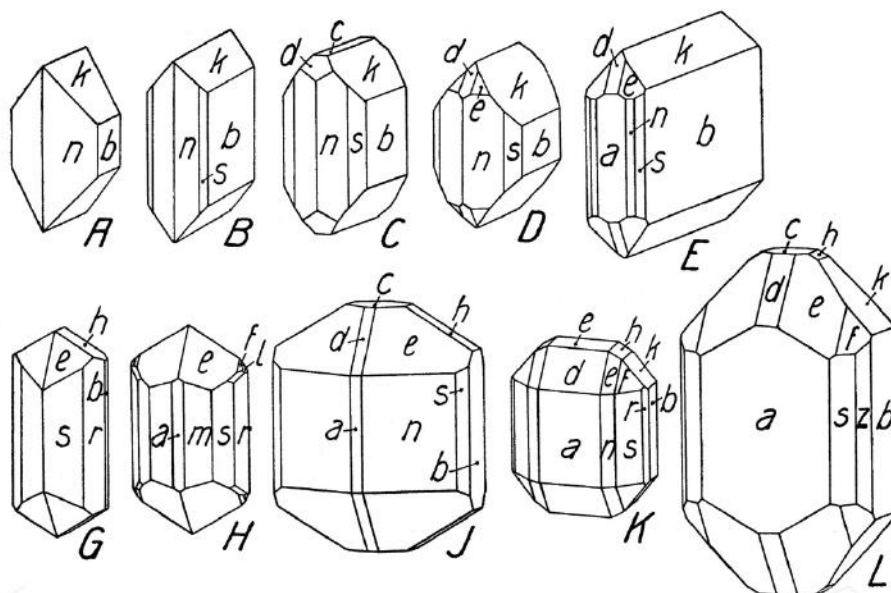
Subhedral and anhedral grain shapes are observed if the mineral's characteristic shape could only develop partly (Fig. 3-5), or not at all, if thermally induced annealing creates polycrystalline grain aggregates (Fig. 3-6), or if dissolution or melting processes lead to a "rounding" of crystal edges.

Fast crystallization from a melt can produce skeletal crystals or hollow shapes (Fig. 3-7). Minute feathery, dendritic or acicular crystals grow in undercooled melt (glass) (Fig. 3-8).

In the two-dimensional thin section image, the 3-D crystal shape of a mineral species has to be deduced from the outlines of the different crystal cross-sections (Fig. 3-9). For the rock-forming minerals, the schematic crystal drawings in the tables of Tröger et al. (1979) may be used as a reference. Fig. 3-10 shows the correlation between crystal shape and crystal sections for a member of the clinopyroxene group.

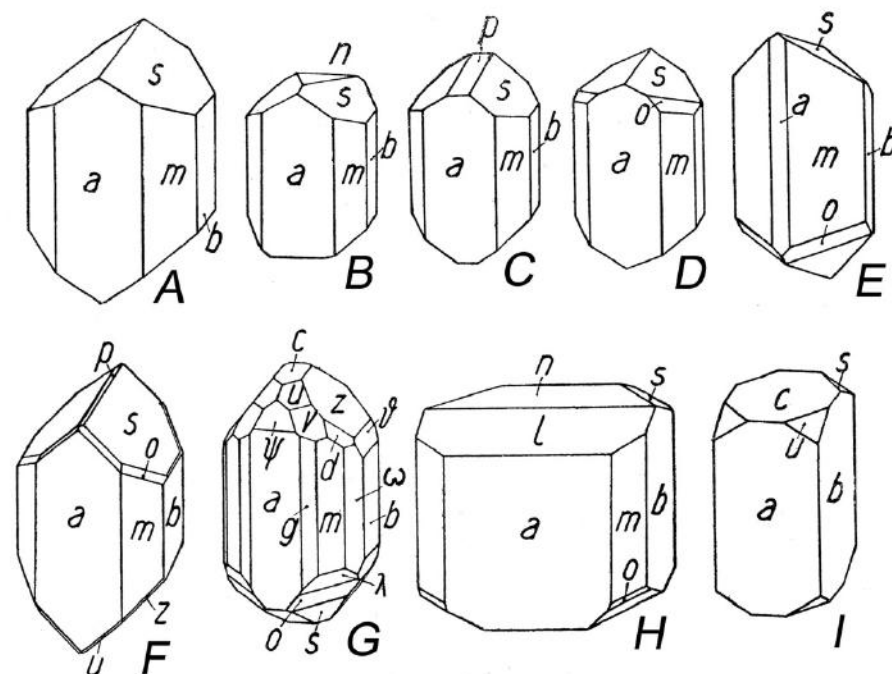
<b>Cubic</b> $a_1 = a_2 = a_3$ $\alpha_1 = \alpha_2 = \alpha_3 = 90^\circ$			garnet, spinel, sodalite, leucite, fluorite, periclase
<b>Tetragonal</b> $a_1 = a_2 \neq c$ $\gamma = \beta_1 = \beta_2 = 90^\circ$			melilite, scapolite, zircon, rutile
<b>Hexagonal</b> $a_1 = a_2 = a_3 \neq c$ $\alpha = \beta = 90^\circ; \gamma = 120^\circ$			nepheline, $\beta$ -quartz, apatite, beryl
<b>Trigonal Rhombohedral</b> $a_1 = a_2 = a_3$ $\alpha_1 = \alpha_2 = \alpha_3 \neq 90^\circ$			$\alpha$ -quartz, carbonates, corundum, tourmaline
<b>Orthorhombic</b> $a \neq b \neq c$ $\alpha = \beta = \gamma = 90^\circ$			olivine, orthopyroxene, anthophyllite, gedrite, sillimanite, andalusite, staurolite, zoisite, anhydrite
<b>Monoclinic</b> $a \neq b \neq c$ $\alpha = \gamma = 90^\circ; \beta \neq 90^\circ$			clinopyroxene, clinoamphibole micas, sanidine, epidote, sapphirine, titanite, gypsum
<b>Triclinic</b> $a \neq b \neq c$ $\alpha \neq \beta \neq \gamma \neq 90^\circ$			plagioclase, microcline, wollastonite, kyanite

**Figure 3-1.** Crystal systems



$a=\{100\}$   $m\{210\}$   $s\{120\}$   $r\{130\}$   $z\{140\}$   $b\{010\}$   $i\{041\}$   $k\{021\}$   $h\{011\}$   $c\{001\}$   
 $d\{101\}$   $e\{111\}$   $f\{121\}$   $l\{131\}$

Crystal forms of olivine-group minerals (A-L) (Niggli, 1927; Fig. 5)



$a=\{100\}$   $f\{310\}$   $g\{210\}$   $m\{110\}$   $i\{130\}$   $b\{010\}$   $δ\{061\}$   $x\{041\}$   $z\{021\}$   $s\{011\}$   
 $c\{001\}$   $l\{103\}$   $ψ\{121\}$   $p\{-011\}$   $n\{-102\}$   $λ\{-331\}$   $o\{-221\}$   $w\{331\}$   $v\{221\}$   $u\{111\}$   
 $d\{131\}$

Crystal forms of augite (A-I) (Niggli, 1927; Fig. 16)

Figure 3-2. Variety of crystal forms shown by single mineral species through combinations of different crystal faces, as seen in augite and olivine

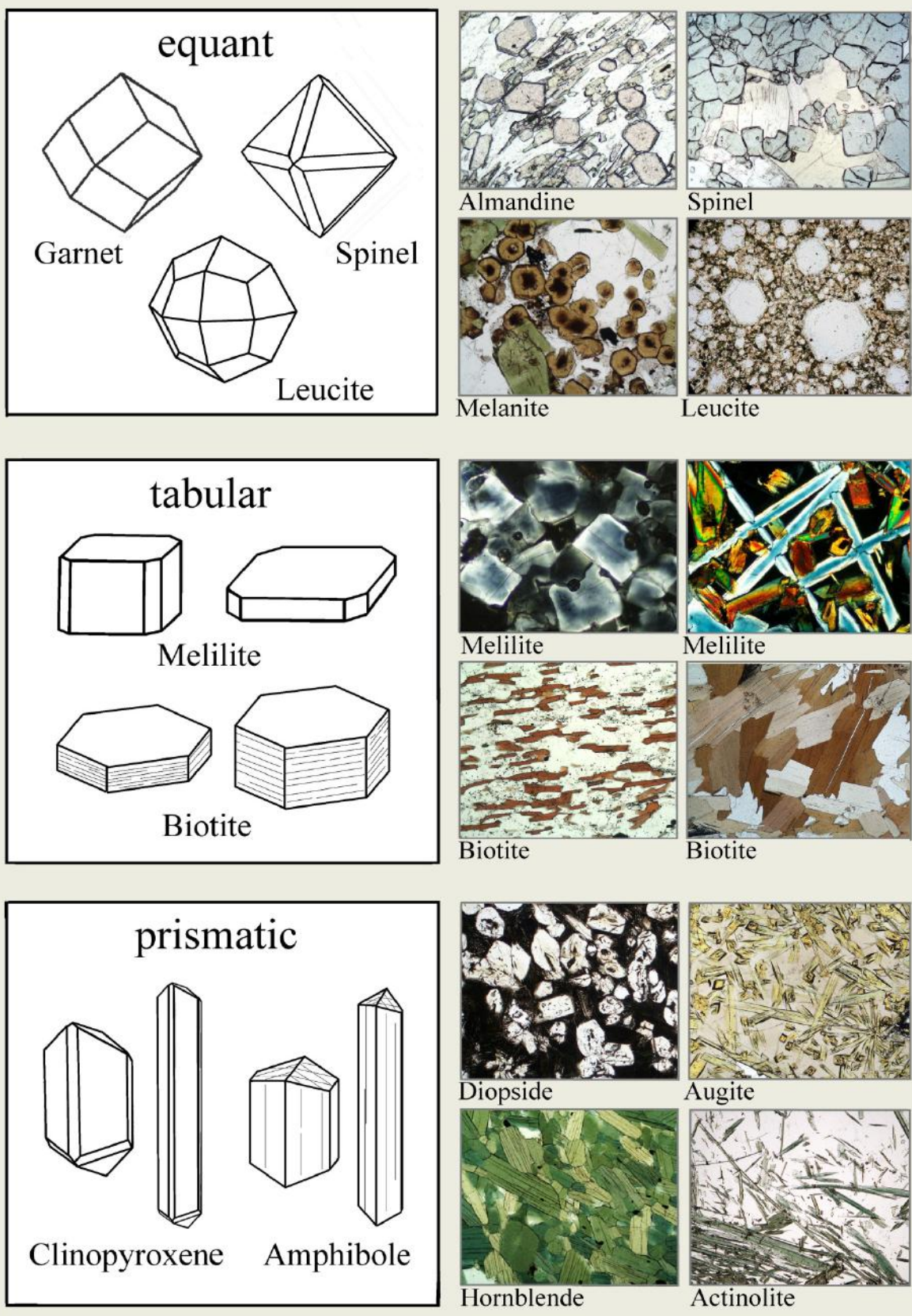


**Figure 3-3.** Habit of crystals

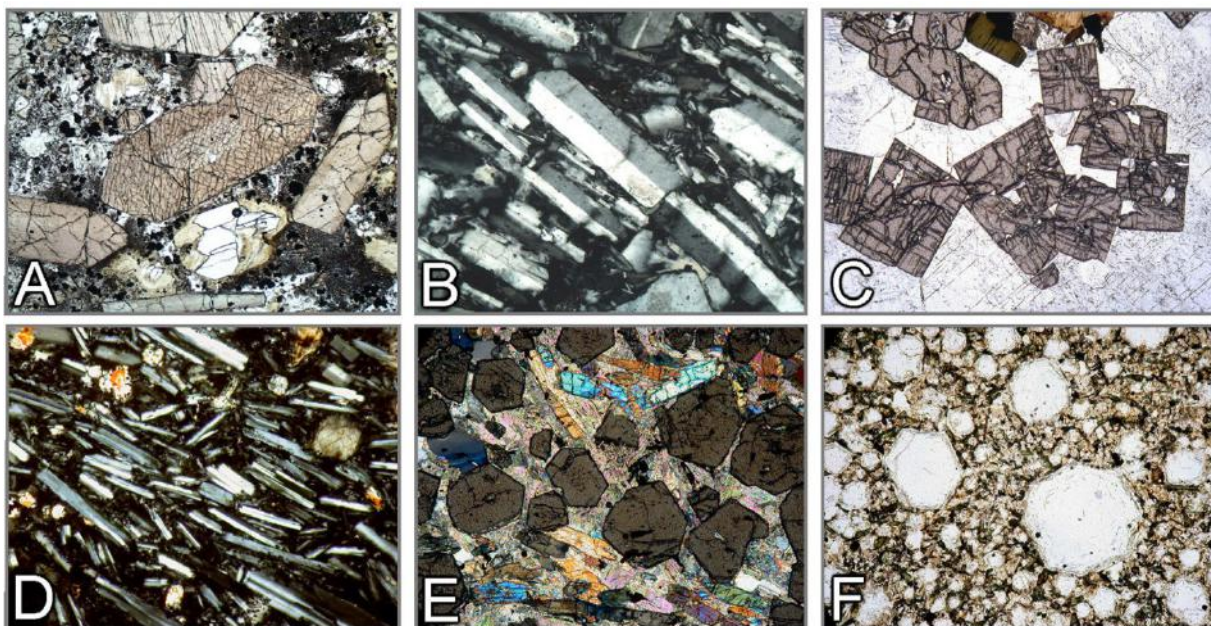


**Figure 3-4.** Euhedral grain shape

A: Augite (basalt). B: Sanidine (trachyte). C: Zircon (syenite pegmatite). D: Plagioclase (basalt). E: Garnet (garnet-kyanite micaschist). F: Leucite (foide).



**Figure 3-5.** Subhedral grain shape

A: Amphibolite. B: Biotite-muscovite schist; C: Olivine in basalt.

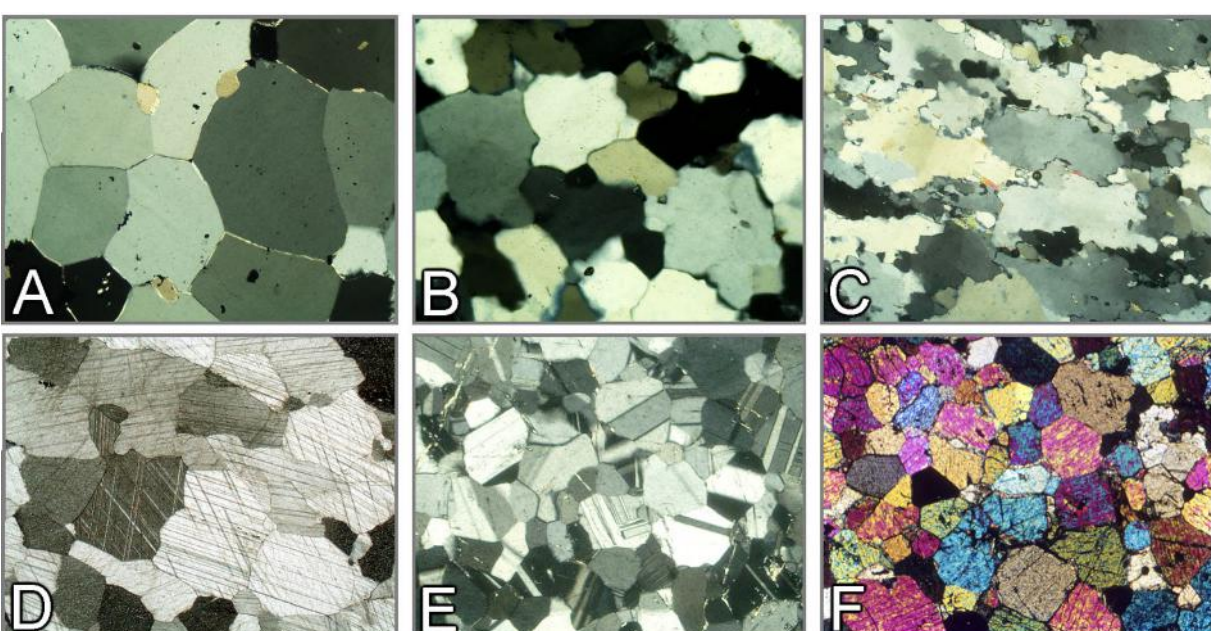


**Figure 3-6.** Anhedral grain shape

Granoblastic textures of quartzite (A to C), marble (D), anorthositic gabbro (E) and fayalite fels (F).

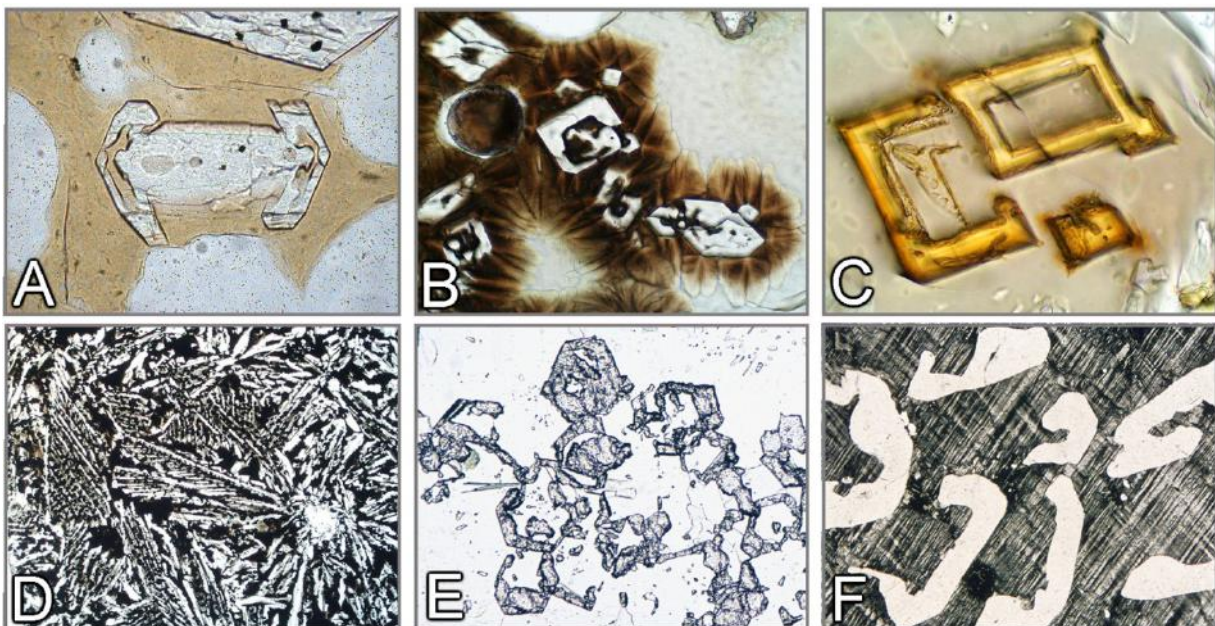


**Figure 3-7.** Skeletal crystal shapes

A: Olivine (basalt). B, C, D: Diopside, ferriclinopyroxene and kirschsteinite (slags). E: Atoll garnet (gneiss). F: Quartz in microcline (graphic granite).

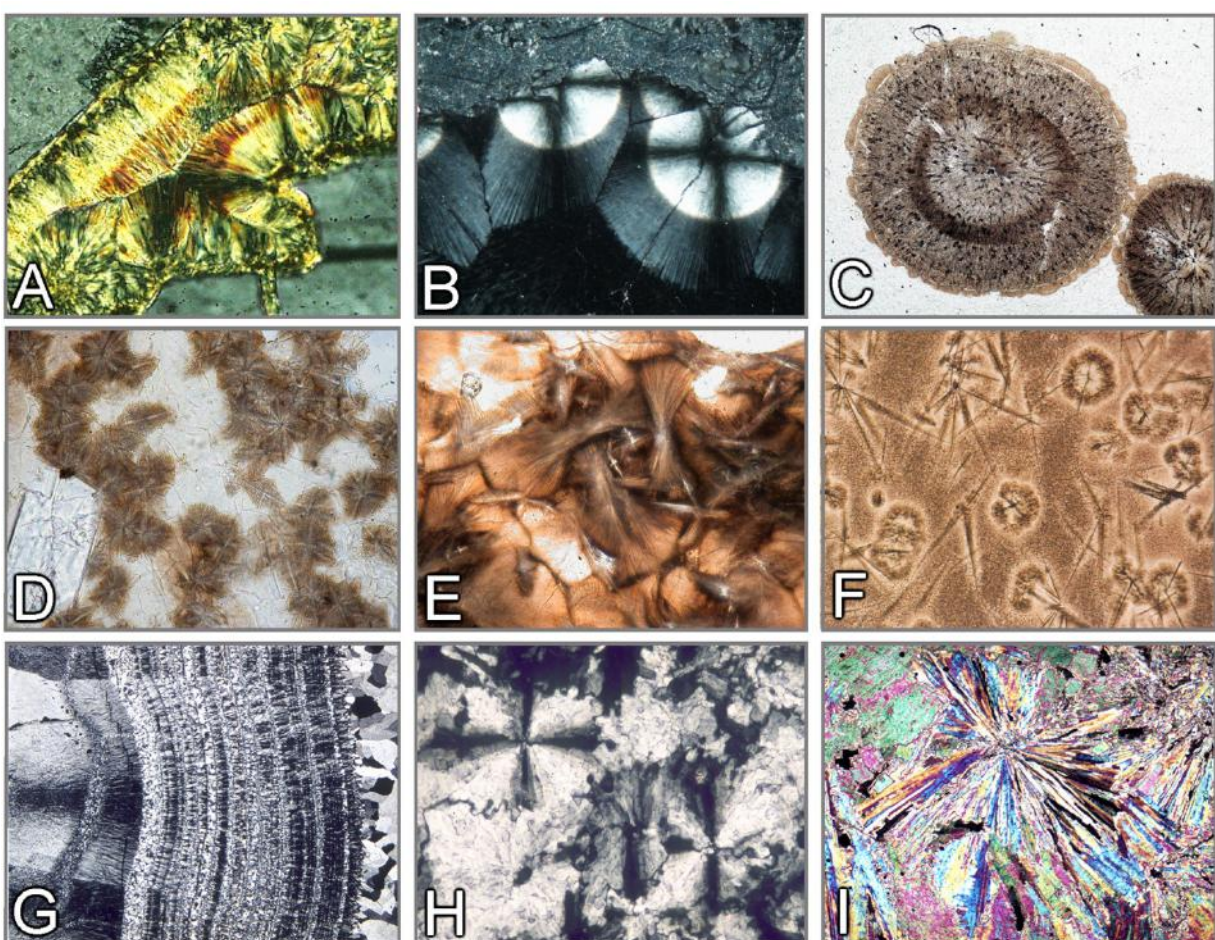


**Figure 3-8.** Spherulitic, dendritic and radiating crystals

A: Chlorite spherulites (charnockite). B: Spherules of radiating zeolite showing Brewster crosses (limburgite; +Pol). C: Spherules (obsidian, Lipari). D: Dendritic devitrification domains (basalt). E: Fan-shaped spherulitic devitrification (obsidian, Arran). F: Microlites with dendritic, fan-shaped devitrification domains (obsidian, Arran). G: Chalcedony (agate). H: Baryte rosettes with Brewster crosses. I: Anhydrite rosette (anhydrite, Zechstein).

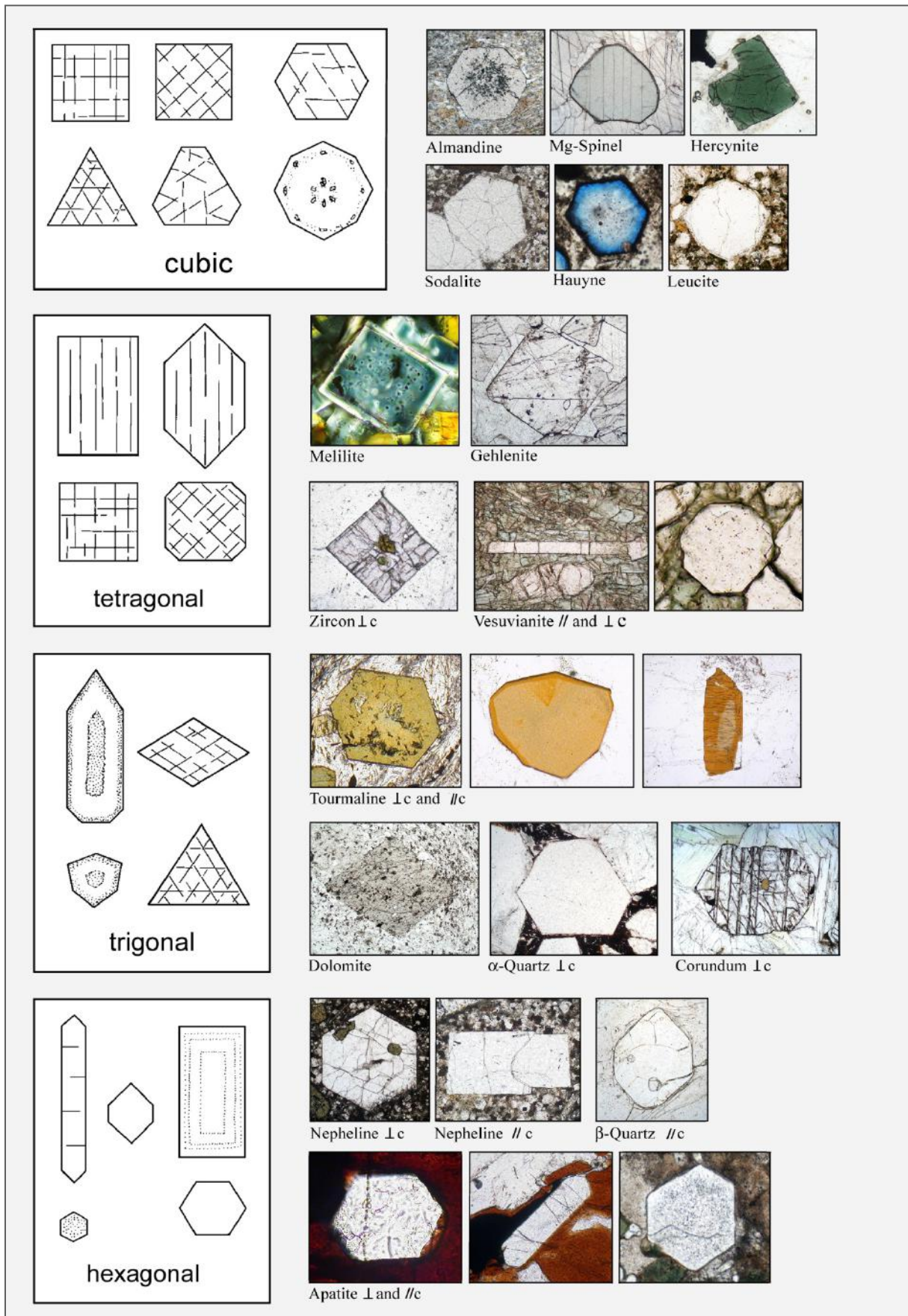


Figure 3-9. Sections of euhedral crystals

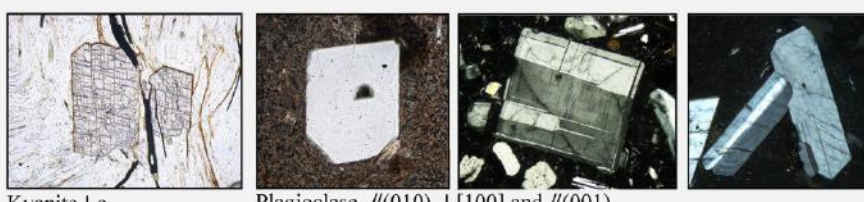
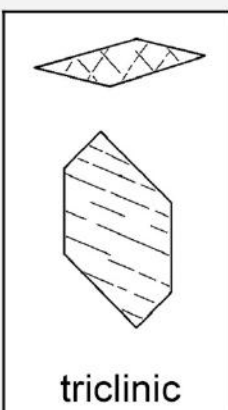
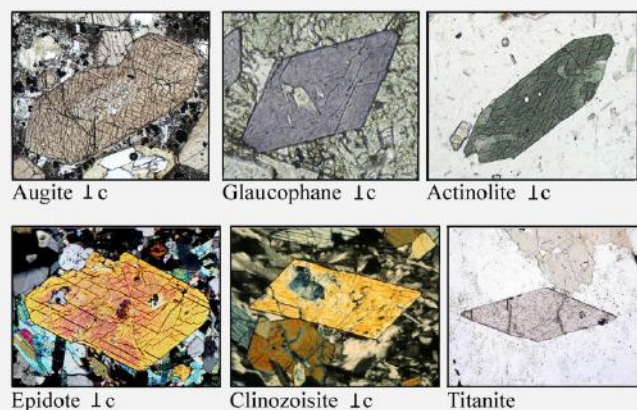
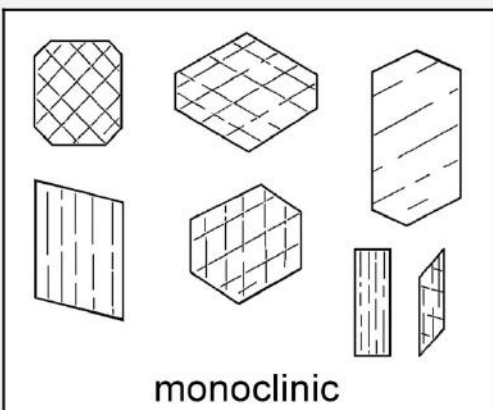
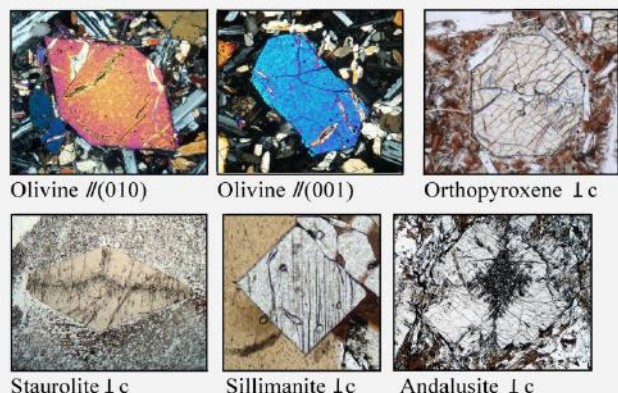
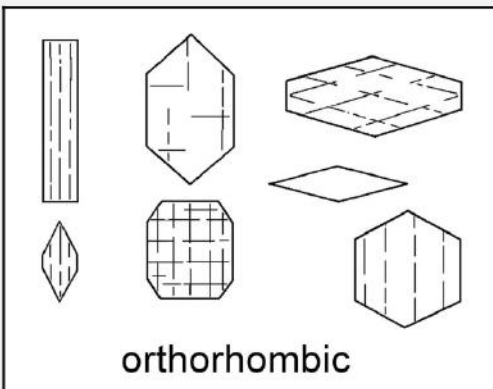
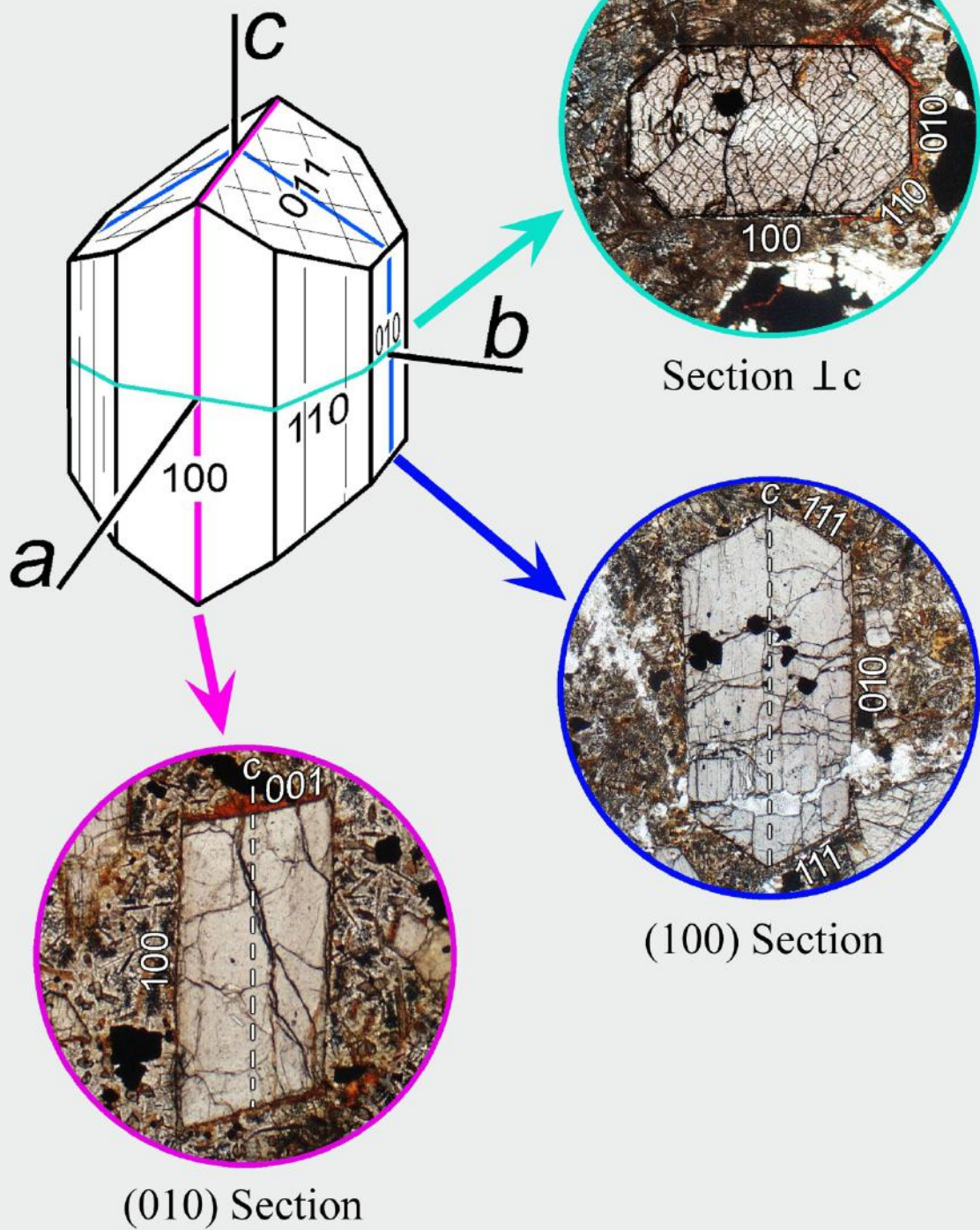


Figure 3-9 contd.. Sections of euhedral crystals

# Titanaugite



**Figure 3-10.** Relation between crystal form and cross-sections using the example of clino-pyroxene (titanaugite). Plane-polarized light

### 3.2 Cleavage, fracture, deformation and recrystallization phenomena

#### Cleavage

Many minerals split preferentially along one or more directions. This is called cleavage. Through the application of mechanical force - whether related to geological processes or to thin section preparation - crystallographically defined planar fractures can be generated in mineral grains. The abundance and quality of cleavage are mineral-specific, but also depend on the level of mechanical stress the mineral grains were subjected to. Cleavage follows crystallographic planes that are characterized by weak bonding and thus reflects a specific crystal structure. Examples are sheet silicates with their prominent basal cleavage and chain silicates showing two prismatic cleavage sets, but no basal cleavage (Fig. 3-11 A-C). It is quite common that cleavage planes have an orientation parallel to dominant crystal faces (Fig. 3-11 A-D,F). However, this cannot be generalized (Fig. 3-11 E).

In mineral cross-sections cleavage is recognised as – in the ideal case – straight traces of planes dissecting the grain. If the cleavage planes are oriented parallel to the viewing direction they appear as thin dark lines. With increasing tilt of the cleavage planes the lines broaden and the traces appear increasingly blurry. If the cleavage orientation is at a small angle to thin section plane, cleavage traces may not be observed.

Cleavage, and also the absence of cleavage (e.g., quartz, staurolite), is an important morphological property for mineral identification. The number of cleavage sets and the specific angles between them can be distinctive for mineral species and also entire mineral groups (pyroxenes, amphiboles, etc.). It should be noted that the often cited cleavage angles that are critical for specific

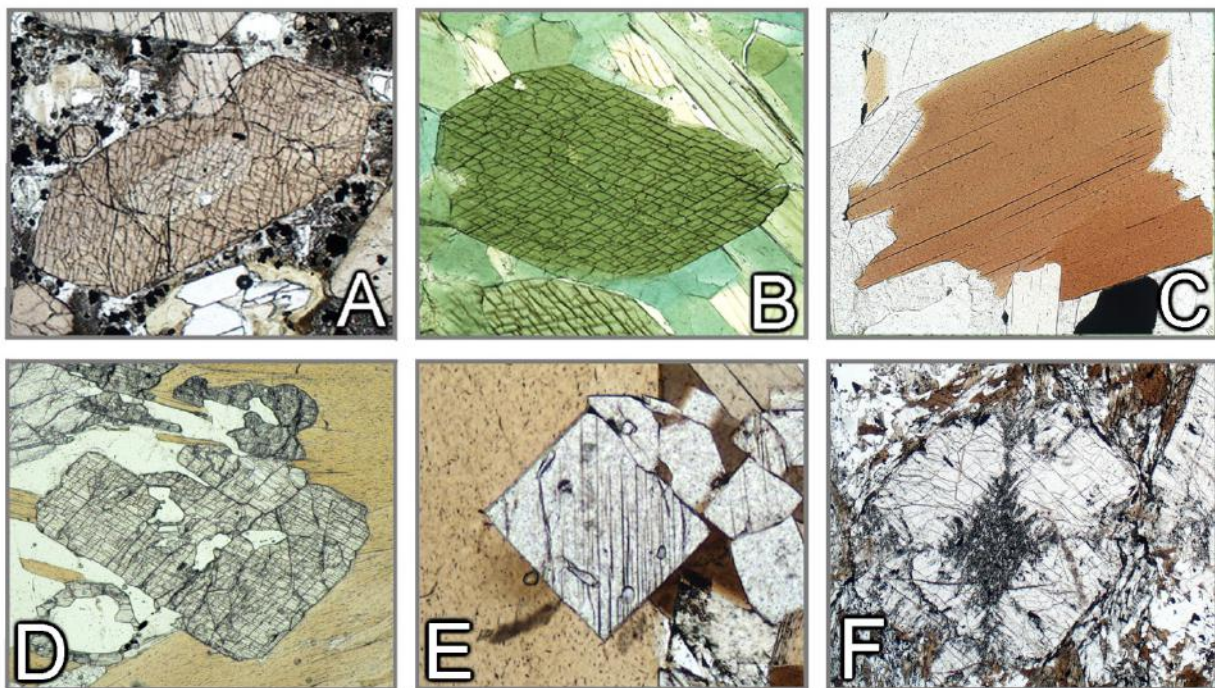


**Figure 3-11. Cleavage**

A: Augite– Section orthogonal to the c axis. The {110} cleavage planes form angles of  $87^\circ$  and  $93^\circ$ . B: Hornblende– Section orthogonal to the c axis. The {110} cleavage planes form angles of  $56^\circ$  and  $124^\circ$ . C: Biotite– Section orthogonal to the perfect cleavage (001).

D: Kyanite– Section approximately orthogonal to c shows the typical pattern of very good cleavage (100) and distinct cleavage (010). E: Sillimanite– The section orthogonal to c shows the good cleavage (010). F: Andalusite– Section orthogonal to the c axis. The good {110} cleavage planes intersect at almost right angles.

minerals can only be observed in appropriate sections (Fig. 3-11 A,B). Once the common axis between two cleavage sets is tilted, the angles of the cleavage traces do no longer correspond to those between the respective planes. For prismatic cleavage sets this common axis is normally c.

Thus, cleavage can also provide clues to the orientation of mineral grains in thin section. For example, amphibole crystals in basal sections (about orthogonal to c) show two intersecting cleavage sets, whereas prismatic sections (parallel to c) show apparently one cleavage only (Figs. 3-11 B, 4-15 – 4-17). Factually, these parallel cleavage traces derive from the two intersecting {110} sets which cannot be readily distinguished in prismatic sections. In other words, the arrangement of cleavage traces in amphiboles (as well as pyroxenes) can be used to identify basal and prismatic sections, in combination with other criteria such as birefringence and, if the minerals are coloured, pleochroism.

## Fracture

Many minerals show poor cleavage only or no cleavage at all. If exposed to external mechanical stress or internal stress during rapid cooling such mineral grains develop irregular fractures. These may still have a preferred orientation (Fig. 3-12).

Cleavage and fracturing are dependent on grain size. Minerals forming small grains commonly show neither cleavage nor fracture.

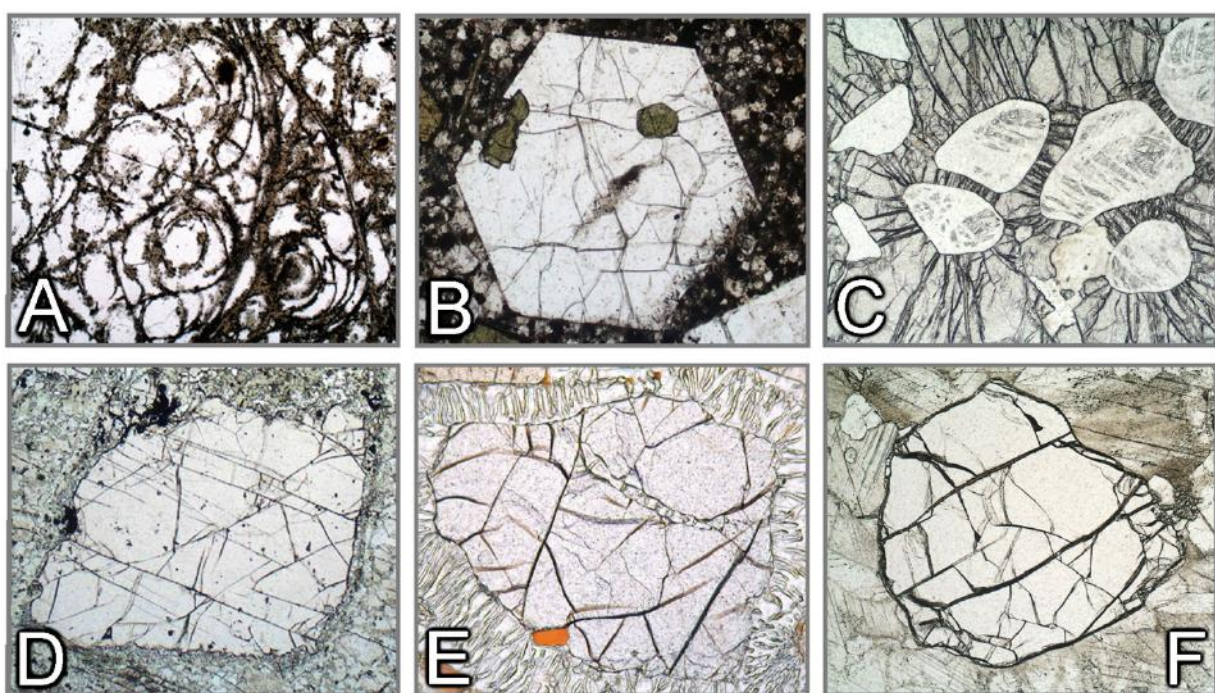


**Figure 3-12.** Fracture

A: Perlite— Due to quenching of the glassy material (obsidian) concentrically curved tension cracks developed.  
 B: Nepheline— Irregular tension cracks caused by rapid cooling. C: Pyrope— Radial cracks emanating from coesite inclusions now largely transformed to quartz. The cause of the fracturing is the volume increase from the coesite-quartz transformation, resulting in increased pressure imposed on the garnet host.

D: Garnet— Fracture planes oriented parallel to narrow-spaced jointing in a basic granulite. E: Garnet— Irregular cracks predating the resorption by orthopyroxene+cordierite symplectite. F: Olivine— The irregular cracks document brittle behaviour of the forsterite grain during plastic deformation of the calcite matrix.

## Deformation and recrystallization

Minerals in metamorphic rocks respond in different ways to tectonic stress, depending on prevailing temperature conditions, deformation rates, level of differential stress and presence or absence of fluids. Generally speaking, minerals at low temperatures tend to show brittle behaviour, whereas they deform plastically at high temperature. The temperatures of the transition between brittle and plastic behaviour are mineral-specific (about 300°C for quartz, 400-500°C for feldspars, at deformation rates that are typical for orogenic processes).

Figure 3-13 shows typical microstructures produced through brittle deformation at low temperature. At the brittle-ductile transition, mineral grains may show features of both brittle (fracturing, cataclasis) and plastic behaviour (undulose extinction, kinking, bending).

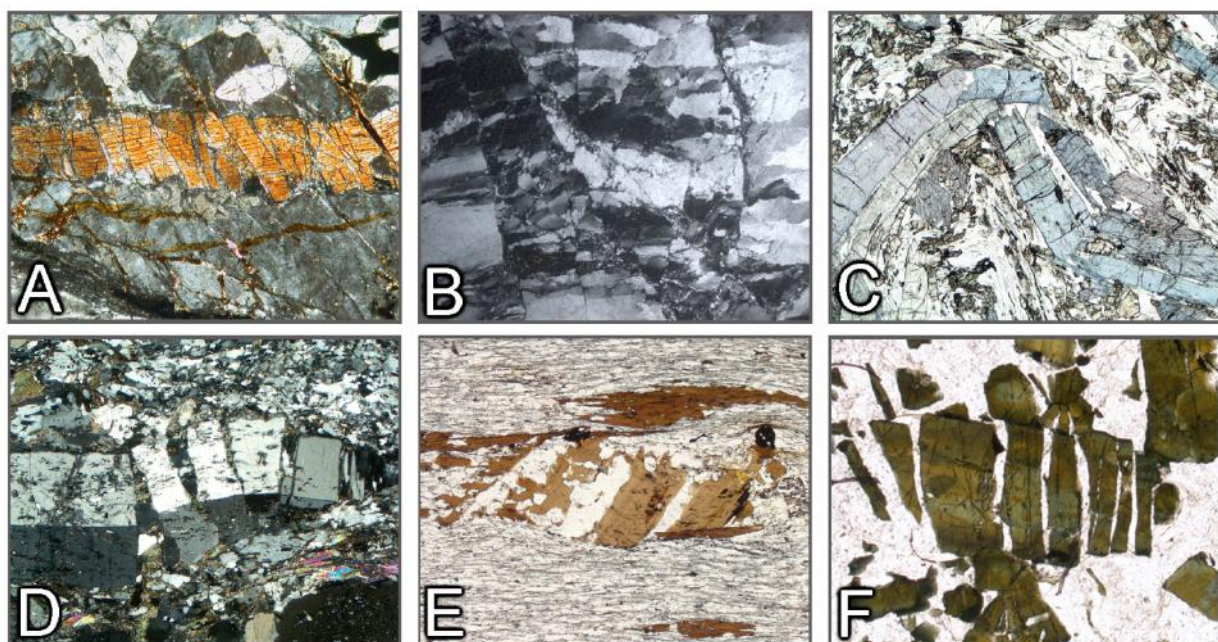


**Figure 3-13.** Brittle deformation behaviour of mineral grains

A: Domino-style fracturing of sillimanite crystal. B: Cataclastic deformation of quartz. C: Broken and kinked glaucophane crystals in microfold. D: Cataclastic deformation of plagioclase. E,F: Microboudinage of biotite and tourmaline. The open fractures are filled with quartz.

(Photomicrographs – B: Michael Stipp, IFM-Geomar Kiel; E,F: Bernardo Cesare, University of Padova)

In the polarized-light microscope, plastic crystal deformation is indicated where mineral grains show bending or kinking of normally planar morphological elements such as cleavage, rational crystal faces or twin planes (Fig. 3-14). The continuous or discontinuous change of crystal lattice orientation within a single mineral grain corresponds to a gradual or abrupt shift of the extinction position as the microscope stage is turned. Even where distinct morphological elements are lacking (as in quartz), deformation can be recognised from the non-uniform extinction positions of different domains within a grain (Fig. 3-14 J,L). These deformation features are caused by stress-induced intracrystalline processes such as dislocation glide and dislocation creep. Plastic deformation of crystal lattices may be continuous over a mineral grain or affect discrete grain domains only. Deformation lamellae or translation lamellae may form along defined glide planes (Fig. 3-14 K; 3-15 H).

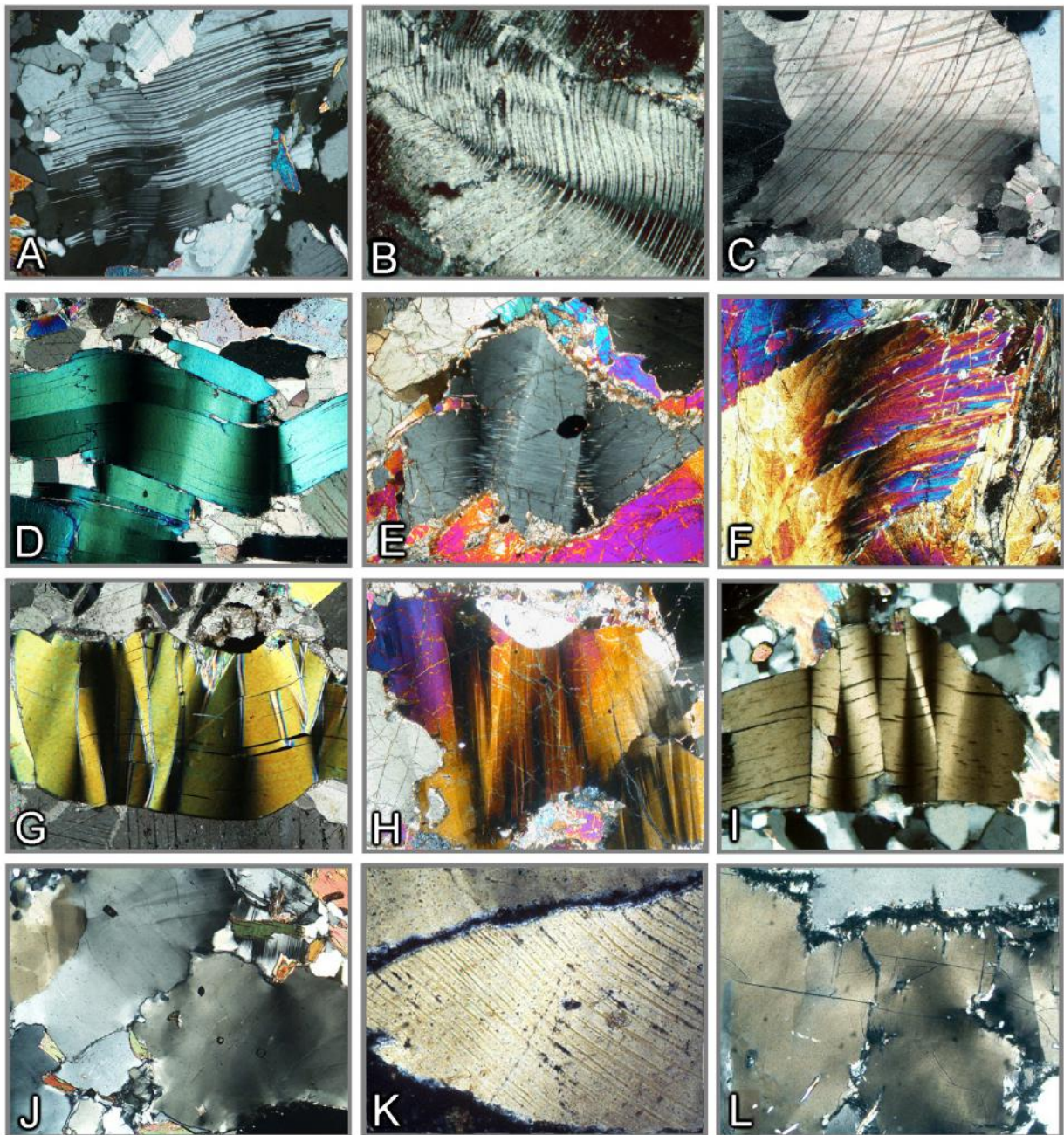


**Figure 3-14.** Plastic deformation of mineral grains (bending, kinking and deformation lamellae)

A-C: Strongly deformed crystals with bent twin lamellae (albite, plagioclase, calcite). D-F: Bent and kinked crystals (mica, orthopyroxene, glaucophane). G: Strongly kinked phlogopite. H: Olivine with kink bands. I: Kyanite with kink bands. J: Quartz with undulatory extinction K: Quartz showing bent translation lamellae on (0001). L: Deformed cordierite showing undulatory extinction and pinitized margins. (Photomicrographs B,K: Jörn Kruhl, TU München)

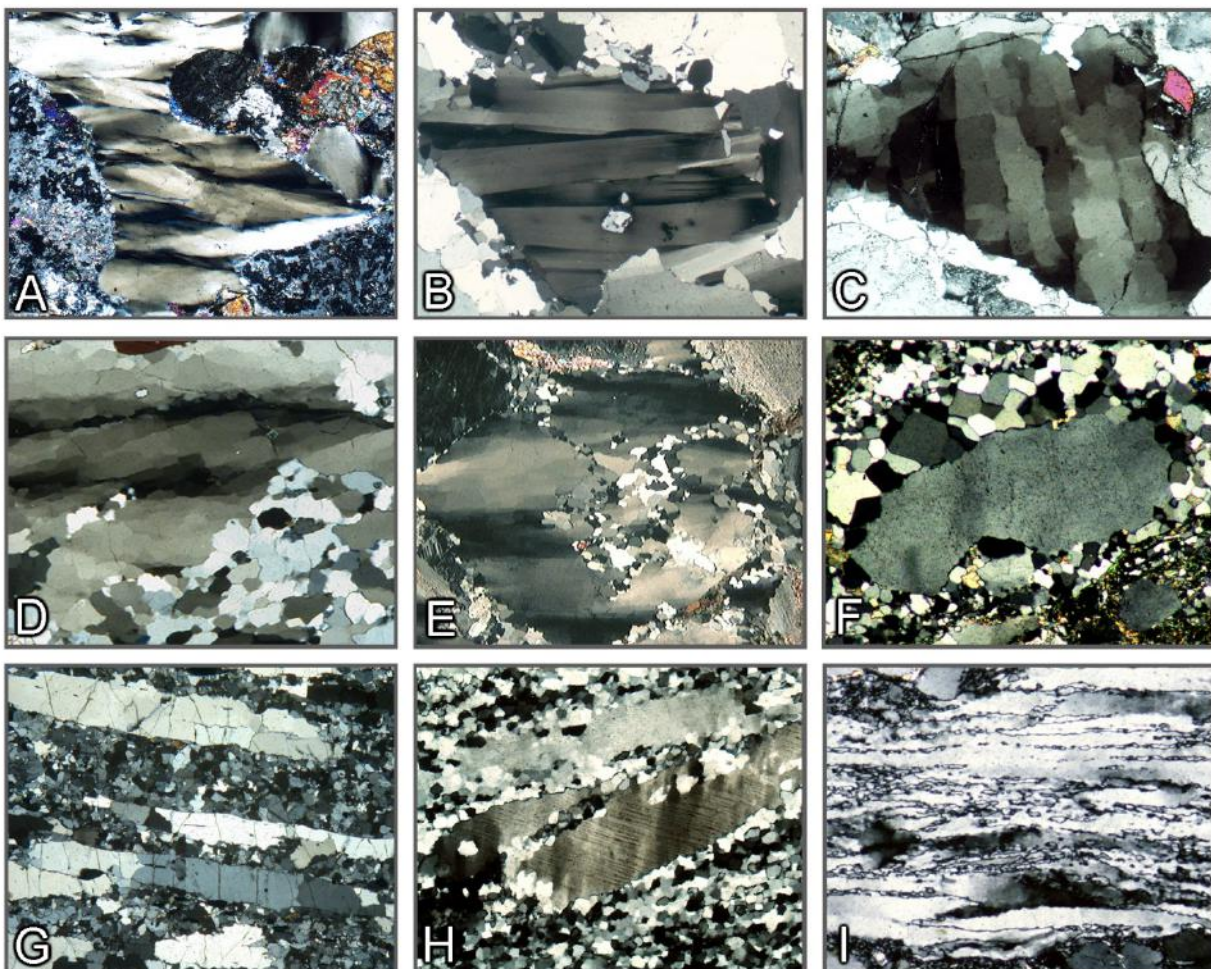


**Figure 3-15.** Plastic deformation and recrystallization of quartz

A,B: Subgrain domains that are elongate parallel to c. D: Chess board pattern. D,E: Partially recrystallized grains showing subgrain domains. F: Static recrystallization of the marginal domain of a turbid quartz crystal. G,H: Platy quartz in a recrystallized matrix of quartz + feldspar (felsic granulite). I: Strongly flattened quartz with serrated grain boundaries.

(Photomicrographs - E: Rainer Kleinschrodt, Universität Köln; F,I: Jörn Kruhl, TU München)

Deformation by mechanical twinning is restricted to certain minerals (e.g., plagioclase, calcite). As opposed to growth twins, deformation twins typically show a wedge-shaped outline (Fig. 3-16 A,B,I).

As the deformation process proceeds, dislocation migration and accumulation of dislocations along preferred zones (subgrain boundaries) within a mineral grain can lead to the formation of aggregates of dislocation-poor crystal domains (subgrains; Fig. 3-15 A-E, Fig. 3-16 D,F,G,H). The crystal lattice between adjacent subgrains is tilted by a few degrees only (low-angle grain boundaries). Between crossed polarizers a distinctly discontinuous change in the direction of extinction can be observed. (domainal undulatory extinction). Subgrain formation is particularly common in quartz, but also observed in other minerals. (Fig. 3-16, D,F,G,H). In quartz, subgrain domains may be elongate in the crystallographic c direction (Fig. 3-15 A,B,D,E). Cross-cutting subgrain patterns do also occur (chess-board pattern; Fig. 3-15 C).

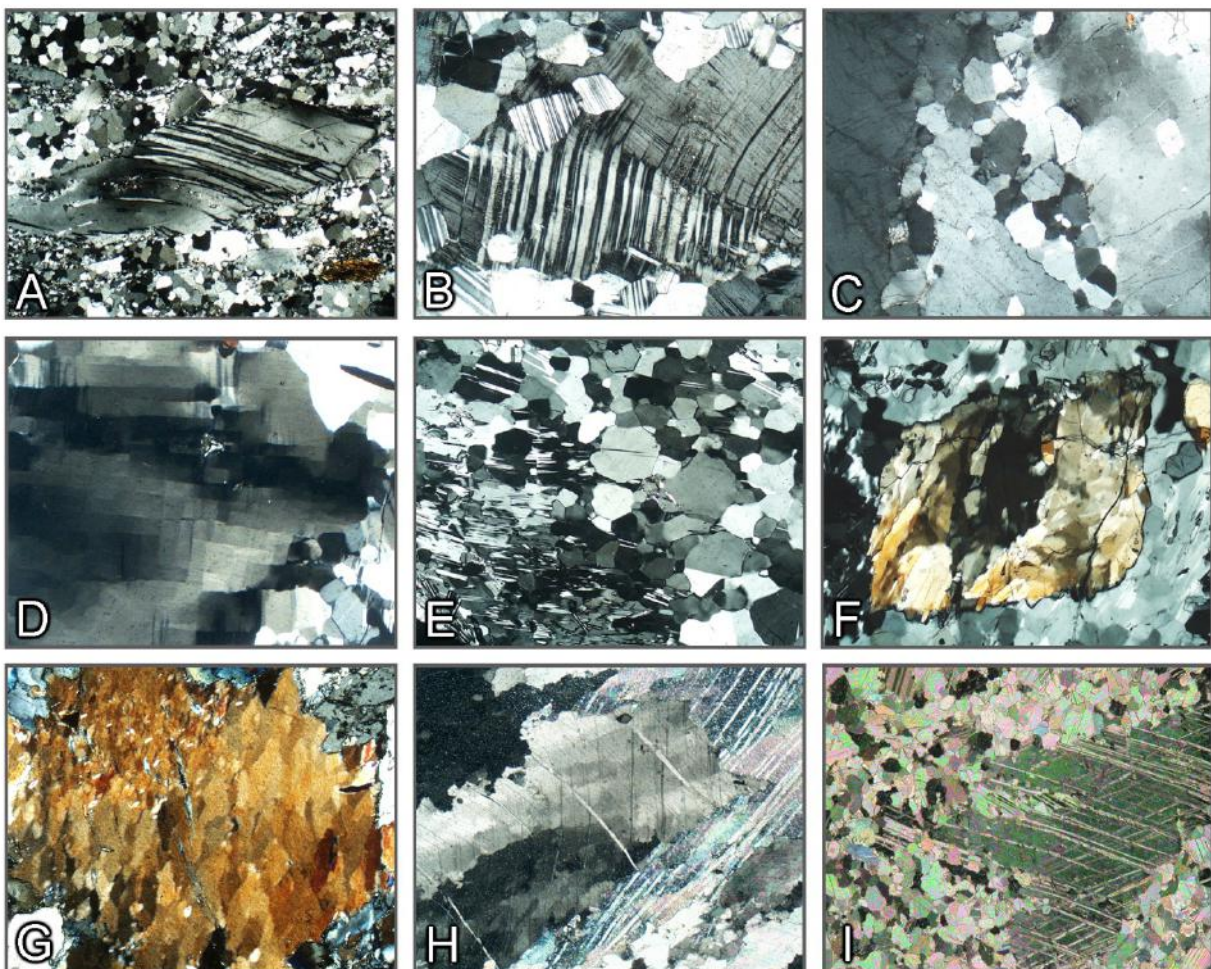


**Figure 3-16.** Plastic deformation and recrystallization

A,B: Deformed and partially recrystallized plagioclase crystals. C: Deformed and partially recrystallized orthoclase. D,E: Deformed cordierite showing a chessboard subgrain structure, partially recrystallized to a polygonal granular aggregate. F: Subgrain domains in sillimanite. G: Subgrain pattern in glaucophane. H: Bent calcite showing undulatory extinction and subgrain formation. I: Calcite with lamellar deformation twins, partially recrystallized statically to form a fine-grained polygonal aggregate.

Plastically deformed crystals tend to recrystallize at high temperatures, whereby crystal defects are eliminated. Recrystallized crystals are typically smaller-grained than the original deformed grains. The individual recrystallized grains show even extinction under crossed polarizers and have high-angle grain boundaries with the adjacent new grains. Recrystallized grains may have lobate to straight grain boundaries (Fig. 3-15 D,F,H; Fig. 3-16 B,C,I). Twin lamellae or inclusions contained in the large deformed crystal are commonly not preserved in the smaller recrystallized grain aggregate (Fig. 3-15 F; Fig. 3-16 E,I).

Recrystallization of deformed crystals may occur while deformation is active, or under static conditions. Typical for dynamic recrystallization is a side-by-side occurrence of larger grains showing undulatory extinction or subgrain structures and domains of finer-grained recrystallized material (Fig. 3-15 G-I). At high temperatures a relatively large grain-size spectrum and strongly curved or embayed grain boundaries are commonly observed.

Static recrystallization typically produces relatively even-grained aggregates of undeformed grains with straight grain boundaries (recovery texture). Minerals with no pronounced inherent shape anisotropy (e.g., quartz, calcite, feldspar) tend to form polygonal aggregates of equant grains (Fig. 3-17). Evidence for post-deformative recrystallization of minerals with a pronounced shape anisotropy (e.g., micas, amphiboles) is perhaps best observed in rocks where such minerals occur in an originally planar arrangement that had been subjected to later folding. Recovery of the deformed grains in microfold hinges leads to the formation of so-called polygonal arcs (Fig. 3-18).

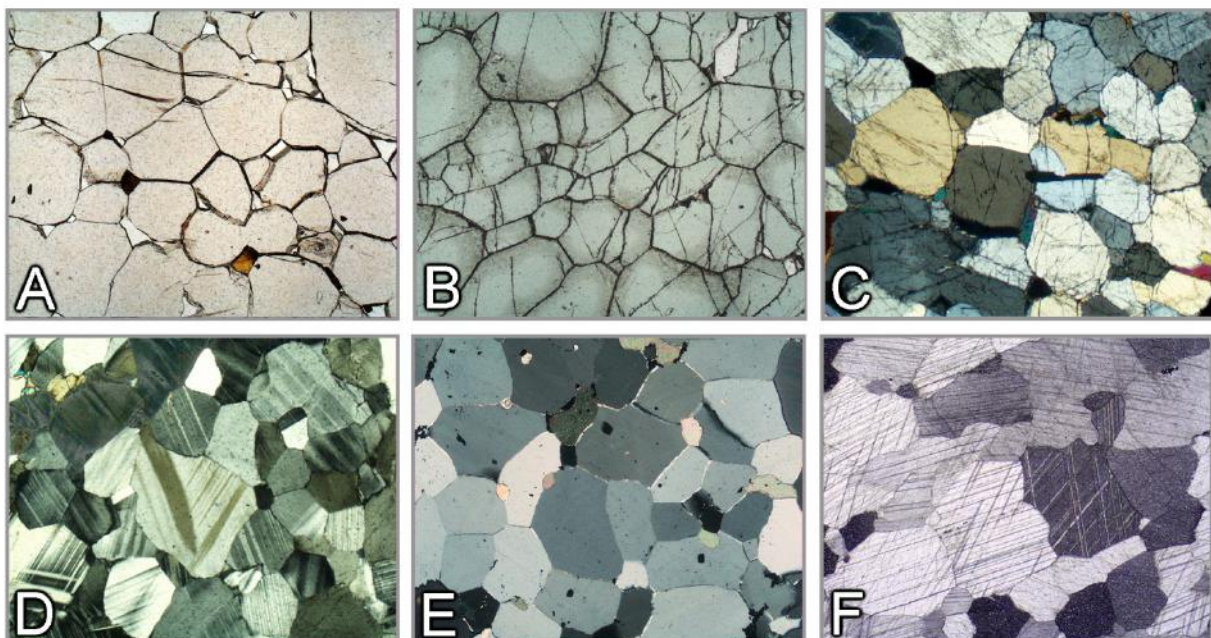


**Figure 3-17:** Static recrystallization and annealing

A-C: Granoblastic-polygonal grain aggregates generated by high-temperature (granulite-facies) static recrystallization or annealing. Garnet (A), spinel (B), orthopyroxene (C), plagioclase (D), quartz (E), calcite (F).

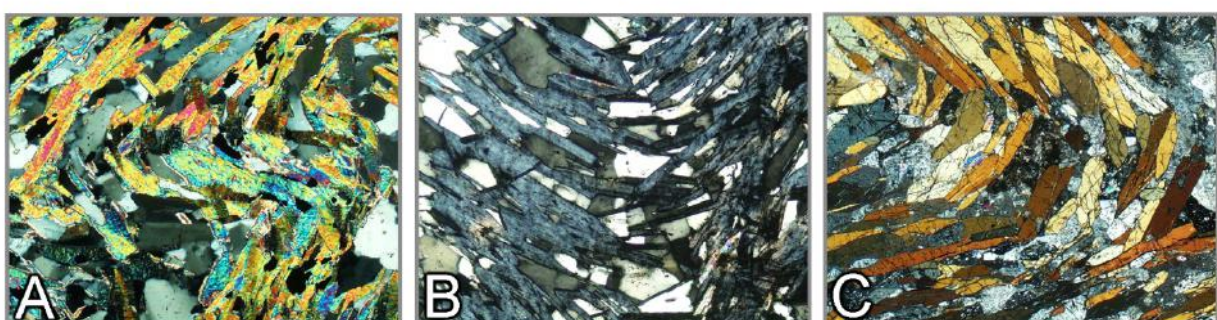


**Figure 3-18:** Static recrystallization of minerals with a strong shape anisotropy

A-C: Static recrystallization in microfold hinges ("polygonal arcs"). Mica (A), chlorite (B), amphibole (C).

### 3.3. Twinning

Twins are generated through crystal-structure-controlled intergrowths of two or more individual crystal segments with a defined symmetrical relationship. Twinning can also result from deformation (as in calcite). The individual parts of a twinned mineral are intergrown such that they either mirror each other's orientation (the mirror plane being the twin plane), or they are rotated against each other by a specific angle (the rotation axis being the twin axis), or both. The twin interface commonly corresponds to the twin plane.

For many mineral species twinning is an important property for identification. There are different kinds of twinning such as contact twins, penetration twins, simple twins, multiple twins, polysynthetic (or lamellar) twins (Fig. 3-19).

In thin section, twinning is commonly easily recognised under crossed polarizers if the mineral is anisotropic. The individual parts of twinned crystals show different brightness and interference colour, and on turning the microscope stage different extinction positions are revealed (Fig. 3-20). There are exceptions, however, as not all types of twins can be recognised under the microscope. If the indicatrix orientation of the individual parts of twinned crystals is identical, they are indistinguishable under crossed polarizers (e.g., the most abundant quartz twins have a twin axis parallel to c, which means the indicatrices are in parallel alignment. Thus, the twins go into extinction simultaneously).

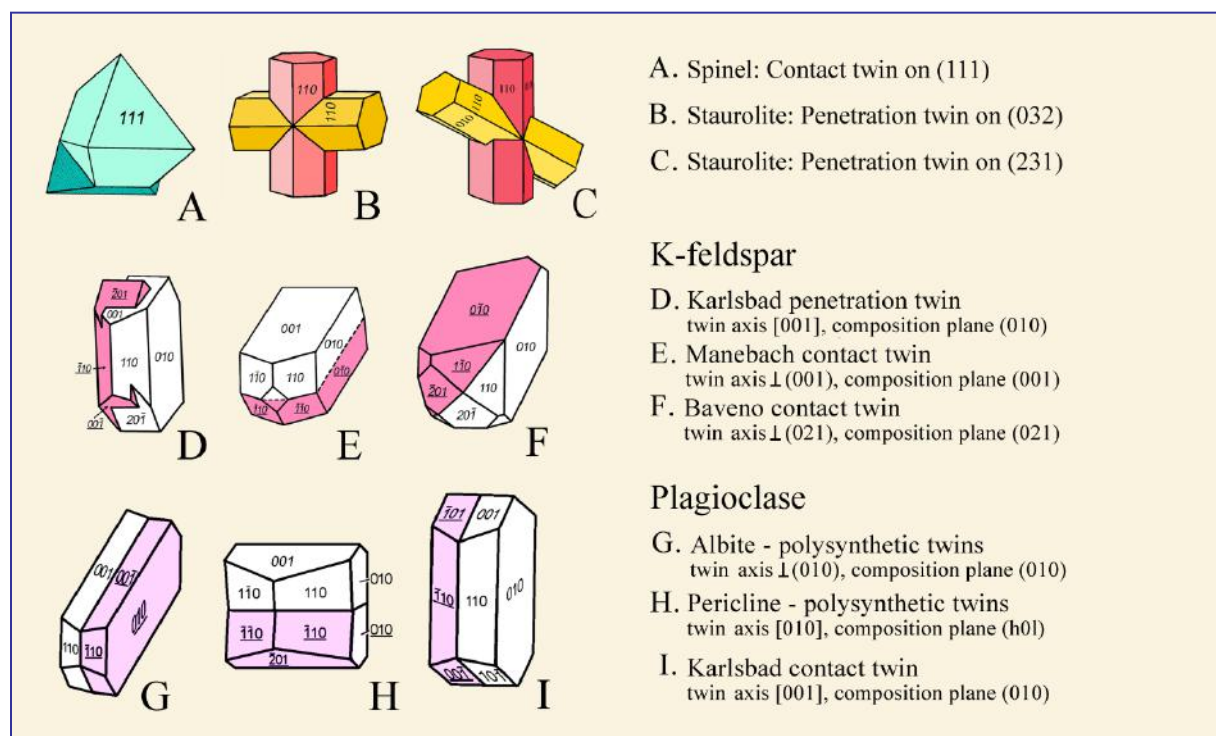


**Figure 3-19.** Types of twinning

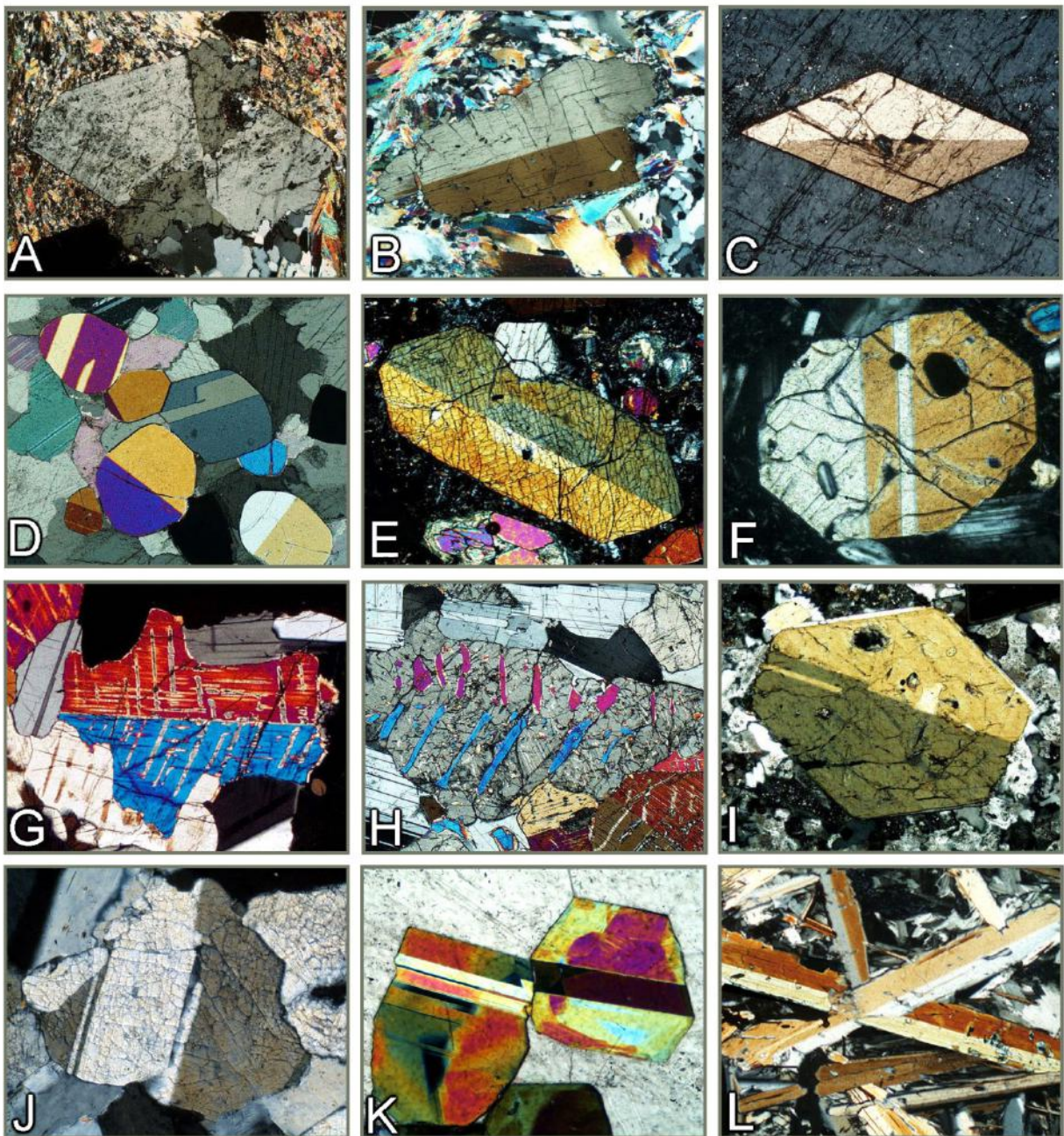


**Figure 3-20.** Twinning in minerals (I)

A: Staurolite, penetration twin on (320). B: Kyanite, simple twin on (100). C: Titanite, simple twin on (100). D: Simple and lamellar twins in chondrodite grains. E-G: Simple and lamellar twins on (100) in augite. H: Pigeonite twin on (100) inverted to orthopyroxene with augite exsolution lamellae on (001). I: Amphibole, simple twin on (100). J: Wollastonite, twins on (100). K: Epidote, lamellar twins on (100). L: Margarite, simple twins on (001).

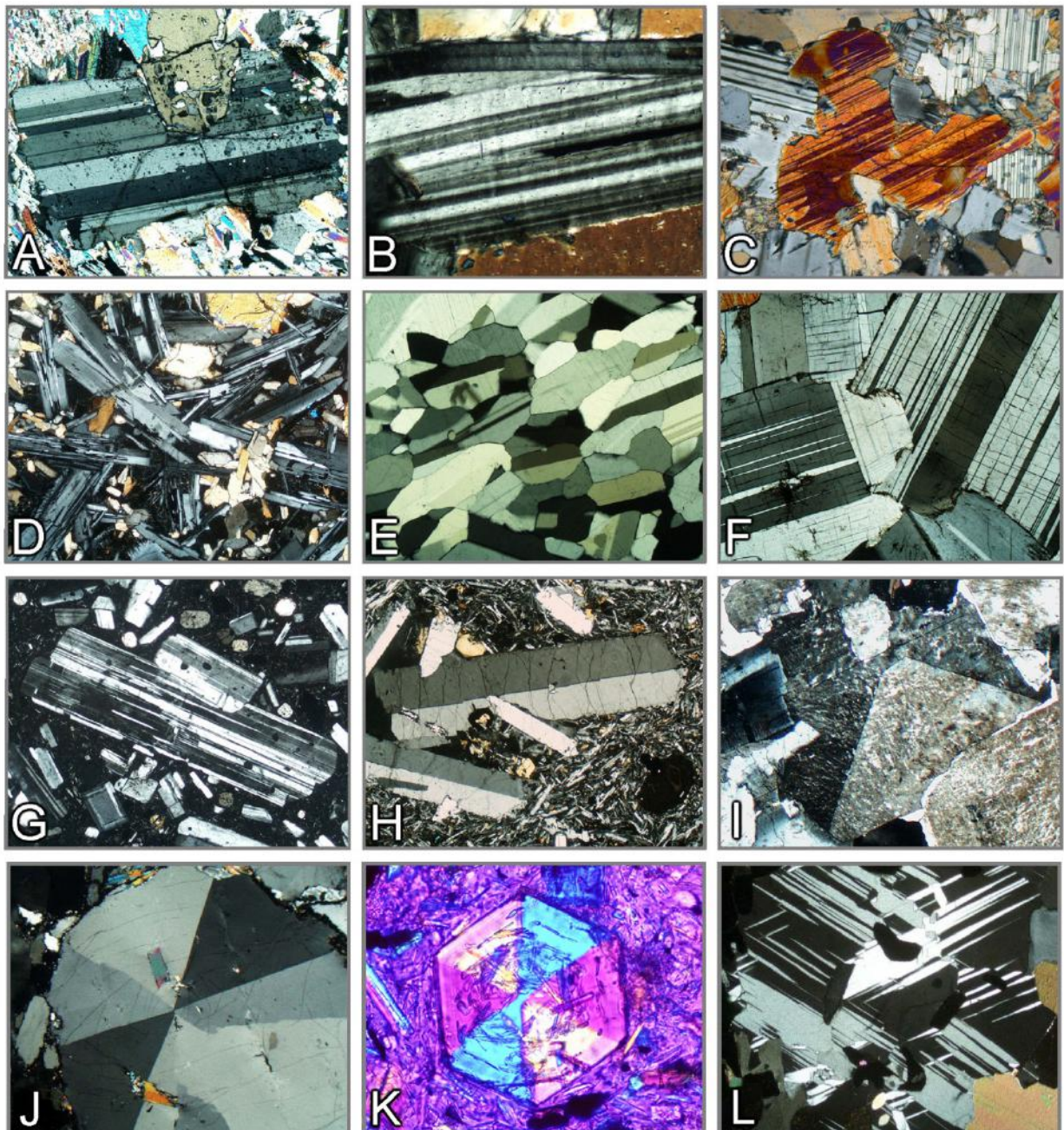


**Figure 3-20.** Twinning in minerals (II)

A: Chloritoid, lamellar twins on (001). B: Mg-rich chlorite (clinochlore), lamellar twins on (001). C: Cummingtonite, thin twin lamellae on (100). D: Plagioclase laths with polysynthetic, lamellar twins. E-G: Polysynthetic twinning in plagioclase. H: Sanidine, Carlsbad twins. I: K-feldspar, Baveno growth twin. J,K: Cordierite, cyclic twinning on {110} (triplet). First-order red plate inserted in K for better birefringence contrast. L: Lamellar twins in cordierite.

(Photomicrograph K: Bernardo Cesare, University of Padova)

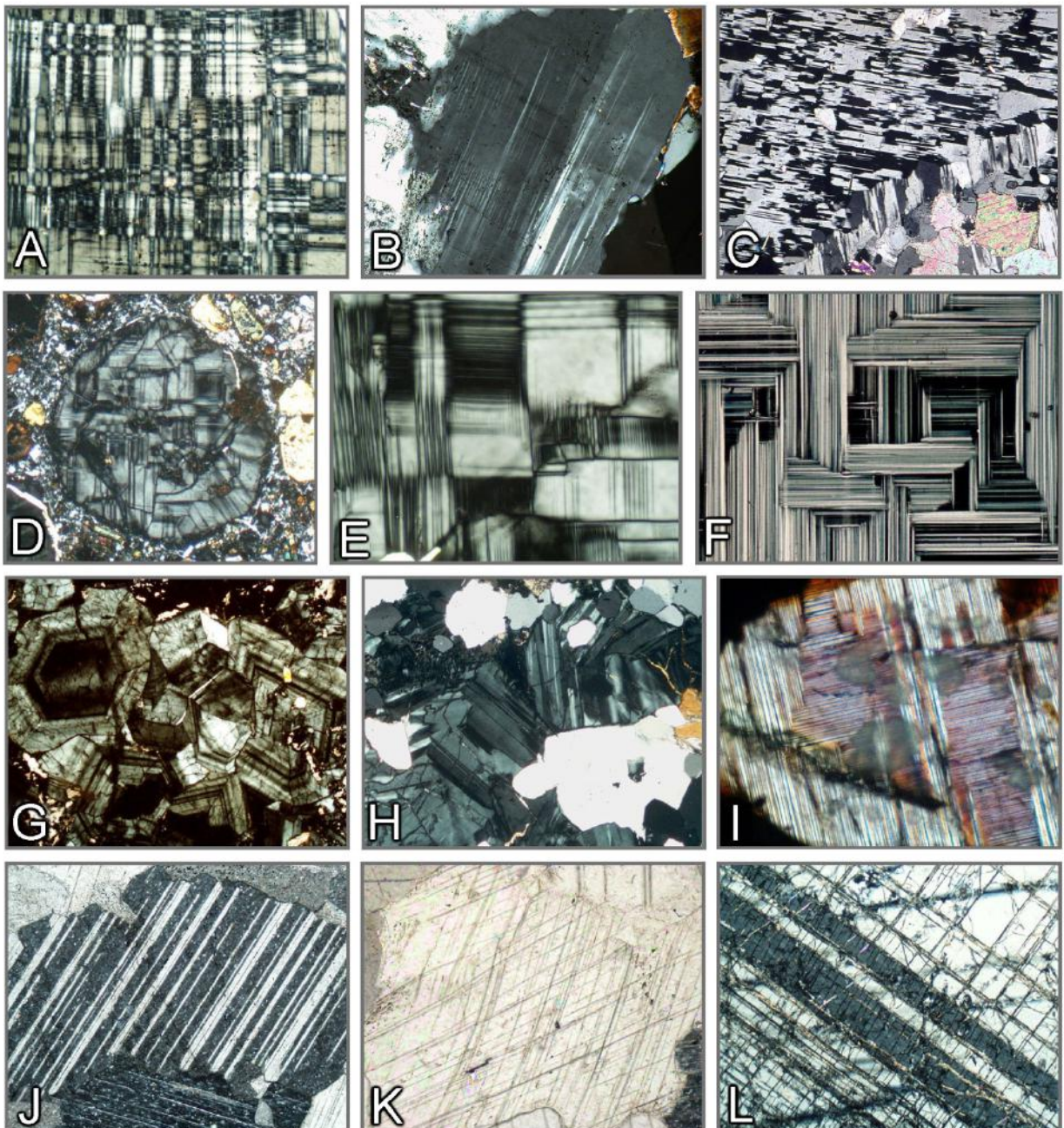


**Figure 3-20.** Twinning in minerals (III)

A: Microcline with characteristic cross-hatched twinning (section approximately parallel to (001)). B: Microcline, twin set (section approximately parallel to (001)). C: Chessboard albite, formed by albitization of microcline. D-F: Leucite with complex lamellar twinning. G: Grossular (anomalous-birefringent) with concentric-oscillating zoning and sector twins. H: Uvarovite (anomalous-birefringent) with sector twins. I: Larnite with thin polysynthetic twins on (100) and (010). J,K. Calcite with polysynthetic glide twins on {0112}. L: Corundum with twin lamellae on {1011}.

### 3.4 Inclusions, intergrowths, alteration products

Additional characteristics that can be used for mineral identification are, on the one hand, inclusions which have been incorporated during crystal growth (primary inclusions) and, on the other hand, inclusions that formed from alteration of the host mineral (secondary inclusions).

Although primary inclusions are not mineral-specific, they can give clues to the growth conditions of the host mineral (pressure-temperature conditions; changes of compositional parameters). Primary fluid and melt inclusions are found in minerals that have grown in the presence of a free fluid or from a melt (Fig. 3.21 A-D, L). Large crystals in metamorphic rocks (porphyroblasts) may contain small-sized inclusions, the orientation and distribution of which provides evidence for timing relationships between crystal growth and deformation (Fig. 3.21 E, F, K). In micaceous metamorphic rocks, Al-rich minerals such as staurolite (Fig. 3.21 G), garnet, andalusite and kyanite commonly form poikiloblasts rich in quartz inclusions. In quartz-rich rocks, skeletal crystals of these minerals can be observed (Fig. 3.21 H). Porphyroblasts with growth sectors that advanced much faster than other sectors of the crystal display a high density of minute primary inclusions (hourglass structure: chloritoid, andalusite; Fig. 3.21 I, J).

Secondary inclusions are, for example, intergrowths of isomorphic minerals that are the result of unmixing from solid solutions, such as pyroxenes, amphiboles and feldspars. The unmixed phases which are commonly lamellar to spindle-shaped show a regular, structurally controlled orientation within the host (Figs. 3.22, 3.23 J). The unmixed phase may, however, also be irregular in shape (e.g., dolomite in calcite; Fig. 3.22 K, L). Other commonly occurring secondary intergrowths are formed by the precipitation of Fe- and Ti-oxides in minerals from high-temperature rocks (pyroxene, amphibole, biotite, garnet, quartz, plagioclase; Fig. 3.23). Precipitation follows the cooling of the rocks whereby the solubility of Ti decreases. Although the crystal structures of host mineral and secondary phases are not isomorphic, the precipitation of Fe- and Ti-oxides may still be structurally controlled by the host mineral.

High-grade metamorphic rocks can show reaction textures that relate to decompression, particularly to episodes of rapid exhumation at relatively high temperatures. Commonly intergrowths of two new minerals form at the expense of a previously stable one (symplectites: Figs. 3.24, 3.25). Less common are fibrous intergrowths of three newly formed minerals (kelyphite: Fig. 3.24 A). Single-phase reaction coronas form during the pseudomorphic transformation of coesite to quartz (Fig. 3.25 I, J), from the pseudomorphic reaction of corundum to spinel (Fig. 3.25 G), or from the hydration of periclase to brucite (Fig. 3.25 E).

Characteristic replacement textures are also generated by retrograde reactions involving hydrous fluids. In the presence of such fluids, hydrous phases grow at the expense of less hydrous or anhydrous minerals. The primary mineral is replaced from the surface inwards, while the reaction proceeds also preferentially along fractures and open cleavage planes (Figs. 3.26, 3.27). During saussuritization and sericitization of plagioclase, consumption of the anorthite component produces fine-grained clinzozoisite, zoisite and sericite, without orientation relationships with the host crystal. (Fig. 3.27 J, K). Apart from hydration, oxidation reactions may be involved as well in such replacement processes (Fig. 3.26 A-E, I).

A special feature are pleochroic haloes around minerals containing a significant amount of radiogenic isotopes. The most common minerals in this group are zircon, monazite and xenotime. The radioactive radiation emitted from these minerals affects the crystal structure of the surrounding host minerals, and these structural defects become visible as coloured concentric haloes around the inclusion (Fig. 3.28). Over geological time, the effect intensifies, and the minerals that carry the radiogenic isotopes may have their own crystal structure modified if not destroyed.

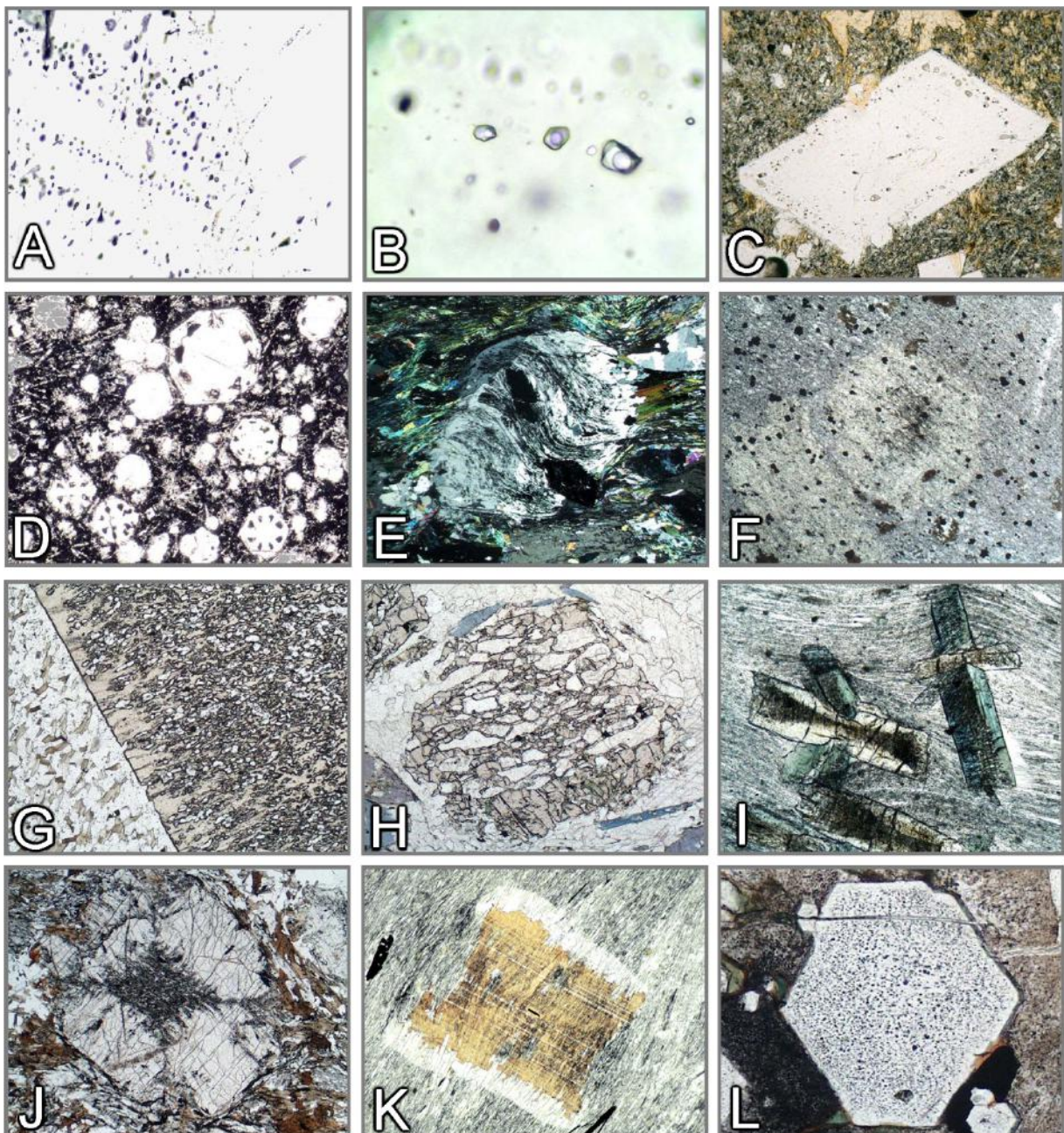


**Figure 3-21.** Inclusions

A,B: Fluid inclusions in quartz. C: Melt inclusions in plagioclase. D: Melt inclusions in leucite. E: Albite porphyroblast with sigmoidal inclusion trails defined by tiny graphite particles. F: Cordierite porphyroblast showing inclusion trails that are identical to matrix foliation. G: Staurolite poikiloblast. H: Skeletal garnet. I: Chloritoid with minute inclusions forming an hour-glass structure. J: Andalusite with fine-grained inclusions (chiastolite). K: Biotite, statically overgrowing the external schistosity. L: Apatite, clouded interior due to tiny fluid inclusions.

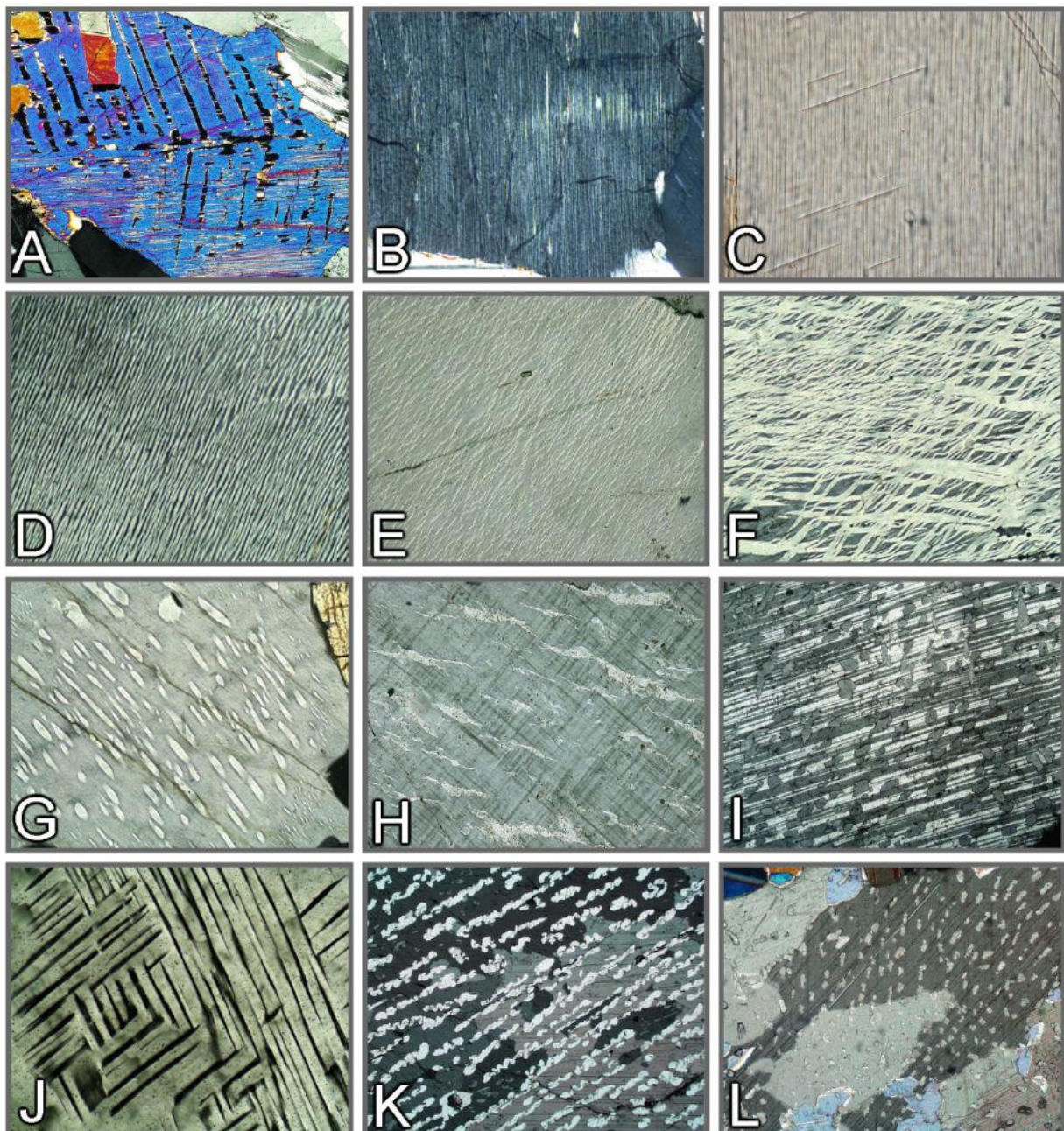


**Figure 3-22** Exsolution textures

A: Augite twin on (100) with pigeonite lamellae on (001). B: Bronzite with thin augite lamellae on (100). C: Exsolution lamellae in grunerite. D-H: Perthitic unmixing in alkali feldspars: mesoperthite, film-like spindle perthite, network-like vein perthite, spindle perthite, coarse vein perthite. I,J: Anti-perthitic unmixing in plagioclase. K,L: Embayed platelets and drop-like crystals of exsolved dolomite in calcite host.

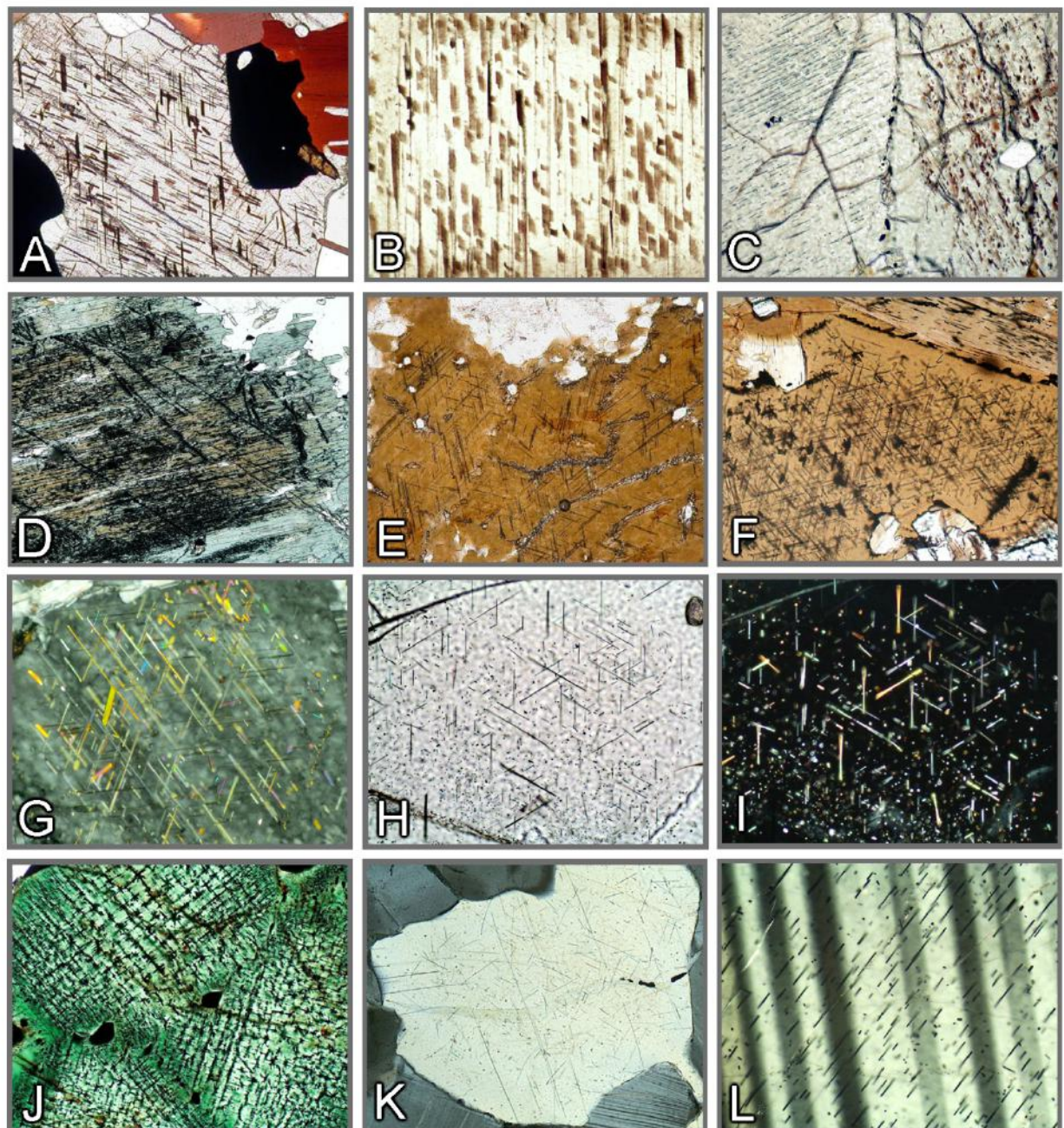
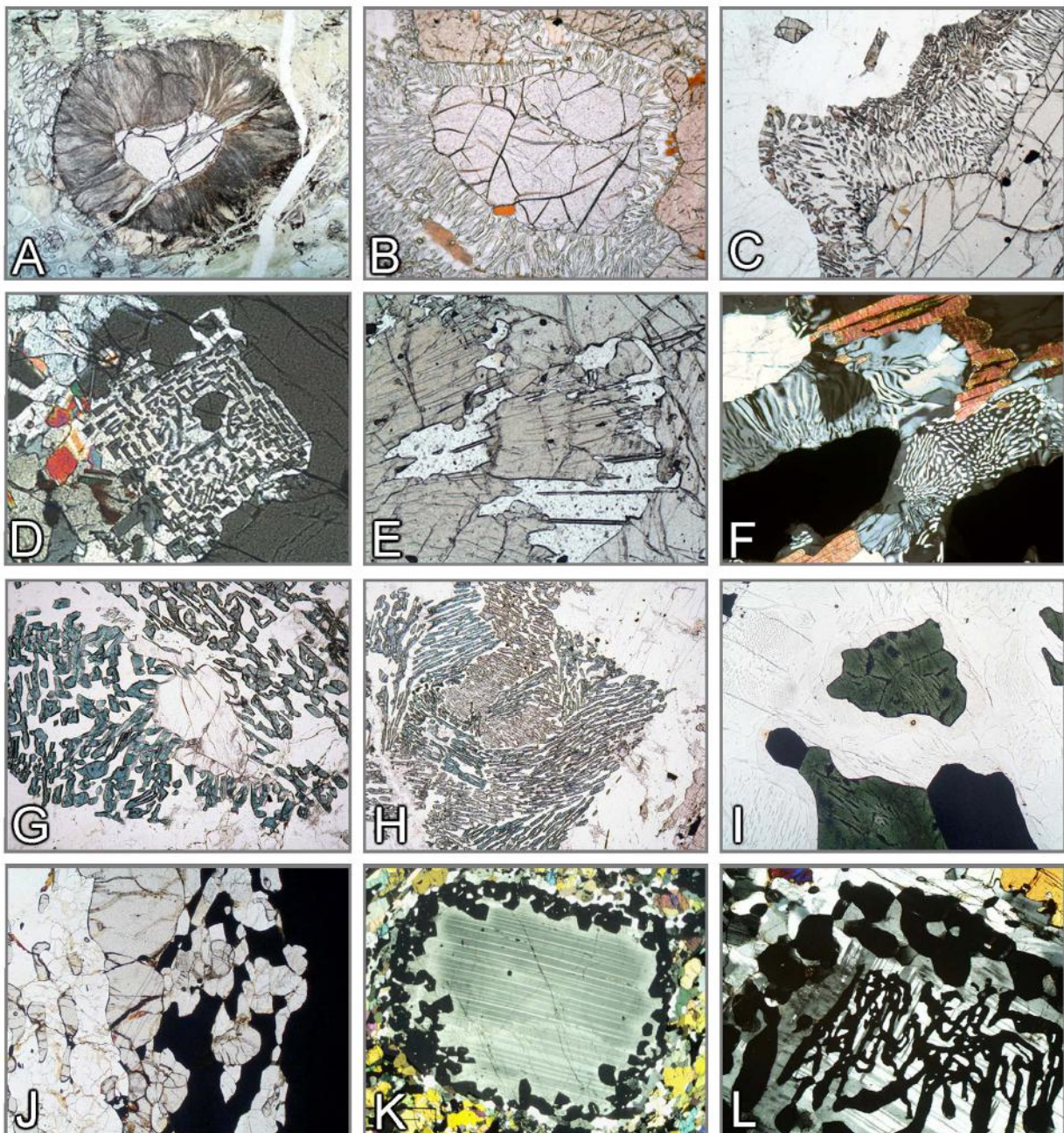


**Figure 3-23.** Oriented exsolution of Fe,Ti-oxides (secondary inclusions)

A-E: Oriented precipitation of ilmenite platelets in orthopyroxene (A,B), clinopyroxene (C), hornblende (D) and biotite (E). F-I: Oriented precipitation of rutile needles in biotite (= sagenite; F,G), garnet (H,I) and quartz (K). J: Hercynite with exsolved magnetite platelets. L: Oriented precipitation of Fe,Ti-oxide needles in plagioclase.



**Figures 3-24.** Reaction textures in granulites

A-F: Garnet breakdown– A: Radiating Hbl-Opx-Spl kelyphite fringe (garnet peridotite). B,C: Opx+Crd symplectite ( $\text{Grt}+\text{Qz}\rightarrow\text{Opx}+\text{Crd}$ ; metapelite; Namibia, Lapland). D: Opx-Sil symplectite ( $\text{Grt}+\text{Qz}\rightarrow\text{Opx}+\text{Sil}$ ; Mg-Al granulite, Kola Peninsula). E: Opx-Spr symplectite ( $\text{Grt}+\text{"Mg"}\rightarrow\text{Opx}+\text{Spr}$ ; Mg-Al granulite, Eastern Ghats, India). F: Crd-Qz symplectite (metapelite, Lapland). G,H: Breakdown of sillimanite to form Spr-Crd symplectite ( $\text{Opx}+\text{Sil}\rightarrow\text{Spr}+\text{Crd}$ ). Mg-Al granulite, southern India). I: Hercynite (Mt-unmixing, ilmenite), with finely pigmented cordierite rim in mesoperthite-quartz matrix ( $\text{Spl}+\text{Qz}\rightarrow\text{Crd}$ ; metapelite, southern Madagascar). J: Sil+Grt double seam between nearly opaque spinel and quartz ( $\text{Spl}+\text{Qz}\rightarrow\text{Grt}+\text{Sil}$ ; Fe-Al granulite, Eastern Ghats, India). K,L: Coronitic and skeletal garnet formation in plagioclase ( $\text{Cpx}+\text{Fa}+\text{Pl}\rightarrow\text{Grt}$ ; ferrodiorite, Eastern Ghats, India).

Mineral abbreviations after Whitney & Evans (American Mineralogist, 95, 185–187, 2010).

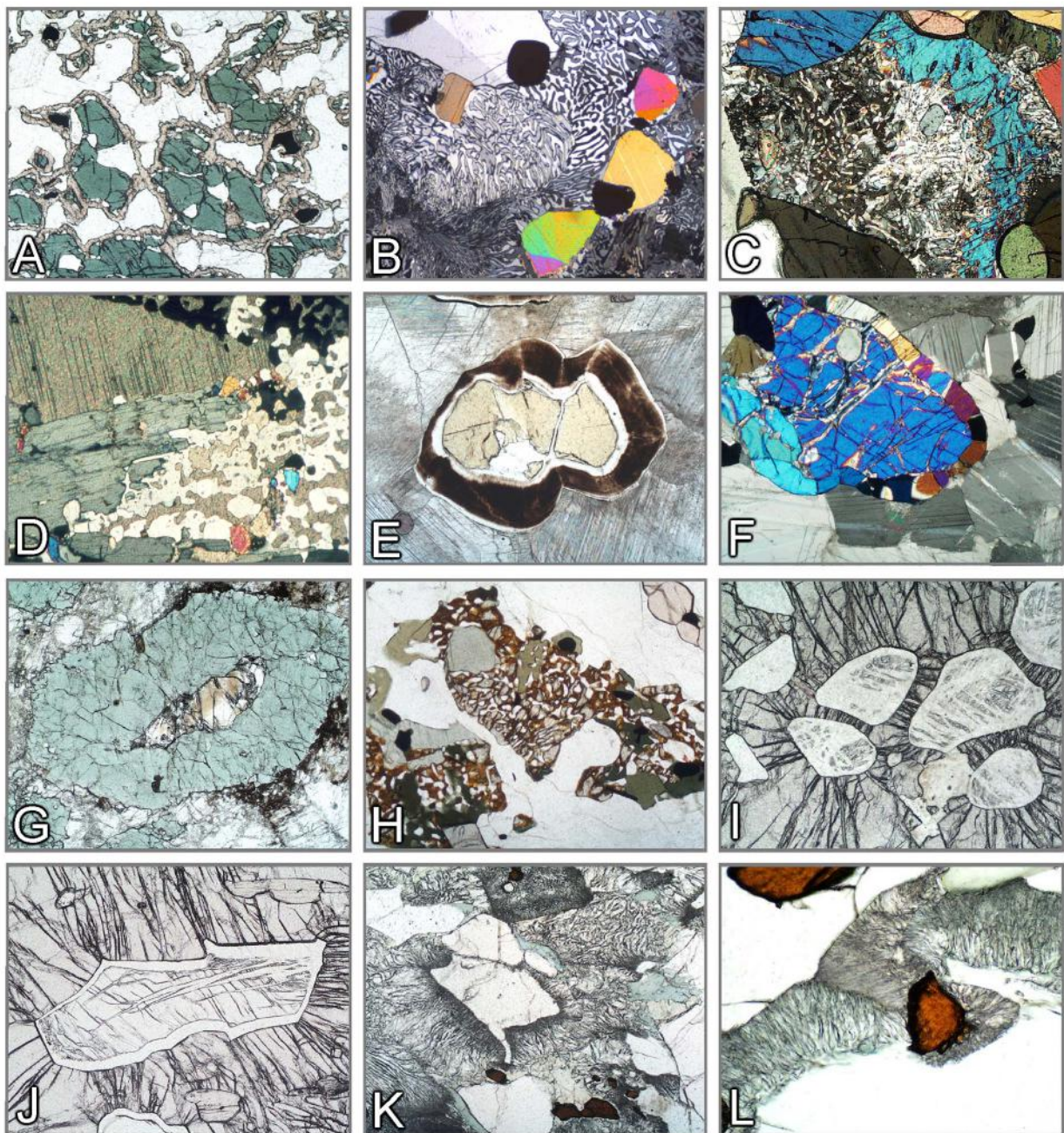


**Figure 3-25.** Reaction textures in granulites and HP- to UHP-metamorphic rocks

A: Garnet coronas around clinopyroxene ( $\text{Cpx}+\text{Pl}\rightarrow\text{Grt}+\text{Qz}$ ; calcsilicate rock, Eastern Ghats Belt, India). B: Monticellite+wollastonite symplectite ( $\text{akermanite}\rightarrow\text{Mtc}+\text{Wol}$ ; calcsilicate rock, Adirondacks, USA). C: Anorthite+calcite symplectite ( $\text{meionite}\rightarrow\text{An}+\text{Cal}$ ; calcsilicate rock, Eastern Ghats Belt, India). D: Cal+Qz aggregate ( $\text{Wol}+\text{CO}_2\rightarrow\text{Cal}+\text{Qz}$ ; South Norway). E: Periclase with brucite fringe ( $\text{Per}+\text{H}_2\text{O}\rightarrow\text{Bru}$ ; calcsilicate marble, Bad Harzburg, Germany). F: Diopside corona around forsterite ( $\text{Fo}+\text{Cal}+\text{CO}_2\rightarrow\text{Di}+\text{Dol}$ ; marble, South Madagascar). G: Pseudomorphic replacement of corundum by spinel ( $\text{Crn}+\text{"MgO"}\rightarrow\text{Spl}$ ; Corundum-anorthite rock, South Madagascar). H: Fayalite+quartz symplectite ( $\text{ferrosilite}\rightarrow\text{Fa}+\text{Qz}$ ; Eastern Ghats Belt, India). I,J: Polymorphic transformation coesite $\rightarrow$ quartz (Dora Maira, Western Alps). K,L: Reaction omphacite+quartz $\rightarrow$ diopside+albite (eclogite; Saualpe, Austria).

Mineral abbreviations after Whitney & Evans (American Mineralogist, 95, 185–187, 2010).

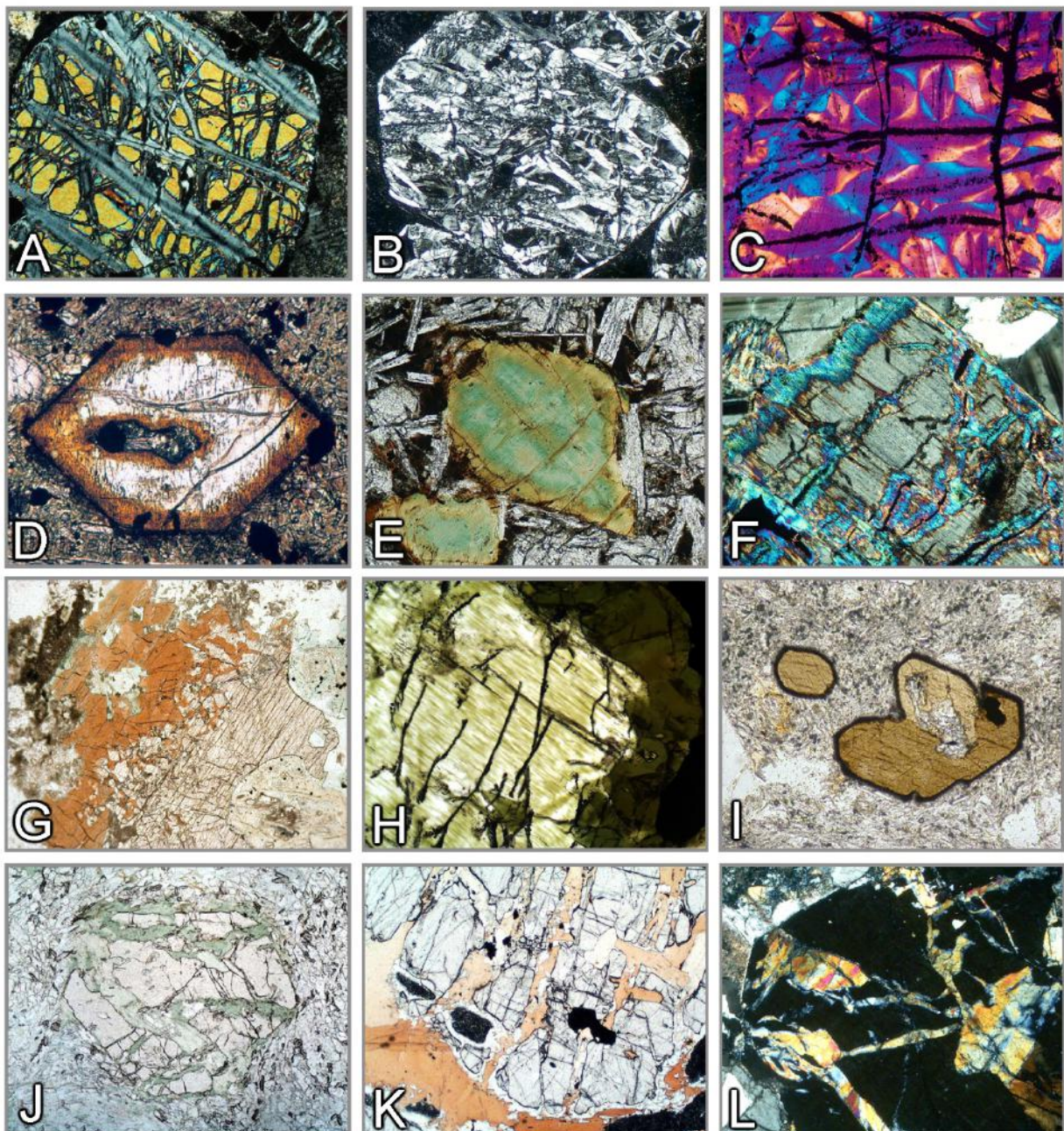


**Figure 3-26.** Secondary alteration through reaction with aqueous fluids (I)

A-C: Serpentinization— $\text{forsterite} \rightarrow \text{serpentine} + \text{magnetite}$ . D,E: Alteration of olivine to “iddingsite” (goethite and clay minerals). F: Oriented replacement of orthopyroxene by talc. G: Reaction clinopyroxene  $\rightarrow$  amphibole. H: Oriented replacement of clinopyroxene by amphibole (uralite). I: Kaersutitic amphibole with microcrystalline alteration seam of magnetite+clinopyroxene (opacite). J-L: Replacement of garnet by chlorite (J), biotite (K) and epidote (L).

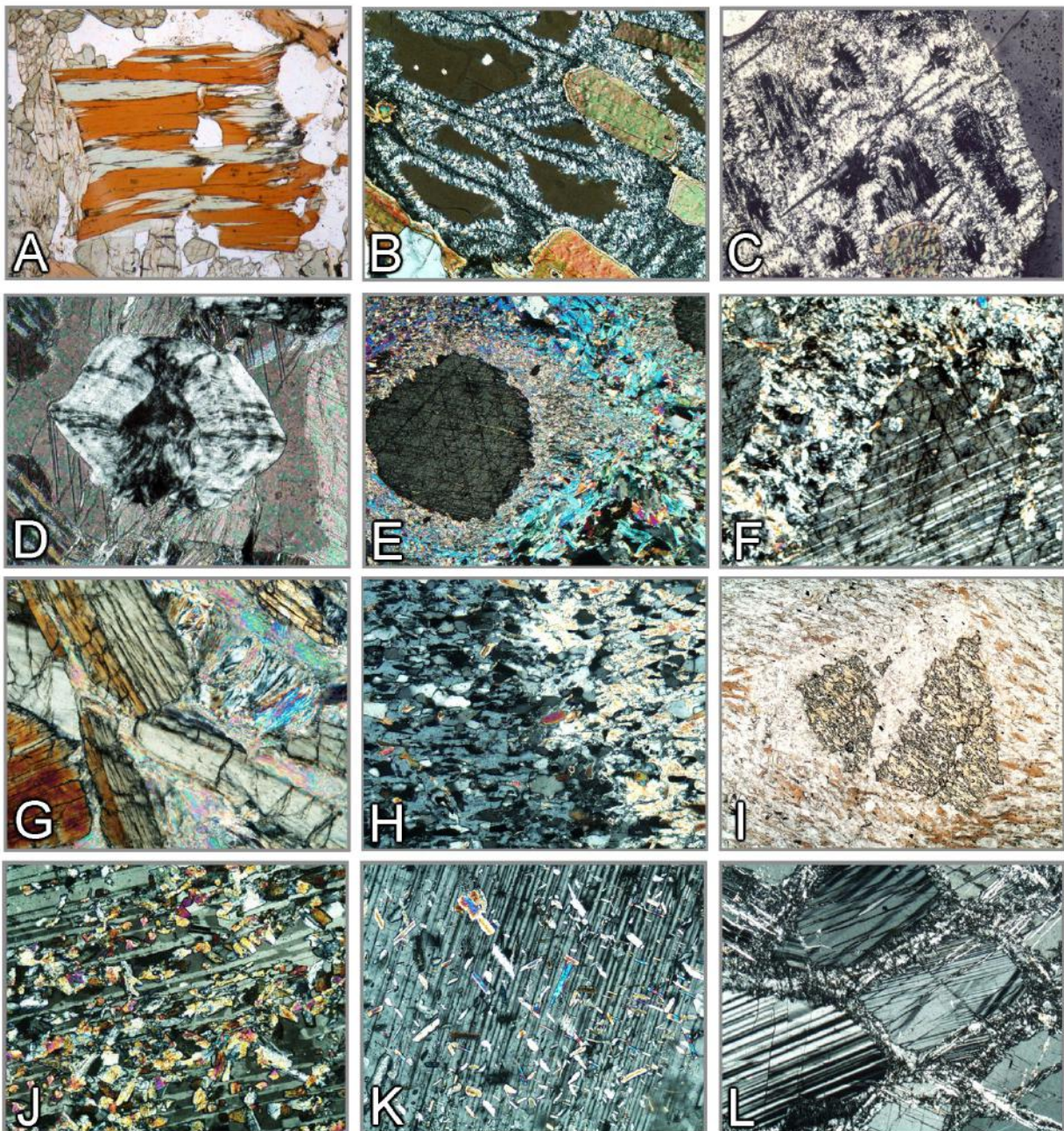


**Figure 3-27.** Secondary alteration through reaction with aqueous fluids (II)

A: Chloritization– biotite. B,C: Pinitization– cordierite→muscovite. D: Brucite pseudomorphing peri-clase. E,F: Replacement of corundum by muscovite (E) and gibbsite (F). G: Alteration of kyanite to pyrophyllite. H,I: Muscovite replacing andalusite (H) and staurolite (I). J: Saussuritization– plagioclase→clinzoisite+albite. K: Sericitization– plagioclase→muscovite. L: Zeolitization– anorthite→thomsonite.

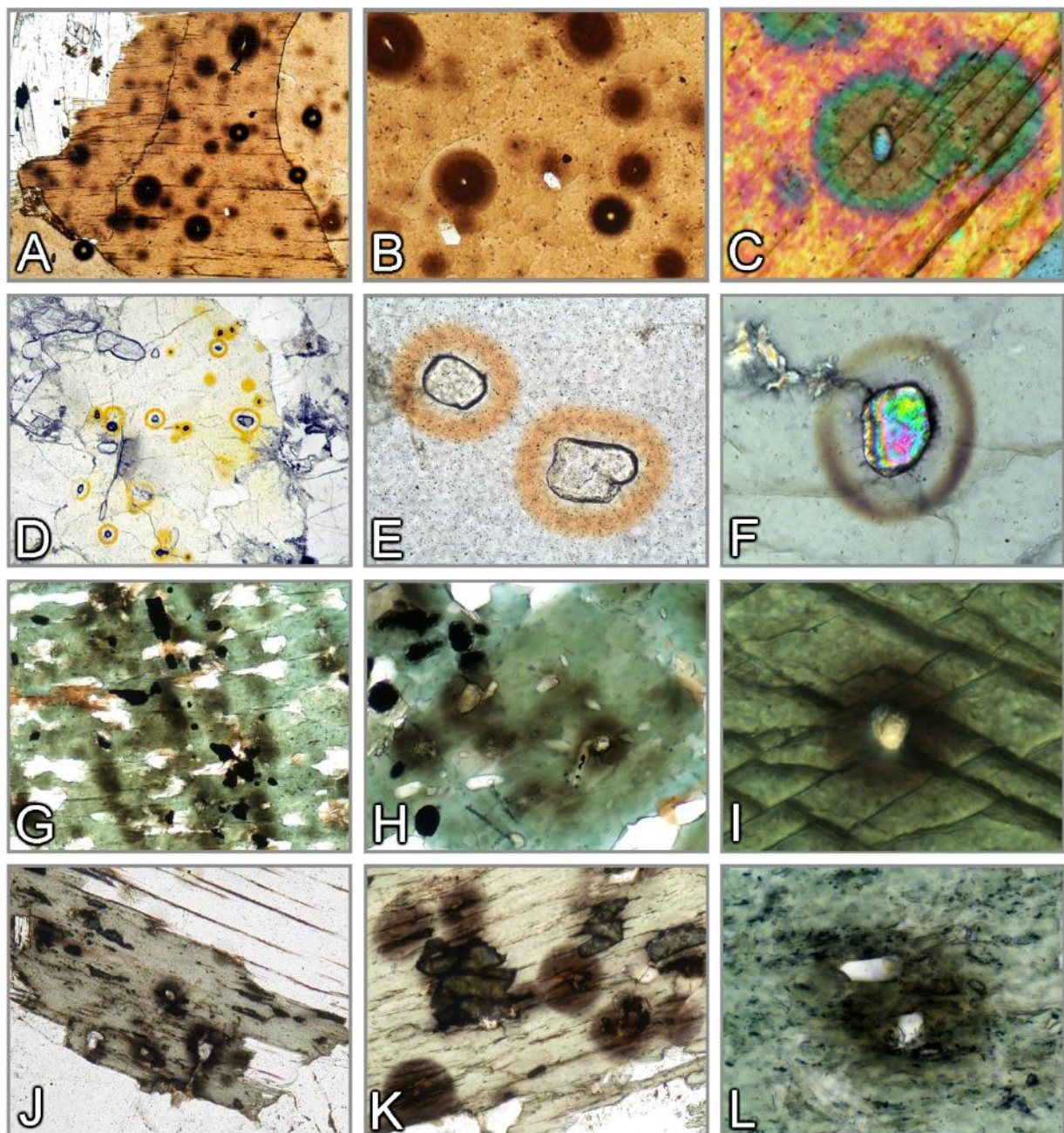


**Figure 3-28.** Pleochroic halos around minerals containing radioactive isotopes

A-L: Pleochroic halos around inclusions of zircon, monazite and xenotime in biotite (A-C), cordierite (D-F), amphibole (G-H) and chlorite (J-L).

## 4. Optical properties

### 4.1 Some basic principles

#### 4.1.1 Nature of light, refraction

In order to describe the interaction of light rays with matter, two physical models can be applied: (a) light as a wave, and (b) light as energy quanta. Most optical phenomena which are observed during microscopic investigation of amorphous or crystalline substances (glass phase, minerals), can be adequately explained with the wave model.

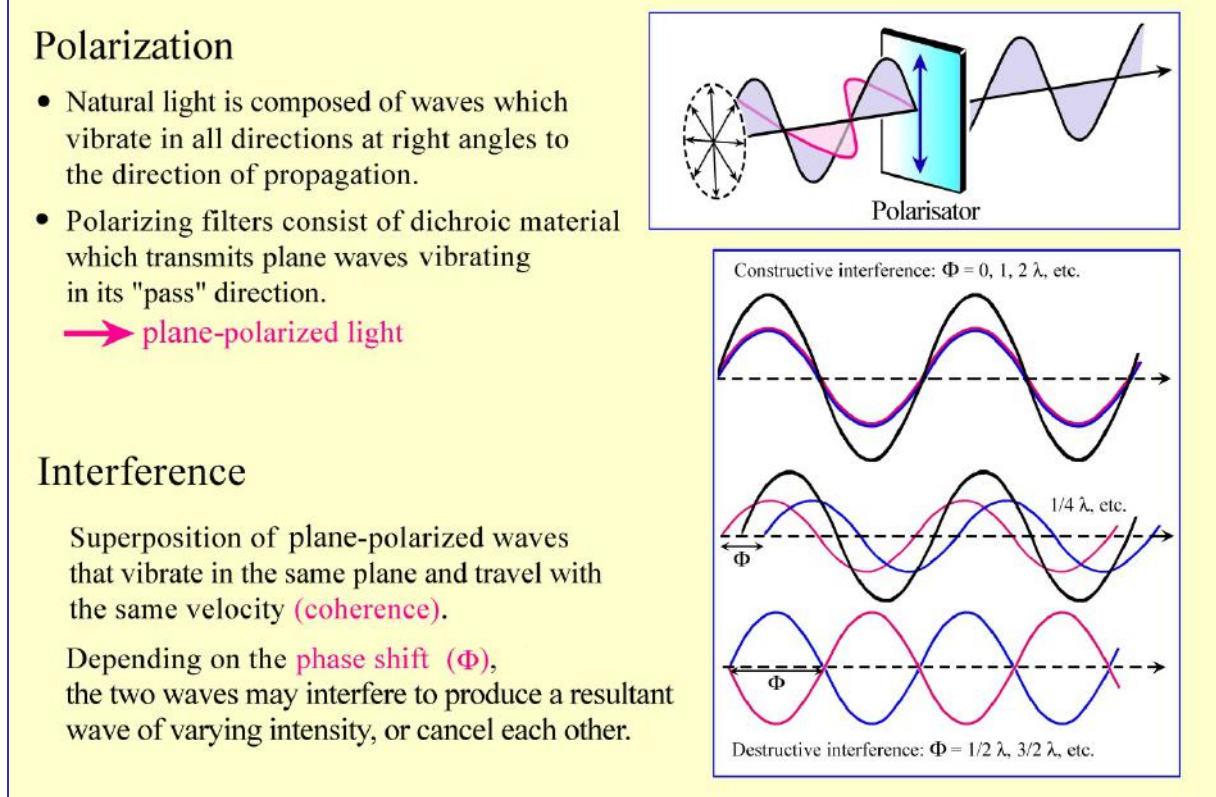
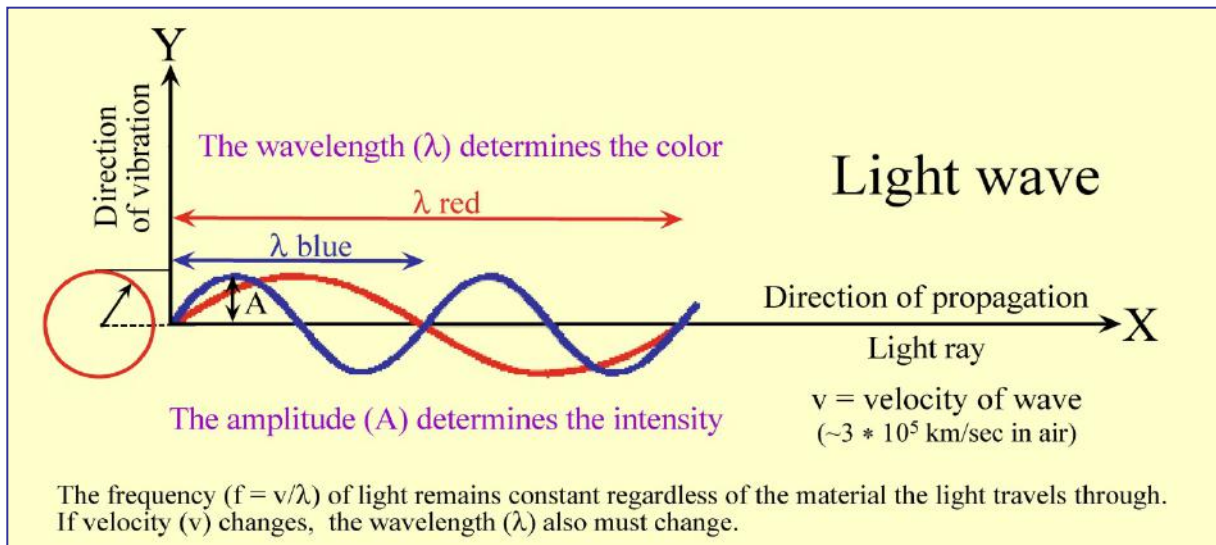
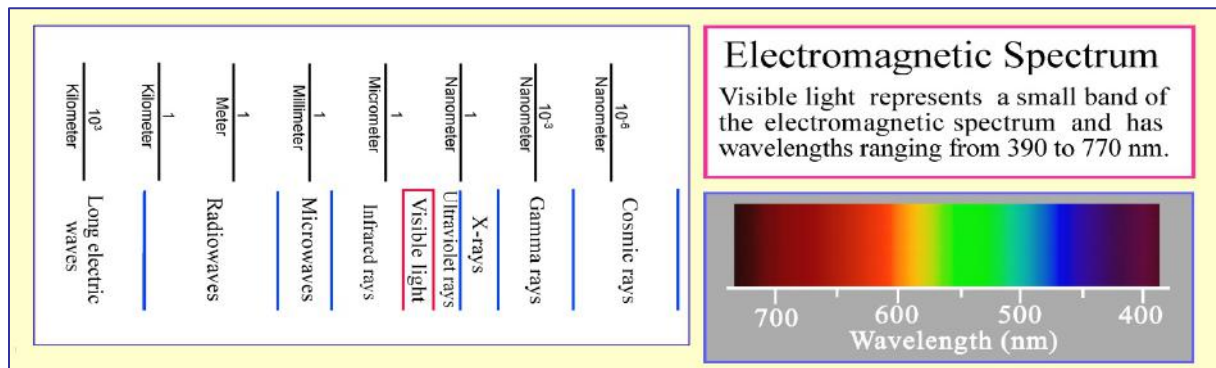
**Wave model:** Light rays propagate as electromagnetic waves. In each wave electric and magnetic vectors oscillate orthogonal to each other and orthogonal to the propagation direction. The optical behaviour of light when passing through amorphous or crystalline substances is essentially controlled by the interaction of the electric vector with the electric field of the ions. Interactions with the magnetic vector are negligible. Thus, each light wave can be described as a harmonic oscillation [ $y = A \sin(x)$ ] (Fig. 4-1).

**Colour:** The human eye can only see a small part of the large spectrum of electromagnetic radiation, namely the spectral domain between about 400 and 800 nm (visible light). This is the colour spectrum from violet to blue, green, yellow, orange and red (Fig. 4-1). Sunlight consists of various proportions of these colours, the combination of which is perceived as white light. In thin section, colour effects are caused if the spectral composition of originally white light is changed as light passes minerals, either by depletion of specific wavelengths (absorption), or by dispersion of white light as a result of refraction or diffraction of light at grain boundaries, inclusions and rough surfaces.

**Intensity:** The intensity of light, of a specific colour, for example, is determined by the amplitude of the light wave. It can be modified by absorption.

**Polarization:** Sunlight or the light emitted from the light source in the microscope consists of waves which vibrate in random directions. In plane-polarized light, the light waves vibrate in a defined direction. Plane-polarized light is generated in modern microscopes by a polarization filter which reduces light of random vibration directions from natural or artificial sources to light of a single vibration direction (Fig. 4-1). The bundle of light waves entering the thin section consists entirely of E-W vibrating light waves if the polarizer is adjusted precisely.

**Interference:** Two coherent light waves generated by the same light source can overlap (i.e., interfere) if they vibrate in the same plane and have the same velocity. This is realised in optically anisotropic minerals when the two orthogonally vibrating light rays, generated through double refraction in the crystal plate, are brought to interference in the analyzer after leaving the thin section (see Ch. 4.2.3). The degree of phase shift ( $\Phi$ ) determines whether the interfering waves are eliminated or produce a resultant wave of decreased or increased intensity (Fig. 4-1). If certain sections of the white light spectrum are eliminated, diminished or amplified, interference colours are generated (see Ch. 4.2.3).

**Figure 4-1.** Properties of light (wave model)

**Refraction of light:** The velocity of light (as measured in air) is reduced if it enters substances of higher density (liquids, glasses, minerals). If the angle between the incident light rays and the phase boundary (e.g., air/glass) is different from 90°, the light rays change the propagation direction; they are refracted. Snell's Law of refraction applies (Fig. 4-2) as long as the materials involved are isotropic (cf. Ch. 4.1.2). In a thin section, the object ( $d = 25 \mu\text{m}$ ) lies embedded between epoxy resin and glass. As light velocity is almost identical in glass and epoxy resin, refraction occurs mainly at boundary surfaces between the object and epoxy resin, but also at phase boundaries within the object (Fig. 4-2).

The light velocity  $v$  of a specified material is an important parameter for its identification. For technical convenience, the refractive index  $n$  is used instead of velocity. The refractive index is defined as the ratio between light velocity  $v_0$  in vacuum (about the same as in air) and light velocity in the material studied. In isotropic materials, it can be determined experimentally by measuring the angles of refraction  $\alpha$  and  $\beta$ , whereby Snell's Law  $n_2/n_1 = \sin\alpha/\sin\beta$  applies. As light velocities in all solid and liquid substances are smaller than  $v_0$  ( $n_1 = n_{\text{air}} = 1$ ), refractive indices are generally larger than 1.

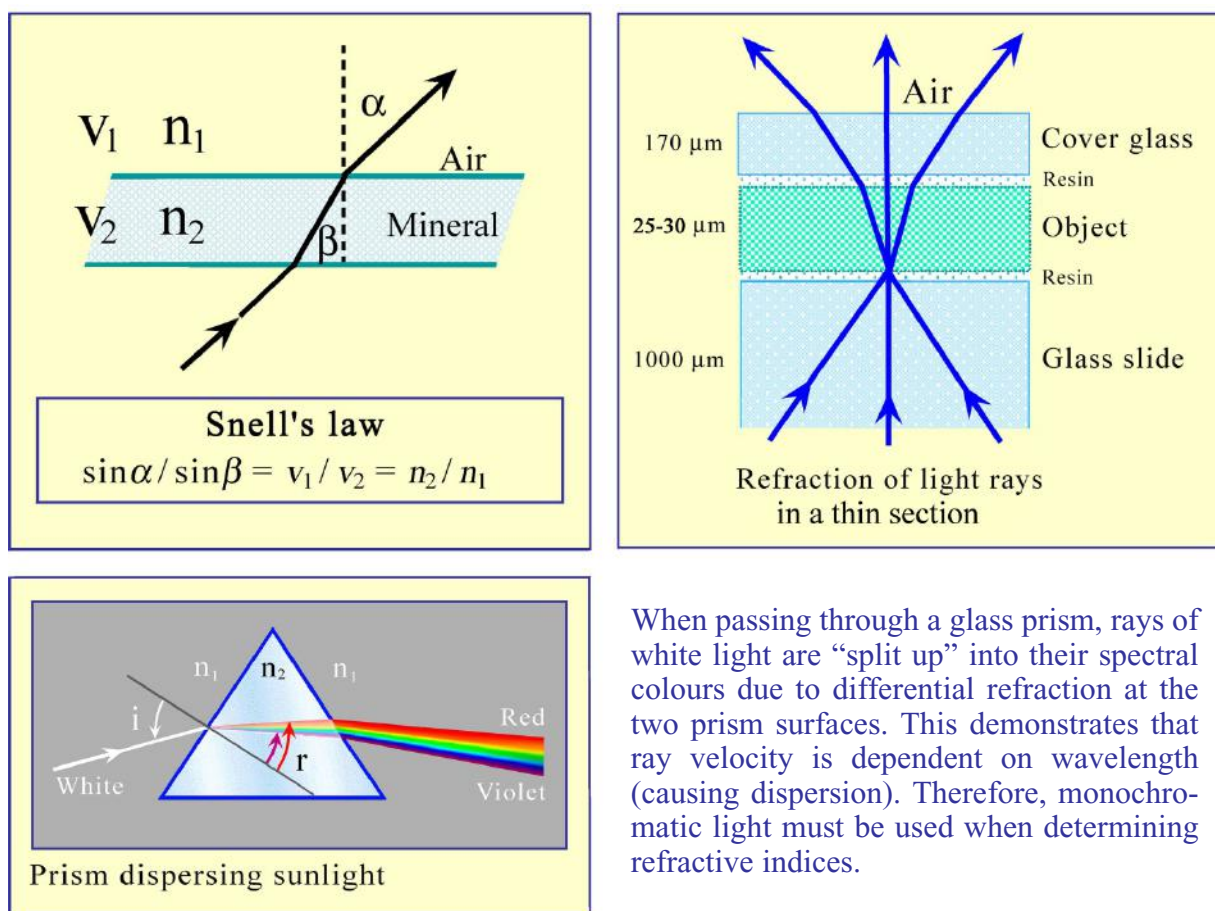


Figure 4-2. Refraction of light, dispersion

## 4.1.2 Isotropy and anisotropy

### Isotropic materials

Optically isotropic substances such as gases, liquids, glasses and the highly symmetric cubic minerals show optical behaviour that is independent of the direction of light propagation. This means, their optical properties (light velocity, refractive index and colour) are identical in all directions.

The three-dimensional propagation of light in an isotropic material can be presented graphically as 3-D models for wave or ray velocity and for refractive index, both of which are spheres (Fig. 4-3). The model preferred by mineralogists is the optical indicatrix, which describes the refractive index as a direction-dependent variable.

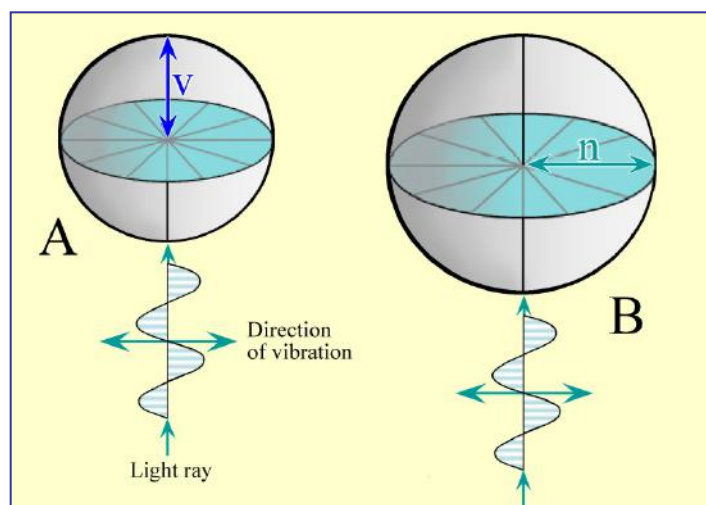


**Figure 4-3.** Isotropic substances; 3D surfaces of  $v$  and  $n$

**A. Ray velocity surface:** For each ray direction, the velocity value is represented by a specific distance from a chosen origin ( $v = 0$ ). The geometric form representing all directions of ray propagation is a sphere with radius  $v$ .

**B. Indicatrix:** For each ray direction, the refractive index is represented by a specific distance from a chosen origin and is marked off parallel to the vibration direction and perpendicular to the ray propagation direction. The geometric form representing the refractive index for all ray propagation directions is a sphere with radius  $n$ . Each ray propagation direction has an infinite number of potential vibration directions.

In thin section microscopy, glasses and cubic minerals generally show a single specific refractive index and colour independent of orientation (Fig. 4-4). An indication of crystal orientation in thin section can therefore only be derived from morphological properties, for example, crystal outlines or cleavage (Fig. 3-9). Another important characteristic of optically isotropic materials is that light waves do not experience any change in vibration direction. This means that E-W vibrating plane-polarized light waves maintain their E-W orientation after passing through the isotropic materials (glass, mineral). Therefore, they are blocked by the analyzer, which is a N-S oriented polarizer (Fig. 4-4 A,E).

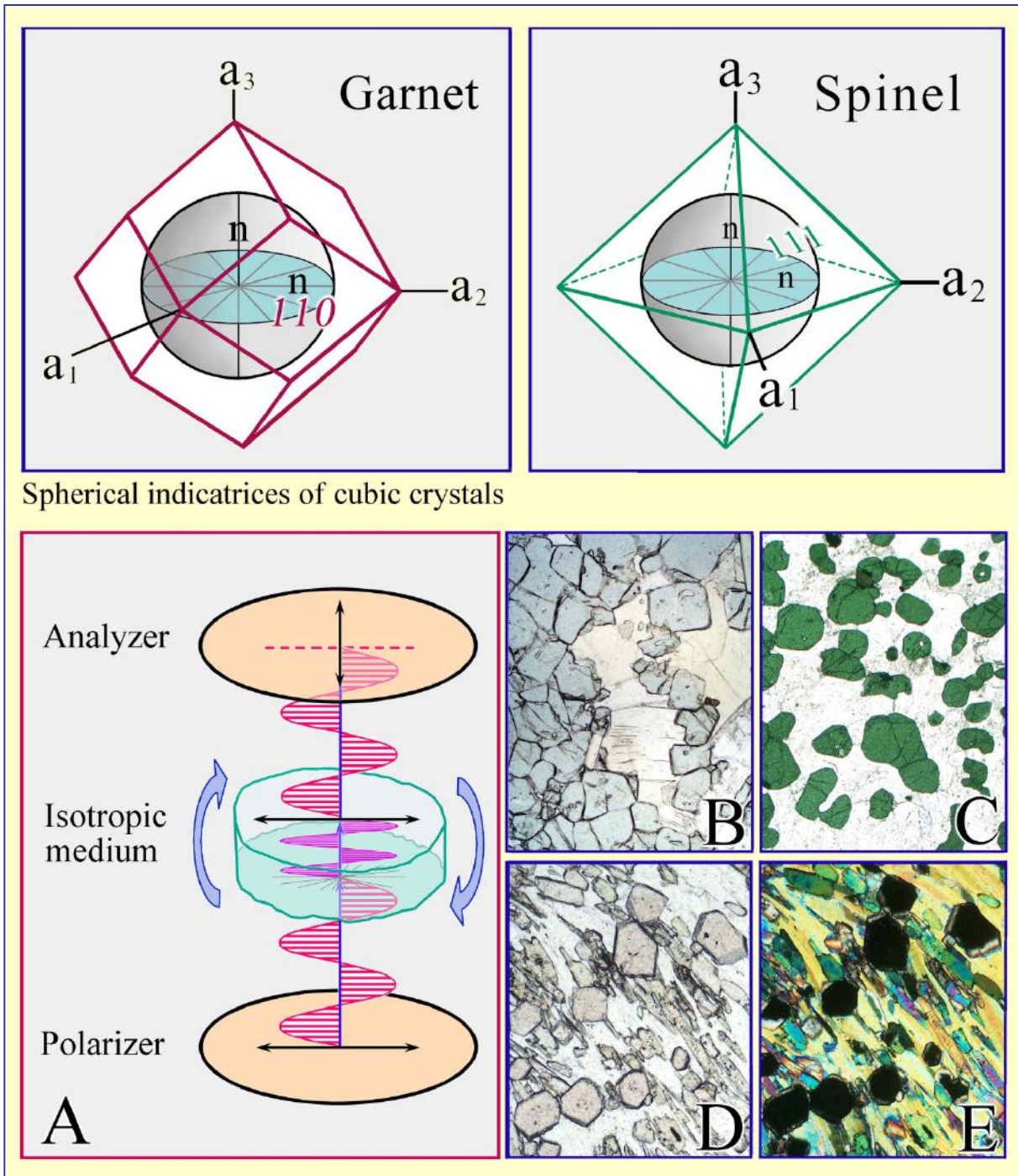


**Figure 4-4.** Isotropic substances

#### Behaviour of light when passing through an isotropic substance (glass or cubic mineral):

In plane-polarized light chemically homogeneous glasses or crystals of cubic minerals show the same colour independent of orientation and rotation of the stage (images B,C: MgFe-spinel; image D: almandine).

Under crossed polarizers (image A), glass and cubic mineral grains appear black independent of orientation and rotation of the stage (image E: almandine).

## Anisotropic materials

Light propagation in optically anisotropic materials is direction-dependent. All non-cubic crystalline substances (Fig. 3-1) are optically anisotropic. Light entering an anisotropic crystal is "split" into two light waves that vibrate orthogonal to each other (with exceptions applying to specific directions in the crystal). The two light waves propagate through the crystal with different velocities. This phenomenon is called double refraction (Fig. 4-5).

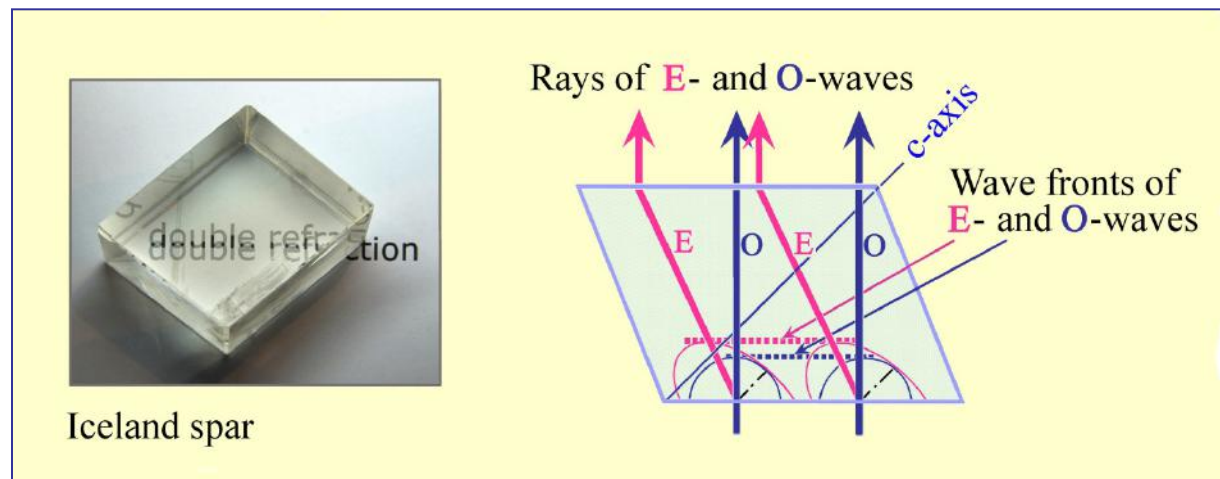


**Figure 4-5.** Double refraction in a calcite rhombohedron (Huygenian construction)

## Crystals of hexagonal, trigonal and tetragonal symmetry

The 3-D models for ray velocities (expressed as  $v$  or  $1/n$ ) in crystals of hexagonal, trigonal and tetragonal symmetry are therefore double surfaces (Fig. 4-6 A). They illustrate that one of the two light waves (O-wave) propagates like light in an isotropic substance, with the same velocity in all directions, while the other wave (E-wave) changes its velocity dependent on the direction in the crystal. The E-wave has either the highest or lowest value ( $v_e$ ) in the direction normal to the crystallographic c-axis. Any rotation away from this direction, towards the c-axis, will shift  $v_e$  towards the  $v_o$  value (decreasing if  $v_e > v_o$ , or increasing if  $v_e < v_o$ ). In an orientation parallel c,  $v_e$  has reached the same value as  $v_o$ . Thus, in this particular direction, the condition of optical isotropy is realised. This specific direction is referred to as the optic axis. Minerals belonging to the group of hexagonal, trigonal and tetragonal symmetry are optically uniaxial. The vibration directions of the waves are fixed within the crystal: the E-wave vibrates within the plane defined by the ray direction and the c-axis; the O-wave vibrates orthogonal to the E-wave.

Mineralogists prefer the single-surface indicatrix model for explaining optical phenomena over the double-surface model of light propagation. The construction principle is illustrated in Fig. 4-6 B: considering the centre of a crystal as the origin, the refractive indices of two light waves belonging to one wave normal and vibrating orthogonal to each other are marked off in proportional distances from the origin. Thus, a "refraction cross" is created which shows the short and long axes of an ellipse. A construction of the ellipses for all possible wave-normal directions in crystal space results in an ellipsoid which is the indicatrix.

The optical indicatrix of the crystal systems discussed here is an ellipsoid of revolution. It has either a prolate form ( $n_e > n_o$ ; optically uniaxial positive) or an oblate form ( $n_e < n_o$ ; optically uniaxial negative) (Fig. 4-6 C,D). The rotation axis (= optical axis) is identical to the c-axis.

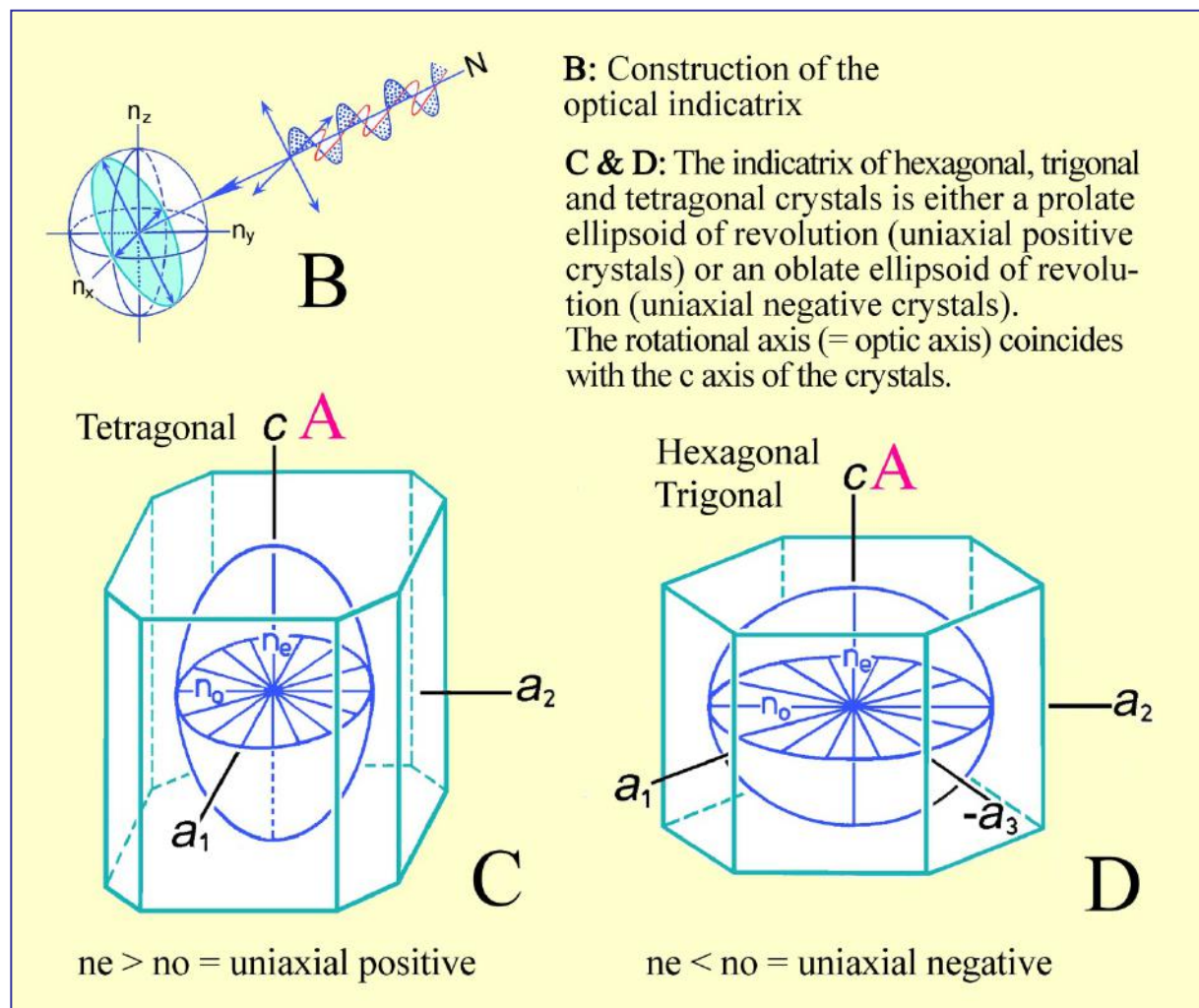
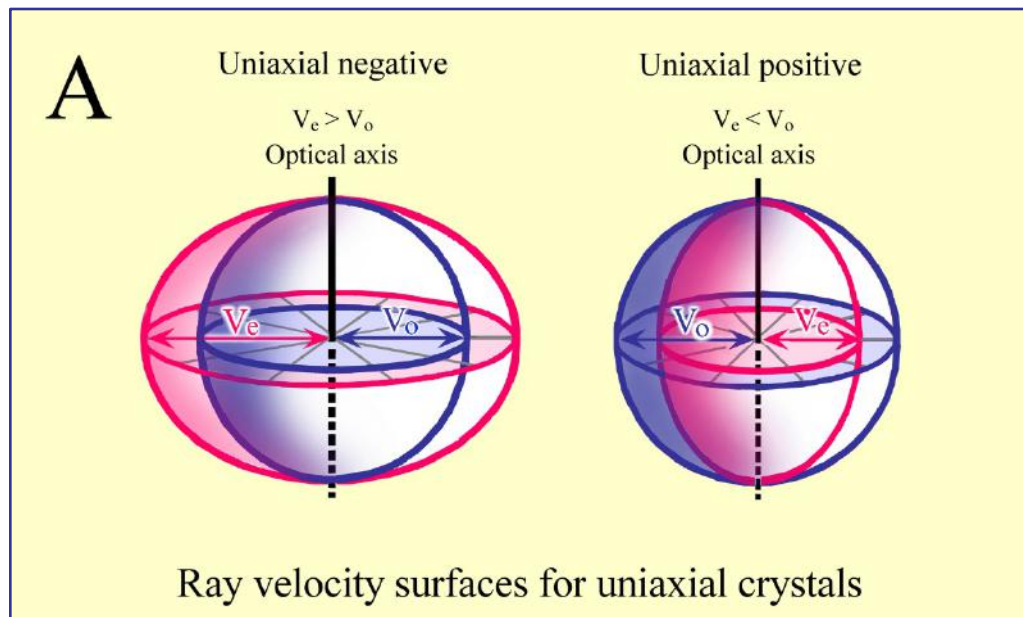


**Figure 4-6.** Optically uniaxial crystals; 3D surfaces of  $v$  and  $n$

A: 3D-surfaces of  $v$  and  $n$ ; B: Construction of the indicatrix; C-D: Indicatrices of optically uniaxial positive and negative crystals.

## Crystals of orthorhombic, monoclinic and triclinic symmetry

The propagation of both waves in crystals of such symmetry is direction-dependent. The resulting 3D two-surface models of ray velocities are complicated and have not had any impact on practical work. Microscopists prefer the single-surface indicatrix model for the explanation of optical phenomena (Fig. 4-7).

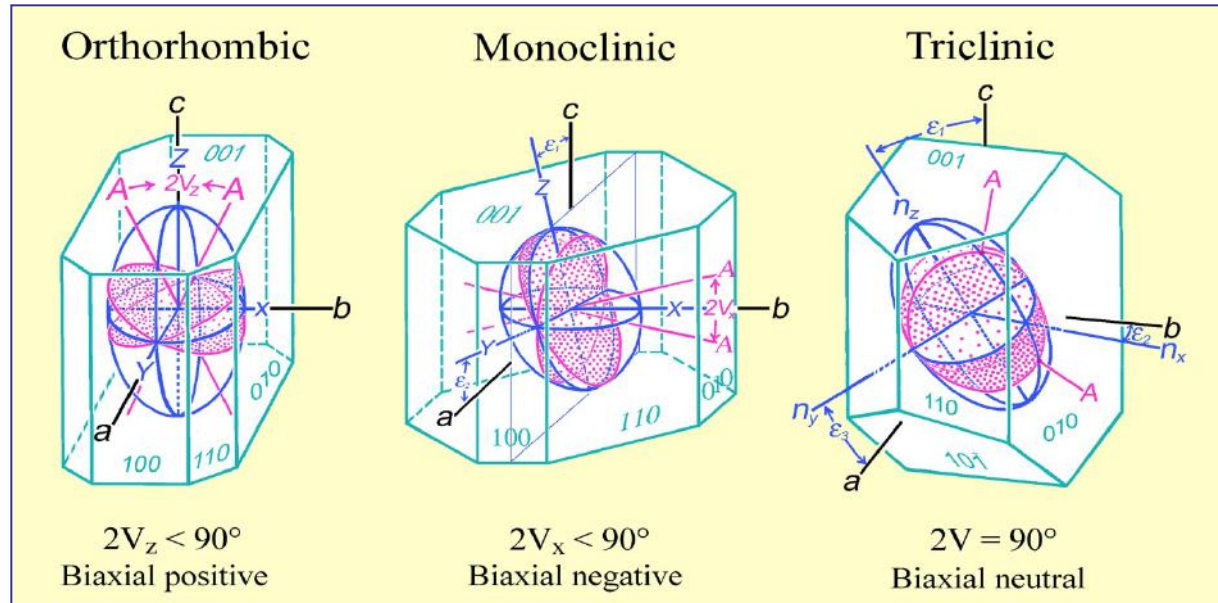


Figure 4-7. Optically biaxial crystals, crystal symmetry and indicatrix

The indicatrix of crystals with orthorhombic, monoclinic and triclinic symmetry is represented in a coordinate system with axes X, Y, Z that are orthogonal to each other. The geometry of the triaxial ellipsoid is defined by the proportional lengths of the refractive indices  $n_x$ ,  $n_y$ ,  $n_z$  on X, Y and Z. Thus, the symmetry of the ellipsoid is generally orthorhombic. The refractive indices are defined as  $n_z > n_y > n_x$  (or  $n_\gamma > n_\beta > n_\alpha$ ).

There are two circular sections with the radius  $n_y$ . Orthogonal to these circular sections, light propagates with the same velocity as in an isotropic substance. These two directions correspond to the two optic axes A. The low-symmetry crystals are therefore optically anisotropic-biaxial.

The optic axes lie in the ZX plane (= optic axial plane OAP). Y is orthogonal to the OAP. The angle between the optic axes ( $2V$ ) is mineral-specific and can attain values between  $0^\circ$  and  $90^\circ$ . If Z dissects the acute angle ( $2V_z < 90^\circ$ ), the crystal is biaxial-positive; if X dissects the acute angle ( $2V_x < 90^\circ$ ), the crystal is biaxial-negative. If the axial angle is  $90^\circ$ , the crystal is optically neutral.

The spatial orientation of the indicatrix in a crystal is defined by the crystal's symmetry:

- In crystals of orthorhombic symmetry, the ellipsoid axes (X, Y, Z) correspond to the crystallographic axes (a,b,c). Which indicatrix axis is parallel to which crystallographic axis depends on the specific mineral.
- In crystals of monoclinic symmetry, it is only the crystallographic b axis and one of the indicatrix axes that are parallel (commonly Y). The other two axes lie in the symmetry plane (010) and form angles with the crystallographic axes a and c.
- In triclinic crystals, none of the axes of the orthorhombic indicatrix is parallel to any of the crystallographic axes. The indicatrix axes form mineral-specific angles with the crystallographic axes.

## 4.2 Optical characteristics used for mineral determination

### 4.2.1 Colour and pleochroism

The intensity of white light can be variably decreased due to absorption as it passes through the thin section. If absorption wavelengths are outside the visible spectrum, glass phase and minerals appear colourless (white to greyish). Colours are generated if selective absorption affects certain parts of the spectrum more than others. Colour and colour intensity are important mineral-specific properties.

Practical hints: Colour intensity increases with sample thickness. In a standard thin section (25-30 µm thickness) wedge-shaped edges of grains or crystals thinner than 25 µm show a distinctly paler colour. In minerals with a high refractive index ( $n > 1.6$ ) weak colours may be masked by the minerals' chagrin (see 4.2.2). Chagrin effects can be minimised if absorption colours are observed at high magnification (objective magnification  $M > 20x$ ), with the auxiliary condenser inserted and aperture diaphragm completely open. Furthermore, it should be noted that the colour hue depends to some degree on the temperature of the light source. This can be adjusted to correspond to the colour temperature of natural light by changing light intensity and using appropriate filters (e.g., a blue filter).

**In optically isotropic substances** (glass phase, cubic minerals) light absorption is identical in all directions. Glasses and cubic crystals therefore show a single colour, no matter how the crystals are sectioned, as long as they are chemically homogeneous. The colour does not change if the stage is turned (Fig. 4-8). Colour and colour intensity provide clues to type and concentration of colour-inducing cations. This can be demonstrated using glasses and spinel group minerals of different composition (Fig. 4-9).

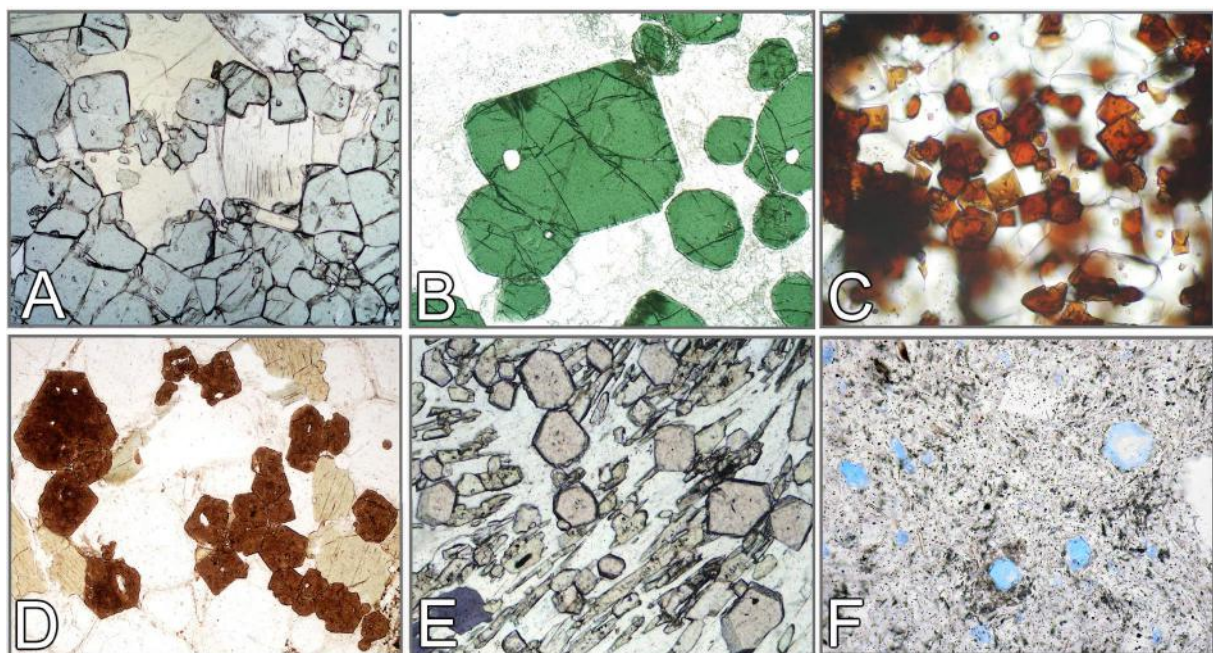


**Figure 4-8.** Optically isotropic phases such as the cubic minerals shown here generally display a single colour, independent of orientation. A-C: MgFe-spinel, hercynite, magnesioferrite. D,E: melanite, almandine. F: hauyne.

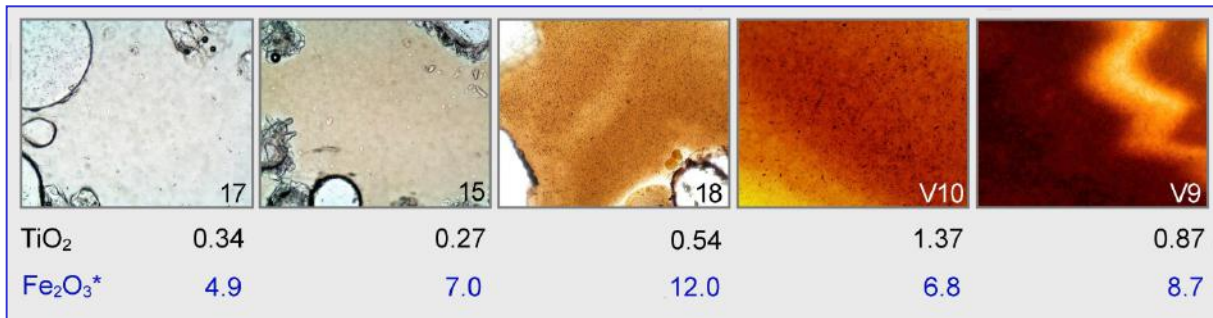


**Figure 4-9 A.** Relationship between colour of the glass phase from slags of coal-fired boilers and the content in staining components TiO<sub>2</sub> and Fe<sub>2</sub>O<sub>3</sub> (wt.%)

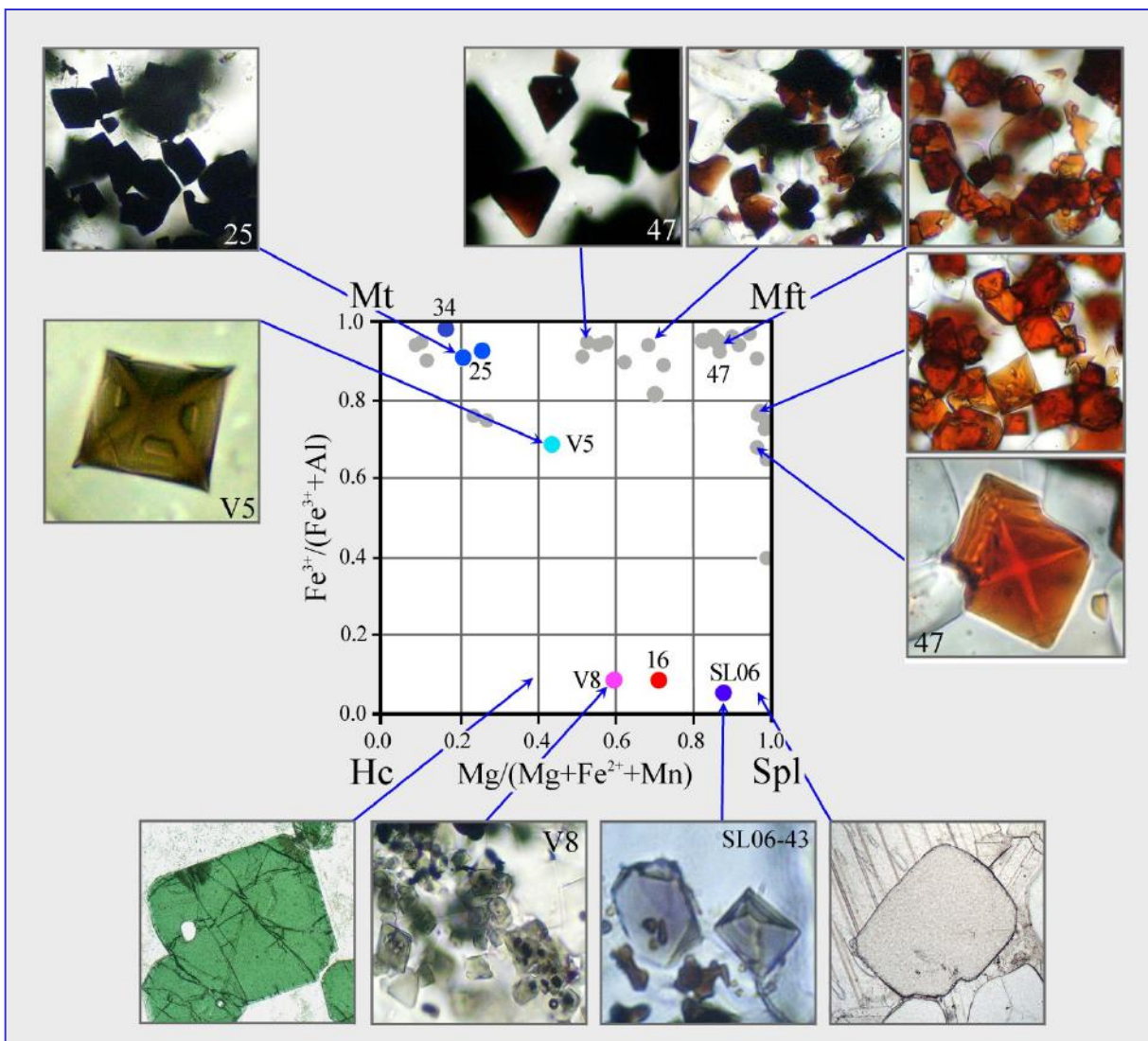


**Figure 4-9 B.** Relationship between mineral colour and composition of spinels in the system magnetite-magnesioferrite-hercynite-spinel. Spinel samples are partly from slags and sinters in coal-fired boilers (numbered samples) and partly from natural rocks.

In optically anisotropic substances (non-cubic minerals), absorption is a directional property. Thus, crystals of a single mineral species can display different colours dependent on their orientation and corresponding light vibration directions. Colours and pleochroism are mineral-specific properties.

The majority of minerals do not show any, or only weak, pleochroism. Exceptions displaying strong pleochroism are tourmaline, members of the amphibole group, Fe-Ti-rich biotites, and less common minerals such as piemontite, sapphirine, dumortierite and yoderite. Fig. 4-10 shows examples of distinct to strong pleochroism.

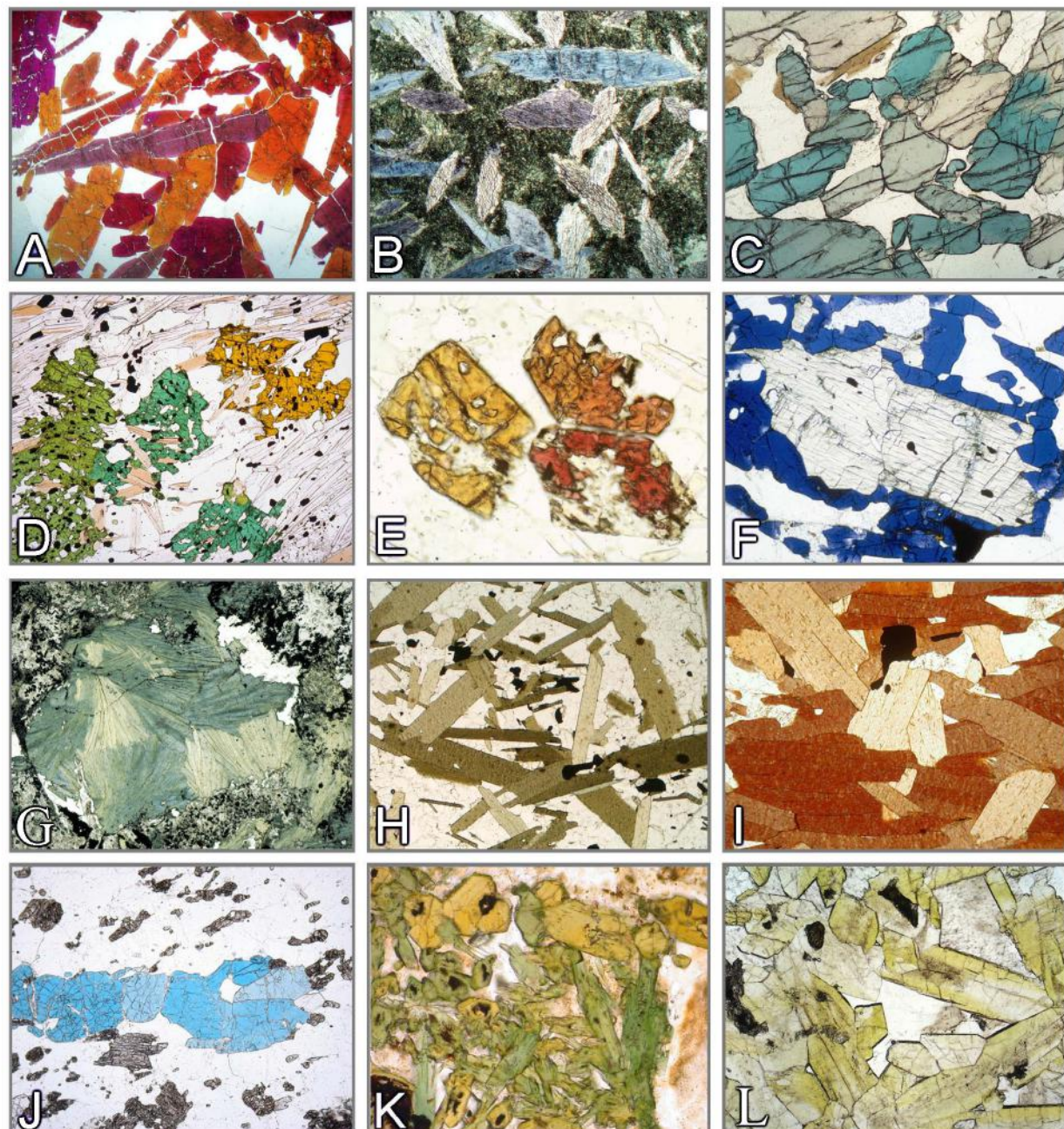


**Figure 4-10.** Examples of distinct to strong pleochroism.

A: Piemontite. B: Glauconaphane. C: Sapphirine. D: Viridine. E: Thulite. F: Yoderite (by courtesy of Dr. N. Jöns, Universität Bremen). G: Chloritoid. H: Biotite. I: Ti-rich biotite. J: Lazulite. K: Aegirine augite. L: Fe<sup>3+</sup>-rich epidote (pistacite).

**Pleochroic minerals of tetragonal, hexagonal and trigonal symmetry** show two specific absorption colours (dichroism), parallel to the vibration directions of the E- and O-waves. Sections orthogonal to the crystallographic c-axis (= optic axis) generally show the absorption colour of the O-wave as the microscope stage is rotated. Sections parallel to the c-axis show an alternation between the absorption colour of the E-wave (E-W orientation of the c-axis) and the O-wave (N-S orientation of the c-axis) for every 90° rotation of the stage (Fig. 4-11 and Fig. 4-12: example tourmaline).

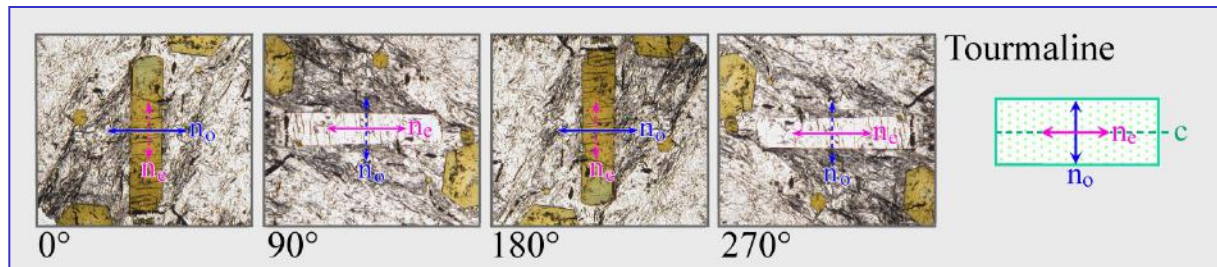


**Figure 4-11.** Change of absorption colour of tourmaline during a 360° rotation of the microscope stage. Shown are the four positions of a crystal section in which the vibration directions of the two waves coincide exactly with the directions of the polarizers. In these orientations, only the E-W vibrating wave passes the crystal; the N-S wave is not activated.

**Pleochroic minerals of orthorhombic, monoclinic and triclinic symmetry** possess three characteristic absorption colours (trichroism) related to vibration directions parallel to the principal indicatrix axes X, Y and Z. The determination of these colours must be performed on selected crystal sections that are parallel to two of these axes (Fig. 4-14 A-C). The relation between crystal orientation, vibration direction and absorption (pleochroism) for members of the amphibole group is explained in Figs. 4-15, 16, 17. As the example of the amphiboles demonstrates beautifully, there is a correlation between absorption colour and chemical composition (Fig. 4-13).

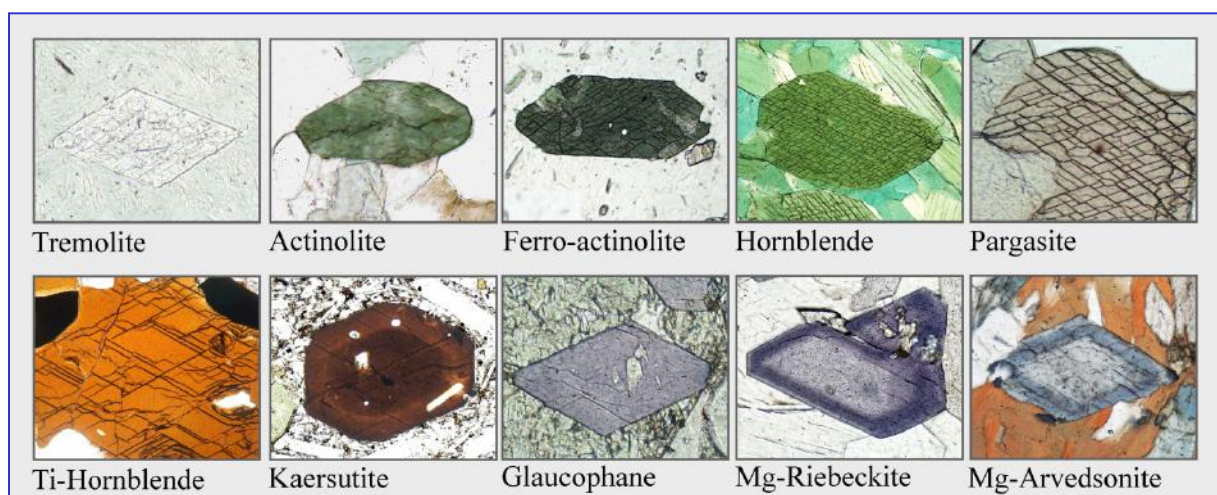
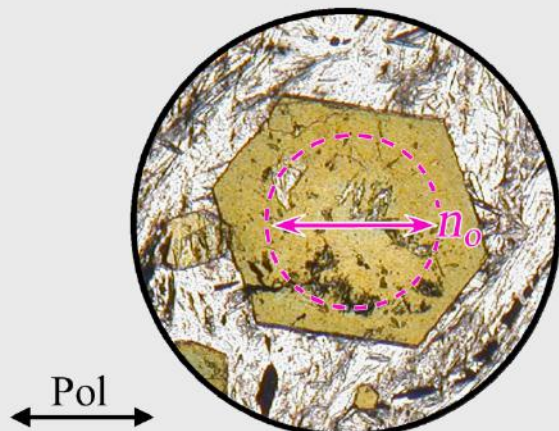
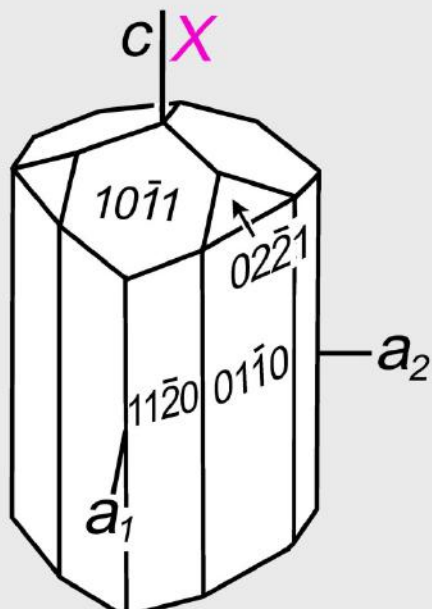


**Figure 4-13.** Colours of amphiboles of different composition, in relation to the principal vibration direction parallel b. The amphibole grains are oriented such that the b-axis is in alignment with the lower polarizer. In these minerals, b is parallel to the indicatrix axis Y. Hence, the colours displayed correlate with Y (cf. Fig. 4-15).

# Tourmaline

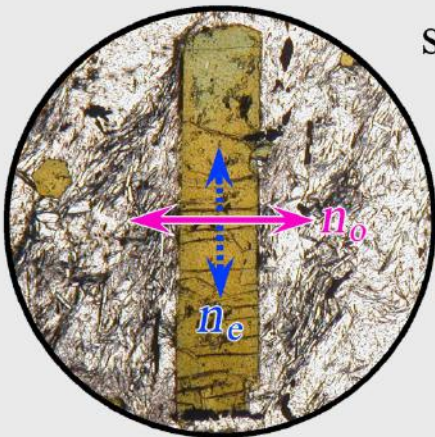
(0001) section



colour || O-wave

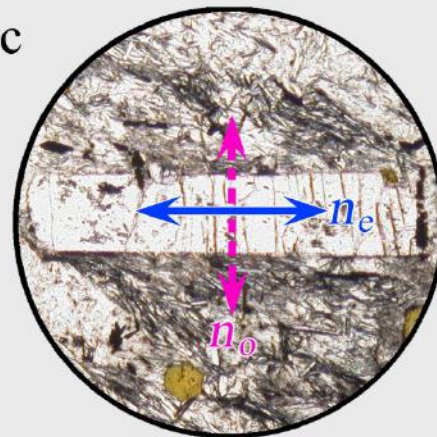
Basal section shows O-waves only, independent of the rotation of the stage (light path parallel to the direction of optical isotropy, i.e., parallel to the optic axis).

section || c



colour || O-wave

Longitudinal section aligned N - S:  
Only O-waves pass through the crystal.



colour || E-wave

Longitudinal section aligned E - W:  
Only E-waves pass through the crystal.

**Figure 4-12.** Determination of the colours relating to the vibration directions of the E- and O-waves of an optically uniaxial mineral, using tourmaline as an example.

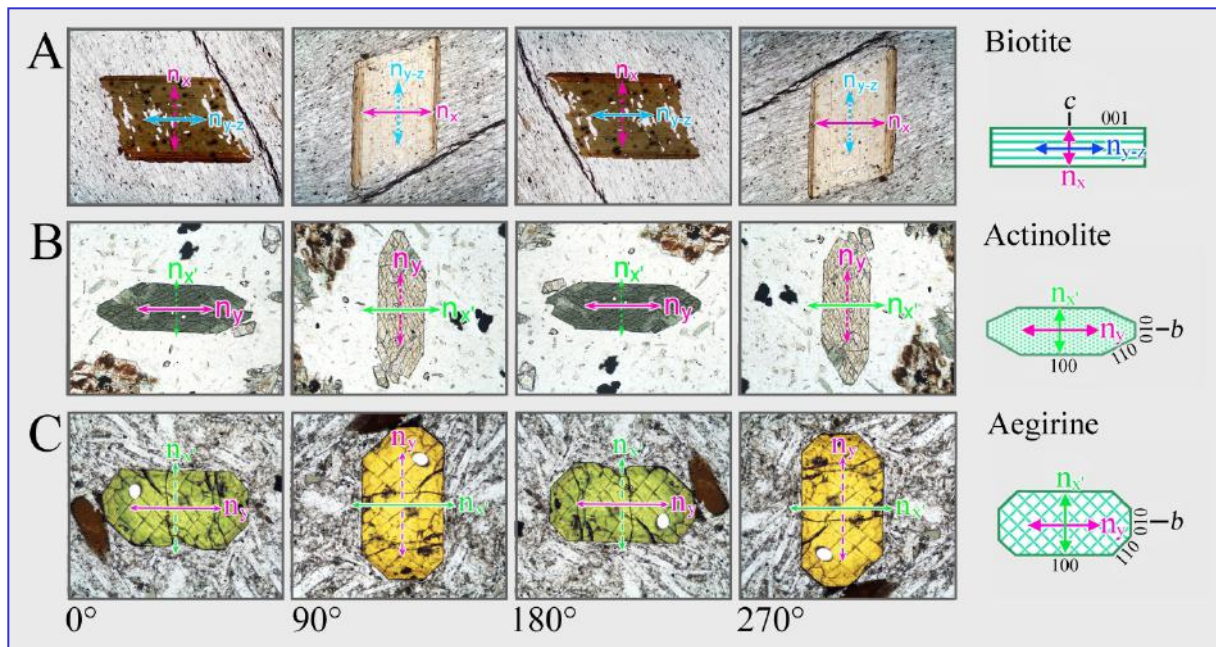


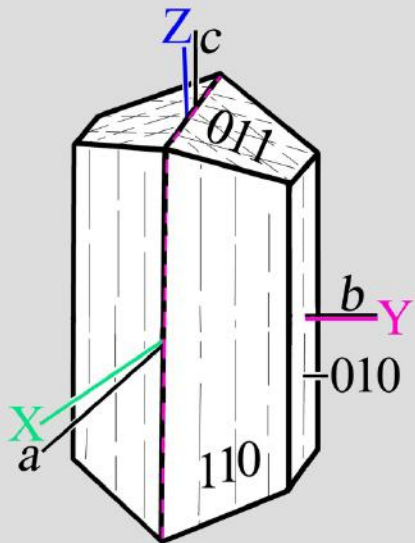
**Figure 4-14 A-C.** Change of absorption colour in crystal sections of biotite, actinolite and aegirine-augite as the stage is rotated 360°. Shown are the four positions in which the vibration directions of the two waves coincide exactly with the directions of the polarizers. In these orientations only the E-W vibrating wave passes the crystal; the N-S wave is not activated. Therefore, these crystal sections change their colour every 90° of rotation. In the actinolite and aegirine-augite sections, these are the colours relating to the  $n_y$  and  $n_x'$  waves, and in biotite, the colours relating to the  $n_{z-y}$  and  $n_x$  waves.

As far as clinoamphiboles are concerned, the absorption colours parallel to X, Y and Z are determined in two specific sections (Figs. 4-15, 16, 17):

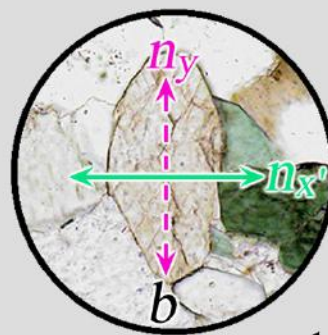
- (1) In crystal sections parallel to (010), the vibration directions Z and X are in the viewing plane, except for some rare alkaline amphiboles. Such sections are commonly prismatic in shape and can be recognised by their high interference colours ( $\Delta n = n_z - n_x$ ) (see Ch. 4.2.3).
- (2) In crystal sections perpendicular to c, the vibration directions Y (parallel to b) and X' are in the viewing plane. These crystal sections are recognised by the characteristic intersection of the {110} cleavage planes.

Crystal sections perpendicular to one of the two optic axes appear in a single colour corresponding to Y as the stage is turned ( $n_y$  wave only).

# Actinolite

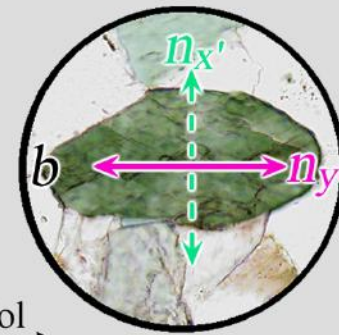


Section  $\perp c$



Colour  $\parallel X'$

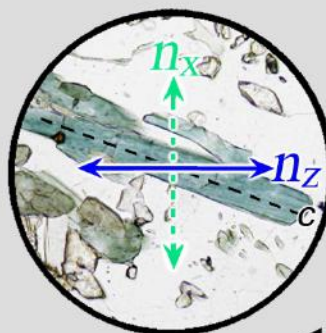
Wave with  $n_x$  vibrates E - W;  
wave with  $n_y$  is not activated.



Colour  $\parallel Y, b$

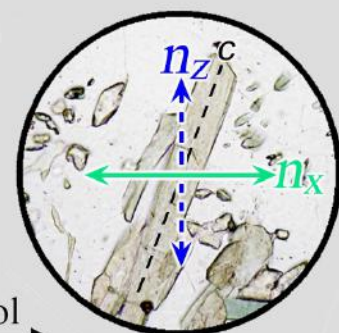
Wave with  $n_y$  vibrates E - W;  
wave with  $n_x$  is not activated

(010) Section



Colour  $\parallel Z$

Wave with  $n_z$  vibrates E - W;  
wave with  $n_x$  is not activated.



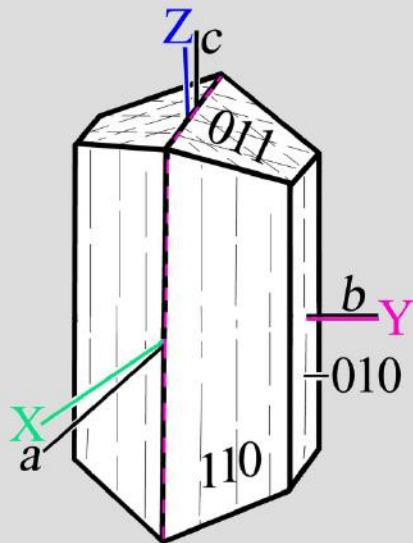
Colour  $\parallel X$

Wave with  $n_x$  vibrates E - W;  
wave with  $n_z$  is not activated.

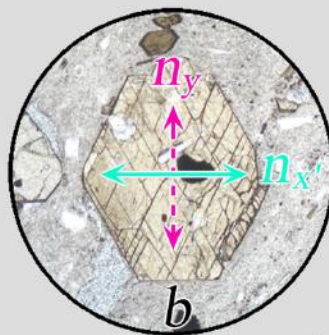
**Actinolite:**  
 $Z$  -- blue-green  
 $Y$  -- green  
 $X$  -- pale yellow-green

**Figure 4-15.** Determination of the colours for the principal vibration directions  $Z$ ,  $Y$  and  $X$  of an optically biaxial mineral, using actinolite,  $\text{Ca}_2(\text{Mg},\text{Fe}^{2+})_5[\text{Si}_8\text{O}_{22}](\text{OH})_2$ , as an example.

# Kaersutite

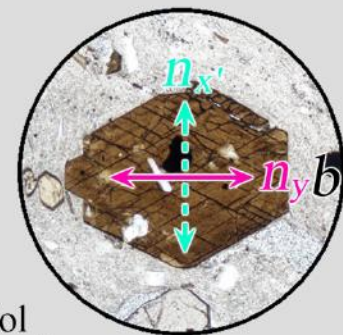


Section  $\perp c$



Colour  $\parallel X'$

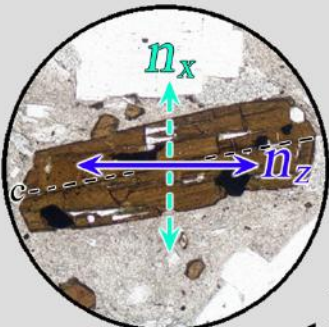
Wave with  $n_{x'}$  vibrates E - W;  
wave with  $n_y$  is not activated.



Colour  $\parallel Y, b$

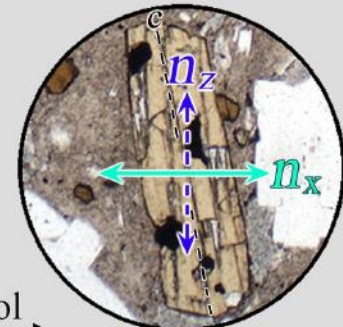
Wave with  $n_y$  vibrates E - W;  
wave with  $n_{x'}$  is not activated.

(010) Section



Colour  $\parallel Z$

Wave with  $n_z$  vibrates E - W;  
wave with  $n_x$  is not activated.



Colour  $\parallel X$

Wave with  $n_x$  vibrates E - W;  
wave with  $n_z$  is not activated.

Kaersutite:

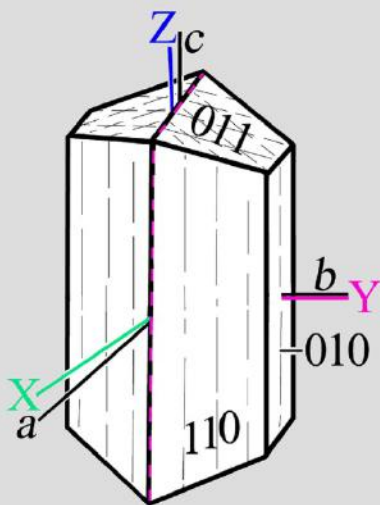
**Z** -- greenish brown

**Y** -- reddish brown

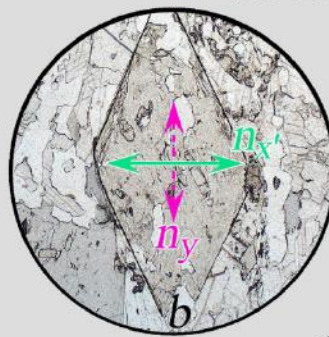
**X** -- brownish yellow

**Figure 4-16.** Determination of the colours in the principal vibration directions **Z**, **Y** and **X** of an optically biaxial mineral, using kaersutite,  $\text{NaCa}_2\text{Mg}_3\text{Fe}^{2+}(\text{Ti},\text{Fe}^{3+})[\text{Al}_2\text{Si}_6\text{O}_{22}](\text{OH})_2$ , as an example.

# Glaucophane

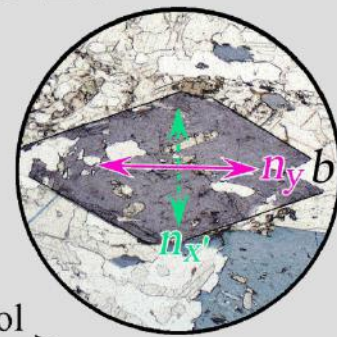


Section  $\perp c$



Colour  $\parallel X'$

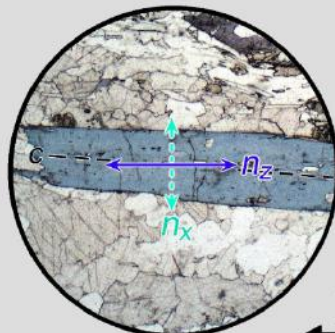
Wave with  $n_x'$  vibrates E - W;  
wave with  $n_y$  is not activated.



Colour  $\parallel Y, b$

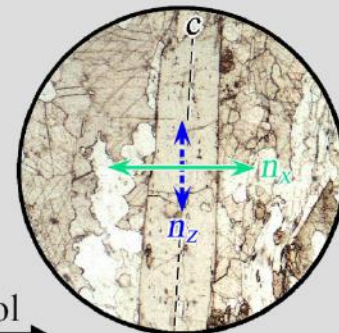
Wave with  $n_y$  vibrates E - W;  
wave with  $n_x'$  is not activated

(010) Section



Colour  $\parallel Z$

Wave with  $n_z$  vibrates E - W;  
wave with  $n_x$  is not activated.



Colour  $\parallel X$

Wave with  $n_x$  vibrates E - W;  
wave with  $n_z$  is not activated.

Glaucophane:

Z -- ultramarine

Y -- lavender-blue

X -- light yellow

**Figure 4-17.** Determination of the colours in the principal vibration directions Z, Y and X of an optically biaxial mineral, using glaucophane,  $\text{Na}_2(\text{Mg},\text{Fe}^{2+})_3(\text{Al},\text{Fe}^{3+})_2[\text{Si}_8\text{O}_{22}](\text{OH})_2$ , as an example.

#### 4.2.2 Light refraction (relief, chagrin, Becke line)

Refractive indices are important characteristics for identifying minerals. Their values cannot be determined directly in thin section, but must be estimated from a comparison with the embedding medium (epoxy resin;  $n$  about 1.54) or with minerals of known refractive indices, using light refraction effects. Criteria for doing this are relief, chagrin and the Becke line.

##### Relief

Mineral grains that have higher or lower refractive indices than their immediate surroundings show distinct contours and appear to lie higher or lower than the adjacent materials. The relief is a result of refraction and internal total reflection of light rays at the interface between the mineral grain and its surroundings. The higher the difference between the respective refractive indices, the more pronounced are grain outline and relief. Both disappear if the refractive indices of adjacent materials are identical (Fig. 4-18).

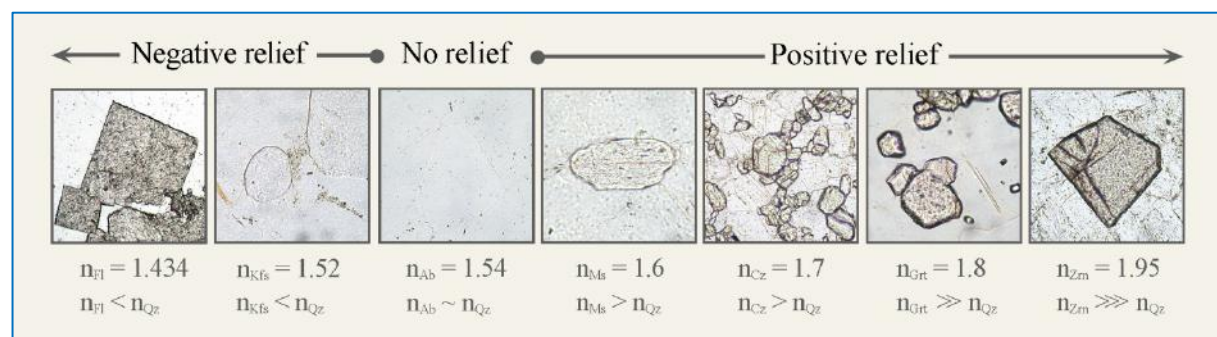
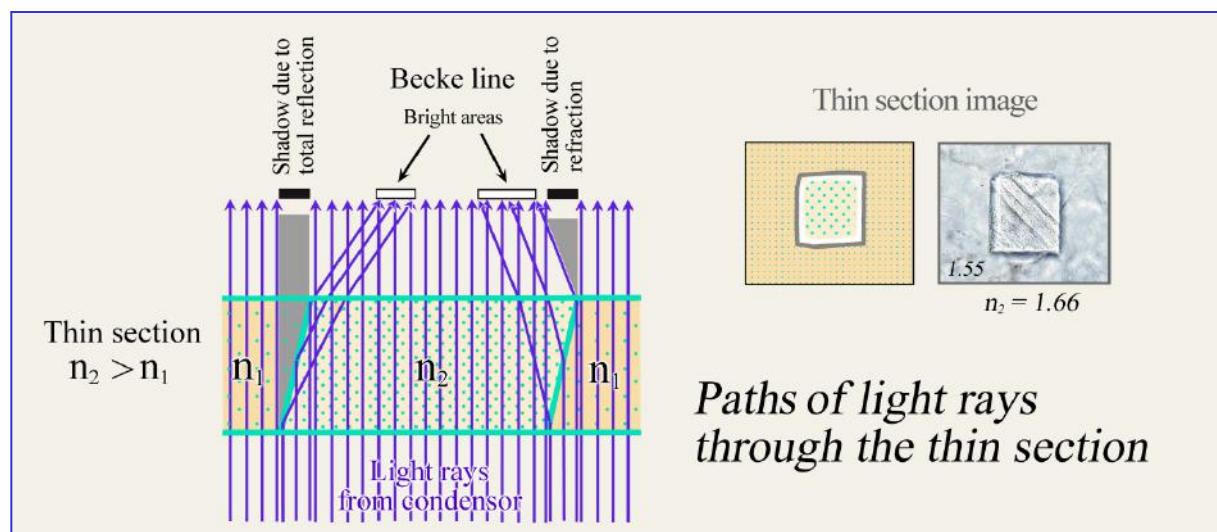


**Figure 4-18.** Generation of relief by refraction of light rays at grain boundaries. The lower sequence shows, from left to right, grains of fluorite (Fl), K-feldspar (Kfs), albite (Ab), muscovite (Ms), clinozoisite (Cz), garnet (Grt) and zircon (Zrn) in quartz ( $n_{\text{Qz}} = 1.544-1.553$ ).

### Chagrin (surface roughness)

The upper and lower surfaces of minerals in thin section (in polished sections only the lower surface) show relief due to minute roughness, unevenness and cracks. If the minerals have higher or lower refractive indices than the embedding medium (epoxy resin,  $n = 1.54$ ), refraction and reflection of light rays will occur at this micro-relief. As a result, the grain surfaces display a finely pitted structure in the microscope, which is referred to as chagrin (French for grained leather). The larger the difference of the refractive indices between mineral and epoxy resin, the more pronounced is the chagrin as the proportion of totally reflected and scattered light increases (Fig. 4-19).

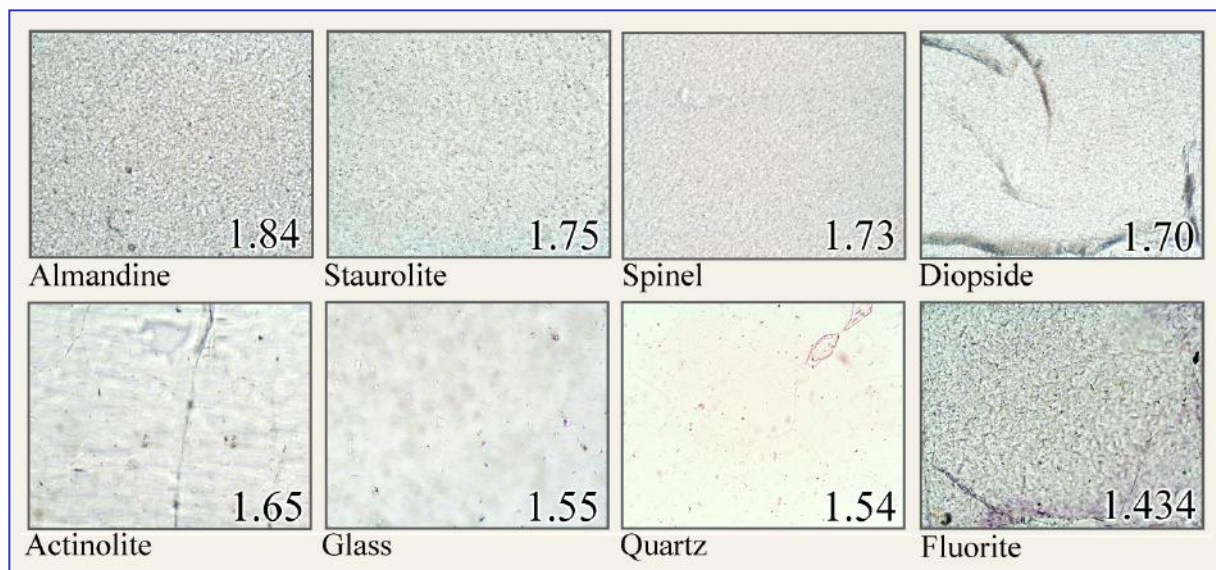


**Figure 4-19** Chagrin in relation to the refractive index of a mineral.

Practical hints: The chagrin contrast may be modified by changing the illumination conditions: (1) putting the auxiliary condenser lens into the light path and opening the aperture diaphragm decrease the chagrin effect; (2) closing the aperture diaphragm and swinging out the condenser lens increases the effect. For an estimation of the light refraction of an unknown mineral using the chagrin contrast, the illumination conditions and magnification should be kept constant (i.e., small aperture by closing the aperture diaphragm; 20x objective).

Furthermore, it should be noted that the chagrin contrast is generally low in polished microprobe sections, as light scattering is only occurring at the rougher lower surface of the minerals.

Note also that a clouding due to finely disseminated mineral and fluid inclusions can give an impression of higher chagrin than the host material actually has.

## Becke Line

At the boundary between two substances of different refractive index (crystal–epoxy resin, crystal–glass, crystal–crystal) a bright fringe, the Becke Line, is observed at high magnification. When closing the aperture diaphragm, this fringe may show colours, particularly if the minerals show a small difference in refractive index but a large difference in dispersion. The Becke Line is named after Friedrich Becke (1855–1931).

If this phase boundary is defocused by raising or lowering the stage slightly, the light fringe moves from one phase into the adjacent one: When lowering the stage it moves into the higher refractive substance, and when raising the stage into the lower-refractive substance. An explanation of this phenomenon is given in Fig. 4-20, left-hand side.

The intensity of the Becke Line decreases as the difference in refractive indices between the adjacent substances decreases. It disappears completely if the indices are identical. Differences in the refractive indices in the order of 0.001 to 0.002 can still be recognised. On the other hand, the Becke Line is obscured at high differences in refractive index by the strong chagrin.

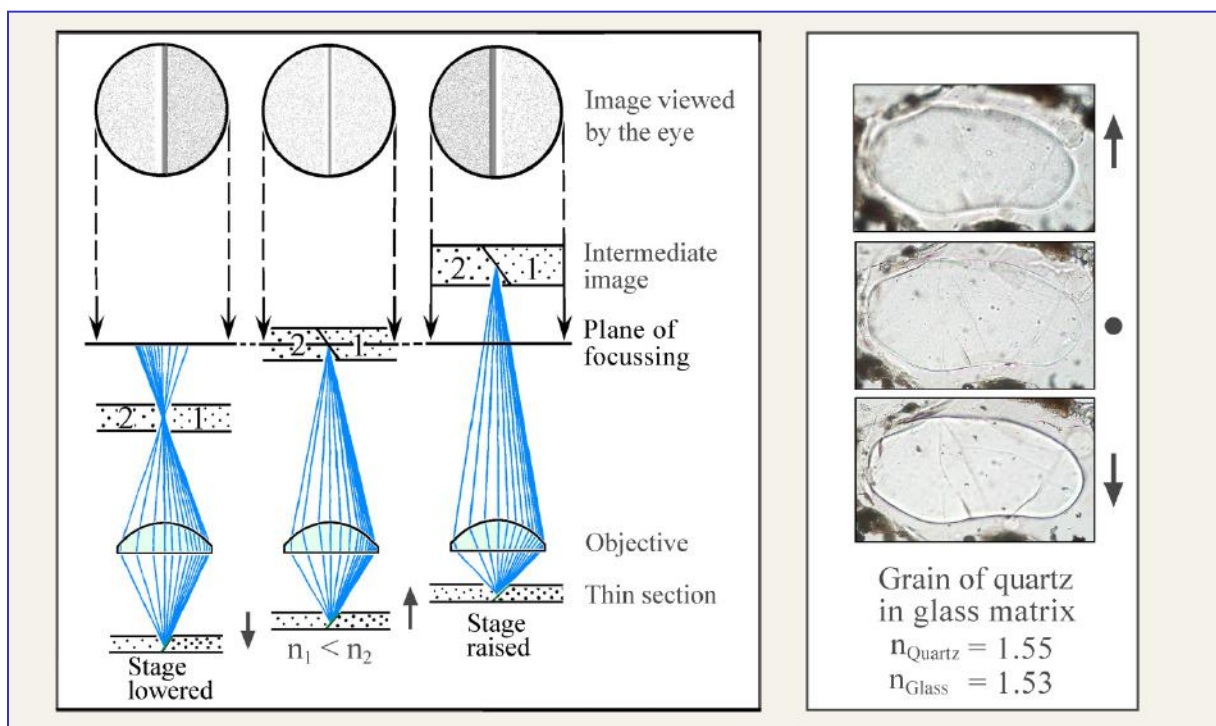


**Figure 4-20.** Generation of the Becke Line (left); movement of the Becke Line at the quartz-glass interface as a result of raising or lowering the stage.

Practical hints: For observation of the Becke Line, a steeply inclined, but not vertical, clean boundary between two phases must be chosen. Suitable are also broken-off grain boundaries bordering on epoxy resin (in break-outs or at the thin section edge). The phase boundary is then viewed with sufficiently high magnification (20x objective), the contrast is optimised by closing the aperture diaphragm, and the sense of movement of the Becke Line is studied by raising and lowering the stage slightly (Fig 4-20, right-hand side).

#### 4.2.3 Double refraction

In non-cubic, optically anisotropic crystals, light propagates in all directions as two sets of orthogonally vibrating plane-polarized waves, except for directions parallel to an optic axis. The two waves have different velocities (and correspondingly different refractive indices  $n_z'$  and  $n_x'$ ).

The specific relation between crystal symmetry and indicatrix in each mineral species defines the orientation of the polarization plane and the refractive index of the two waves (Ch. 4.1.2; Figs. 4-6,7). For every crystal section seen in thin section, these parameters can be derived from the ellipse created by the intersection of the indicatrix and the thin section plane (Fig. 4-21).

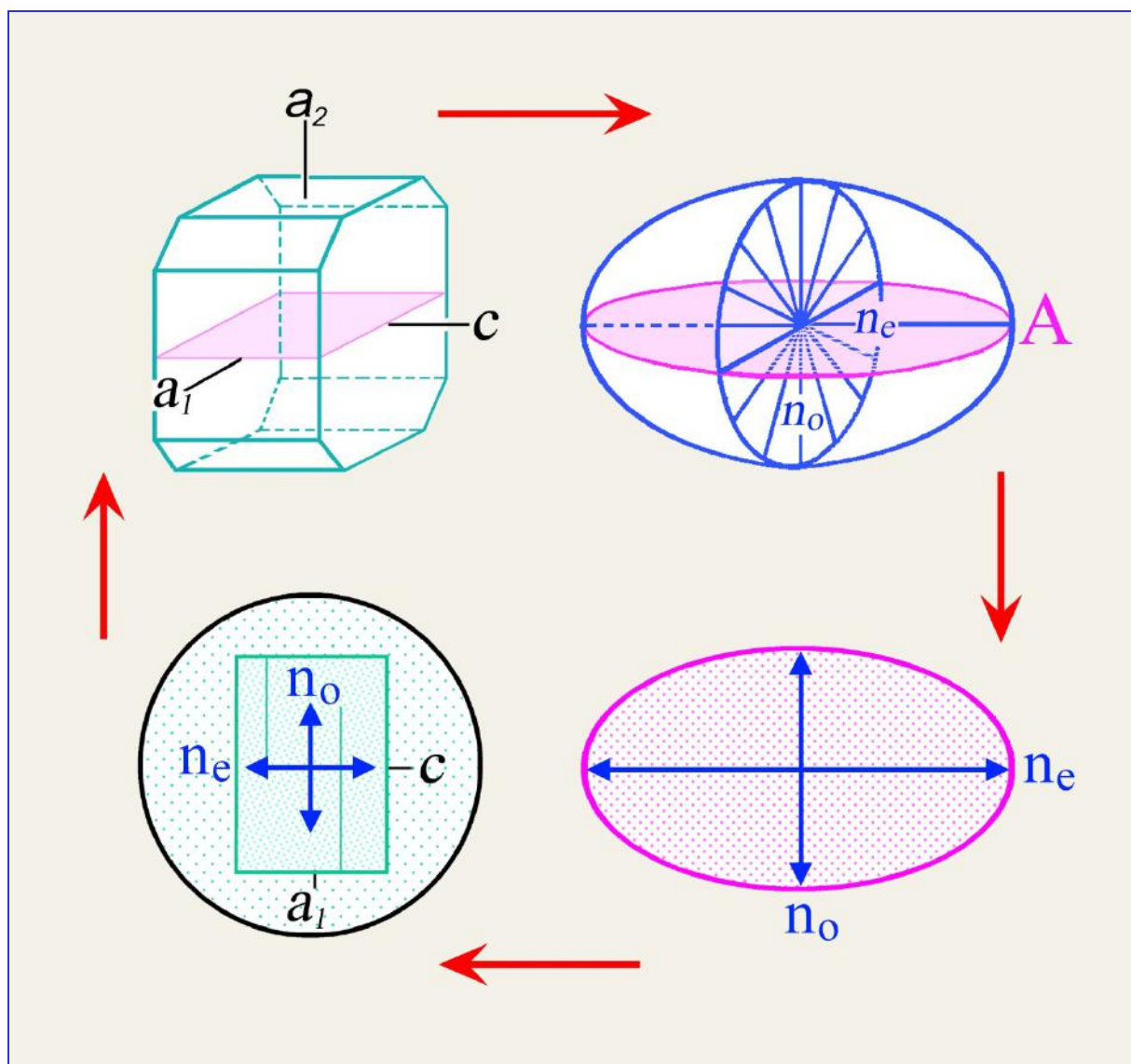


**Figure 4-21.** Relationship between crystal section, crystal orientation and indicatrix orientation using melilite as an example.

#### 4.2.3.1 Observation without analyzer (plane-polarized light mode)

In plane-polarized light, anisotropic minerals can only be distinguished from isotropic minerals if characteristic grain shapes are observed (e.g., elongate or platy habit), if the grains display relief changes such as chagrin contrast as the stage is turned (only in minerals with large differences in  $n_z'$  and  $n_x'$ ), or if the absorption colour changes with changing orientation (pleochroism).

The birefringence ( $\Delta n$ ) of minerals is commonly not large enough to create distinct chagrin effects, with the exception of carbonates. Fig. 4-22 shows the striking change of chagrin in calcite and dolomite due to their extreme birefringence ( $\Delta n = 0.172_{\text{Cal}}$  resp.  $0.177_{\text{Dol}}$ ).

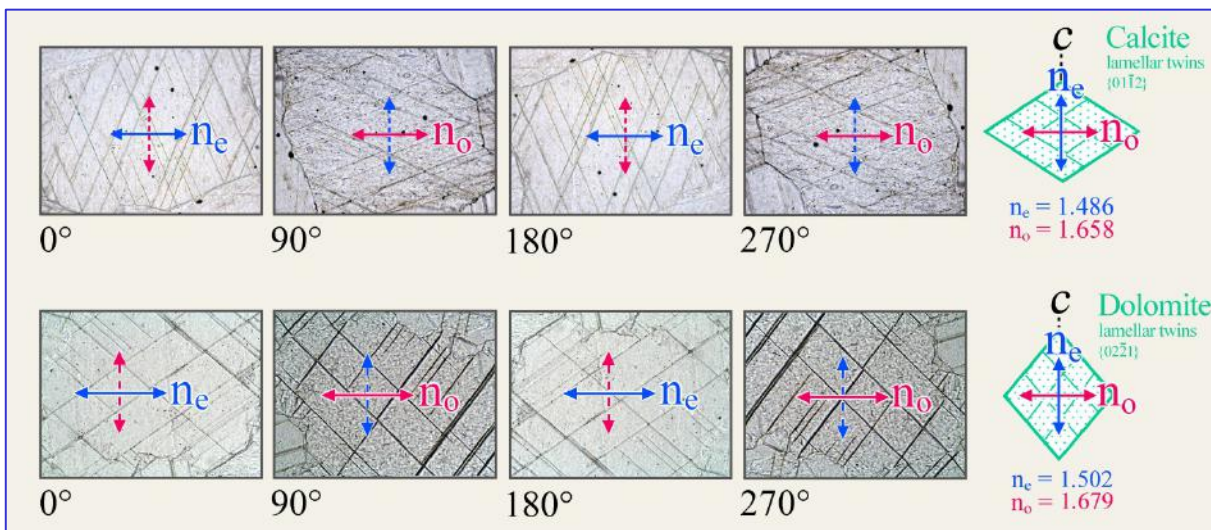


**Figure 4-22.** Change of chagrin in calcite and dolomite during a 360° rotation of the stage.

Crystal sections are oriented parallel to the c axis. Shown are the four positions where the vibration directions of the two waves in the crystal coincide exactly with the polarizer directions. In these positions, only the E-W vibrating wave is passing through the crystal. The large difference between the refractive indices of the O- and E-waves causes the change in chagrin ( $\Delta n = 0.172_{\text{Cal}}$  resp.  $0.177_{\text{Dol}}$ ).

The majority of minerals show no or very little pleochroism. Exceptions include tourmaline, members of the amphibole group, Fe-Ti-rich biotites as well as less common minerals such as piemontite, sapphirine, dumortierite, yoderite and lazulite (Fig. 4-10).

*Pleochroic minerals of tetragonal, hexagonal and trigonal symmetry* show two characteristic absorption colours parallel to the vibration directions of the E- and O-waves (dichroism). Crystal sections normal to the crystallographic c-axis (= optic axis) only show the absorption colour of the O-wave as the stage is rotated. Crystal sections parallel to the c-axis show an alternation between the absorption colour of the E-wave (E-W orientation of c) and the O-wave (N-S orientation of c) every 90° during stage rotation (Ch. 4.2.1, Figs. 4-11,12).

*Pleochroic minerals of orthorhombic, monoclinic and triclinic symmetry* show three characteristic absorption colours parallel to the principal indicatrix axes X, Y and Z (trichroism). Crystal sections normal to one of the two optic axes show the absorption colour of the Y vibration direction as the stage is rotated. An identification of the absorption colours in the X, Y and Z directions requires specific crystal sections (Ch. 4.2.1, Figs. 4-14–17).

#### 4.2.3.2 Observation with analyzer inserted (crossed-polarizers mode)

**Extinction behaviour:** The rotation of a birefringent crystal section between crossed polarizers involves a periodic change between a bright image and a dark image. A full rotation of the stage involves four extinction positions separated by  $90^\circ$  and four bright images in between (Fig. 4-23). The four orientations of maximum brightness are also referred to as diagonal positions.

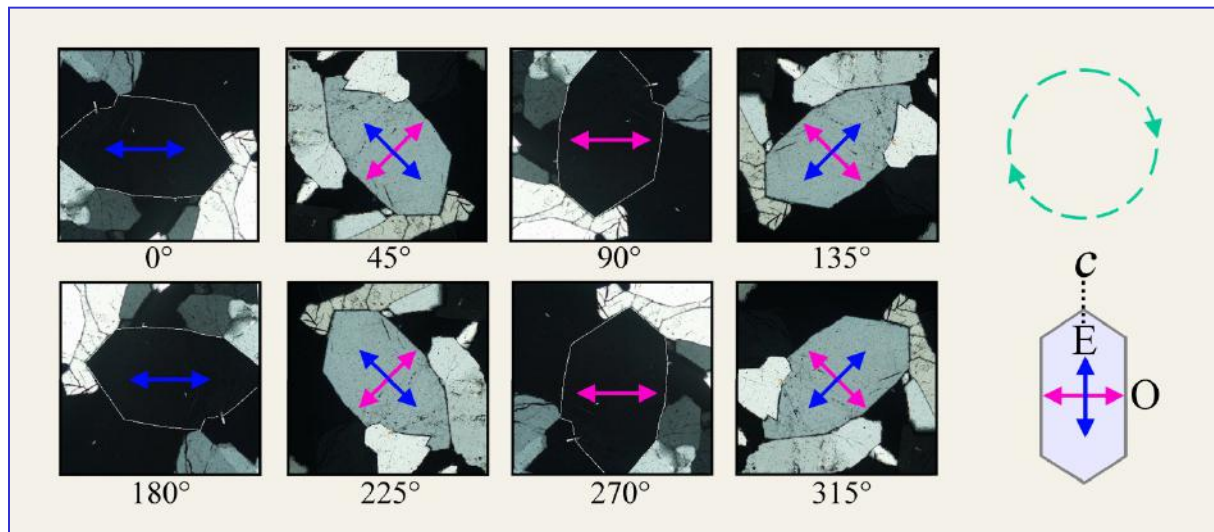


**Figure 4-23.** Extinction positions and diagonal positions of a quartz grain during a  $360^\circ$  rotation of the stage.

In the **extinction position** the E-W vibrating waves leaving the polarizer are exactly parallel to one of the two possible vibration directions of the crystal (Fig. 4-23). Hence, the waves are not split up and pass the mineral without any change in vibration direction as E-W vibrating waves which propagate with the velocity specific to that direction in the crystal. Taking the optically uniaxial quartz as an example, either the E- or the O-waves with the refractive indices  $n_e'$  resp.  $n_o$  are parallel to the polarizer. In the general case of an anisotropic mineral, the waves are those that relate to the refractive indices  $n_z'$  and  $n_x'$ . After leaving the crystal, the E-W vibrating waves are blocked by the N-S-oriented analyzer, and the crystal appears black.

If the crystal is rotated out of the extinction position, the plane of polarisation of the light entering the crystal is no longer parallel to any of the principal vibration directions in the crystal ( $n_o$ ,  $n_e'$ ,  $n_z'$ ,  $n_x'$ ). The E-W vibrating waves leaving the polarizer are therefore split up in the crystal into two orthogonally vibrating waves with refractive indices  $n_e'$  and  $n_o$  resp.  $n_z'$  and  $n_x'$  in the general case of an anisotropic mineral (Fig. 4-23,24). As light enters the crystal, the relative amplitudes  $a_1$  and  $a_2$  of the two newly generated waves depend entirely on the orientation of  $n_x'$  and  $n_z'$  (or  $n_o$  and  $n_e'$ ) with respect to the polarizer (Fig. 4-24, bottom row). At small angles, one of the two waves very much dominates in terms of light intensity. In the  $45^\circ$  diagonal position the  $a_1$  and  $a_2$  amplitudes are identical. However, without the analyzer

there is no discernible change in light intensity as the stage is rotated (at least in colourless minerals), simply because the total light intensity from  $a_1$  and  $a_2$  remains constant. Anisotropic coloured minerals are, of course, expected to show a variation of absorption as the stage is turned (Ch. 4.2.1), and high-birefringent minerals may show variable refraction effects (Fig. 4-22).

As both waves propagate in the crystal with different velocities (and correspondingly different refractive indices  $n_z'$  and  $n_x'$ ), a specific phase shift (= retardation gamma) is created by the time the light reaches the upper crystal surface (Fig. 4-24; in this example, the phase shift  $\Gamma$  is  $\lambda/2$ ).

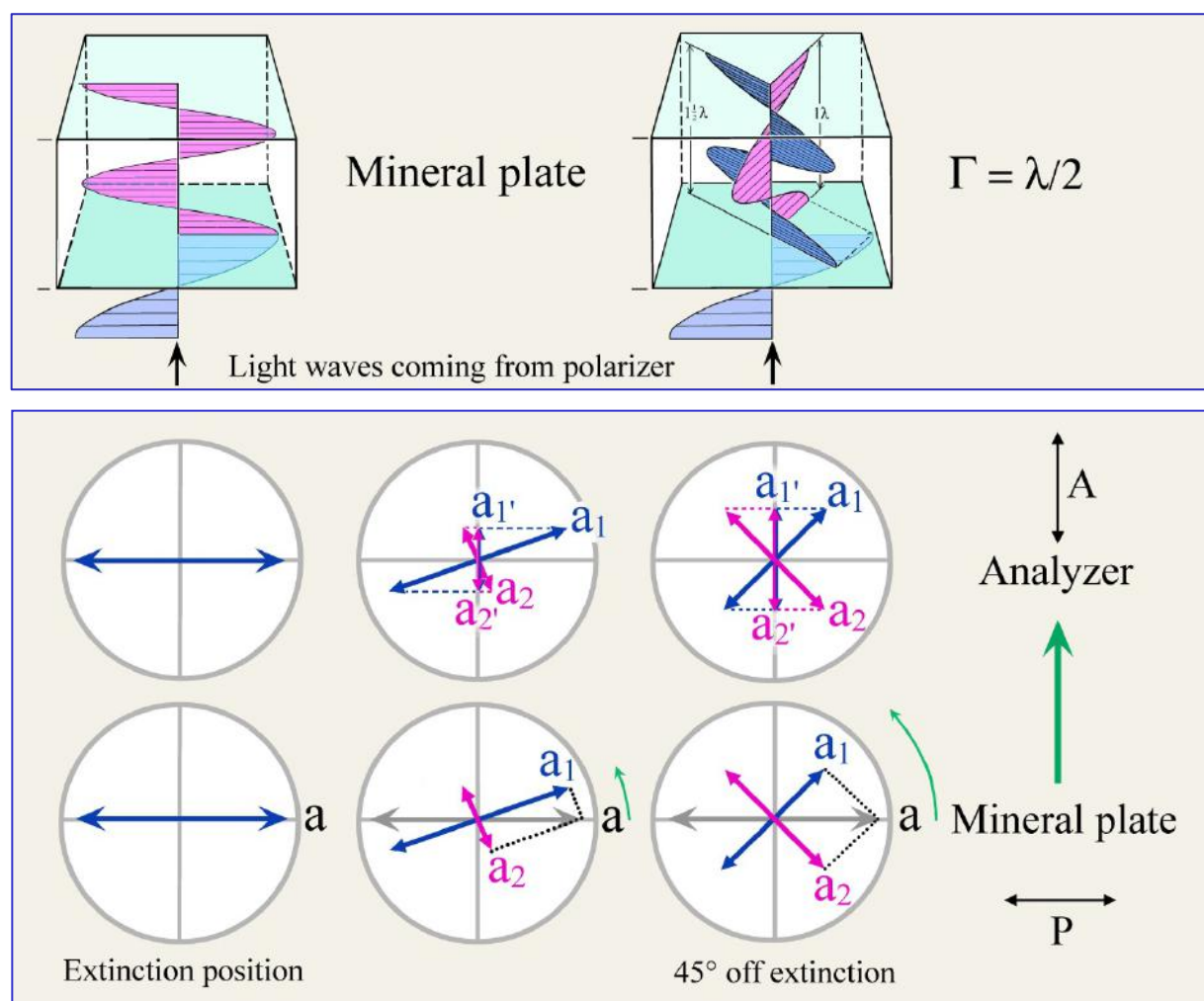


**Figure 4-24.** Vector construction for light intensities as the mineral is rotated from the extinction position into a 45° diagonal position.

Retardation refers to the accumulated distance between the wave front of the fast wave (correlating with  $n_x'$ ) and that of the slow wave (correlating with  $n_z'$ ) by the time the slow wave reaches the crystal surface. As both waves revert back to identical wave velocity after leaving the crystal, retardation remains constant in the microscope from that point onwards, unless these light waves pass through another crystal (which they do if an accessory plate is inserted; see Ch. 4.2.4). In thin section microscopy, retardation is expressed in nm. In macroscopic crystals, retardation can be in the order of millimetres. Taking calcite as an example, O-wave and E-wave passing through a cleavage rhombohedron of 2 cm thickness have accumulated a retardation of 1.84 mm as they exit the crystal (light path orthogonal to rhomb faces).

The amount of retardation is determined by two factors, (1) the difference between the two wave velocities, or expressed differently, by the birefringence value ( $\Delta n = n_z' - n_x'$ ) of the particular crystal section observed; and (2) by the thickness (d) of the crystal plate in the thin section. Thus,  $\Gamma = d * (n_z' - n_x')$ .

The distance between bottom and top of the crystal plate (i.e., thickness d) can also be expressed as multiples of wavelengths ( $d = m * \lambda$ ). As light of an initial wavelength  $\lambda_i$  enters the crystal, two waves with different wavelengths are generated (slow wave:  $\lambda_{z'} = \lambda_i/n_z'$ ; fast wave:  $\lambda_{x'} = \lambda_i/n_x'$ ). If d is expressed as multiples of  $\lambda_{z'}$  and  $\lambda_{x'}$ , we get

$$d = m_1 * \lambda_{z'} = m_2 * \lambda_{x'} \quad \text{or} \quad m_1 = d/\lambda_{z'} \quad \text{and} \quad m_2 = d/\lambda_{x'}$$

Retardation is the difference between the multipliers  $m_1$  and  $m_2$ , multiplied by wavelength  $\lambda_i$ :

$$\Gamma = (m_1 - m_2) * \lambda_i.$$

Note that by the time the slow wave reaches the upper crystal surface, the fast wave has reverted to  $\lambda_i$  and travelled the distance  $\Gamma$  outside the crystal.

$$\text{Thus, } \Gamma = (d/\lambda_{z'} - d/\lambda_{x'}) * \lambda_i$$

$$\text{as } \lambda_{z'} = \lambda_i/n_{z'} \quad \text{and} \quad \lambda_{x'} = \lambda_i/n_{x'},$$

$$\Gamma = (d * n_{z'}/\lambda_i - d * n_{x'}/\lambda_i) * \lambda_i = d * (n_{z'} - n_{x'}).$$

After leaving the crystal, the two waves with amplitudes  $a_1$  and  $a_2$  enter the analyzer with the retardation obtained within the crystal plate. As shown by vector decomposition (Fig. 4-24) two waves of the same wavelength but reduced amplitudes ( $a_1'$  and  $a_2'$ ) come to lie in the analyzer's plane of polarization. The orthogonally oriented wave components are blocked by the analyzer. The relative amplitudes  $a_1'$  and  $a_2'$  of the transmitted waves depend entirely on the orientation of the vibration directions with respect to the polarizer and analyzer directions. They have their minimum (zero) in the dark image (= extinction) position and reach their maximum after rotation of 45° from the extinction position, in the diagonal position (Figs. 4-23, 4-24).

As the light waves enter the analyzer, they are reduced to their analyzer-parallel components, and are thus subject to interference. The amount of retardation controls whether two related waves obliterate each other completely, or whether they generate a resulting wave with an amplitude from anything above zero to maximum height (Fig. 4-25). It is important here to appreciate the conditions for constructive and destructive interference of originally orthogonal waves which interfere in the analyzer (Figs. 4-24, 4-25) as opposed to the simple case of interference of two waves vibrating in a single plane (cf. Fig. 4-1).

Considering interference of light waves in the N-S transmission direction of the analyzer, two extreme cases can be distinguished:

**Case A:** If the retardation of the two waves corresponds to a phase shift of zero or whole-number multiples of  $\lambda$ , the condition of complete destructive interference is realized. The analyzer-parallel wave components of this particular wavelength vibrate in opposite directions and hence obliterate each other. No light is passing the analyzer (Fig. 4-25A).

**Case B:** If the retardation of the two waves corresponds to a phase shift of  $\lambda/2$  or odd-number multiples of  $\lambda/2$ , the condition of maximum constructive interference is realized. The analyzer-parallel wave components of this particular wavelength vibrate parallel ("in phase") and thus are superimposed to form an interference wave of maximum amplitude (i.e., maximum light intensity). The light is completely transmitted by the analyzer (Fig. 4-25B), if absorption effects of the polarizing filter are disregarded.

For any retardation between these extremes the intensity of the light transmitted by the analyzer is reduced to a certain degree, depending on the exact phase shift (e.g., 50% for  $1/4 \lambda$  and  $3/4 \lambda$ ). If monochromatic light was used, mineral grains of variable orientation in a thin section would show different levels of brightness, between black and maximum brightness, as  $\Delta n$  depends on crystal orientation, and retardation is a function of  $\Delta n$  ( $\Gamma = d * \Delta n$ ;  $d = \text{const}$ ). Mineral grains with wedging-out edges would show a bright-and-dark-striped pattern corresponding to a continuous variation in  $\Gamma$  relating to the change in  $d$  ( $\Delta n = \text{const}$ ).

Crystal sections observed in white light under crossed polarizers appear in characteristic interference colours that vary only in intensity as the microscope stage is turned, as long as the mineral is in an off-extinction position (Fig. 4-26).

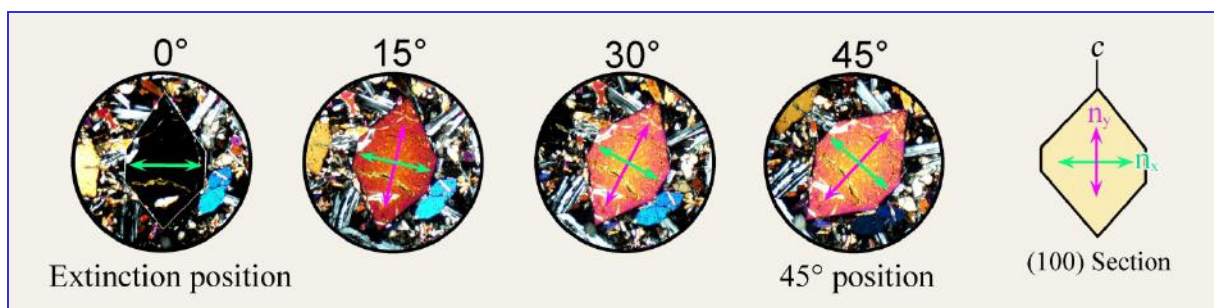


**Figure 4-26.** Interference colour of a forsterite crystal as the stage is rotated from the extinction position into a  $45^\circ$  diagonal position. The interference colour does not change during rotation, but its intensity does. In the crystal section parallel (100) birefringence is  $(n_y - n_x) = 0.015$  and retardation thus amounts to  $25 * 10^3 \text{ nm} * 0.015 = 375 \text{ nm}$ .

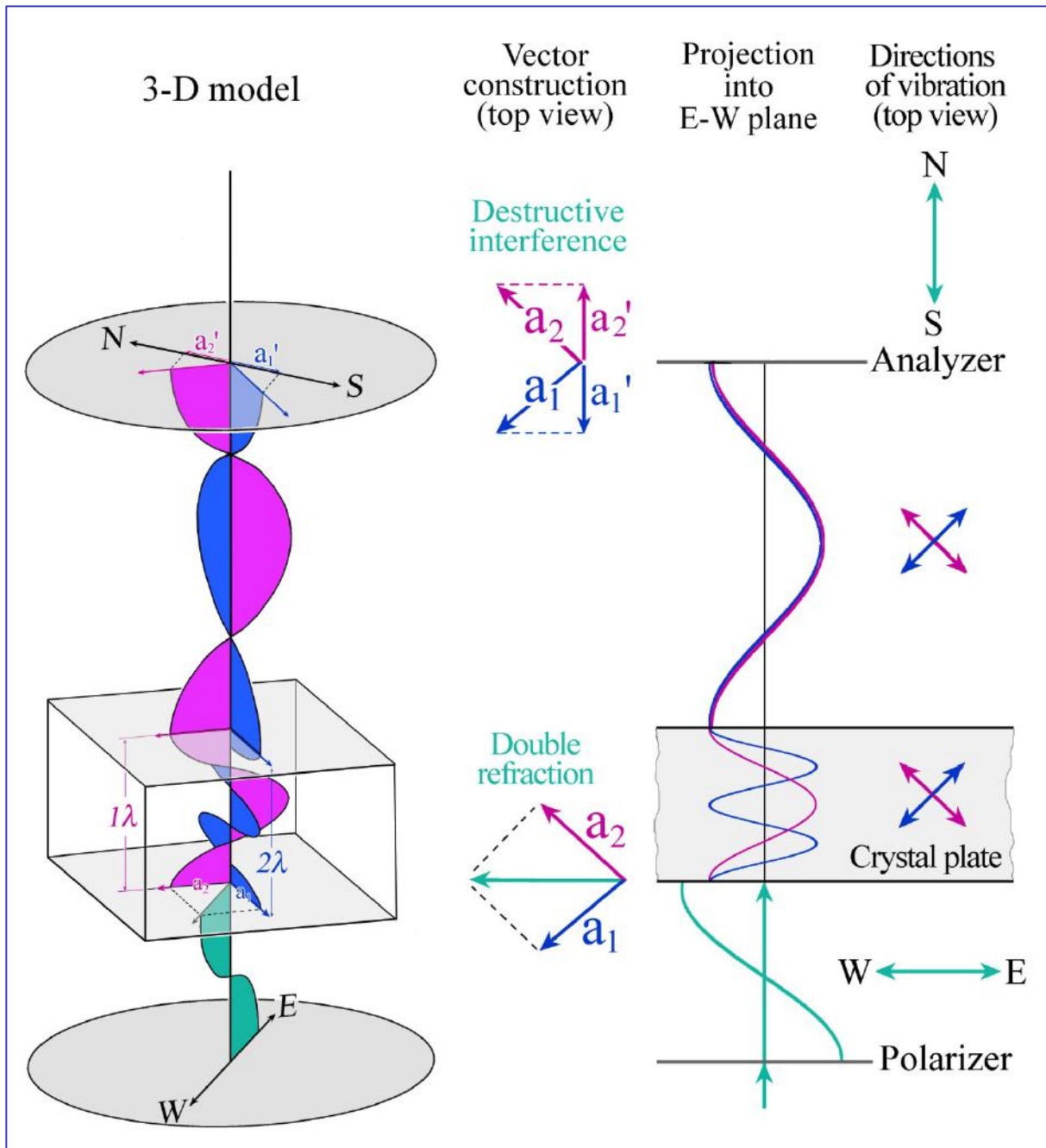


**Figure 4-25A.** Schematic presentation of the behaviour of light passing through a birefringent crystal which is in a diagonal position. Polarizers are crossed. For simplicity, only monochromatic light is shown. Retardation is  $1\lambda$ . For explanations see p. 88.

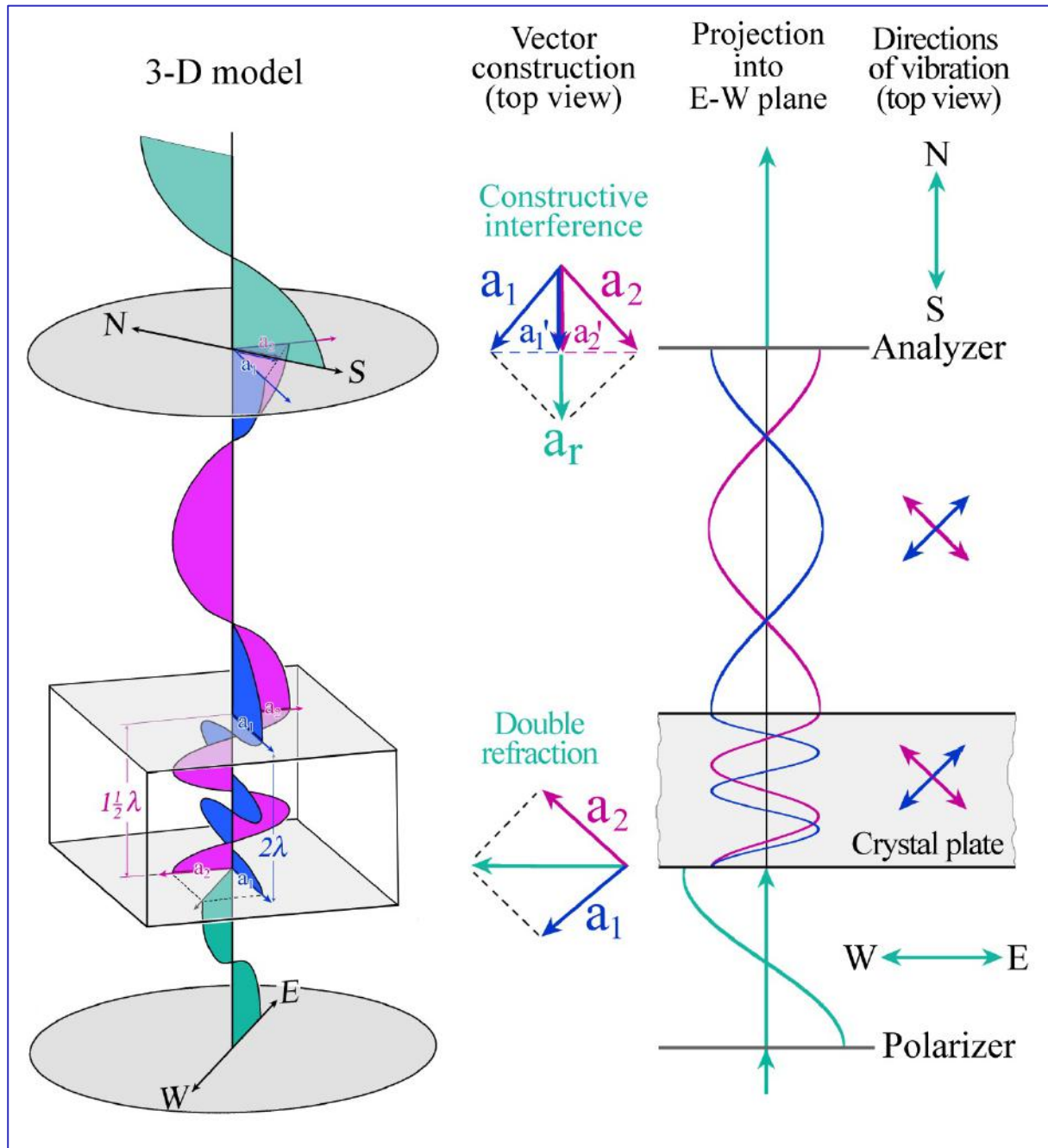


**Figure 4-25B.** Schematic presentation of the behaviour of light passing through a birefringent crystal which is in a diagonal position. Polarizers are crossed. For simplicity, only monochromatic light is shown. Retardation is  $\frac{1}{2}\lambda$ . For explanations see p. 88.

## Explanations for Figures 4-25A and 4-25B

**Case A:** Maximum destructive interference (0% transmission by the analyzer) if the retardation accumulated in the crystal is  $1\lambda$ . The same applies if the retardation is zero or a whole-number multiple of  $\lambda$  [ $\Gamma = n*\lambda$ ;  $n = 0,1,2,3,\dots$ ].

A light wave emitted from a light source experiences the following modifications (3-D model): E-W polarization in the lower polarizer; splitting up into two light waves with mutually perpendicular vibration directions as the light enters a birefringent crystal. Inside the crystal the two waves travel at different velocity and have different wavelengths. As the two waves exit the crystal they maintain their vibration directions but revert back to the wavelength and velocity of light below the crystal. From the point of exit the retardation accumulated within the crystal remains constant. The analyzer-parallel (N-S) components of the two waves entering the analyzer vibrate in opposite directions and thus eliminate each other by interference.

**Case B:** Maximum constructive interference (transmission by the analyzer at maximum amplitude) if the retardation accumulated in the crystal is  $\lambda/2$ . The same applies if the retardation is an odd-number multiple of  $\lambda/2$  [ $\Gamma = (2n+1)*\lambda/2$ ;  $n = 0,1,2,3,\dots$ ].

A light wave emitted from a light source experiences the following modifications (3-D model): E-W polarization in the lower polarizer; splitting up into two light waves with mutually perpendicular vibration directions as the light enters a birefringent crystal. Inside the crystal the two waves travel at different velocity and have different wavelengths. As the two waves exit the crystal they maintain their vibration directions but revert back to the wavelength and velocity of light below the crystal. From the point of exit the retardation accumulated within the crystal remains constant. The analyzer-parallel (N-S) components of the two waves entering the analyzer vibrate in parallel arrangement and thus produce a resulting wave of maximum amplitude.

Green: Plane-polarized light exiting the polarizer. Red: fast wave inside the crystal (correlates with  $n_x'$ ) and its corresponding wave outside the crystal; blue: slow wave inside the crystal (correlates with  $n_z'$ ) and its corresponding wave outside the crystal.

The left-hand side of Figs. A and B (column 1) displays schematic 3-D presentations of the crystal, the polarizers and the light waves. The vector decomposition of the original light wave as it enters the crystal as well as the vector relationships in the analyzer are shown in a view from the top (i.e., in the direction of the microscope axis; column 2). The same viewing direction applies to the vibration directions at the various positions of light transmission in the microscope (column 4). Column 3 represents a projection of the light waves into an E-W plane containing the microscope axis. It should be noted that the red and blue light waves vibrate at  $45^\circ$  to the drawing plane and perpendicular to each other (as seen in the 3-D models). The light exiting the analyzer in the case of constructive interference (case B) vibrates N-S and hence perpendicular to the projection plane.

## Interference colours:

In contrast to monochromatic light, the use of white light provides a full spectrum of wavelengths (spectral colours) which, for a given retardation, is modified in the analyzer through interference such that certain wavelengths are transmitted at full intensity; others are reduced to a variable degree or are obliterated entirely. White light exiting a colourless anisotropic crystal comprises an infinite number of wave couples corresponding to all spectral colours, each wavelength represented by a wave couple with mutually orthogonal vibration directions that are fixed by the crystal's orientation (cf. Figs. 4-25A and B which show such single wave couples). Interference in the analyzer between the two waves of each couple across the light spectrum is a way of making retardation visible and also quantifiable. Any specific retardation modifies the full white-light spectrum, generating a characteristic wavelength spectrum and wave amplitude pattern, which in combination produce a unique interference colour. Evidently, interference colours can only be generated from polychromatic light. They correlate directly with retardation. The sequence of interference colours in relation to increasing retardation is explained graphically in Figs. 4-27 and 4-28.

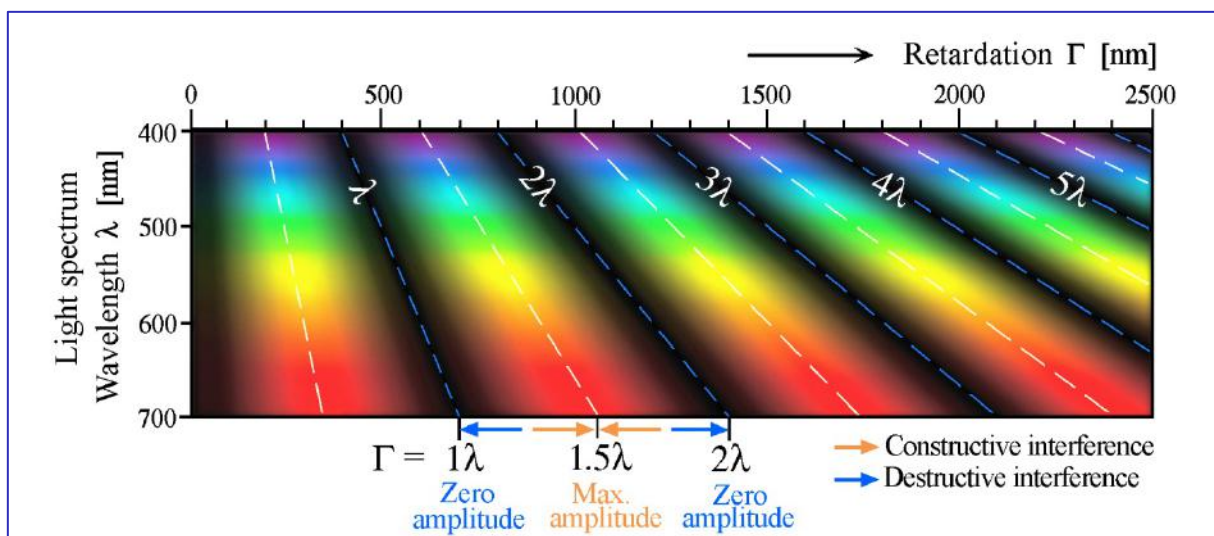
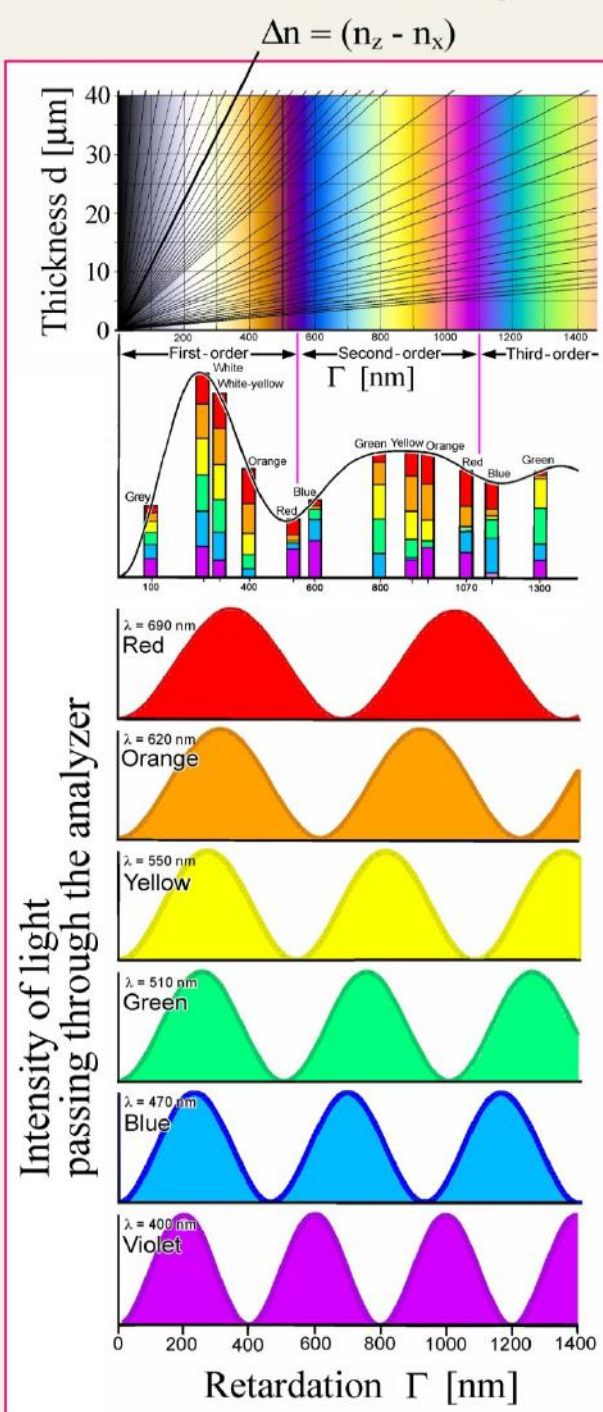


**Figure 4-27.** Constructive and destructive interference as a function of wavelength  $\lambda$  and retardation  $\Gamma$  in the spectral range of visible light (see also Fig. 4-28). The variation of the intensity of the light being transmitted by the analyzer is described by the equation  $I = 100[\sin^2(\Gamma/\lambda)180^\circ]$ .

To give a few examples: In the lower range of retardation ( $\Gamma = 0 \leftrightarrow 200$  nm) black and grey colour tones dominate as the complete colour spectrum of white light is affected by a reduction of intensities. At around  $\Gamma = 250$  nm only wavelengths from both ends of the spectrum are slightly diminished which is perceived as close to white ("first-order white"). The range  $\Gamma = 400 \leftrightarrow 500$  nm shows characteristic orange to light red interference colours, as blue and green wavelengths are suppressed, while longer wavelengths dominate the spectrum. This situation is reverse in the range  $\Gamma = 600 \leftrightarrow 650$  nm. Here, the shorter wavelengths dominate, which results in a blue interference colour. The distinctive purple colour at  $\Gamma = 551$  nm ("first-order red") lies in a position where the intermediate wavelengths (green to orange)

## Interference colour sequence



## Michel-Lévy Colour Chart

$$\Gamma = d * (n_z - n_x)$$

The summation of variably intensified or attenuated colours results in a characteristic interference colour for each value of retardation.

Depending on the retardation of waves interfering in the analyzer, the colour components of white light are intensified, attenuated or erased.

The amount of light transmitted by the analyzer is given by the equation  $I = 100\sin^2(\Gamma/\lambda)180^\circ$ .

**Figure 4-28.** Graphical presentation explaining the sequence of interference colours. The interference colour for a specific value of  $\Gamma$  derives from the sum of all wavelength amplitudes in the visible spectrum that have been modified by interference in the analyzer (or, in other words, the sum of intensities of all wavelengths across the spectrum after interference in the analyzer). As can be derived from the figure, a specific interference colour in its precise spectral composition cannot occur more than once in the colour chart (cf. Fig. 4-27).

are "filtered out", while red and blue hues dominate. The range  $\Gamma = 500 \leftrightarrow 1500$  nm is characterized by relatively intense colours due to elimination or reduction of one or two relatively narrow spectral intervals for each  $\Gamma$  value. For high retardation values ( $\Gamma > 1500$  nm) an increasing number of spectral domains distributed over the full wavelength spectrum is subtracted which produces increasingly pale colour tones and, at very high  $\Gamma$ , an interference colour that is perceived as white. As can be derived from Fig. 4-27, at very high retardation the interference colour spectrum consists of a narrow-spaced and evenly distributed arrangement of domains of constructive and destructive interference, such that none of the major colour bands is cut out completely.

Thus, the interference colour spectrum starts with black ( $\Gamma = 0$ ) and progresses through grey, white, yellow, and orange to a succession of intense colours of red  $\rightarrow$  blue  $\rightarrow$  green  $\rightarrow$  yellow  $\rightarrow$  orange  $\rightarrow$  red, which repeats itself with increasing retardation, while getting more and more pale (Fig. 4-29; Michel-Lévy colour chart). The colour sequence is subdivided into colour orders using the distinctive purplish reds (in steps of 551 nm). From the 4<sup>th</sup> order upwards, the interference colours are dominated by alternating greenish and reddish hues. With increasing retardation these fade more and more and eventually approach white (Fig. 4-33). This is referred to as high-order white (in contrast to first-order white).

The first graphical presentation between retardation, crystal thickness and birefringence [ $\Gamma = d*(n_z - n_x)$ ] was published by Michel-Lévy (1888, Tableau des biréfringences in "Les Minéraux des Roches", Paris). This interference colour chart which shows just over four colour orders is used to this day as a useful standard tool for mineral determination at the microscope. Improvements in printing technique over time ensured that modern colour charts are a reasonably close reproduction of the interference colour spectrum observed in polarized-light microscopes (such as the colour charts of Zeiss and Leica). Nevertheless, some weaknesses in colour reproduction are evident like the second-order green which is far too prominent in most colour charts. The Michel-Lévy colour chart of this guide provides an improved reproduction of the colour spectrum (Fig. 4-29). It has been calculated by Dr. Bjørn Eske Sørensen (Department of Geology and Mineral Resources Engineering, NTNU-Trondheim, Norway) using MATLAB. The spectrum has been calculated taking into account human colour perception (CIE-calibrated curves of sensitivity for the primary colours red, green, blue) and the RGB colour space of the computer. Conformity between calculated and observed interference colours was further optimised using the gamma correction of the intensity values.

When redesigning the Michel-Lévy colour chart for this guide we modified the presentation such that the application principle for mineral determination is easy to grasp, compared with the widely distributed standard charts of Zeiss or Leica (Figs. 4-29 and 4-32). Guided by our experience with microscopy courses we also developed an alternative concept for the interference colour chart. We believe this chart is easier to read where birefringence values or crystal thickness need to be determined, compared with the classic colour chart. The difference to the standard Michel-Lévy colour chart is that the colours representing retardation are

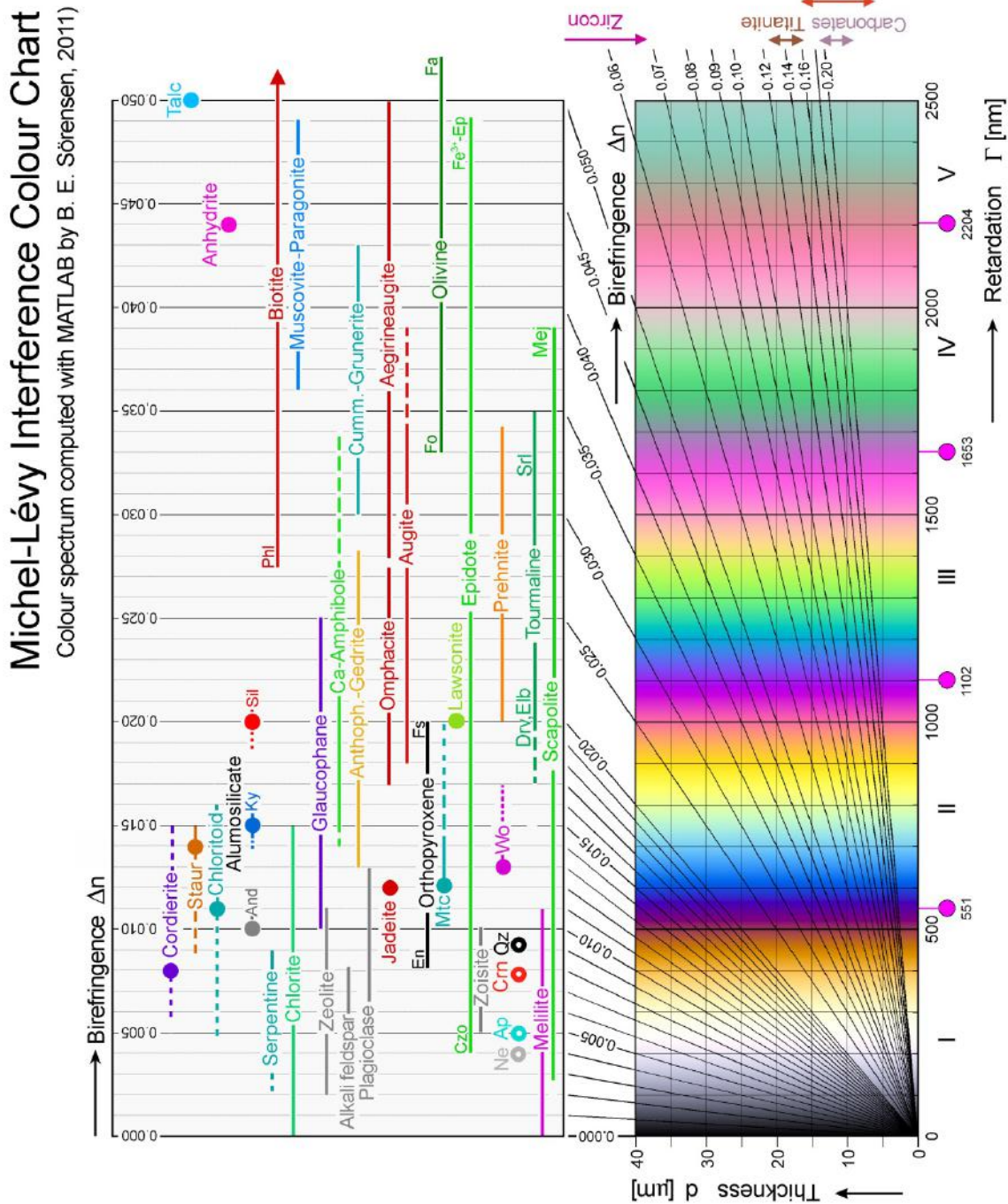


**Figure 4-29.**  $\Gamma$ -d Interference colour chart after Michel-Lévy.

The birefringence values of the radial lines in the colour chart are correlated with common rock-forming minerals. The use of the colour chart for mineral identification and determination of crystal thickness is explained in the text and is further demonstrated in Fig. 4-32.

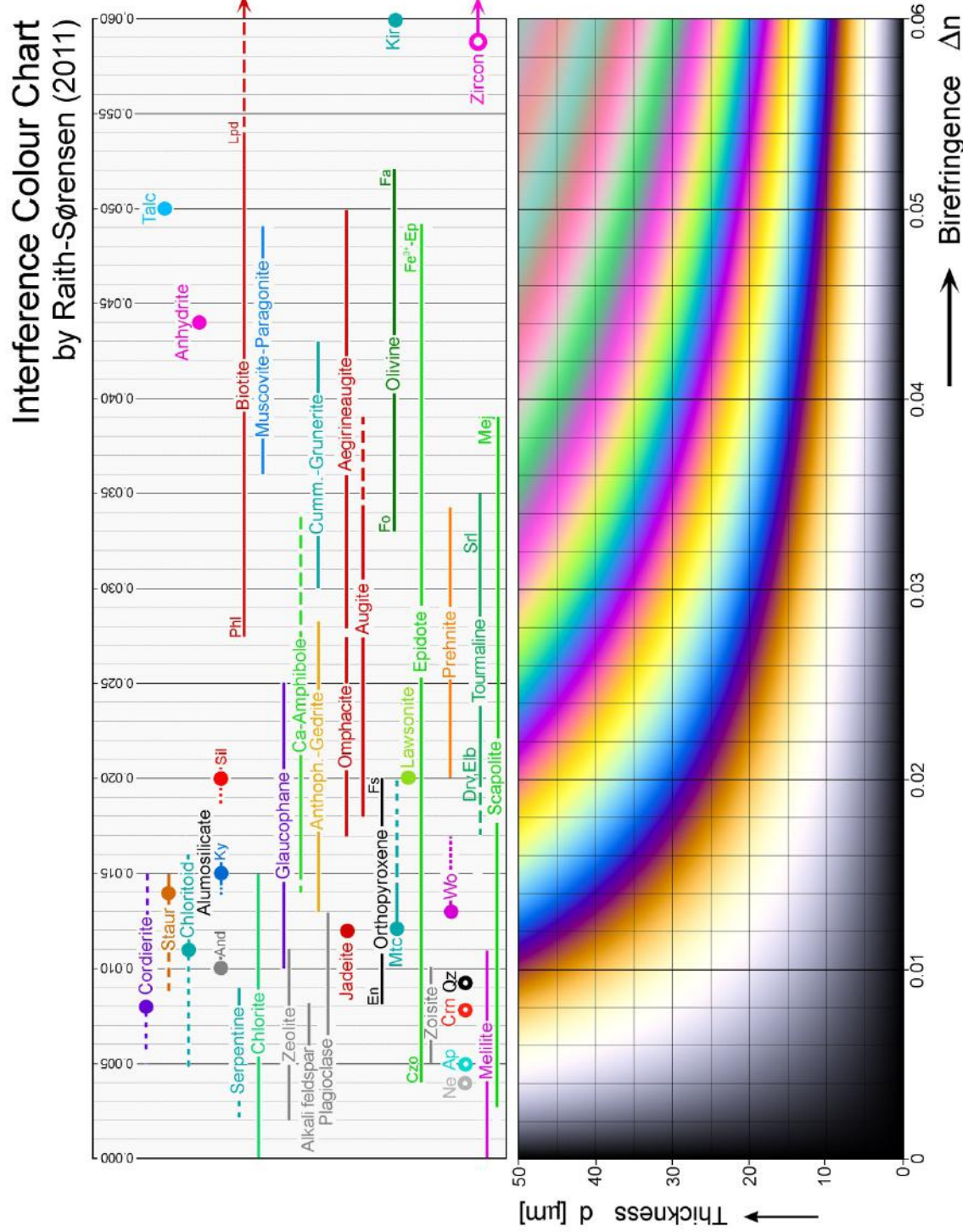


**Figure 4-30.**  $\Delta n-d$  Interference colour chart after Raith-Sørensen.

The birefringence values of the colour chart are correlated with common rock-forming minerals. The use of the colour chart for mineral identification and determination of crystal thickness is explained in the text and is further demonstrated in Fig. 4-32.

arranged as a function of birefringence and crystal (or thin section) thickness (Fig. 4-30). The resulting, more complex hyperbolic colour arrangement has been calculated by Bjørn Eske Sørensen using MATLAB. The correlation between the birefringence value of an unknown mineral in a section of known thickness and the mineral's interference colour can be conceived intuitively (Fig. 4-32, right-hand side). Similarly, reading the thin section thickness from the reconfigured colour chart using the maximum interference colour of a known mineral is straightforward. The dependence of interference colour on thin section thickness is immediately evident. However, for getting the numerical correlation between retardation and  $\Delta n$ , or between retardation and  $d$ , the Michel-Lévy chart is the better choice.

When using interference colours for the determination of minerals it has to be kept in mind that the retardation which accumulates as the waves pass through the crystal is not only dependent on  $\Delta n$  of that particular crystal section, but also on the thickness of the sample. In order to correlate interference colours and birefringence values directly, the thin section thickness has to be known. Therefore, thin sections are prepared with a defined standard thickness (commonly 25 or 30  $\mu\text{m}$ ). However, there may be reasons to deviate from these standard values, for example, if the contrast of interference colours between low-birefringent phases is to be increased; or, to improve the contrast between differently oriented grains of extremely high-birefringent minerals, the interference colours can be reduced to a lower order (as in ultra-thin sections of carbonates).



**Figure 4-31.** Relation between interference colour and grain (crystal) orientation of anisotropic minerals, using quartz, diopside and anhydrite as examples.

A: The euhedral quartz crystals from a vein show creamy-white to dark grey first-order interference colours. Creamy-white crystals: sections parallel to the c-axis [max. birefringence ( $n_e - n_o$ ) = 0.009]; dark grey crystal: section nearly orthogonal to c [circular indicatrix section showing  $n_o$ ; birefringence = 0].

B: The diopside grains in a calcsilicate rock show different interference colours, dependent on crystal orientation, ranging from second-order blue-green to first-order dark grey. Blue-green grain: section parallel to (010) resp. optic axial plane [max. birefringence ( $n_z - n_x$ ) = 0.031]; dark grey grain: section nearly orthogonal to one of the two optic axes [circular indicatrix section showing  $n_y$ ; birefringence = 0].

C: The anhydrite grains show different interference colours, dependent on crystal orientation, ranging from third-order red to first-order (near-)black. Pale red grains: section parallel to (010) resp. optic axial plane [max. birefringence ( $n_z - n_x$ ) = 0.044]; black grain: section orthogonal to one of the two optic axes [circular indicatrix section showing  $n_y$ ; birefringence = 0].

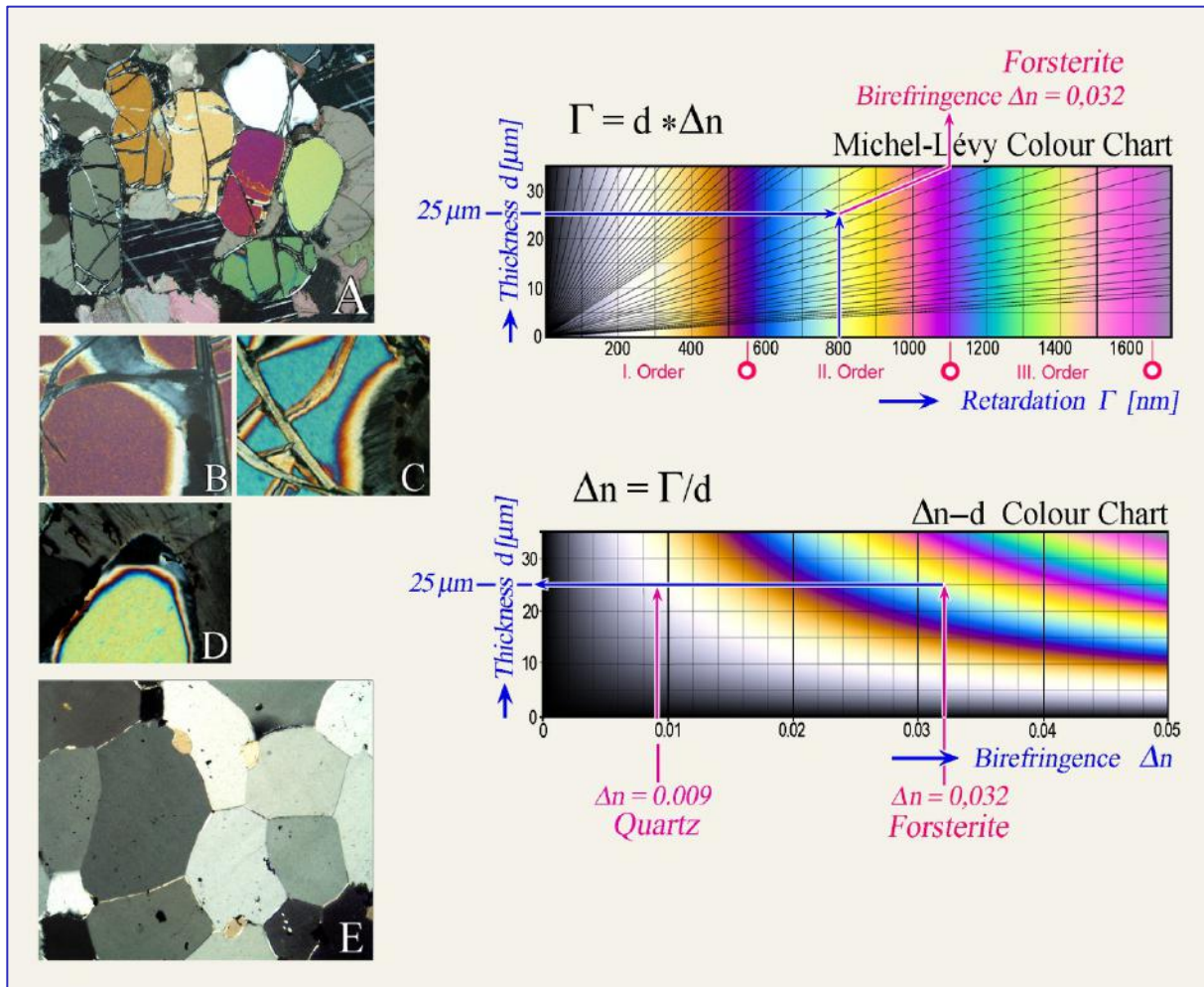


**Figure 4-32.** Determination of birefringence and thin section thickness using interference colour.

*Left-hand side:* (A) Variation of interference colours in differently oriented forsterite grains; (B) to (D) Decreasing interference colours at wedge-shaped grain edges of forsterite grains in different crystallographic orientation. The crystal section D shows the highest interference colour (2<sup>nd</sup> order yellow-green) and is oriented orthogonal to c, i.e. parallel to (001) with principal vibration directions Z//a and X//b. (E) In this quartzite thin section, grains sectioned parallel to c show the highest interference colour (1<sup>st</sup> order creamy white); these are sections containing the principal vibration directions E = Z//c and O = X⊥c.

*Right-hand side, top:* Determination of birefringence ( $n_z - n_x$ ) of forsterite (section D) in a standard thin section of known thickness (25 μm) taking the maximum interference colour observed in thin section [( $\Gamma$ -d colour chart after Michel-Lévy)].

*Right-hand side, bottom:* Determination of thin section thickness from the maximum interference colour observed for a mineral with known birefringence. Examples are shown for forsterite ( $\Delta n = 0.032$ ; grain section D) and quartz ( $\Delta n = 0.009$ ; creamy white grains in section E) [ $\Delta n$ -d colour chart after Raith-Sørensen].

The determination procedures as shown on the right-hand side may be applied in reverse, of course, with both types of colour charts.

**Determination of birefringence using the interference colour:** Birefringence is an important property of anisotropic minerals and is crucial for mineral determination. However, the amount of birefringence of a specific mineral depends on the orientation of the section. In optically uniaxial minerals it varies from zero in the section perpendicular to the optic axis (direction of optical isotropy), to a maximum value ( $|n_e - n_o|$ ) in sections parallel to the optic axis. In optically biaxial minerals it varies from zero in sections perpendicular to one of the two optic axes, to a maximum value ( $n_z - n_x$ ) in the section parallel to the optic plane. For this reason, the grains of each anisotropic mineral show different interference colours in thin section dependent on their crystallographic orientation (Figs. 4-31). For routine mineral identification, only the maximum birefringence ( $\Delta n = n_z - n_x$ ) values are critical (Fig. 4-32), and these values are commonly listed in mineral-optical tables or compilations.

The determination of interference colours may be difficult in highly birefringent minerals (such as carbonates: so-called high-order white). Wedge-shaped grain boundaries provide a means to observe the colour spectrum, in relation to decreasing crystal thickness, down to first-order black (Fig. 4-33).

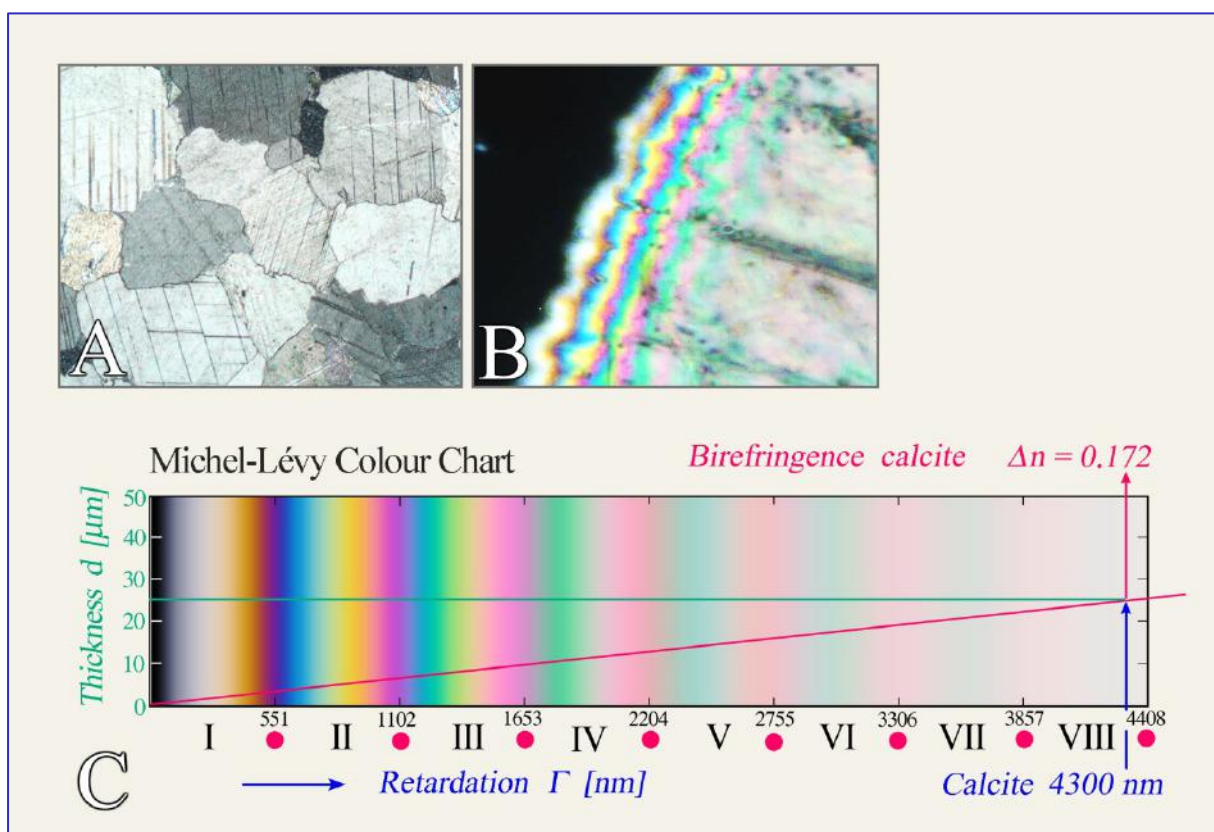


**Figure 4-33.** A. Calcite grains in a thin section of marble appear in high-order white (+Pol). B. The wedge-shaped margin of a calcite grain shows a spectrum of decreasing interference colours from the interior plateau to the outer edge as the crystal thickness decreases from 25 to 0 μm. Five colour orders can be recognised using the red bands as a reference. C. A calcite grain cut exactly parallel to the c axis would show an 8<sup>th</sup> order white at a standard thickness of 25 μm.

**Interference colour and zoning of minerals:** In minerals with extensive solid solution, the optical properties vary with chemical composition, including birefringence. Chemical zoning in crystals can then be recognised from the conspicuous zoning of the interference colour. Particularly impressive examples are plagioclases and titanaugites with oscillatory zoning, as found in certain volcanic rocks, zoned melilite in slags, and epidote in metamorphic rocks (Fig. 4-34).

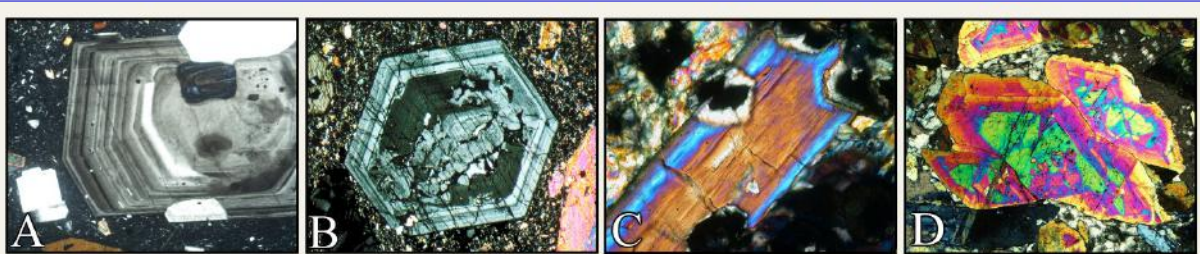


**Figure 4-34.** Zoning of interference colour in plagioclase (A), titanaugite (B), sodic amphibole (C) and epidote (D).

Growth zoning with oscillatory variations in composition characterises the volcanic plagioclase and augite. The sodic amphibole has a  $\text{Fe}^{3+}$ -rich core (crossite) and a  $\text{Fe}^{3+}$ -poor rim (glaucophane). The decrease of interference colours towards the edge of the epidote grain indicates decreasing  $\text{Fe}^{3+}$  contents during grain growth.

The interference colours of coloured minerals may be masked significantly as they overlap with the minerals' own colour (examples: hornblende, biotite). In strongly coloured minerals of high birefringence, the primary mineral colour will be dominant under crossed polarizers. A relatively pale interference colour or a high-order white can hardly impose a noticeable spectral shift on the mineral's own colour as the two overlie each other (example: rutile).

**Anomalous interference colours:** The interference colours of certain minerals deviate from the normal colour scheme. Instead of the grey to white colours in the first order of the interference colour spectrum, leather brown, ink blue to grey-blue colours are observed (Fig. 4-35,36). Such "anomalous" interference colours are generated by a strong dispersion of birefringence, which means that the latter attains distinctly different values for different wavelengths (colours). In the melilite example, the value of birefringence becomes zero for wavelengths in the range orange-yellow-green. Hence, these colours are not contributing to the interference colour (cf. Fig. 4-28).



**Figure 4-35.** Examples of anomalous interference colours: A. Titanaugite (sector structure and oscillatory zoning); B. Clinzoisite; C. Zoisite; D. Vesuvianite; E. Melilite (continuous zoning with åkermanite-rich core and gehlenite-rich rim).

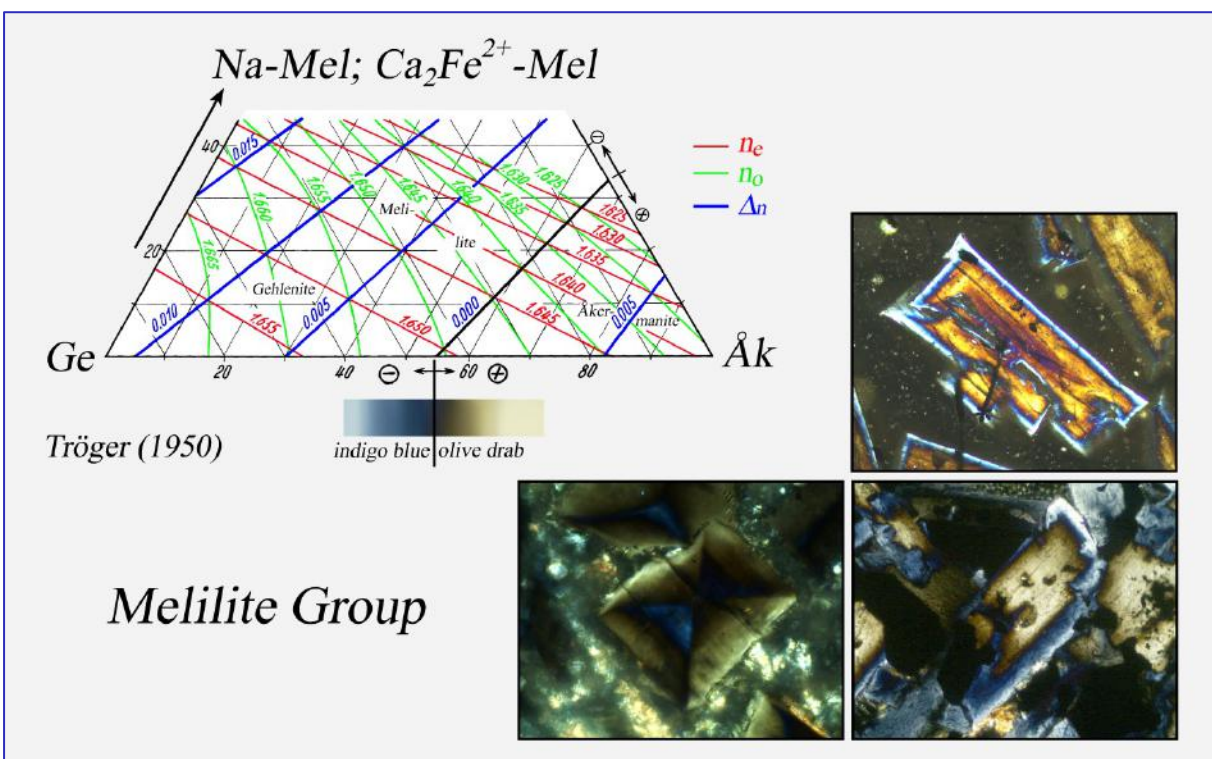
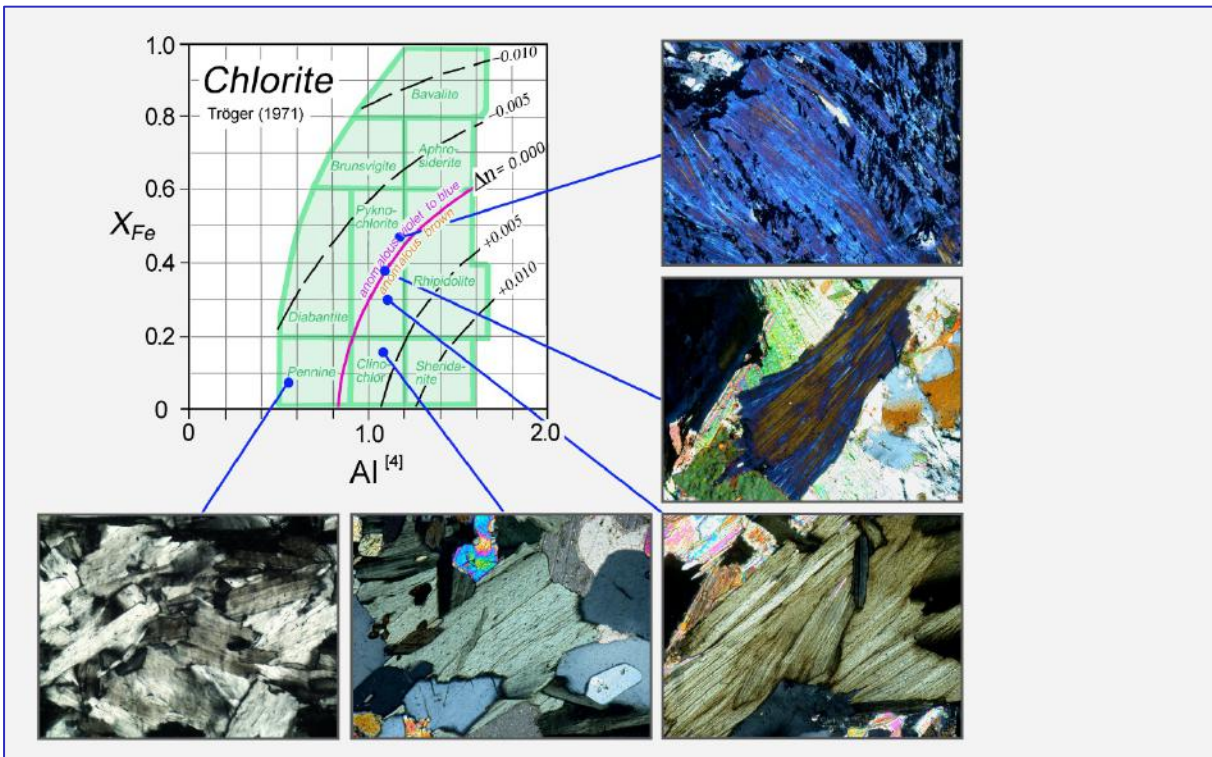


**Figure 4-36.** Anomalous interference colours in chlorite and melilite. Anomalous blue or leather-brown interference colours occur in solid solutions with birefringence values close to zero. The higher birefringent members of the solid solution series show normal light grey to creamy white interference colours of the first order.

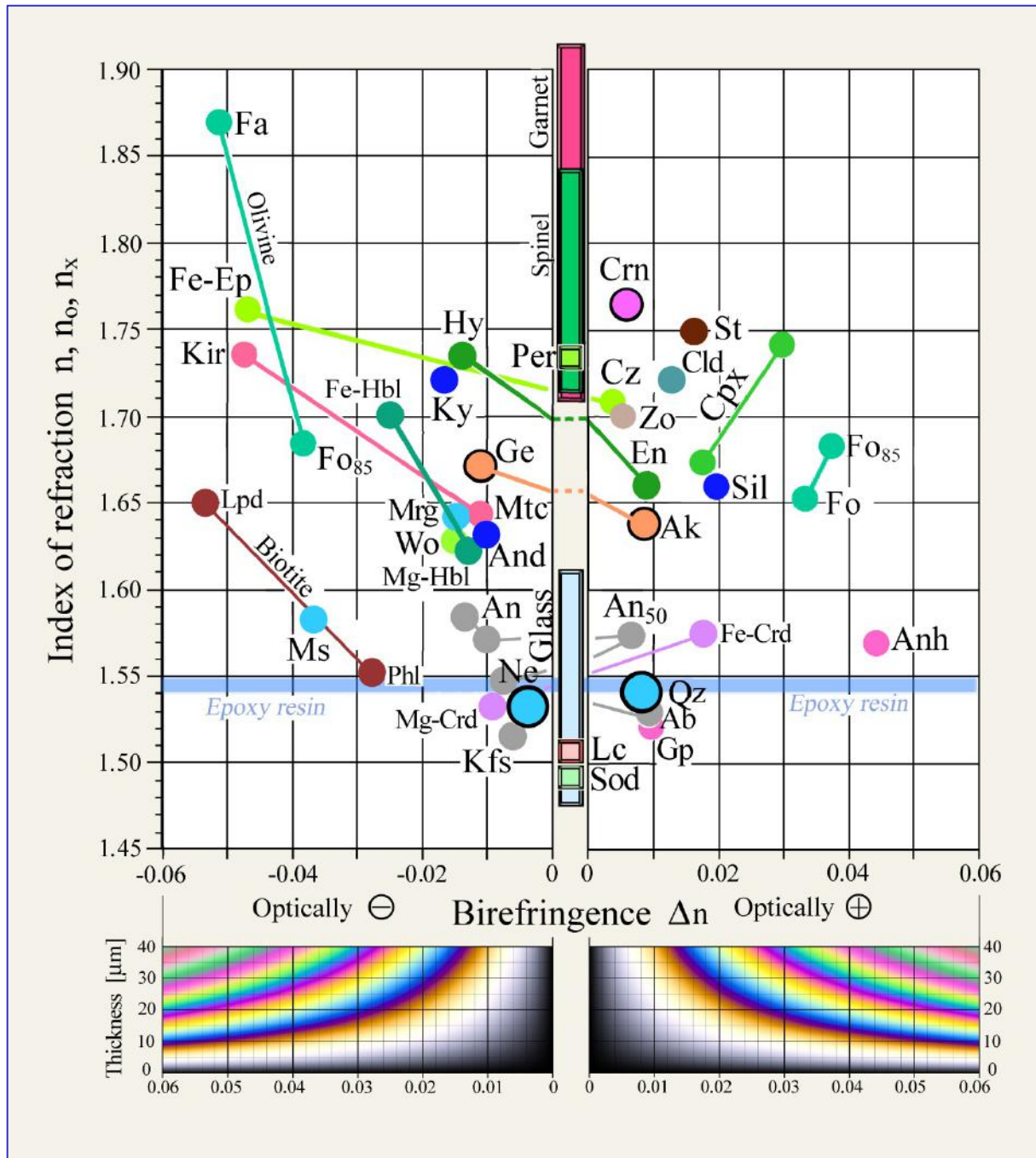


**Figure 4-37.** Diagram showing refractive index versus birefringence for rock-forming minerals.

Optic class and sign (uniaxial – biaxial; positive – negative), if unknown, must be determined with conoscopic methods. Bold circles mark the optically uniaxial minerals. Glasses and cubic minerals are optically isotropic ( $\Delta n = 0$ ). For each anisotropic mineral in a thin section of given thickness, the highest interference colour can be read from the  $\Delta n$ -d interference colour chart of Raith-Sørensen.

Mineral abbreviations after Whitney & Evans (American Mineralogist, 95, 185-187, 2010).

#### 4.2.4 Extinction positions in birefringent crystal sections

##### Vibration direction and extinction character

In optically anisotropic crystals, crystal symmetry, and in low-symmetry solid solutions also composition, controls the form and spatial orientation of the indicatrix (Figs. 4-6,7). The regular spatial relationships imply that the orientation of vibration directions with respect to morphological elements (crystal faces, crystal edges, cleavage planes, twin planes) is fixed in birefringent crystal sections. The resulting extinction behaviour allows a distinction between minerals of higher symmetry (hexagonal, trigonal, tetragonal and orthorhombic) and those of lower symmetry (monoclinic, triclinic) (Fig. 4-38). Three general types of extinction can be distinguished:

Straight extinction: the vibration directions lie parallel to the morphological reference directions ( $\varepsilon = 0^\circ$ ).

Symmetrical extinction: the vibration directions bisect the angles between two equivalent morphological reference directions ( $\varepsilon_1 = \varepsilon_2$ ).

Inclined extinction: the vibration directions form any angle ( $\varepsilon \neq 0^\circ, \neq 90^\circ$ ) with morphological reference directions.

Extinction			
	parallel $\varepsilon = 0$	symmetrical $\varepsilon_1 = \varepsilon_2$	inclined $\varepsilon_1 \neq \varepsilon_2$
Hexagonal Trigonal Tetragonal			
	c in E-W or N-S plane; $a_1, a_2, a_3$ in N-S		Sections $\perp$ (hkl)
O'rhombic			
	Sections parallel [100], [010], [001]		all other sections
Monoclinic			
	Sections parallel [010]		all other sections
Triclinic			
			all sections

Examples:

melilite, nepheline, apatite, corundum, zircon, tourmaline, rutile

olivine, orthopyroxene, sillimanite, andalusite, staurolite, zoisite, anhydrite

clinopyroxene, clinoamphibole, epidote, sanidine

plagioclase, kyanite, wollastonite

**Figure 4-38.** Crystal symmetry and extinction behaviour.

The orientation of the crystals shown here corresponds to the extinction position. The cross in each figure indicates the two polarizer directions resp. the crosshairs.

## Extinction angle

The angle between a vibration direction and the morphological reference element (crystal edge, cleavage, twin plane) in a crystal section is referred to as the extinction angle. Extinction angles are useful for the characterisation of monoclinic and triclinic minerals.

Example clinopyroxene: The monoclinic members of the pyroxene group show a correlation between extinction angle  $\varepsilon$ , measured between vibration direction Z ( $n_z$ ) and the trace of (100) in a crystal section parallel to (010), and chemical composition, i.e. the type of clinopyroxene (Fig. 4-39). The angle can be expressed as  $\varepsilon = Z \wedge c$ .

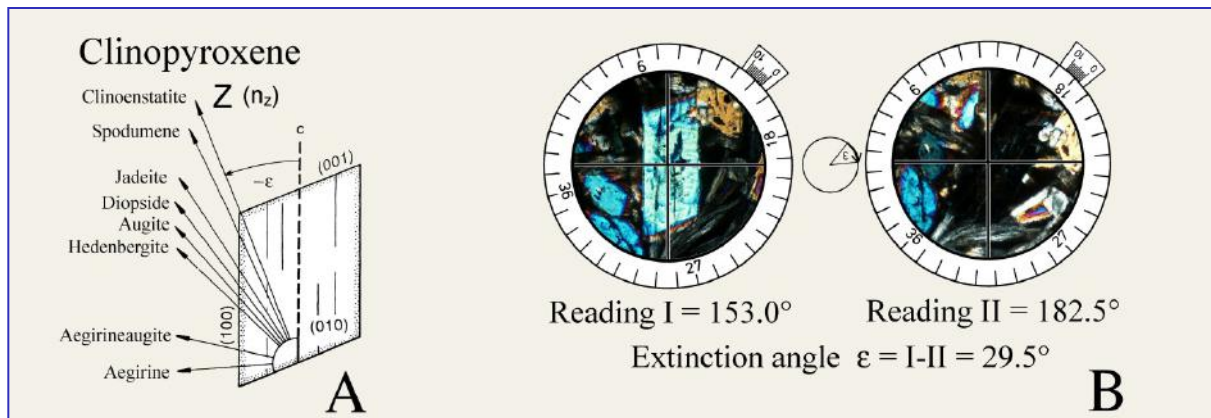


**Figure 4-39.** Extinction angle in clinopyroxenes

A: Relation between composition and extinction angle  $\varepsilon = Z \wedge c$  in crystal sections parallel to (010) for some important members of the clinopyroxene group. The c-direction corresponds to the traces of (100) crystal faces or the traces of the {110} cleavage. B: Method of determining the extinction angle. Reading I: position of reference morphological element parallel to the N-S line of the crosshairs. Reading II: extinction position.

Practical hints: The precise determination of extinction angles requires specific crystal orientations. In the case of clinopyroxene, these are crystal sections with the highest interference colour (Fig. 4-39). The extinction angle is determined in the same way as measuring angles between morphological planes (e.g., cleavage planes), whereby the polarizers must be exactly oriented in E-W resp. N-S direction. The measurement is done in two steps (Figs. 4-39 B): (1) Rotation of the morphological reference direction (trace of a crystal face or cleavage) into N-S direction (= N-S line of the crosshairs) and reading the angle value I from the vernier on the microscope stage; (2) rotation of the vibration direction into N-S direction (which is equivalent to the extinction position of the crystal section) and reading the angle value II at the vernier. The difference between the values is the extinction angle  $\varepsilon$ .

Example clinoamphibole: The monoclinic members of the amphibole group show a correlation between extinction angle  $\varepsilon$ , measured between vibration directions Z, Y or X and the trace of (100) in a crystal section parallel to (010), and chemical composition, i.e. the type of clinoamphibole (Fig. 4-40 A). The measurement of the extinction angle is shown in Fig. 4-40 B and is carried out in the same way as for clinopyroxene.

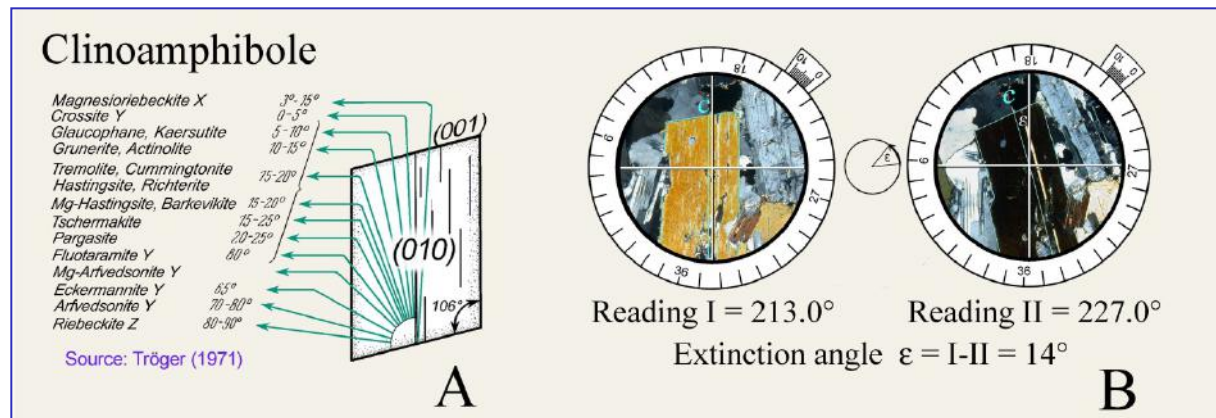


**Figure 4-40.** Extinction angle in clinoamphiboles

A: Relation between composition and extinction angle  $\varepsilon = X, Y, Z \wedge c$  in crystal sections parallel to (010) for some important members of the clinoamphibole group; B: Method of determining the extinction angle.

Example plagioclase: In plagioclase solid solutions, the orientation of the indicatrix in relation to the axes *a*, *b* and *c* of the triclinic crystal varies, dependent on anorthite content and the degree of Al/Si ordering. The vibration directions of the pair of waves change accordingly in crystal sections of defined orientation. At a constant degree of ordering, the vibration directions depend on anorthite content alone (Fig. 4-41 A,B).

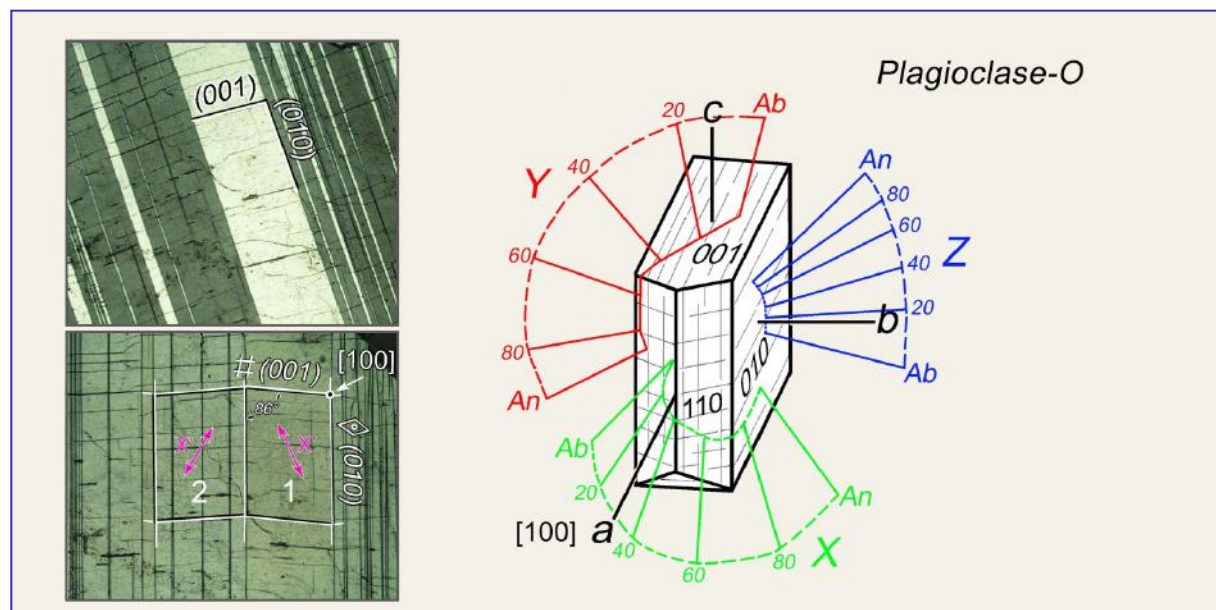


**Figure 4-41 A.** Relation between indicatrix orientation and anorthite content in plagioclase with maximum Al-Si order (from slowly cooled plutonic and metamorphic rocks).

The anorthite content of plagioclase solid solutions in such rocks can be determined reasonably well by measuring the extinction angle  $\varepsilon$ .  $\varepsilon$  is the angle between the vibration direction  $X'$  and the trace of (010) in a section orthogonal to the direction [100] (Method of Rittmann, 1929).

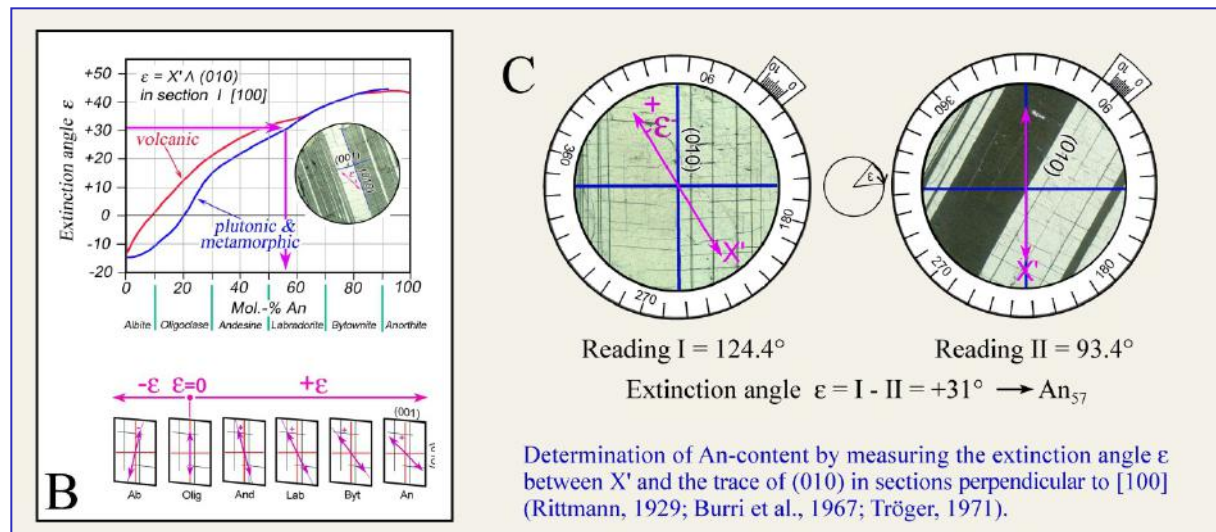


**Figure 4-41 B,C.** Extinction angle  $\varepsilon$  in plagioclase crystal sections  $\perp [100]$

Practical hints: The determination of anorthite content by measuring the extinction angle  $\varepsilon$  ("zone method" of Rittmann 1929; Burri et al., 1967) requires crystal sections that are oriented exactly orthogonal to [100]. In such crystal sections, the (010) interfaces of albite twins as well as the (001) cleavage traces occur as sharply defined, thin lines (Fig. 4-41 A,C). They form an acute angle of  $86^\circ$ . Wider (010) lamellae relating to the Carlsbad twin law do not show (001) cleavage traces. If the (010) traces are rotated into N-S direction, the two sets of albite twin lamellae show identical interference colours if the grain is appropriately oriented (Fig. 4-41 C). Carlsbad twins display a different interference colour if placed in this position. In order to distinguish albite lamellae from the common pericline twin lamellae oriented nearly parallel to (001), one of the two twin lamellae sets is rotated out of the extinction position anticlockwise by  $45^\circ$ , and the first-order red plate is inserted. Increase of interference colours  $\rightarrow$  albite twins; decrease of interference colours  $\rightarrow$  pericline lamellae.

The measurement of the anorthite content involves two steps (Fig. 4-41 C): (1) Rotation of the morphological reference direction ((010) twin plane) into N-S orientation (= N-S line of the ocular crosshairs) and reading of the angle value I from the vernier of the microscope stage; (2) rotation of the vibration direction  $X'$  into N-S orientation (which corresponds to the extinction position of one set of twin lamellae) and reading of the angle value II at the vernier. The difference of both angle values equates to the extinction angle  $\varepsilon$ . (3) In order to obtain the sign of the extinction angle  $\varepsilon$ , it must be checked whether  $X'$  lies in the acute or in the obtuse angle between the morphological reference directions (010) and (001) inside the respective twin lamellae. Since the observed twin set is in extinction, it is advisable to insert the first-order red plate. If  $X'$  lies in the obtuse angle ( $An_{0-20}$ ),  $\varepsilon$  is negative; if  $X'$  lies in the acute angle ( $An_{20-100}$ ),  $\varepsilon$  is positive (Fig. 4-41 B).

For the example shown (plagioclase from Lindenfels Gabbro, Germany), the measured extinction angle of  $31^\circ$  indicates an anorthite content of 57 mole% (Fig. 4-41 B).

## Optical character of the extinction directions

If a birefringent crystal section is in extinction position, the vibration directions  $Z'$  and  $X'$  are parallel to the N-S and E-W directions of the crosshairs (cf. Fig. 4-23). For a variety of applications it may be important to know which direction corresponds to the higher, respectively lower, refractive index:

- Determination of mineral colour in a specific vibration direction (cf. Ch. 4.2.1).
- Determination of optical sign of optically uniaxial minerals which are elongate in c direction or platy having the basal plane ( $\{001\}$ ,  $\{0001\}$ ) as the dominant crystal face.
- Determination of sign of elongation ( $l$ ) of acicular to columnar, platy or flaky minerals in elongate crystal sections.

For a distinction between vibration directions  $Z'$  and  $X'$ , compensator plates are used. These are anisotropic crystal plates of constant or variable retardation with known orientation of the  $X$  and  $Z$  wave vibration directions ( $\alpha = n_x$  and  $\gamma = n_z$ ). The vibration direction of the  $Z$  wave ( $\gamma = n_z$ ) is engraved in the metal casing of the compensators. Commonly used compensators (Fig. 4-42):

The first-order red plate (lambda plate,  $\lambda$  plate, sensitive tint plate) consists of a quartz or gypsum plate that is cut parallel to the optic axis, about 62  $\mu\text{m}$  thick, which shows a first-order red interference colour in diagonal position ( $\Gamma = 551 \text{ nm}$ ).

The  $\lambda/4$  (lambda quarter) plate consists of a thin quartz or mica plate which shows a grey interference colour in diagonal position ( $\Gamma = 130-150 \text{ nm}$ , depending on manufacturer).

The quartz wedge consists of a wedge-shaped quartz plate with the long axis parallel to the optic axis. In diagonal position, this quartz wedge shows interference colours ranging across four orders ( $\Gamma = 0$  to  $2200 \text{ nm}$ ).

Most commonly, the compensators are inserted diagonally into the microscope tube below the analyzer. The wave corresponding to  $n_z$  ( $\gamma$  or  $Z'$ ) vibrates in NE-SW direction, the wave corresponding to  $n_x$  ( $\alpha$  or  $X'$ ) in NW-SE direction.

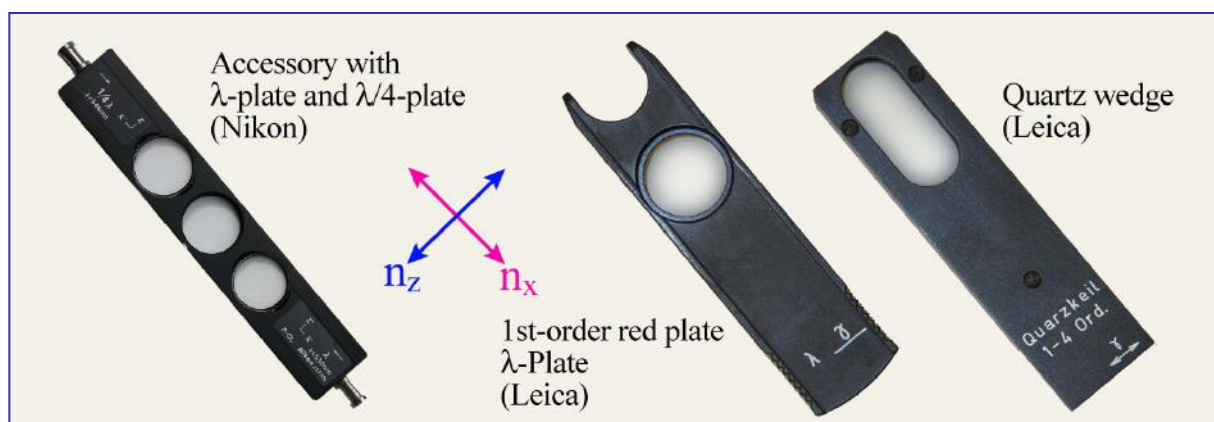


**Figure 4-42.** Compensators— first-order red plate ( $\lambda$  plate), lambda/4 plate and quartz wedge

In order to distinguish between the extinction directions  $X'$  and  $Z'$  (with corresponding refractive indices  $n_x'$  and  $n_z'$ ), the mineral grain is put exactly in an extinction position and then rotated anticlockwise by  $45^\circ$  into a diagonal position (Fig. 4-43). Some modern microscopes have a device attached to the stage that can be activated in extinction position such that every  $45^\circ$  rotation is indicated by a mechanical click.

In diagonal position, the mineral displays its characteristic interference colour in maximum brightness. In this position, the originally E-W vibrating wave is now vibrating NE-SW (in quadrants I and III); the originally N-S vibrating wave is now oriented NW-SE (in quadrants II and IV).

Two different optical orientations of the mineral are possible in diagonal position (Fig. 4-43):

- I. The NE-SW vibrating wave is the slower wave; its refractive index is  $n_z'$ . The NW-SE vibrating wave is the faster wave; its refractive index is  $n_x'$ .
- II. The NE-SW vibrating wave is the faster wave; its refractive index is  $n_x'$ . The NW-SE vibrating wave is the slower wave; its refractive index is  $n_z'$ .

By inserting the first-order red plate or the lambda/4 plate into the light path, with the compensator direction  $Z'$  ( $\gamma$ ) in diagonal NE-SW orientation, the two different positions I and II can be distinguished as follows:

#### I. $Z'$ (mineral) || Z (compensator); $X'$ (mineral) || X (compensator)

The interference colours of the mineral shift to colours of a higher order: this is called addition.

Minerals with low birefringence (quartz and feldspars, for example) and white to grey first-order interference colours show blue to greenish-yellow second-order colours as the first-order red plate is inserted, and first-order yellow if the lambda/4 plate is inserted (Fig. 4-43).

The colour shift to a higher order is not always easily identified in minerals with high birefringence and interference colours of the 3<sup>rd</sup> or higher order, particularly for the novice. In such cases the quartz wedge may be used instead of the first-order red plate. By inserting the quartz wedge, the continuous change of the interference colours towards paler hues can be observed whereby the colours eventually reach a high-order white if the minerals have sufficiently high birefringence (such as carbonates).

For the assessment of high interference colours, the observations at wedging-out edges of crystal plates are particularly useful. From the grain interior to the outer edge the crystal plate thickness decreases. The interference colours change correspondingly displaying a continuous sequence of decreasing orders down to first-order black. If the quartz wedge is inserted, the colour bands shift towards the grain edge, which is particularly well recognised in the reds of first and second order (Fig. 4-44). The outer edge of the grain eventually shows a fourth-order red, the grain interior shows higher interference colours.

Interpretation:

In an anisotropic mineral, the  $n_x'$  wave advances faster in the crystal plate than the  $n_z'$  wave. Both waves have different wavelengths. After leaving the mineral, both waves have the same velocity and wavelength, but with an accumulated retardation of  $\Gamma_{\text{Min}} = d * (n_z' - n_x')$ .

With this retardation, the waves enter the crystal plate of the compensator, whereby the mineral's  $n_x'$  wave is again the faster wave  $n_{x\text{Comp}}$ , the original  $n_z'$  wave transforms to the slower wave  $n_{z\text{Comp}}$ . Therefore, the retardation accumulated in the mineral is now further increased by the retardation of the compensator. There is an increase of interference colours:

$$\Gamma_{\text{Min}} + \Gamma_{\text{Comp}} = \Gamma_{\text{total}}$$

When inserting the first-order red plate or the quartz wedge with the mineral in this position it should be noted that the colours are always increasing towards a higher order.

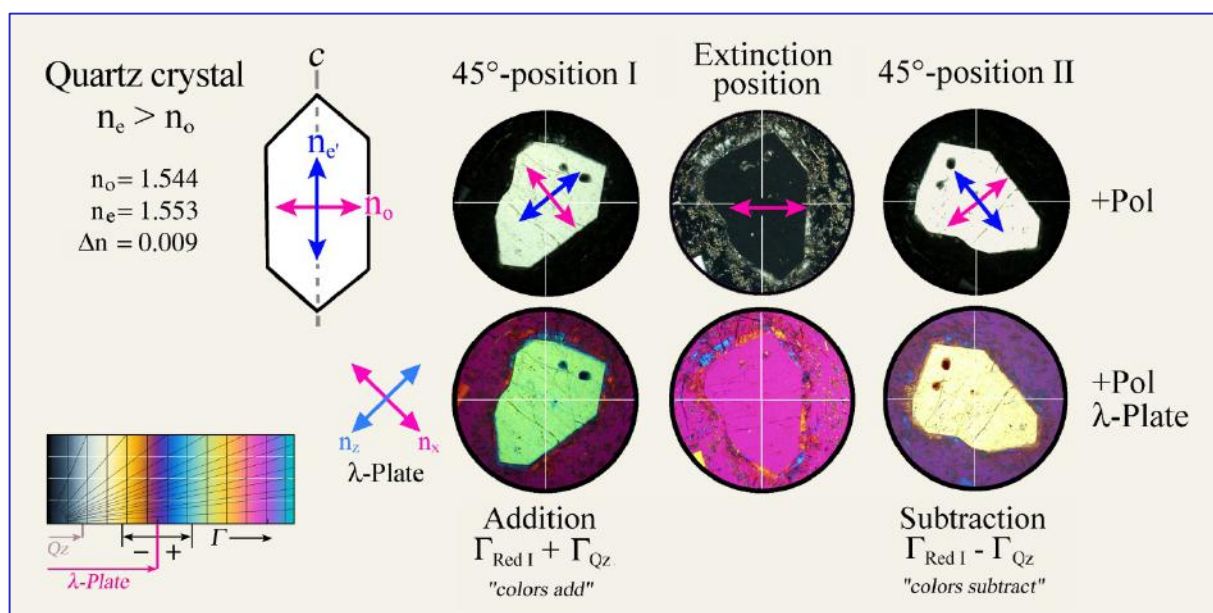


**Figure 4-43.** Addition and subtraction in the two diagonal positions of a quartz grain cut oblique to its c axis. The E-wave vibrates parallel to c, whereby  $n_e' = n_z'$ ; the O-wave vibrates orthogonal to c, with  $n_o = n_x$ .

## II. Z' (mineral) || X (compensator); X' (mineral) || Z (compensator)

The interference colours of the mineral section shift to colours of a lower order: this is referred to as subtraction.

Minerals with low birefringence (quartz and feldspars, for example) and white to grey first-order interference colours show orange to grey first-order colours as the first-order red plate is inserted, and first-order dark grey if the lambda/4 plate is inserted (Fig. 4-43).

The colour shift to a lower order is not always easily identified in minerals with high birefringence and interference colours of the 3<sup>rd</sup> or higher order, particularly for the novice. In such cases, the quartz wedge may be used instead of the first-order red plate. By inserting the quartz wedge, the continuous change of the interference colours towards more saturated hues can be observed while the colours shift to lower orders. In minerals with low birefringence first-order black is reached initially. With further insertion of the quartz wedge, the colour sequence reverts to increasing interference colours (e.g., olivine and white mica). At thinning-out crystal plate edges, the colour bands move towards the grain interior as the quartz wedge is inserted (Fig. 4-44). This effect is particularly evident from the red tones of the first, second and third order. The dark grey colour band of the first order at the outermost edge of the mineral migrates into the grain interior and is replaced by colours of the first to third order, if the interference colours of the mineral lie in the first to second order (e.g., olivine, white mica, pyroxenes).

#### Interpretation:

In an anisotropic mineral, the  $n_x'$  wave advances faster in the crystal plate than the  $n_z'$  wave. Both waves have different wavelengths. After exciting the mineral, both waves have the same velocity and wavelength, but with an accumulated retardation of  $\Gamma_{\text{Min}} = d * (n_z' - n_x')$ .

With this retardation, the waves enter the crystal plate in the compensator in which the fast and slow wave directions are at 90° to those of the mineral. The mineral's  $n_x'$  wave now becomes the slower wave  $n_{z\text{Comp}}$ , the original  $n_z'$  wave transforms to the faster wave  $n_{x\text{Comp}}$ . Therefore, the retardation accumulated in the mineral is now reduced by the retardation of the compensator. There is a decrease of interference colours:

$$\Gamma_{\text{Min}} - \Gamma_{\text{Comp}} = \Gamma_{\text{total}}$$

When inserting the first-order red plate or the quartz wedge, the following is to be noted:

1. If the retardation of the mineral is larger than that of the compensator, only decreasing colours of a lower order are observed.
2. If the retardation of the mineral is the same as that of the compensator, the mineral appears in first-order black ( $\Gamma_{\text{total}} = 0$ ). The retardation of the mineral is fully compensated.
3. If the retardation of the mineral is smaller than that of the compensator, the interference colour are reduced to a value corresponding to the difference  $\Gamma_{\text{Comp}} - \Gamma_{\text{Min}}$ . When inserting the quartz wedge, decreasing colours will be observed initially, down to first-order black, after which colours will increase again.

# Anhydrite

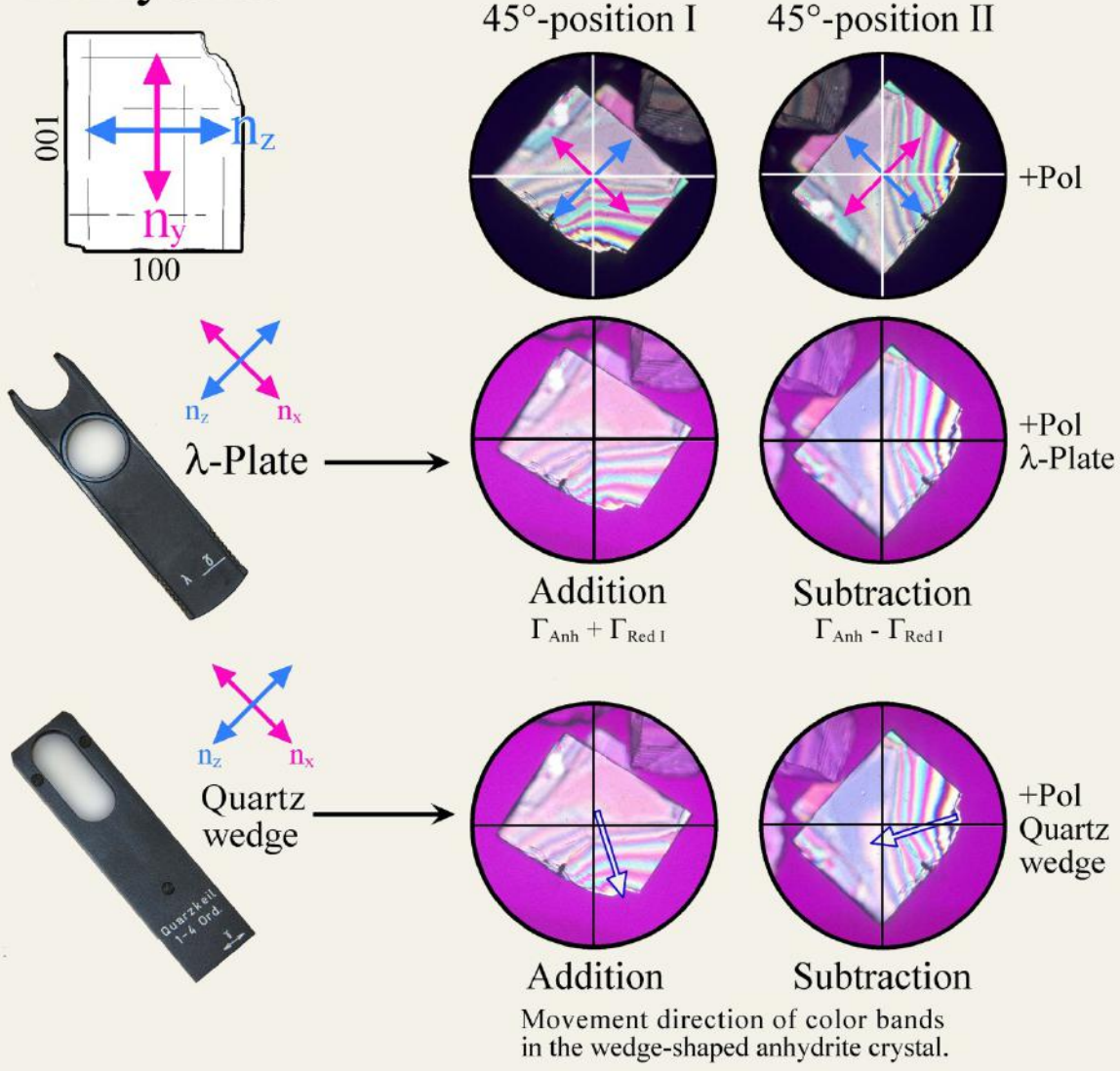


**Figure 4-44.** Anhydrite grain showing a colour sequence covering seven orders.

Addition and subtraction can be easily recognised by observing the changes in the colour sequence along the wedge-shaped edge of the grain. Compensation with first-order red shifts the colour sequence into the grain interior by one order (subtraction), or towards the grain edge by one order (addition). When using the quartz wedge for compensation, the colour sequence moves either into the grain interior by four orders (subtraction) or out of the grain (addition).

The interference colours of minerals that are strongly coloured in plane-polarized light may be masked significantly such that addition and subtraction positions with inserted first-order red plate are not easily distinguished by a novice. In such cases, it is recommended to use the quartz wedge and to observe the movement of colour bands at the wedging-out edges of the mineral grains.



## Sign of elongation I

Crystals with columnar to acicular or platy to flaky habits show elongate sections if cut parallel to their long morphological axis or perpendicular to a dominantly developed basal plane. If such elongate sections are rotated into a diagonal position (i.e., long axis l parallel to NE-SW) they show under crossed polarizers and compensator-in (first-order red plate or  $\lambda/4$  plate) either addition ( $\Gamma_{\text{Comp}} + \Gamma_{\text{Min}} = \Gamma_{\text{total}}$ ) or subtraction ( $\Gamma_{\text{Comp}} - \Gamma_{\text{Min}} = \Gamma_{\text{total}}$ ), depending on their optic sign (Fig. 4-45).

Addition is observed if the wave with the larger refractive index ( $n_z'$ ) vibrates parallel or at a small angle to the long dimension of the crystal section: l (+) = positive sign of elongation or "length-slow". Examples: acicular-columnar crystals— sillimanite, gedrite, anthophyllite; platy crystals— gehlenite, micas, antigorite, pennine.

Subtraction is observed if the wave with the smaller refractive index ( $n_x'$ ) vibrates parallel or at a small angle to the long dimension of the crystal section: l (-) = negative sign of elongation or "length-fast". Examples: acicular-columnar crystals— tourmaline, apatite; platy crystals— åkermanite, brucite, clinochlore.

For optically uniaxial mineral species with acicular-columnar habit, the sign of elongation corresponds to the optic sign. For platy uniaxial minerals, the two signs are opposite.

Elongate sections in which  $n_y$  is parallel (or at a small angle) to the morphological long axis of the crystal or perpendicular to the planar dimension of platy crystals show a variable sign of elongation, l(+) or l(-), depending on the exact orientation of the crystal in thin section. Examples of such elongate crystals— wollastonite, epidote.

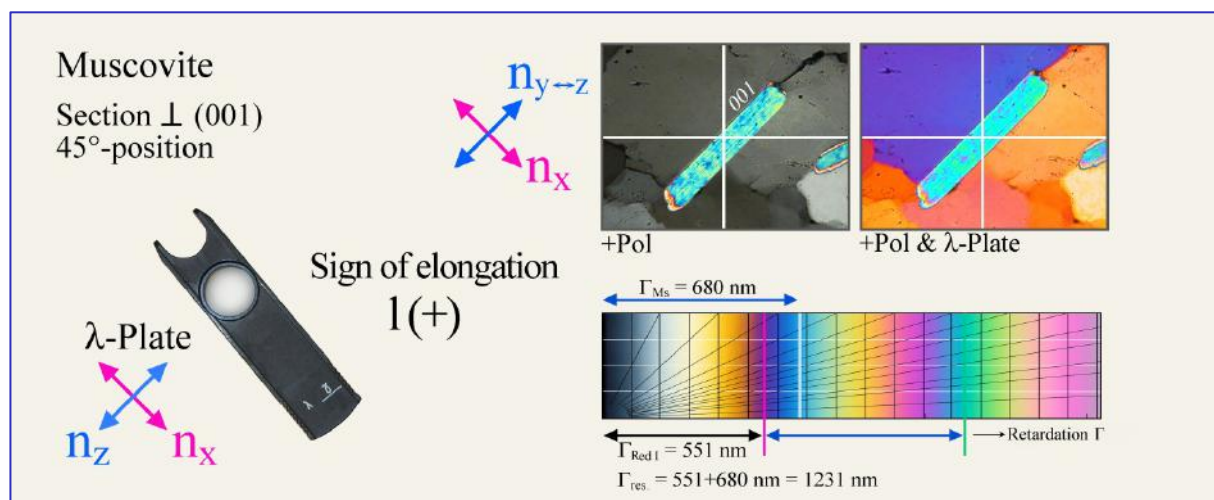


**Figure 4-45 A.** Platy muscovite showing positive sign of elongation. In muscovite and first-order red plate, fast ( $n_x$ ) and slow ( $n_y \leftrightarrow n_z$ ) waves vibrate in identical orientation. Therefore, the retardation adds up and increased interference colours result ( $\Gamma_{\text{res.}} = \Gamma_{\text{Red1}} + \Gamma_{\text{Ms}} = 1231 \text{ nm}$ ; second-order blue-green).

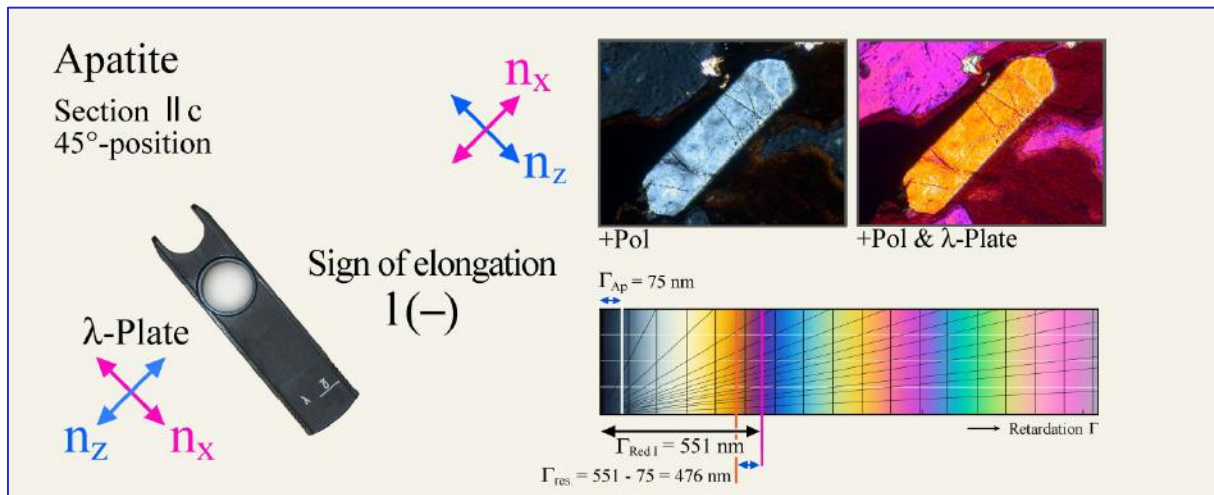


**Figure 4-45 B.** Prismatic apatite showing negative sign of elongation. In apatite, the fast wave vibrates parallel to the slow wave of the first-order red plate, and the slow wave in apatite parallel to the fast wave of the first-order red plate. Hence, retardation is reduced and subtraction results ( $\Gamma_{res} = \Gamma_{Red1} + \Gamma_{Ap} = 476 \text{ nm}$ ; first-order orange-yellow).

If the extinction direction deviates significantly from the long axis of the crystal section, it is convention to use the extinction position that forms an angle smaller than  $45^\circ$  with the long axis, and to rotate it into the diagonal position before the first-order red plate or lambda/4 plate is inserted for determining the sign of elongation. However, if extinction angles are close to  $40\text{--}50^\circ$ , the use of  $l(+)$  and  $l(-)$  becomes impractical.

### Determination of the optic sign of optically uniaxial minerals

Optically uniaxial minerals that are elongate in  $c$  direction (e.g., quartz, apatite, tourmaline) and are present in thin section in a cut that is roughly parallel to that long axis, will have the E-wave ( $n_e$ ) vibrating parallel to  $c$  and the O-wave ( $n_o$ ) orthogonal to  $c$ . If the habit of optically uniaxial minerals is platy (e.g., melilite), the same applies, but the O-wave now vibrates parallel to the elongate section.

For both crystal habits, the optic sign can be determined easily by compensation, that is, whether  $n_e > n_o$  (= optically uniaxial positive) or  $n_e < n_o$  (= optically uniaxial negative) (Fig. 4-46). The long axis of the crystal section is rotated into diagonal position (NE-SW orientation), and the first-order red plate or lambda/4 plate is inserted. For crystals elongate in  $c$ ,  $n_e$  is now parallel to  $n_{zComp}$  and  $n_o$  is parallel to  $n_{xComp}$ . For platy minerals, the relation is reverse as  $c$  is perpendicular to the long dimension of the crystal sections. The retardation between the waves which are created in the optically uniaxial mineral ( $\Gamma_{Min}$ ) and in the compensator plate will be increased through addition or decreased through subtraction, depending on optical sign. Correspondingly, the crystal section shows higher or lower interference colours if the compensator is inserted.

Elongate section through an elongate-prismatic crystal:  $n_e$  is aligned with the long axis of the section;  $n_o$  is orthogonal to it. Addition occurs if  $n_e < n_o$ ; the mineral is optically uniaxial-positive. Subtraction occurs if  $n_e > n_o$ ; the mineral is optically uniaxial-negative.

Profile section through a platy mineral:  $n_o$  lies parallel to the long axis of the elongate cross-section;  $n_e$  is orthogonal to it. Addition occurs if  $n_e < n_o$ ; the mineral is optically uniaxial-negative. Subtraction occurs if  $n_e > n_o$ ; the mineral is optically uniaxial-positive.

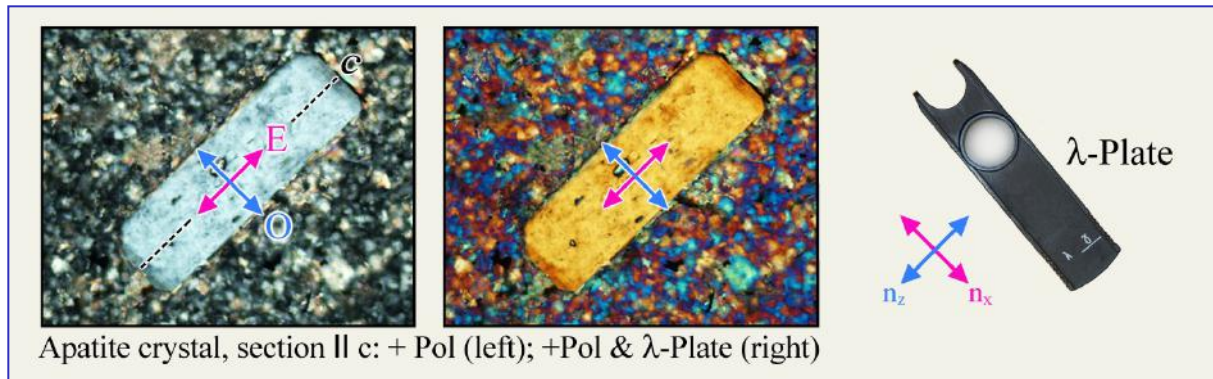


**Figure 4-46 A.** Hexagonal apatite forms elongate crystals that show subtraction with the first-order red plate inserted, when placed in diagonal position. Hence, the optic sign is negative ( $n_e < n_o$ ).

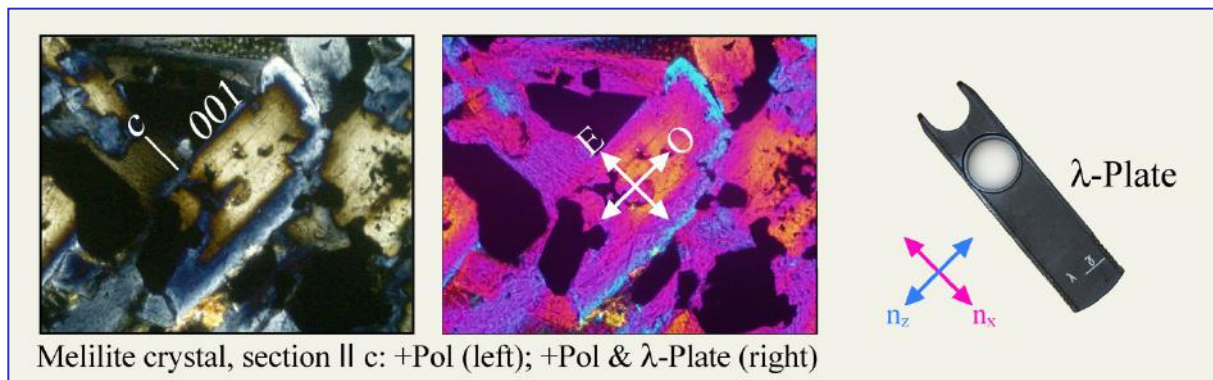


**Figure 4-46 B.** Tetragonal melilite forms platy crystals that show either addition or subtraction with the first-order red plate inserted, depending on composition. In this example, the core domain is optically positive (high akermanite content), whereas the rim is optically negative (high Na-melilite + gehlenite components).

## 4.2.5 Conoscopic methods

### 4.2.5.1 Some basic principles

In "**normal**" **orthoscopic view** light enters the thin section orthogonally as a set of parallel, E-W vibrating light waves. The objective creates an enlarged, real, inverted image of the thin section, which is then further enlarged and viewed through the ocular. The light rays entering the thin section travel through the mineral grains in defined crystallographic directions that depend on the respective orientation of the crystals. In order to record the optical behaviour of an anisotropic mineral species, crystal sections of different orientations must be studied, as outlined in previous chapters (e.g., crystal sections with maximum interference colour are needed to determine birefringence).

*Optic axial angle and optic sign cannot be determined directly in the orthoscopic mode of operation, except in specific circumstances where the crystal symmetry is known to be high (hexagonal, trigonal, tetragonal) and where the crystal shape allows to identify the c-axis direction (cf. Ch. 4.2.4).*

As opposed to orthoscopy, the **conoscopic view** involves a convergent set of light rays, which means that a wide-angle cone of differently inclined light rays transmits the thin section (Fig. 4-47). To achieve this, the illumination aperture is enlarged to a maximum by putting the auxiliary condenser lens into the light path and opening the substage iris diaphragm.

Dependent on their propagation direction, the rays of this light cone will form an image in the focal plane above the objective, whereby the maximum opening angle of the cone of rays forming that image depends on the aperture of the objective used (Fig. 4-48). Since two orthogonally vibrating waves propagate generally in all directions within optically anisotropic minerals, these wave couplets are brought into interference in the analyzer, generating an interference figure. This interference figure can be viewed, either as an enlarged image by putting an auxiliary lens (Amici-Bertrand lens) into the light path, or with the naked eye by removing an ocular and looking down the ocular tube. Light waves that travel in the direction of the microscope axis, and are thus oriented orthogonal to the thin section plane, form the centre of the interference figure. The larger the angle of the ray propagation direction to the microscope axis, the larger the distance of the image point from the centre of the interference figure. Thus, the conoscopic interference figure allows to study the propagation behaviour of light in an anisotropic crystal quasi-simultaneously for a multitude of crystallographic directions within that crystal.

*From the geometry of the interference figure and its modification through the use of compensators, the number of optic axes (uniaxial vs. biaxial), the optic axial angle ( $2V$ ) and the optic sign (positive vs. negative) can be determined.*

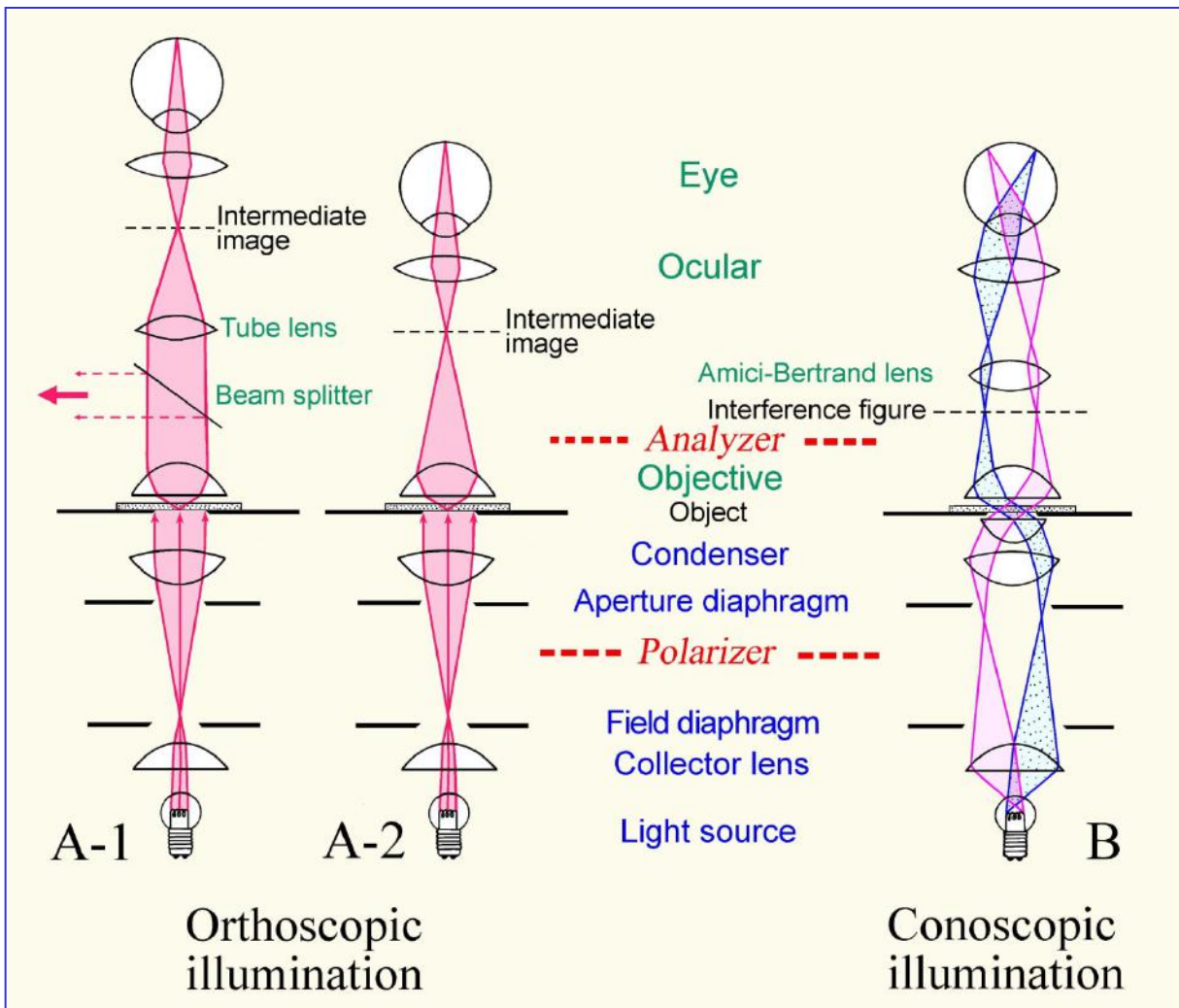


Figure 4-47. Light paths in the polarized-light microscope

**A: Orthoscopic illumination mode.** In finite tube-length microscopes, the objective produces a real inverted image (intermediate image) of the specimen which then is viewed with further enlargement through the ocular (A-2). In infinity-corrected microscopes, the objective projects the image of the specimen to infinity, and a second lens placed in the tube (tube lens) forms the intermediate image which then is viewed through the ocular (A-1). This imaging design allows to insert accessory components such as analyzer, compensators or beam splitters into the light path of parallel rays between the objective and the tube lens with only minor effects on the image quality.

**B: Conoscopic illumination mode.** Parallel rays of the light cone which illuminates the specimen create an image in the upper focal plane of the objective (B). In the case of anisotropic crystals, an interference image is generated which can be viewed as an enlargement by inserting an auxiliary lens (Amici-Bertrand lens). The interference image can also be directly observed in the tube through a pinhole which replaces the ocular.

#### 4.2.5.2 Conoscopy of optically anisotropic crystals

In the conoscopic mode, waves deviating from vertical incidence by increasing tilt angles travel increasing distances within the birefringent crystal. According to the relationship  $\Gamma = d * (n_z' - n_x')$  described in chapter 4.2.3, it has to be concluded that the retardation  $\Gamma$  of the waves increases with increasing angles due to the continuous increase of  $d'$  (= length of the light path in the crystal plate). Accordingly, the interference colours in a conoscopic interference figure should generally increase outwards. However, the interference figure is to a much larger extent controlled by the orientation of the vibration directions and the birefringence values of the wave couplets within the observed volume of the anisotropic crystal. As described previously, the birefringence for waves parallel to optic axes is zero. It increases as the angle between the optic axis and ray propagation direction (or wave normal, to be precise) increases.

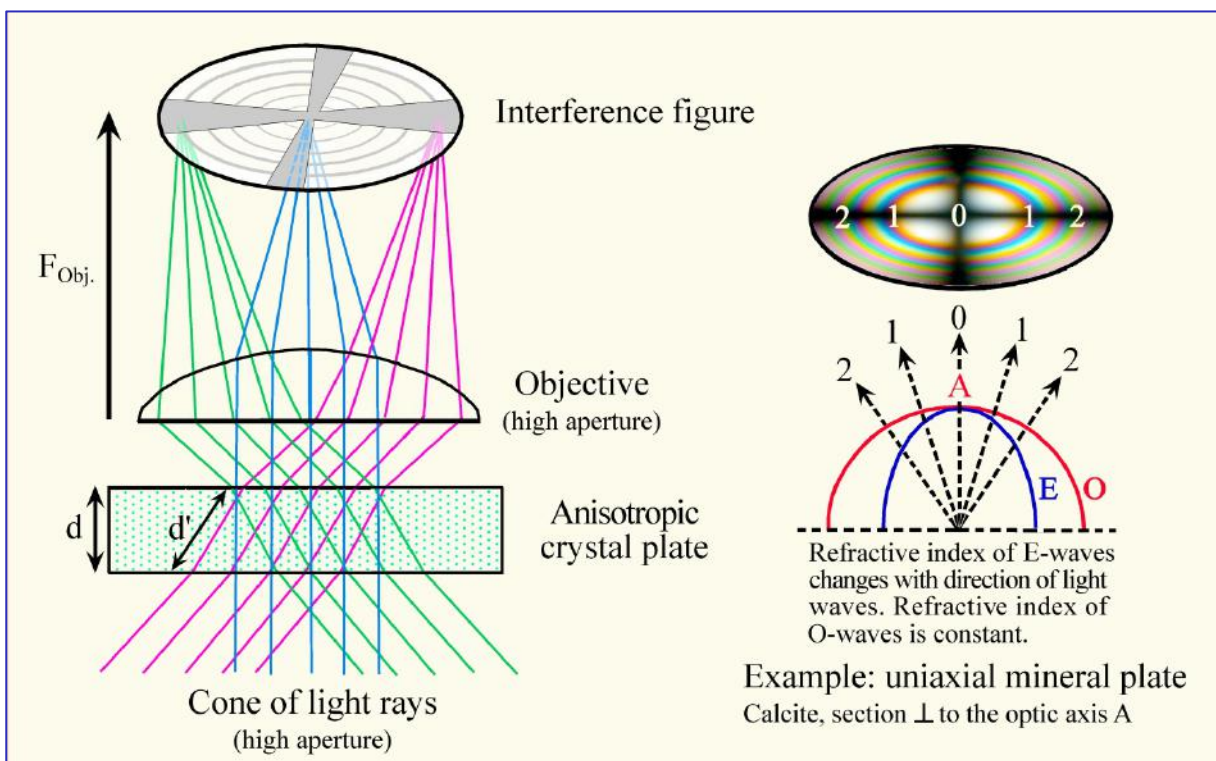


**Figure 4-48:** Generation of an interference figure in the upper focal plane of the objective by imaging of parallel sets of rays that pass the crystal plate at different angles. The example shows these relationships for a uniaxial crystal (calcite) cut perpendicular to the optic axis.

The geometry of interference figures obtained from anisotropic crystals can be illustrated with the model of the skiodrome sphere developed by Becke (1905). The crystal is considered to occupy the centre of a sphere. Each ray propagation direction of light waves within the crystal has a corresponding point on the spherical surface where the ray pierces that surface. In each of these points, the vibration directions of the related waves can be shown as a tangent (e.g., O and E in case of optically uniaxial minerals). When connecting all the tangents of equal vibration direction, a geometric mesh of vibration directions is generated that depends on the optical symmetry of the crystal (Fig. 4-49,50).

## Skiodrome sphere

For the optically uniaxial mineral species, a net of longitudinal and latitudinal circles, which has rotational symmetry, forms the surface of the sphere (Fig. 4-49). The meridians (longitudes) represent the vibration directions of the E-waves and the circles of latitude the O-waves. The optic axis A is the rotation axis of the net.

For the optically biaxial mineral species, the spherical surface consists of an arrangement of two sets of cross-cutting ellipses with orthorhombic symmetry (Fig. 4-50). The optic axes  $A_1$  and  $A_2$  emerge at the common foci of the ellipses. The symmetry planes of the net correspond to the principal sections ZX, ZY and YX.

## Skiodrome net (projected)

For practical reasons, the part of the surface of the skiodrome sphere that is captured in the conoscopic cone of light rays as it emerges from a crystal sections is projected onto the thin section plane (Fig. 4-49,50). The skiodrome nets and the corresponding interference figures for diagnostically important orientations of optically uniaxial and biaxial minerals are presented in Figs. 4-51 to 4-54.

## Interference figure

In the interference figure, those domains are in extinction in which the vibration directions of the waves are parallel to the polarizer and analyzer directions. [Analogy to the orthoscopic extinction position: light entering the crystal in such directions will vibrate exclusively E-W and hence will be blocked by the analyzer; N-S vibrating waves are not generated!]. The domains of extinction are called "isogyres". Their geometry is dependent on the optical symmetry and the orientation of the crystal, and it may change as the microscope stage is turned (Figs. 4-51 to 4-54).

The domains in which the vibration directions of the waves deviate from the polarizer and analyzer directions appear in different brightness and different interference colours. [Analogy to the orthoscopic diagonal position: the light entering the birefringent crystal plate in such directions is split into two sets of orthogonally vibrating waves, which interfere afterwards in the analyzer]. Curved lines of equal colour (or equal retardation  $\Gamma$ ) are called "isochromes". Their geometry depends on the optical symmetry and the orientation of the crystal (Fig. 4-51,53). The range of the colour spectrum, i.e. the number of isochromes, is determined by the birefringence values, the thickness of the crystal plate [ $\Gamma = d * (n_z' - n_x')$ ] and the aperture of the objective (Figs. 4-52 to 4-54).

## Skidrome Sphere

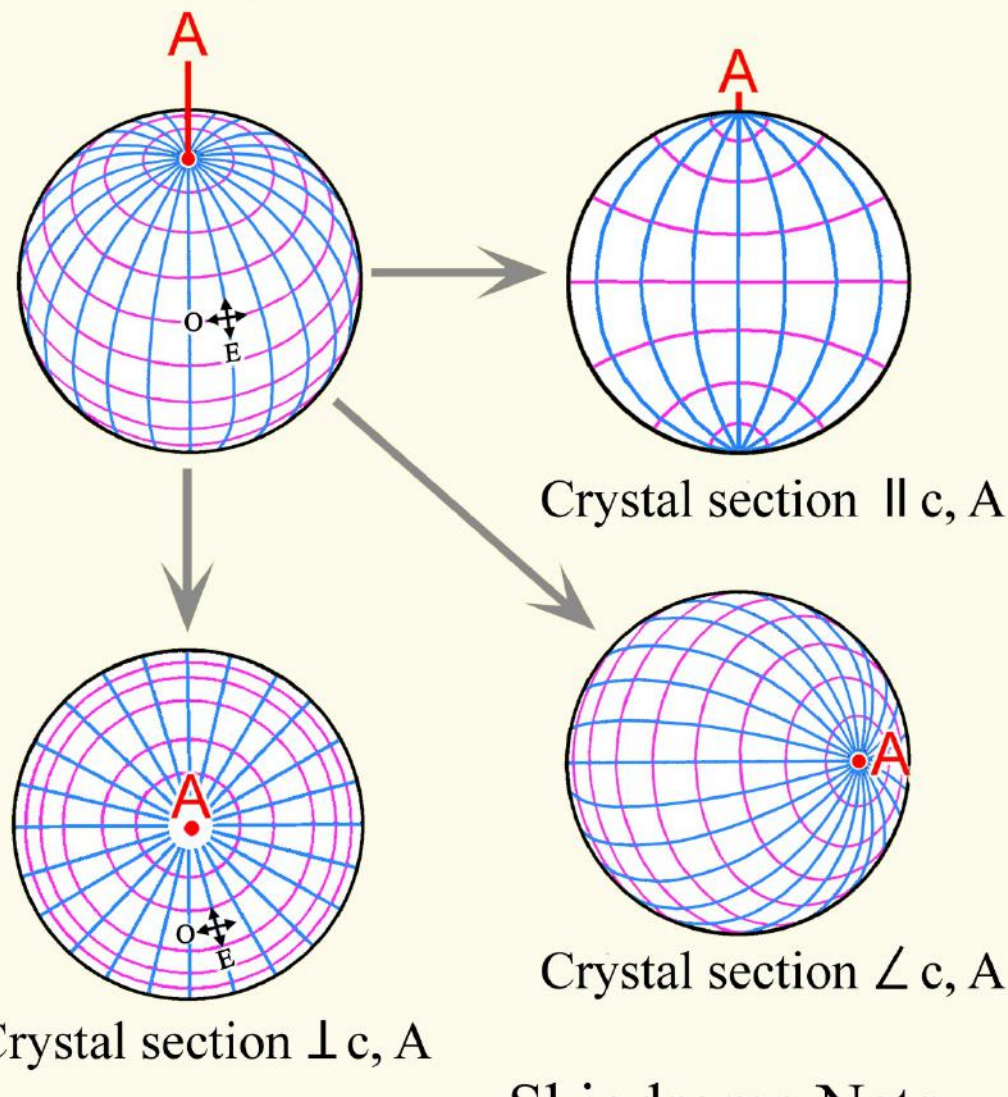
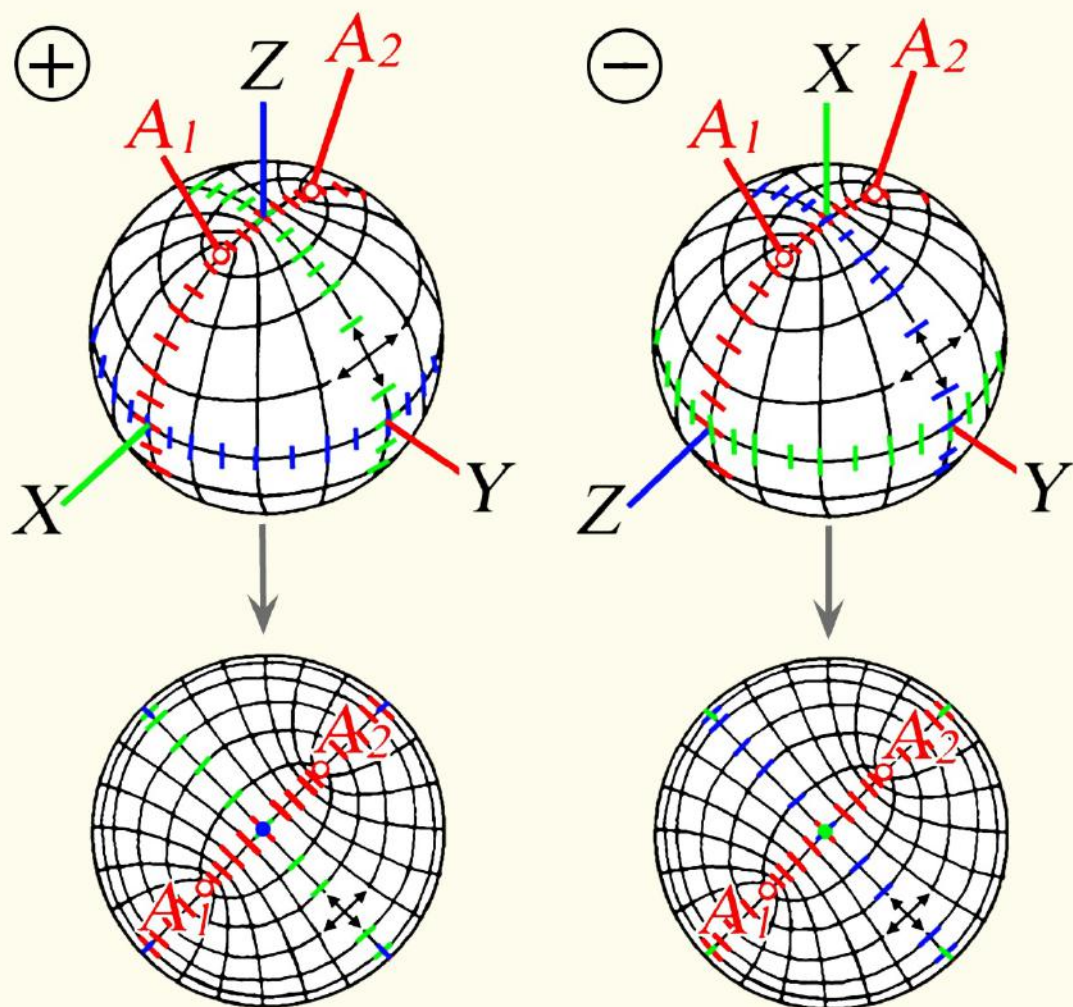


**Figure 4-49.** Skidrome sphere and projections for optically uniaxial crystals.

On the skidrome sphere the vibration directions of the orthogonally vibrating O- and E-waves are fixed for all ray propagation directions. The O-waves (red) vibrate always latitudinally, the E-waves (blue) vibrate longitudinally. Projections of the 3-D skidrome net onto the plane of view are most useful for the interpretation of interference figures which result from different orientations of the uniaxial crystal. The figure shows such projections for crystal sections orthogonal to, oblique to, and parallel to the optic axis (resp. c-axis) of the crystal.

## Skiodrome Spheres: biaxial crystals



**Skiodrome Nets**  
sections  $\perp$  acute bisectrix

**Figure 4-50.** Skiodrome sphere and projections for optically biaxial crystals.

On the skiodrome sphere, the vibration directions of the orthogonally vibrating waves are fixed for all ray propagation directions. The net shows two sets of cross-cutting ellipses. The two optic axes  $A_{1,2}$  emerge at the common foci of the ellipses. Vibration directions with the principal refractive indices  $n_z$ ,  $n_y$  and  $n_x$  lie within the XY, ZX and ZY principal sections and are shown here in blue, red and green, respectively. For the investigation of optic sign and optic axial angle  $2V$ , interference figures of crystal sections orthogonal to the acute bisectrix (Z or X, for  $2V < 45^\circ$ ) or perpendicular to one of the optic axes ( $A_{1,2}$ , for  $2V > 45^\circ$ ) are most useful.

#### 4.2.5.3 Optically uniaxial minerals

For the optically uniaxial mineral species a net of meridional and latitudinal circles, which has rotational symmetry, forms the spherical surface of the skiodrome (Fig. 4-49). The meridians represent the vibration directions of the E-waves and the circles of latitude the O-waves. The optic axis A is the rotation axis of the net.

**Crystal sections perpendicular to the optic axis A** are recognised in orthoscopic view by their isotropic behaviour. In conoscopic view, these sections show a characteristic interference figure which is a black cross. The isogyes become broader towards the margin of the field of view, and the four sectors are filled by concentric coloured circles. The optic axis forms the centre (melatope) of the cross (Figs. 4-49, 51, 52). If the microscope stage is turned, the interference figure does not change.

##### Interpretation of the interference figure

The vibration directions of the O- and E-waves are orthogonal to each other and are arranged concentrically around the optic axis. In the N-S and E-W directions of the interference figure, the vibration directions coincide with the polarizer and analyzer directions. In these directions only E-W vibrating waves pass the crystal plate (O-waves along the N-S isogyre; E-waves along the E-W isogyre), but these will be blocked by the analyzer. Due to the rotational symmetry of the indicatrix (and the skiodrome net) and the particular orientation of the crystal plate (viewing direction parallel to the optic axis), the interference figure does not move or change if the stage is rotated.

The increase of the interference colours towards the edge of the field of view is caused by the increase of the retardation  $\Gamma$  of the O-waves and E-waves from the centre [ $\Delta n = 0$  in the direction of the optic axis] to the periphery, whereby the potential range of visible colours is limited by the mineral-specific maximum birefringence perpendicular to the optic axis. [ $\Delta n = |n_e - n_o|$ ]. The circular arrangement of isochromes is a result of the rotational symmetry of the indicatrix and the specific crystal orientation perpendicular to the optic axis. The range of the colour spectrum (i.e., the number of isochromes) depends on birefringence and crystal plate thickness [ $\Gamma = d * (n_e' - n_o)$ ] as well as on the numerical aperture of the objective. For example, in a thin section of 25 $\mu\text{m}$  thickness, the interference figure of highly birefringent calcite ( $\Delta n = 0.172$ ) comprises about six orders of interference colour, while quartz ( $\Delta n = 0.009$ ) shows first-order colours only (Fig. 4-52).

**In crystal sections oblique to the optic axis A**, the isogyre cross shifts towards the periphery of the field of view and moves in a circular fashion if the microscope stage is rotated. The distance of the melatope to the centre of the field of view reflects the tilt angle between the optic axis and the microscope axis. The E-W and N-S portions of the isogyre cross move through the field of view without rotation (Fig. 4-51 B,C).

Crystal sections parallel to the optic axis show maximum birefringence in orthoscopic view. The conoscopic interference figure shows a broad black cross which, at minimal rotation of the stage, quickly opens up ("flash figure", Fig. 4-51D). Due to their similarity with interference figures of optically biaxial minerals, interference figures of such orientations have no practical significance.

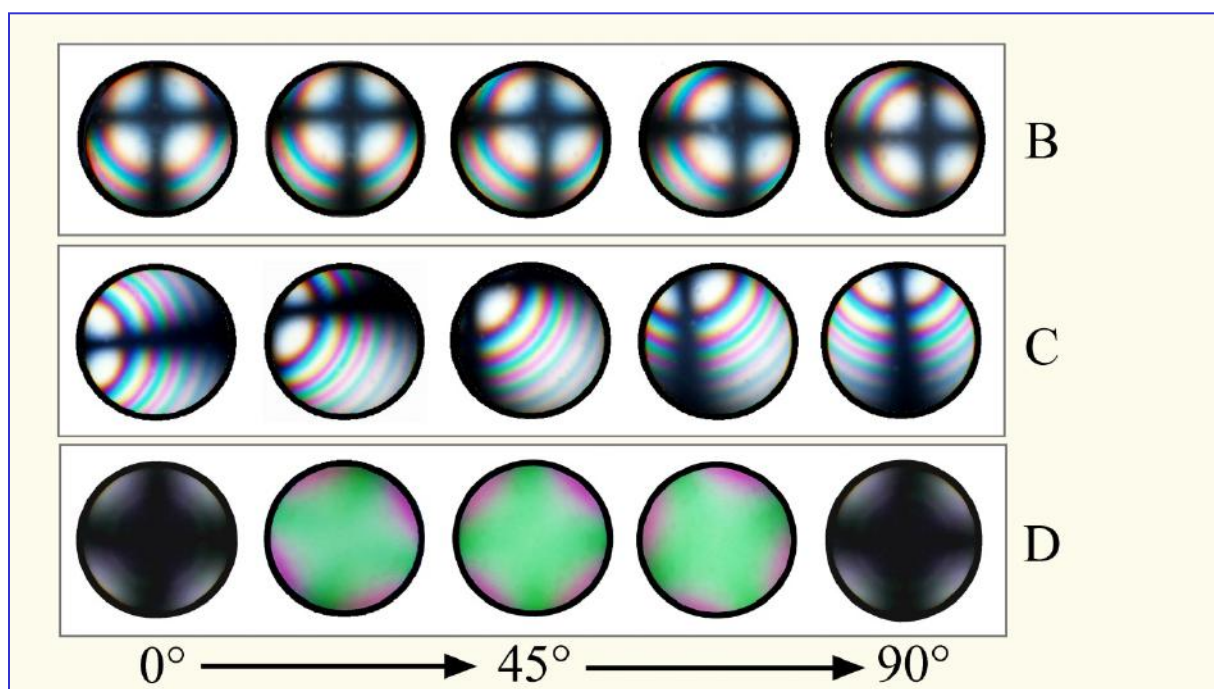
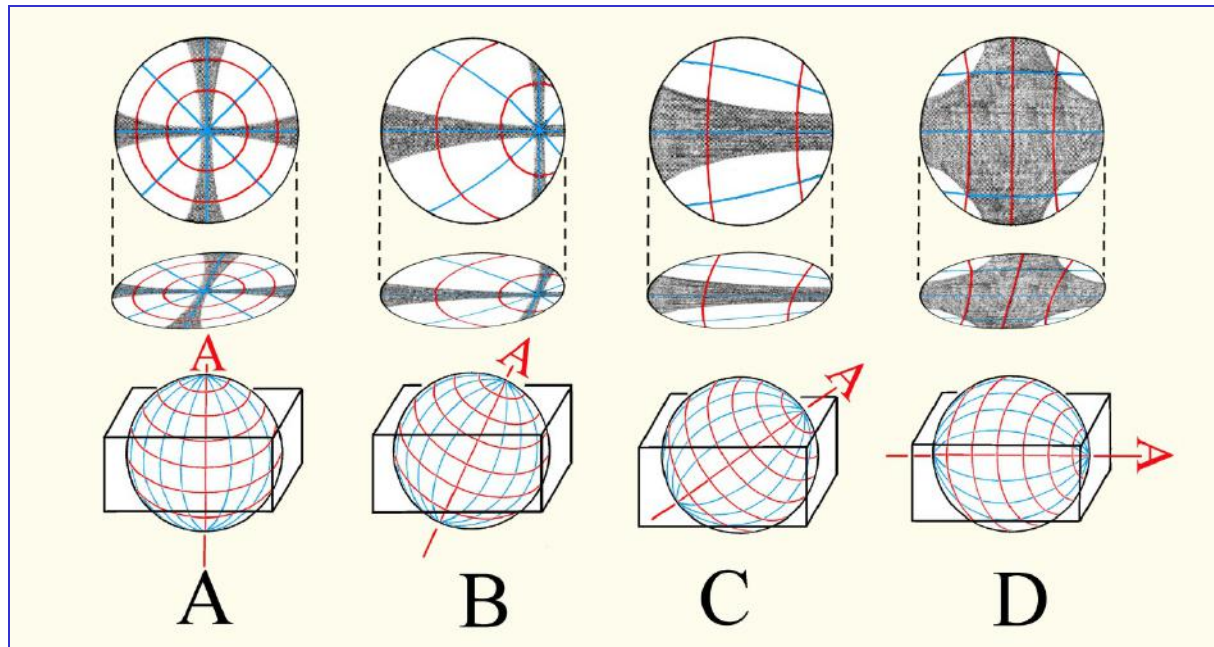


**Figure 4-51.** Interference figures of optically uniaxial minerals

Upper section: Skiodrome presentations and isogyres for differently oriented crystal sections of a uniaxial crystal. The vibration directions are shown in red (O-wave) and blue (E-wave).

Lower section: Shift of isogyres and isochromes for crystal orientations B, C and D during a 90° rotation of the microscope stage.

## Determining the optic sign of uniaxial minerals

For the determination of optic sign, crystal sections are required that are either isotropic or show very low interference colours in orthoscopic view. The conoscopic interference figure will then show a more or less centred, dark isogyre cross.

If the first-order red plate is inserted, the cross will appear in 1<sup>st</sup>-order red, while the four quadrants display two different sequences of interference colours, depending on the vibration direction of the E- and O-waves. Two cases have to be distinguished:

**Case A:** In quadrants I and III the interference colours increase by one order (= addition), while in quadrants II and IV the interference colours decrease by one order (= subtraction). Thus,  $n_e' > n_o$ , and hence the optic sign of the minerals is positive (Fig. 4-52; example quartz).

**Case B:** In quadrants I and III the interference colours decrease by one order (= subtraction), while in quadrants II and IV the interference colours increase by one order (= addition). Thus,  $n_e' < n_o$ , and hence the optic sign of the minerals is negative (Fig. 4-52; example calcite).

The interference figure in high-birefringent minerals shows multiple isochromes. In order to distinguish clearly between cases A and B, it is suggested to use the quartz wedge instead of the first-order red plate. When inserting the quartz wedge, the isochromes in the four quadrants shift in a characteristic way (Fig. 4-52,55).

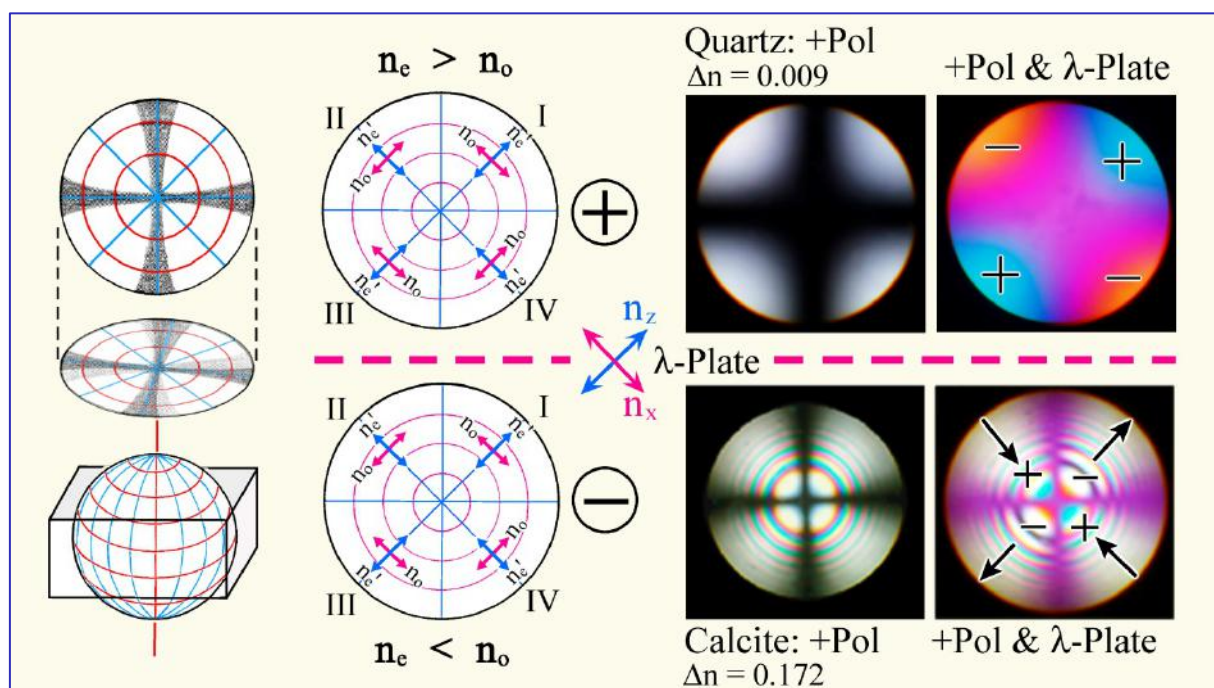


**Figure 4-52.** Determination of the optic sign of a uniaxial crystal.

The distinction between positive and negative optic sign is made in sections perpendicular to the optic axis by observing the addition and subtraction phenomena caused by insertion of the first-order red plate.

#### 4.2.5.4 Optically biaxial minerals

The skiodrome sphere of optically biaxial mineral species shows an arrangement of overlapping ellipses that possesses an orthorhombic symmetry (Fig. 4-50). The optic axes  $A_1$  and  $A_2$  emerge at the common foci of the ellipses. They enclose the axial angle  $2V$  which can attain mineral-specific values between  $0^\circ$  and  $90^\circ$ . The bisector (acute bisectrix) of  $2V$  is either  $Z$  ( $2V_z < 90^\circ$  = optically positive) or  $X$  ( $2V_x < 90^\circ$  = optically negative). The symmetry plane of the net corresponds to the principal sections  $ZX$  (= optic axial plane),  $ZY$  and  $YX$  of the indicatrix.

**Crystal sections orthogonal to the acute bisectrix** (at small  $2V$ ) or **orthogonal to one of the optic axes** provide the diagnostically least ambiguous interference figures. As opposed to the interference figure of optically uniaxial crystals, the isogyres change their shape as the stage is rotated (Fig. 4-53 A,B).

**Interference figures of crystal sections oriented orthogonal to the acute bisectrix ( $2V < 60^\circ$ ).**

In extinction positions (orthoscopic view), the axial plane is oriented either N-S or E-W. In this position, the conoscopic image shows a black cross, with one isogyre being wider than the other. The thinner one represents the optic axial plane and appears tighter at the emerging points of the optic axes (melatopes). When examining highly birefringent minerals, multiple isochromes can be seen to surround the two melatopes (Fig. 4-53 A).

When turning the stage  $45^\circ$  into the diagonal position, the isogyre cross opens to form two hyperbolas which, depending on the sense of rotation, come to lie in quadrants I and III or in II and IV. The optic axes emerge in the inflection points of the hyperbolas. By rotating the stage  $360^\circ$ , the isogyres separate and converge, corresponding to the change between bright-image and extinction position in the orthoscopic mode of view (Fig. 4-53). With an increase in optic axial angle, the distance between the two hyperbola-shaped isogyres increases, while their curvature decreases (Fig. 4-53, bottom right).

**Interference figures of crystal sections oriented orthogonal to an optic axis ( $2V > 60^\circ$ ).**

The determination of the optic sign of minerals with a large optic axial angle requires crystal sections orthogonal to one of the two optic axes, or sections in which the viewing direction does not deviate significantly from the optic axis orientation. Such crystal sections appear in orthoscopic mode either isotropic or show low interference colours. The interference figure shows a more or less curving isogyre, with the optic axis emerging from the inflection point. As the stage is rotated, the isogyre rotates through the field of view (Fig. 4-53 C). [Conversely, the isogyres of optically uniaxial minerals move parallel to the polarizer-analyzer directions (E-W and N-S), Fig. 4-51]. The blue and also red fringes of the isogyres, as seen in Figs. 4-54 and 4-56 (mica), are caused by dispersion of the optic axes, which means that the position of the optic axes varies with the wavelength of light. Such colour fringes must not be confused with isochromes.

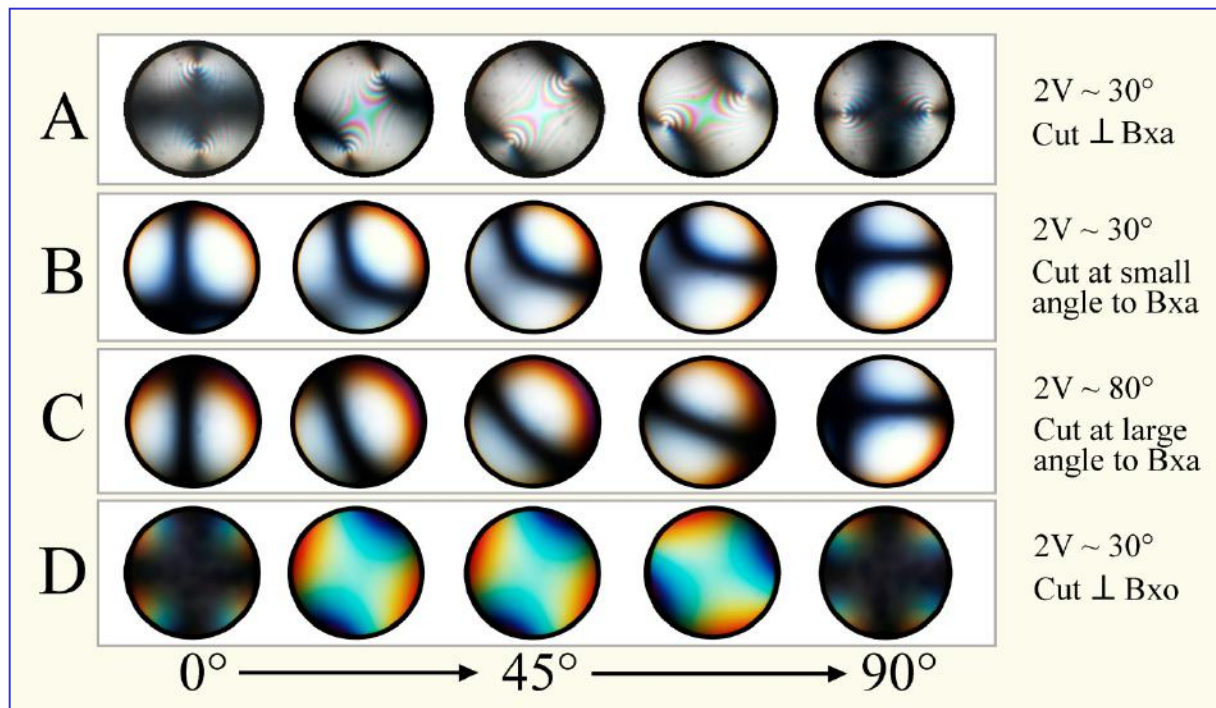
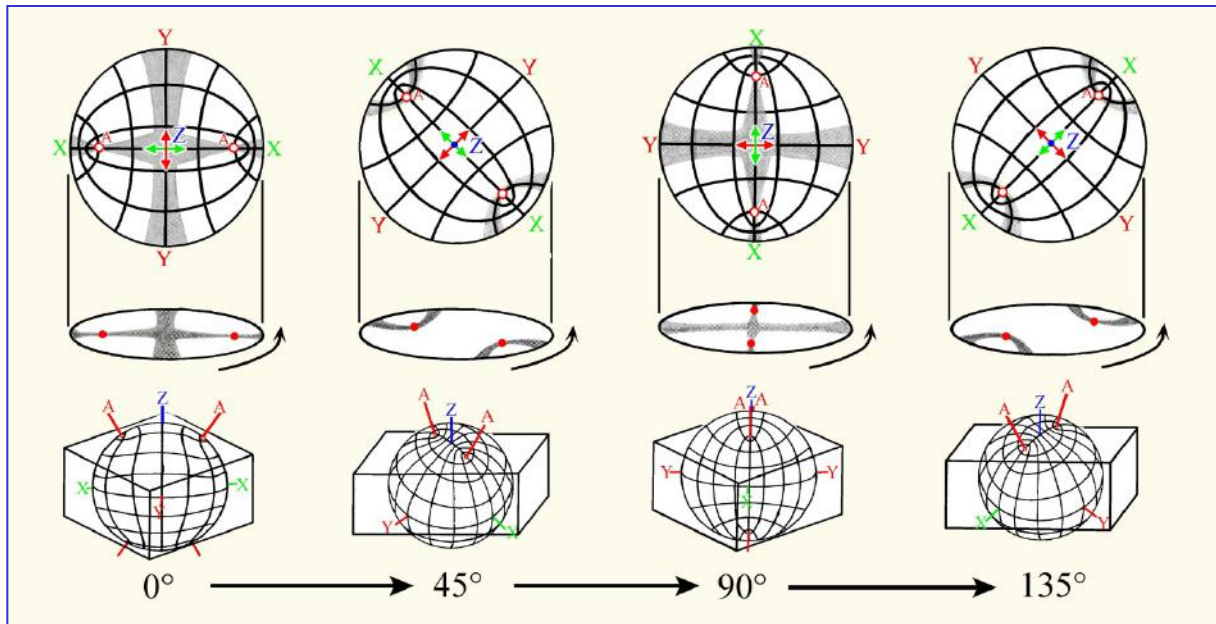
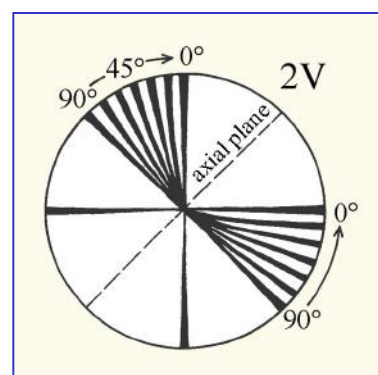


**Figure 4-53.** Interference figures of optically biaxial minerals.

Top: Modification of the interference figure of a crystal section orthogonal to the acute bisectrix during rotation of the microscope stage. Normal positions at 0° and 90°; diagonal positions at 45° and 135°.

Middle: Variation in interference figures of optically biaxial crystals depending on orientation, 2V and rotation position of the microscope stage. Shown are sequences corresponding to a rotation of 0 to 90°. Bxa—acute bisectrix, Bxo—obtuse bisectrix.

Bottom: Relation between 2V and isogyre curvature for crystal sections perpendicular to an optic axis.



## Determining the optic sign of biaxial minerals

For the determination of the optic sign, crystal sections with lowest-possible interference colours should be selected. For minerals with low 2V, acute bisectrix figures are also suitable (Fig. 4-54). Appropriate grains will show low, but not zero birefringence in orthoscopic mode. In general, it is sufficient to see one optic axis (melatope) within the field of view. Ideally, the point of maximum curvature (melatope) of the isogyre should lie in the centre of the field of view, such that the direction of curvature can be seen clearly. The convex side of the hyperbola points to the acute bisectrix, the concave side to the obtuse bisectrix.

For the observation of the change of interference colour when a compensator is inserted, the isogyres should be positioned such that the optic axial plane is in diagonal, NE-SW orientation. In this orientation, the concave sides of the isogyres point NE and SW, or either direction, if only a single isogyre is in the field of view. After inserting the first-order red plate, the isogyres appear in 1<sup>st</sup>-order red, while the interference colours in between the isogyres change in accordance with the optic sign of the mineral (Fig. 4-54):

**Case A:** On the convex sides of the isogyres subtraction occurs (1<sup>st</sup>-order orange-yellow close to the melatope), while the concave domains show addition (2<sup>nd</sup>-order blue close to the melatope). The acute bisectrix is Z; the optic sign of the minerals is therefore positive (Fig. 4-54; example aragonite).

**Case B:** On the convex sides of the isogyres addition occurs (2<sup>nd</sup>-order blue), while the concave domains show subtraction (1<sup>st</sup>-order orange-yellow). The acute bisectrix is X; the optic sign of the minerals is therefore negative (Fig. 4-54; example muscovite).

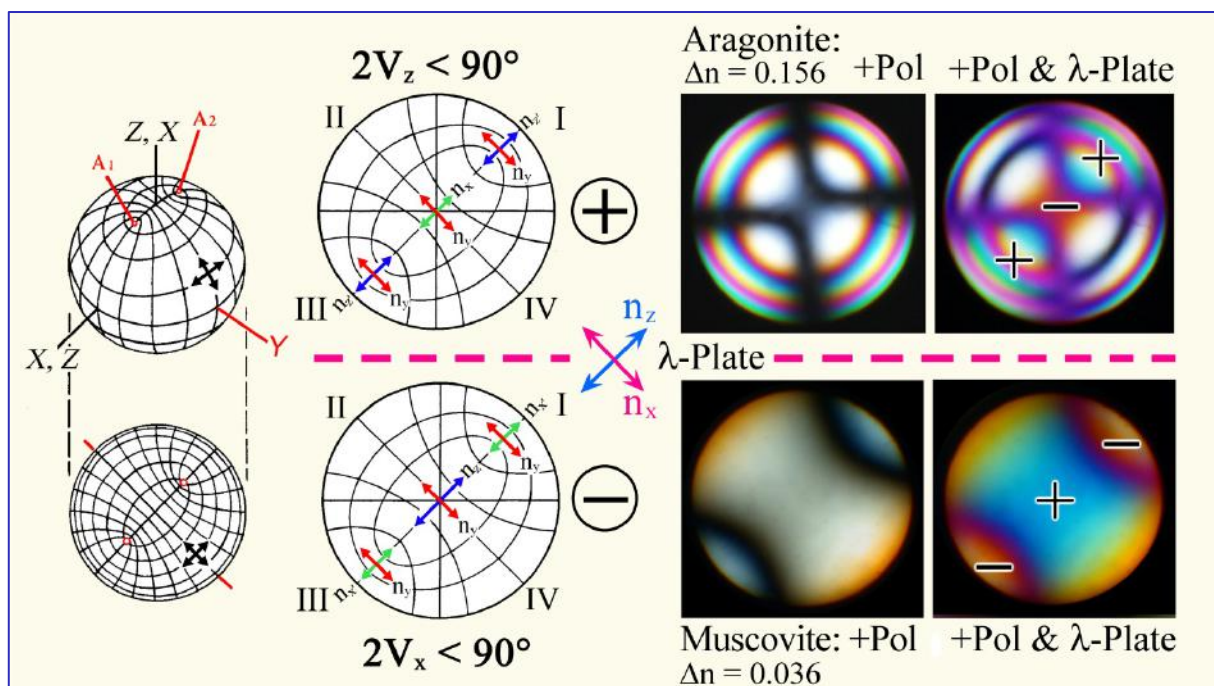


**Figure 4-54.** Determination of the optic sign of a biaxial crystal.

The optic sign can be determined in sections perpendicular to the acute bisectrix or perpendicular to one of the two optic axes. The distinction between positive and negative optic sign is made by observing the addition and subtraction phenomena resulting from insertion of the first-order red plate. The isogyres of the mica show distinct blue fringes of their concave side due to dispersion of the optic axes.

When studying high-birefringent minerals, it is suggested that the quartz wedge is used instead of the first-order red plate. When inserting the quartz wedge, the isochromes in the four quadrants migrate in a characteristic way (Fig. 4-55).

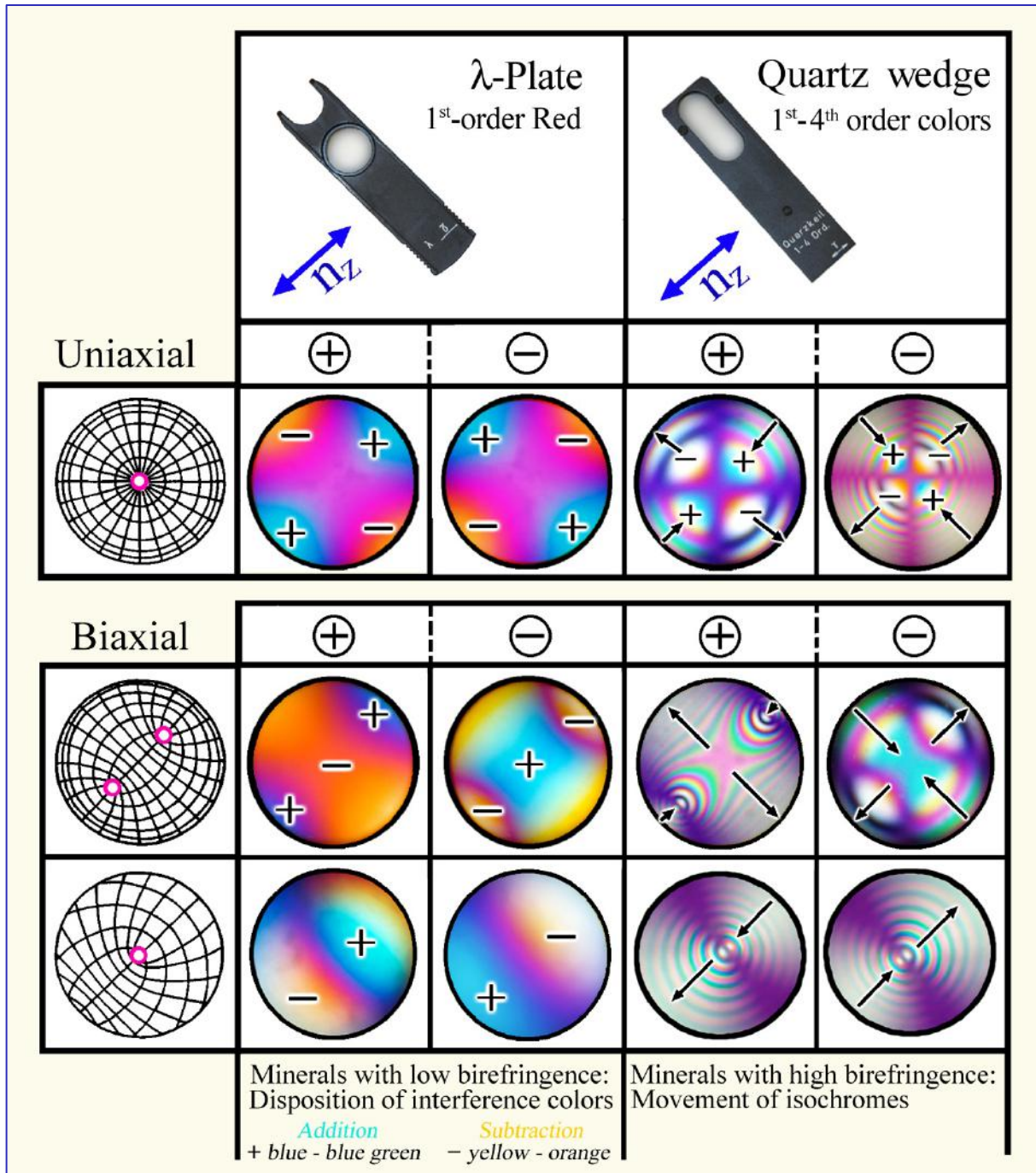


Figure 4-55. Determination of the optic sign of anisotropic minerals



#### 4.2.5.5 Practical hints for conoscopic observation

**Mineral grains that are to be investigated conoscopically should meet specific requirements:**

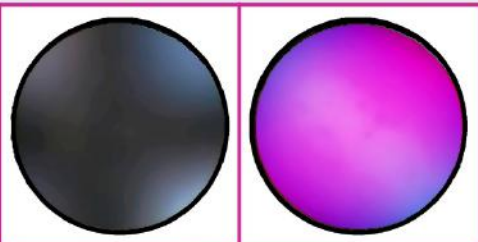
- a. When using a strongly magnifying objective ( $M_O = 40x, 50x, 63x$  or oil immersion  $100x$ ) with a large numerical aperture ( $>0.6$ ), the mineral grain should cover the field of view completely.
- b. The mineral grain must not be twinned within the observed frame, nor must it show alteration effects or exsolution phases.
- c. The mineral grain should have a suitable orientation.

**The procedure of obtaining the conoscopic interference figure is carried out as follows:**

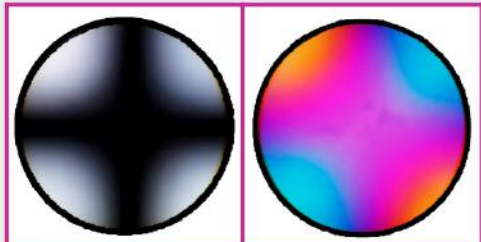
- a. Move the mineral grain into the centre of the crosshairs, use a high-magnification objective (40x minimum) and focus.
- b. Open all diaphragms below the stage.
- c. Move the condenser into the uppermost position and put the auxiliary condenser into the light path.
- d. Put the analyzer in. Take out the ocular; use a pinhole if included with the microscope, observe the image in the ocular tube or use the Amici-Bertrand lens and observe the enlarged image through the ocular. In some microscopes, the Amici-Bertrand lens can be centred and focused separately, which is important for quantitative work.
- e. If the mineral grain is too small to fully occupy the field of view, an upper diaphragm that is included in some microscopes can be used to reduce or eliminate the periphery around the grain. If there is no Amici-Bertrand lens with upper diaphragm, a sharp conoscopic interference figure may be obtained using a simple pinhole in place of the ocular.

Minerals that are strongly coloured may cause problems for the determination of their optic sign if the first-order red plate is used. Therefore, the quartz wedge is recommended for compensation, which allows observing the direction of movement of the isochromes.

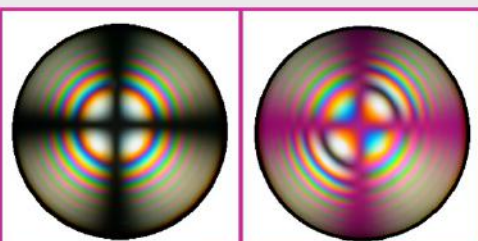
### Optically uniaxial minerals



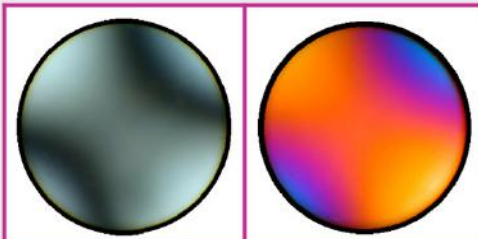
Apatite cut  $\perp$  optic axis  
 $2V_x = 0^\circ \Delta n = 0.003$



Quartz cut  $\perp$  optic axis  
 $2V_z = 0^\circ \Delta n = 0.0091$

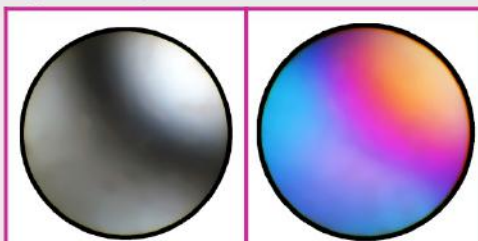


Calcite cut  $\perp$  optic axis  
 $2V_x = 0^\circ \Delta n = 0.1719$

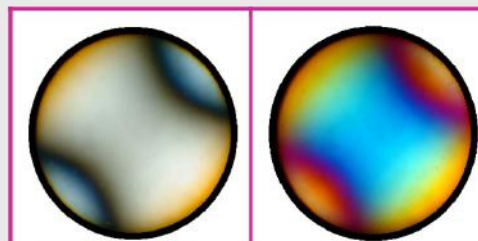


Sillimanite cut  $\perp$  acute bisectrix  
 $2V_z \sim 25^\circ \Delta n = 0.020$

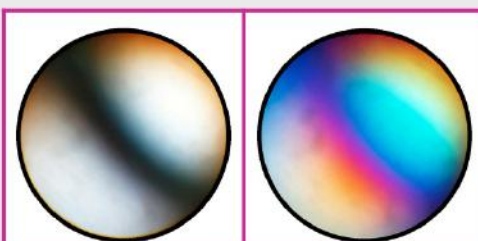
### Optically biaxial minerals



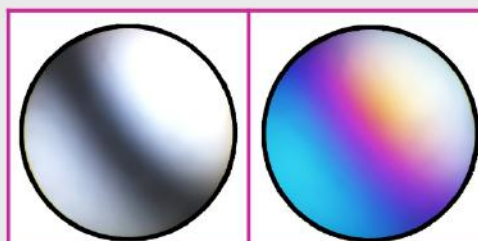
Wollastonite cut  $\perp$  optic axis  
 $2V_x = 36-42^\circ \Delta n = 0.014$



Muscovite cut  $\perp$  acute bisectrix  
 $2V_x \sim 40^\circ \Delta n \sim 0.040$



Clinopyroxene cut  $\perp$  optic axis  
 $2V_z \sim 60^\circ \Delta n \sim 0.030$



Forsterite cut  $\perp$  optic axis  
 $2V_x \sim 90^\circ \Delta n = 0.033$

**Figure 4-56.** Conoscopic interference figures of selected minerals, viewed in grain sections perpendicular to the optic axis or the acute bisectrix. Left-hand side: Interference figure without compensator; right-hand side: first-order red plate inserted.

## 5. Routine mineral determination

### Observations in plane-polarized light mode

#### Mineral colour

Colour tone and intensity,  
Colour distribution  
Pleochroism  
*Ch. 4.2.1*

Pleochroism, changing relief/chagrin = anisotropic  
*non-cubic minerals*

#### Light refraction

Relief, chagrin,  
Becke-Line:  
Refractive index n  
*Ch. 4.2.2*

#### Morphological characteristics

Grain form, twins,  
fractures, cleavage,  
zoning, inclusions,  
decomposition, alteration  
*Ch. 3.1 – 3.4*

### Observations in crossed polarizers mode

#### Mineral section remains black during rotation of stage

##### a. isotropic

no optic axis interference figure  
*Glasses; cubic minerals*

##### b. anisotropic: Section $\perp$ optic axis

optic axis interference figure:  
uniaxial, biaxial; *Ch. 4.2.5*  
*non-cubic minerals*

Mineral section changes from bright to dark during stage rotation = anisotropic

#### Interference colour

low, high  
normal, anomalous  
*Ch. 4.2.3*

#### Morphological features

Twins and intergrowths;  
Subgrains, undulose extinction;  
Zoning, unmixing;  
Brewster crosses in spherulites  
*Ch. 3.3, 3.4, 4.2.3*

Sections of maximum  
interference colour

Sections with low  
interference colour

↓  
birefringence  
*Ch. 4.2.3*

↓  
a. optically uniaxial, optic sign  
Sections  $\sim \perp$  opt. axis

↓  
b. optically biaxial, optic sign  
Sections  $\sim \perp$  acute bisectrix, or  $\perp$  optic axis  
*Ch. 4.2.5*

#### Extinction

*orthorhombic*  
*monoclinic*

$\left\{ \begin{array}{l} \text{straight} \\ \text{symmetrical} \\ \text{inclined} \end{array} \right.$	$\left. \begin{array}{l} \text{hexagonal} \\ \text{trigonal} \\ \text{tetragonal} \\ \text{triclinic} \end{array} \right\}$
---	---

**Sign of elongation:** I (+), I (-)  
*Ch. 4.2.4*

**Extinction angle  $\epsilon$**   
*Ch. 4.2.4*